T.R.
ONDOKUZ MAYIS UNIVERSITY
INSTITUTE OF GRADUATE STUDIES
DEPARTMENT OF HISTOLOGY AND EMBRYOLOGY

THE POSSIBLE PROTECTIVE ROLE OF GUM ARABIC AGAINST THE EFFECTS OF DICLOFENAC SODIUM EXPOSURE ON THE HEART TISSUE IN RATS

Ph.D. Thesis

Abuzar Mubarak OMER OSMAN

Supervisor

Assoc. Prof. Dr. Mehmet Emin ÖNGER

SAMSUN

2023

ACCEPTANCE AND APPROVAL OF THE THESIS

The study entitled **"THE POSSIBLE PROTECTIVE ROLE OF GUM ARABIC AGAINST THE EFFECTS OF DICLOFENAC SODIUM EXPOSURE ON THE HEART TISSUE IN RATS"** prepared by **Abuzar Mubarak OMER OSMAN** and supervised by **Assoc. Prof. Dr. Mehmet Emin ÖNGER** was found successful and unanimously accepted by committee members as Ph.D. thesis, following the examination on the date (28.08.2023)

	Title Name SURNAME **University** **Department/Art**	**Final Decision**
Chairman	Prof. Dr. Süleyman KAPLAN Ondokuz Mayıs University Department of Histology and Embryology	☒ Accept ☐ Reject
Member	Assoc. Prof. Dr. Mehmet Emin ÖNGER, Ondokuz Mayıs University Department of Histology and Embryology	☒ Accept ☐ Reject
Member	Assis. Prof. Dr. Mehmet Alper ARSLAN Ondokuz Mayıs University Department of Medical Biology	☒ Accept ☐ Reject
Member	Assist. Prof. Dr. Ömür Gülsüm DENİZ Bolu Abant İzzet Baysal University Department of Histology and Embryology	☒ Accept ☐ Reject
Member	Assist. Prof. Dr. Işinsu ALKAN Nevsehir Haci Bektas Veli University Department of Histology and Embryology	☒ Accept ☐ Reject

This thesis has been approved by the committee members that already stated above and determined by the Institute Executive Board.

Prof. Dr. Ahmet TABAK

Head of Institute of Graduate Studies

DECLARATION OF COMPLIANCE WITH SCIENTIFIC ETHIC

I hereby declare and undertake that I complied with scientific ethics and academic rules in all stages of my Ph. D. Thesis , that I have referred to each quotation that I use directly or indirectly in the study, and that the works I have used consist of those shown in the sources, that it was written in accordance with the institute writing guide and that the situations stated in the article 3, section 9 of the Regulation for TÜBİTAK Research and Publication Ethics Board were not violated.

Is the Ethics Committee Necessary?

Yes ☒

No ☐

21 / 06/ 2023

Abuzar Mubarak OMER OSMAN

DECLARATION OF THE THESIS STUDY ORIGINALITY REPORT

Thesis Title: THE POSSIBLE PROTECTIVE ROLE OF GUM ARABIC AGAINST THE EFFECTS OF DICLOFENAC SODIUM EXPOSURE ON THE HEART TISSUE IN RATS.

As a result of the originality report taken by me from the plagiarism detection program on 21/06 /2023 for the thesis titled above,

Similarity ratio: % 8

Single resource rate: % 1 has been released.

21/06/ 2023

Assoc. Prof. Dr. Mehmet Emin ÖNGER

ÖZET

RATLARDA DİKLOFENAK SODYUM MARUZİYETİNİN KALP DOKUSU ÜZERİNDEKİ ETKİLERİNE KARŞI GUM ARABIC'İN MUHTEMEL KORUYUCU ROLÜ

Abuzar Mubarak OMER OSMAN
Ondokuz Mayıs Üniversitesi
Lisansüstü Eğitim Enstitüsü
Histoloji ve Embriyoloji Ana Bilim Dalı
Doktora, Temmuz/2023
Danışman: Doç. Dr. Mehmet Emin ÖNGER

Diklofenak sodyum (DS), en yaygın olarak reçete edilen non-steroid bir anti-inflamatuvar ilaçtır. DS, antipiretik, analjezik, antiinflamatuvar ve antikoagülan olarak işlev görmektedir ve ciddi kardiyovasküler olaylara neden olmaktadır. Gum Arabic (GA), Akasya Senegal ağacının bir sızıntısıdır. GA çeşitli dejeneratif hastalıklar için olumlu tedavi özelliklerine sahiptir . Bu çalışmanın amacı, sıçan modelinde diklofenak sodyum maruziyeti sonucu oluşan kalp dokusu hasarının iyileşmesinde GA' nın etkisini stereolojik teknikler kullanarak araştırmaktır.

40 adet Wistar albino erkek sıçan dört gruba ayrıldı: Kontrol grubu (n=10); herhangi bir uygulama yapılmadı. DS grubu (n=10); 15 gün boyunca oral gavaj yoluyla 3.6 mg/kg/gün dozunda DS uygulandı. GA grubu (n=10);15 gün boyunca oral gavaj yoluyla 7.5 g/kg/gün GA uygulandı. GA+DS grubu (n=10); 15 gün boyunca oral gavaj yoluyla sırasıyla 3,6 mg/kg/gün ve 7.5 g/kg/gün dozunda DS ve GA uygulandı.

Bu çalışmada GA'nın DS'nin dejeneratif etkisine karşı olası iyileştirici etkileri histolojik ve stereolojik yöntemlerle incelenmiştir. Tüm gruplar arasında her bir hayvanın sol ventriküllerindeki kardiyomiyosit sayısındaki farklılığı araştırmak için fiziksel disektör yöntemleri uygulandı. Çalışma, oral gavaj yoluyla uygulanan DS'nin sol ventrikül yapısı ve işlevi üzerinde herhangi bir zararlı etkisinin olmadığını buldu. Biyokimyasal araştırmalar gruplar arasında antioksidan düzeylerinde herhangi bir değişiklik olmadığını gösterdi. Kardiyomiyosit sayımı açısından gruplar arasında anlamlı fark bulunmadı. Ancak niteliksel analizimiz DS' nin kalp dokusu hücreleri üzerinde toksik etkisini gösterdi.

Gruplar arasında gözlenen bazı küçük değişikliklerin muhtemelen DS'nin toksik etkilerinden kaynaklandığı ancak bunların istatistiksel düzeylere ulaşmadığı sonucuna varılabilir. Yine GA'nın faydalı etkisine bakıldığında gruplar arasında anlamlı bir fark olmadığı sonucuna varabiliriz.

Anahtar Sözcükler: Gum Arabic, Diklofenak, NSAID, Kalp dokusu, Stereoloji

ABSTRACT

THE POSSIBLE PROTECTIVE ROLE OF GUM ARABIC AGAINST THE EFFECTS OF DICLOFENAC SODIUM EXPOSURE ON THE HEART TISSUE IN RATS

Abuzar Mubarak OMER OSMAN
Ondokuz Mayıs University
Institute of Graduate Studies
Department of Histology and Embryology
Ph.D., July/2023
Supervisor: Assoc. Prof. Dr. Mehmet Emin ÖNGER

Diclofenac sodium (DS) is a non-steroidal anti-inflammatory drug most widely prescribed. DS acts as an antipyretic, analgesic, anti-inflammatory, and anti-coagulant. It causes serious cardiovascular events. Gum Arabic (GA) is an exudate of the Acacia Senegal tree. GA has positive treatments for several degenerative diseases. The aim of this study is to investigate the effect of GA on the healing of heart tissue damage caused by DS exposure in rat model using stereological techniques.

40 Wistar albino male rats were divided into four groups as follows: The Control group (n=10) was assigned as a control group. However, this group received no treatment. DS group (n=10); was treated by DS with a dose of 3.6 mg/kg/day orally for 15 days. GA group (n=10); was treated by GA only with a dose of 7.5 g/kg/day orally by oral gavage for 15 days. GA+DS group (n=10); was treated by DS and GA with a dose of 3.6 mg/kg/day, 7.5 g/kg/day respectively, orally for 15 days.

In this study, possible healing effects of GA against the degenerative effect of DS were examined by histological and stereological methods. The physical dissector methods were performed to investigate the difference in counts of the cardiomyocytes of the left ventricles of each animal among all groups. The study found that DS has no harmful effects on the left ventricles' structure and function when administered by oral gavage. Biochemical investigations showed no change in antioxidant levels between the groups. There is no significant difference between groups in terms of cardiomyocyte counting. However, our qualitative analysis showed a toxic effect of DS on the heart tissue cells.

It can be concluded that despite some minor changes that were observed between the groups, they have not reached statistical levels, and they likely tend to be due to the toxic effects of DS. Regarding the beneficial effect of GA, we can conclude that there are no significant differences between the groups.

Keywords: Gum Arabic, Diclofenac, NSAID, Heart tissue, Stereology

ACKNOWLEDGEMENT

First and foremost, I would like to thank Allah Almighty for providing the strength and encouragement to embark on this research project and to persevere and complete it.

I would like to express my robust gratitude and appreciation to my supervisor, Assoc. Prof. Dr. Mehmet Emin ÖNGER who encouraged me throughout my Ph.D. journey with his continuous and everlasting support, advice, and stimulating suggestions. I express my most honest and sincere gratitude to my mentor, Prof. Dr. Süleyman KAPLAN, who supported me with his constant and precious advice and offered me valuable opportunities to learn and gain experience in stereology. My gratefulness and thanks to Assist. Prof. Dr. Mehmet Alper ARSLAN who supported me throughout my Ph.D. journey and provided me the giudance and advice. Valuable appreciation and blessings to Assist. Prof. Dr. Ömür Gülsüm DENİZ and Assist. Prof. Dr. Işinsu ALKAN for their precious time and effort during the assessment and correction of the thesis.

My heartfelt thanks and sincere gratitude were expressed to Prof. Dr. Ayman Ahmed WARILLE for his constant encouragement and unlimited support, which always encouraged me to work harder. My gratefulness to Assist. Prof. Dr. Abubaker Elhaj FARG, my former colleague from the Department of Histology and Embryology, I want to thank him for his help and huge support. Especial thanks to those who supported me in my research work, Dr. Gamze ALTUN, and my colleague Ph.D. student Aysenur KAYA, and the department's staff, technician Hüseyin SARÇAOLU. I offer valuable appreciation and blessings to all the Sudanese colleagues in the Department of Histology and Embryology who supported me in any way during my study. I will not forget to especially thank Abubaker ALAMIN and Juman ALMASAAD for all great the help and support.

I would like to thank, with profound gratitude from the bottom of my heart, my wife, Dr. Azza Badri, my children, my sisters, and my brothers for their unquestionable and unlimited encouragement and support to complete my work. I dedicate this accomplishment to them and to the soles of my parents.

Abuzar Mubarak OMER OSMAN

CONTENTS

ACCEPTANCE AND APPROVAL OF THE THESIS ..... **İ**
DECLARATION OF COMPLIANCE WITH SCIENTIFIC ETHIC ..... **İİ**
DECLARATION OF THE THESIS STUDY ORIGINALITY REPORT ..... **İİ**
ÖZET ..... **İİİ**
ABSTRACT ..... **İV**
ACKNOWLEDGEMENT ..... **V**
CONTENTS ..... **Vİ**
SYMBOLS AND ABBREVIATIONS ..... **Vİİ**
FIGURES LEGENDS ..... **Vİİİ**
TABLES LEGENDS ..... **İX**
1. INTRODUCTION **1**
2. GENERAL INFORMATION **4**
2.1. Diclofenac Sodium as (NSAIDS) 4
2.1.1. Pharmacodynamics Properties of Diclofenac Sodium 4
2.1.2. DS the Mechanism of Action 5
2.1.3. Prostaglandin and Cyclo-Oxygenase Production Inhibition 5
2.1.4. Adverse Effects of DS on the All Body Organs 6
2.1.5. The Effects of DS on the (CVS) 7
2.2. Gum Arabic (GA) 9
2.2.1. Chemical Components of the GA 9
2.2.2. Traditional Medicine Uses of GA 10
2.2.3. Antioxidant Properties of GA 11
2.3. Anatomy of the Rat Heart 11
2.3.1. Background and Development 11
2.4. Stereology 14
2.5. Objectives 14
2.5.1. General Objective 14
2.5.2. Special Objectives 15
2.6. Justification 15
3. MATERIALS AND METHODS **16**
3.1. Experimental Animals 16
3.1.1. Formation of Experimental Animal Groups 16
3.2. Materials 17
3.2.1. Diclofenac Sodium 17
3.2.2. Gum Arabic 18
3.3. Histological Procedures and Tissue Preparation 18
3.3.1. Perfusion 18
3.3.2. Routine Histological Tissue Processing 18
3.3.3. Toluidine Blue Staining Process 20
3.3.4. Sectioning Methods 20
3.3.5. H&E Stain 21
3.3.6. Masson Trichrome Stain 22
3.3.7. Tissue Preparation for Ultra-Thin Sectioning Process. 23
3.4. Stereology 24
3.4.1. Stereological Analysis: 25
3.5. Biochemical Methods 29
3.5.1. Analysis of Superoxide Dismutase Enzyme Activity 30
3.5.2. Analysis of Catalase Enzyme Activity 31

3.5.3. Total Phenolic Content and Antioxidant Power Determination 32
3.5.4. Method to Assess the Total Phenolic Content 32
3.5.5. Methods to Assess The Antioxidant Power 33
3.6. Statistical Analysis 33
4. RESULTS 34
4.1. Stereological Findings 34
4.1.1. The Counted Particles of Cardiomyocytes of The Left Ventricle 35
4.1.2. The Total Volume of The Left Ventricle 35
4.1.3. The Total Number of Cardiomyocytes in The left Ventricle 36
4.1.4. The Numerical Density of Cardiomyocytes in The left Ventricle 37
4.2. Analysis of Enzyme's Activities 39
4.2.1. Analysis of Catalase Enzyme Activity 39
4.2.2. Analysis of Superoxide Dismutase Enzyme Activity 39
4.3. Light Microscopic Findings 40
4.3.1. Light Microscopic Findings of H&E-Stained Sections 40
4.3.2. Light Microscopic Findings of Toluidine Blue - Stained Sections 52
4.3.3. Findings of Toluidine Blue - Stained Sections 87
4.3.4. Light Microscopic Findings of Masson Trichrome- Stained Sections 88
5. DISCUSSION 114
6. CONCLUSIONS AND RECOMMENDATIONS 119
6.1. Conclusions 119
6.2. Recommendations 119
REFERENCES 120
APPENDIX 1: ETHICAL COMMITTEE DICISTION 129
CURRICULUM VITEA 130

SYMBOLS AND ABBREVIATIONS

AG	: Arabinogalactan
AGP	: Arabinogalactan-Protein Complex.
BC	: Before Christ
CE	: Coefficient of Error
CV	: Coefficient of variance
COX-1	: Cyclooxygenase 1 Enzyme
COX-2	: Cyclooxygenase 2 Enzyme
DS	: Diclofenac Sodium
GA	: Gum Arabic
GSH	: Glutathione
GPx	: Glutathione Peroxidase
H_2O_2	: Hydrogen Peroxide
LV	: Left Ventricle
NSAIDs	: Non-steroidal anti-inflammatory Drugs
OS	: Oxidative Stress
PG	: Prostaglandin
ROS	: Reactive Oxygen Species
SOD	: Superoxide Dismutase

FIGURES LEGENDS

Figure 2.1. Chemical structure of DS drug products 5

Figure 2.2. Biosynthetic pathway of prostanoids and action, redrawn from (Ricciotti and FitzGerald, 2011)..... 6

Figure 2.3. Gum Arabic (dry exudates particles)..... 9

Figure 3.1. Housing conditions of the animal..... 16

Figure 3.2. Wistar albino rats in a cage..... 17

Figure 3.3. Automated dehydration 19

Figure 3.4. A rotary microtome (Leica RM2125RT, Nussloch, Germany)..... 20

Figure 4.1. Indicates the significant differences between the groups in terms of the counted particles of the left ventricle 35

Figure 4.2. Indicates the differences between the groups regarding the volume of the left ventricle of the rat heart..... 36

Figure 4.3. The graph shows the differences between the groups in terms of the total number of myocytes in the left ventricle of the rat heart..... 37

Figure 4.4. The graph shows the differences between the groups in terms of mean of the numerical density of cardiomyocytes in the left ventricle of the rat heart. 38

Figure 4.5. The mean and SEM of CAT enzyme activity nmol/min/ml 540 nm among all groups: CON, DS, GA, and GA+DS. 39

Figure 4.6. SOD enzyme activity (U/ml (450 nm)), among all groups: CON, DS, GA, and GA+DS. 40

Figure 4.7. (A, B) Histological images of the left ventricle of CON stained with H&E staining are seen. 41

Figure 4.8. (A, B) Histological images of the left ventricle stained with H&E staining are seen. 42

Figure 4.9. (A, B) Histological images of the left ventricle stained with H&E staining are seen of DS..... 43

Figure 4.10. (A, B) Histological images of the left ventricle stained with H&E staining are seen. 44

Figure 4.11. (A, B) Histological images of the left ventricle stained with H&E staining are seen. 45

Figure 4.12. (A, B) Histological images of the left ventricle stained with H&E staining are seen. 46

Figure 4.13. (A, B) Histological images of the left ventricle stained with H&E staining are seen. 47

Figure 4.14. (A, B) Histological images of the left ventricle stained with H&E staining are seen. 48

Figure 4.15. (A, B) Histological images of the left ventricle stained with H&E staining are seen. 49

Figure 4.16. (A, B) Histological images of the left ventricle stained with H&E staining are seen. 50

Figure 4.17. (A, B) Histological images of the left ventricle stained with H&E staining are seen. 51
Figure 4.18. (A, B) Images of the heart tissue of the left ventricle are seen in the CON. 52
Figure 4.19. (A, B) Images of the heart tissue of the left ventricle are seen in the CON. 53
Figure 4.20. (A, B) Images of the heart tissue of the left ventricle are seen in the CON. 54
Figure 4.21. (A, B) Images of the heart tissue of the left ventricle are seen in the CON. 55
Figure 4.22. (A, B) Images of the heart tissue of the left ventricle are seen in the CON. 56
Figure 4.23. (A, B) Images of the heart tissue of the left ventricle are seen in the CON. 57
Figure 4.24. (A, B) Images of the heart tissue of the left ventricle are seen in the CON. 58
Figure 4.25. (A, B) Images of the heart tissue of the left ventricle are seen in the CON. 59
Figure 4.26. (A, B) Images of the heart tissue of the left ventricle are seen in the CON. 60
Figure 4.27. (A, B) Images of the heart tissue of the left ventricle are seen in the DS..... 61
Figure 4.28. (A, B) Images of the heart tissue of the left ventricle are seen in the DS..... 62
Figure 4.29. (A, B) Images of the heart tissue of the left ventricle are seen in the DS..... 63
Figure 4.30. (A, B) Images of the heart tissue of the left ventricle are seen in the DS..... 64
Figure 4.31. (A, B) Images of the heart tissue of the left ventricle are seen in the DS..... 65
Figure 4.32. (A, B) Images of the heart tissue of the left ventricle are seen in the DS..... 66
Figure 4.33. (A, B) Images of the heart tissue of the left ventricle are seen in the DS..... 67
Figure 4.34. (A, B) Images of the heart tissue of the left ventricle are seen in the DS..... 68
Figure 4.35. (A, B) Images of the heart tissue of the left ventricle are seen in the GA. 69
Figure 4.36. (A, B) Images of the heart tissue of the left ventricle are seen in the GA. 70
Figure 4.37. (A, B) Images of the heart tissue of the left ventricle are seen in the GA. 71
Figure 4.38. (A, B) Images of the heart tissue of the left ventricle are seen in the GA. 72
Figure 4.39. (A, B) Images of the heart tissue of the left ventricle are seen in the GA. 73
Figure 4.40. (A, B) Images of the heart tissue of the left ventricle are seen in the GA. 74
Figure 4.41. (A, B) Images of the heart tissue of the left ventricle are seen in the GA. 75
Figure 4.42. (A, B) Images of the heart tissue of the left ventricle are seen in the GA. 76
Figure 4.43. (A, B) Images of the heart tissue of the left ventricle are seen in the GA. 77
Figure 4.44. (A, B) Images of the heart tissue of the left ventricle are seen in the GA. 78
Figure 4.45. (A, B) Images of the heart tissue of the left ventricle are seen in the GA+DS.. 79
Figure 4.46. (A, B) Images of the heart tissue of the left ventricle are seen in the GA+DS.. 80
Figure 4.47. (A, B) Images of the heart tissue of the left ventricle are seen in the GA+DS.. 81
Figure 4.48. (A, B) Images of the heart tissue of the left ventricle are seen in the GA+DS.. 82
Figure 4.49. (A, B) Images of the heart tissue of the left ventricle are seen in the GA+DS.. 83
Figure 4.50. (A, B) Images of the heart tissue of the left ventricle are seen in the GA+DS.. 84
Figure 4.51. (A, B) Images of the heart tissue of the left ventricle are seen in the GA+DS.. 85
Figure 4.52. (A, B) Images of the heart tissue of the left ventricle are seen in the GA+DS.. 86

Figure 4.53. (A, B) Images of the heart tissue of the left ventricle are seen in the CON. 88
Figure 4.54. (A, B) Images of the heart tissue of the left ventricle are seen in the CON. 89
Figure 4.55. (A, B) Images of the heart tissue of the left ventricle are seen in the CON. 90
Figure 4.56. (A, B) Images of the heart tissue of the left ventricle are seen in the CON. 91
Figure 4.57. (A, B) Images of the heart tissue of the left ventricle are seen in the CON. 92
Figure 4.58. (A, B) Images of the heart tissue of the left ventricle are seen in the DS..... 93
Figure 4.59. (A, B) Images of the heart tissue of the left ventricle are seen in the DS..... 94
Figure 4.60. (A, B) Images of the heart tissue of the left ventricle are seen in the DS..... 95
Figure 4.61. (A, B) Images of the heart tissue of the left ventricle are seen in the DS..... 96
Figure 4.62. (A, B) Images of the heart tissue of the left ventricle are seen in the DS..... 97
Figure 4.63. (A, B) Images of the heart tissue of the left ventricle are seen in the DS..... 98
Figure 4.64. (A, B) Images of the heart tissue of the left ventricle are seen in the GA. 99
Figure 4.65. (A, B) Images of the heart tissue of the left ventricle are seen in the GA. 100
Figure 4.66. (A, B) Images of the heart tissue of the left ventricle are seen in the GA. 101
Figure 4.67. (A, B) Images of the heart tissue of the left ventricle are seen in the GA. 102
Figure 4.68. (A, B) Images of the heart tissue of the left ventricle are seen in the GA. 103
Figure 4.69. (A, B) Images of the heart tissue of the left ventricle are seen in the GA. 104
Figure 4.70. (A, B) Images of the heart tissue of the left ventricle are seen in the GA. 105
Figure 4.71. (A, B) Images of the heart tissue of the left ventricle are seen in the GA+DS.106
Figure 4.72. (A, B) Images of the heart tissue of the left ventricle are seen in the GA+DS.107
Figure 4.73. (A, B) Images of the heart tissue of the left ventricle are seen in the GA+DS.108
Figure 4.74. (A, B) Images of the heart tissue of the left ventricle are seen in the GA+DS 109
Figure 4.75. (A, B) Images of the heart tissue of the left ventricle are seen in the GA+DS 111
Figure 4.76. (A, B) Images of the heart tissue of the left ventricle are seen in the GA+DS.112

TABLES LGENDS

Table 2.1. Shared toxicities of NSAIDs (Crofford, 2013) 7

Table 3.1. Time spent treating cardiac tissues processing procedures protocol 19

Table 3.2. Tissue staining procedures protocol H&E staining procedure..... 22

Table 3.3. Tissue staining procedures protocol for Masson trichrome stain..... 23

Table 3.4 Tissue embedding silicone mold procedures protocol. 24

Table 4.1. Estimation of mean and SD of volume, total number, and numerıcal density of the left ventricle..... 34

Table 4.2. The mean, SD, SEM, CE and CV of counted particles of cardiomyocytes of the left ventricle..... 35

Table 4.3. Estimation of mean, SD and SEM of volume of the left ventricle (μm^3) 36

Table 4.4. The mean, SD and SEM of the total number of cardiomyocytes of the left ventricle among all groups: CON, DS, GA, and GA+DS 37

Table 4.5. The mean and SD numerical density (count/μm^3) among all groups: CON, DS, GA, and GA+DS 38

Table 4.6. The mean and SEM of CAT enzyme activity nmol/min/ml 540 nm 39

Table 4.7. The mean, the SEM of SOD enzyme activity U/ml450 nm..... 40

1. INTRODUCTION

Since the 1970s, Diclofenac Sodium DS, composed of salicylic and acetylsalicylic acids, has been the most frequently prescribed medication among non-steroidal anti-inflammatory drugs (NSAIDs)(Gan, 2010). It acts as an analgesic, antipyretic, anti-inflammatory, and anti-coagulant (Pountos, Theodora, Howard, and Giannoudis, 2011; Ricciotti and FitzGerald, 2011). It works by inhibiting the cyclo-oxygenase enzymes (COX-1 and COX-2), which are responsible for producing prostaglandins and are made from the arachidonic acid found in cell membranes. Arachidonic acid is transformed into endoperoxides (prostaglandin, prostacyclin, and thromboxane) by these enzymes (Ricciotti and FitzGerald, 2011). Endoperoxides are crucial for controlling inflammation, fever, and pain. In addition to regulating renal blood circulation, platelet aggregation, and gastric mucosa protection, COX-1 is also involved in platelet expression. COX-2, in contrast, contributes to inflammation mediation (Atzeni, Masala, and Sarzi-Puttini, 2018). The prostaglandin of pain and inflammation-mediated reactions, COX-2, controls blood flow and cardiovascular system (CVS) homeostasis (Ricciotti and FitzGerald, 2011).

Selective and non-selective are the main two types of NSAIDs. Due to the significant adverse effects that non-selective NSAIDs have on the GIT when they block COX-1, selective COX-2 inhibitors were created. (Ong, Lirk, Tan, and Seymour, 2007) found that they also have a detrimental effect on the cardiovascular system. DS is not selective; however, according to reports (Gan, 2010), it is four times more selective for COX-2 than COX-1. To treat the pain associated with osteoarthritis and rheumatoid arthritis, Japan developed the slow-release tablet Voltaren, DS in 1974 (Gan, 2010).

In the USA, more than 111 million prescriptions every year, and more than 30 million individuals use them daily, with a mortality rate of 6 per 100,000 people (Peterson et al., 2006). Ibuprofen and DS constitute 60% of all sales of NSAIDs worldwide, making them the most popular NSAIDs (Conaghan, 2012). Arthritis sufferers make up most consumers (Hawkey, 2000). According to a recent DS meta-analysis study, DS increases the chance of having a heart attack or stroke. The risk of congestive heart failure (CHF), particularly in patients with a history of cardiac illness, is considerable (Varas-Lorenzo, et al., 2013). Other research demonstrated that DS decreases smooth muscle cell development and may contribute to lesion formation at

vascular injury sites (Baskar, Sparatore, Del Soldato and Moore, 2008). A recent study shows that DS reduces the size and quantity of myocytes, which leads to a reduction in the heart ventricular wall mass in rats exposed to DS in utero (Gevrek, Kara, RAĞBETLİ and ASLAN, 2015). Research on domesticated white leghorn birds (Gallus domesticus) revealed that DS toxicity causes cardiac cell necrosis, edema, and thickening of the epicardium (Jain, et al., 2009). However, in accordance with another meta-analysis study on the adverse effects of DS, the risk of developing severe cardiovascular events such as myocardial infarction, angina, stroke, transient ischemic attack, cardiovascular death, hypertension, and congestive heart failure (Haugen, et al., 2015). A recent study revealed a strong correlation between symptomatic hand osteoarthritis and coronary heart disease (myocardial infarction, coronary insufficiency syndrome) (Haugen,et al., 2015; Nair and Taylor-Gjevre, 2010). The American College of Rheumatology (ACR) and the European League Against Rheumatism (EULAR) recommend topical NSAIDs for treating osteoarthritis if other oral pharmacologic approaches are impossible. There is a risk of thrombotic cardiovascular events, according to long-term medication. According to (Nair and Taylor-Gjevre, 2010) 50% of NSAID users were unaware of potential adverse effects.

Gum Arabic (GA) is also known by many names as follows: GA Acacia Senegal, Gum hashab, Kordofan Gum, GA Acacia Seyal, Gum Talha, Acacia gum, and Arabic Gum. Only two species, Acacia Senegal and Acacia Seyal, are relevant for commercial uses out of the more than 1000 species of the GA trees (Nair and Taylor-Gjevre, 2010). Due to their low tannin content, Acacia Senegal is classified as having the highest quality and constitutes most of the global trade (Egadu, Mucunguzi and Obua, 2007).

Most of the gum trees were growing in the Sahelian belt of Africa, which extends from Senegal in the west to Somalia in the east, it is an estimated 3,860-kilometer-long arc-shaped continent that lies directly south of the Sahara Desert. Almost all a tree's parts can release GA exudate. The process of "tapping," which involves removing portions of the bark, stimulates the production of GA. On the trees, the gooey, sticky stuff dries and hardens into nodules. They are hand-collected and categorized by size and color, according to (Phillips and Williams, 2000).

GA is the best sort of gum and was recognized as Saharan food as early as the Stone era (Sanchez, et al., 2018). GA is a viscous secretion of the tropical plant (Acacia

Senegal) (Cornelsen, et al., 2015). Constructed of a water-soluble polysaccharide (molecular weight about 850000) comprising rhamnose, arabinose, glucuronic acid, and galactose, and extensively used as an additive and stabilizer in various food and medicine items (B. H. Ali, et al., 2011). Over 3000 global pharmaceutical, food, drinks, and cosmetics institutions and companies utilize GA in their business (Glover, Ushida, Phillips and Riley, 2009).

GA has several positive impacts on the body, including acting as an antioxidant, lowering plasma cholesterol levels in both animals and humans, and having an anti-carcinogenic action with a preventive function against hepatic and cardiac cancer (Abd-Allah, et al., 2002; Khalid, et al., 2014). Furthermore, GA relieves the symptoms of chronic renal failure in human beings; the influence of GA on lipid metabolism and GA consumption can lower plasma cholesterol levels in rats (Nair and Taylor-Gjevre, 2010; Nasir, Babiker and Salim, 2016). It has significant beneficial effects, including monitoring cell proliferation, apoptosis, angiogenesis regulation, and inflammation (B. H. Ali,et al., 2011). Whenever utilized in therapies and medication for degenerative diseases such as hepatic, renal failure, cardiovascular, and gastrointestinal problems, GA has shown therapeutic efficacy and positive results (Nasir,et al., 2016). Furthermore, there are various advantageous effects on diabetics' and rats' blood pressure. There have been no serious adverse or harmful effects related to the use of (GA) (Nair and Taylor-Gjevre, 2010).

2. GENERAL INFORMATION

2.1. Diclofenac Sodium as (NSAIDS)

Diclofenac Sodium (DS) is one of the nonsteroidal anti-inflammatory drugs NSAID; DS(sodium-((2,6-dichlorophenyl)-amino)-phenyl)-acetate) (Aygun, Kaplan, Odaci, Onger and Altunkaynak, 2012). It functions as an anti-inflammatory, analgesic, and antipyretic agent. It is usable in various forms, including oral, rectal, and intramuscular injection (Todd and Sorkin, 1988). The drug works by restricting prostaglandin production by inhibiting cyclo-oxygenase (COX2) and (COX1) enzymes (Altman, Bosch, Brune, Patrignani and Young, 2015). The DS is the NSAID of "first choice" for relieving acute and chronic pain and inflammation. Considering that it can be tolerated well in comparison to other NSAIDs and has a short elimination the half-life, minimal risk of adverse effects on the body organs. It is an analgesic with a rapid onset and a longer duration of action (Todd and Sorkin, 1988). NSAIDs can cause a variety of side effects, including convulsions, platelet dysfunction, gastrointestinal and heart damage, and convulsions (Aygun,et al., 2012). appropriate to the case, such as rheumatoid arthritis, osteoarthritis, and ankylosing spondylitis (Chan, et al., 2010). DS dosage of 75 to 150mg daily supplied according to the case.

2.1.1. Pharmacodynamics Properties of Diclofenac Sodium

DS treats strains, osteoarthritis, neuropathic pain, acute and chronic inflammation-related problems, and heat. According to (Chan,et al., 2010; Zhao, et al., 2016), DS is more effective than aspirin, ibuprofen, naproxen, and phenylbutazone and causes less gastrointestinal adversely impact than aspirin, feprazone, indomethacin, and naproxen. By blocking the cyclo-oxygenase enzymes, resulting in an inhibiting impact on the production of prostaglandins, prostacyclin, and thromboxane products (Antman et al., 2007). The prostanoids include (prostacyclin [PGI2], prostaglandin [PG]-E2, PGD2, PGF2, and thromboxane [TX] A2). According to Roy Altman et al. (2015), PGE2 is the prostanoid of inflammation, and NSAIDs must be able to inhibit its production to become efficient analgesic and anti-inflammatory drugs (Figure 1.1.). Due to its effects on chemotaxis, superoxide generation, and protease synthesis, DS reduces polymorphonuclear leucocyte function (Chan,et al., 2010). In terms of prostaglandin E2 (PGE2) inhibition, DS is 3 to 1000 times more

powerful than other NSAIDs at inhibiting COX (Gan, 2010; N. Morioka, K. Kumagai, K. Morita, S. Kitayama and T. Dohi, 2004). To provide patients with osteoarthritis (OA), rheumatoid arthritis (RA), and ankylospondylitis with prolonged-lasting pain relief, DS (Voltaren) is an enteric-coated, slow-release designed treatment (Gan, 2010).

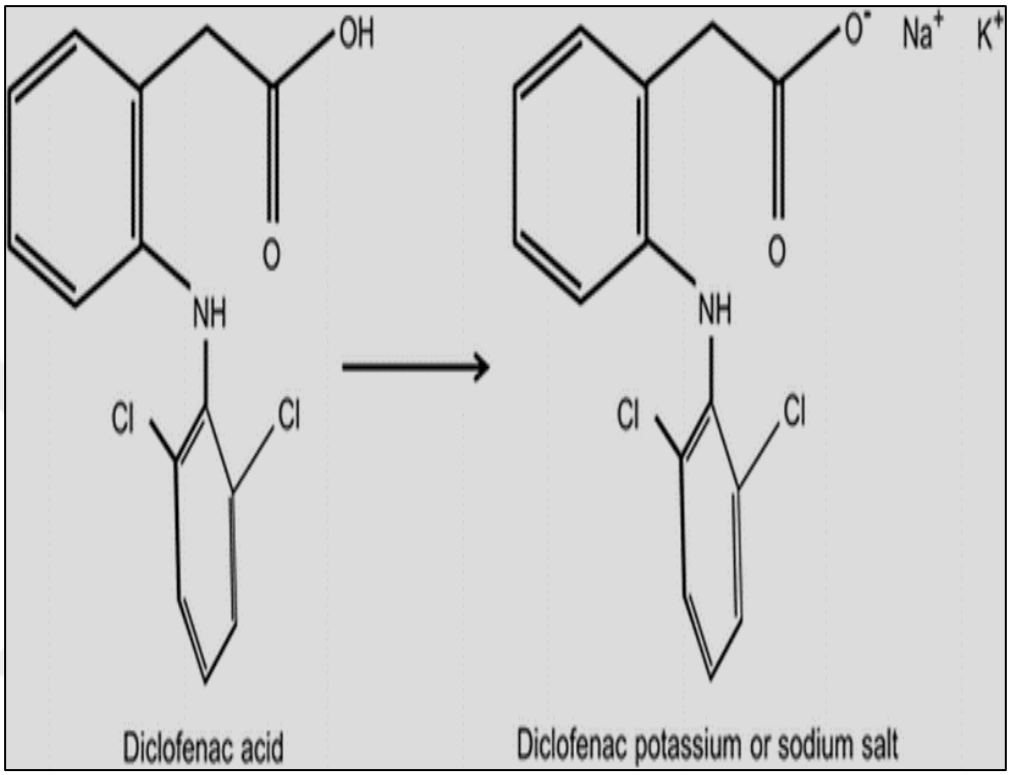


Figure 2.1. Chemical structure of DS drug products , redrawn from (Altman, et al., 2015)

2.1.2. DS the Mechanism of Action

2.1.3. Prostaglandin and Cyclo-Oxygenase Production Inhibition

DS inhibits the enzymes COX-1 and COX-2. By attaching COX isozymes and (cyclic guanosine monophosphate) GMP, DS prevents the formation of prostanoids. In contrast to the majority of other NSAIDs, DS has a more substantial selectivity for COX-2 than COX-1 (Altman,et al., 2015; Ong, et al., 2007). Research findings showed that DS might decrease the production of leukotriene C4 and 5-hydroxy eicosatetraenoic acid (5-HETE) in rat leukocytes and macrophages. These effects required DS concentrations above the therapeutic range, and a similar response was seen with indomethacin, naproxen, and ibuprofen (Gan, 2010)

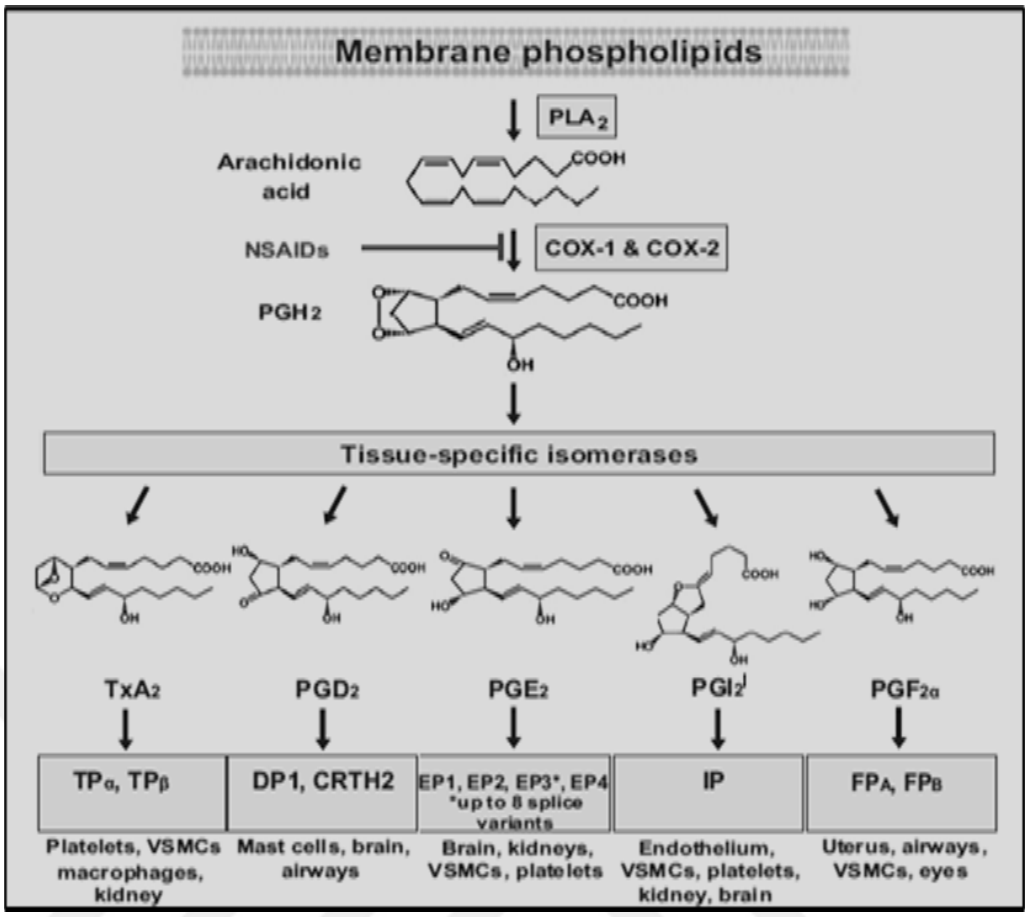


Figure 2.2. Biosynthetic pathway of prostanoids and action, redrawn from (Ricciotti and FitzGerald, 2011)

2.1.4. Adverse Effects of DS on the All Body Organs

NSAIDs have a distinct mechanism of action that allows them to be extremely successful therapeutically despite causing adverse reactions, which are especially frequent with oral administration (Varas-Lorenzo,et al., 2013). NSAIDs are suspected to be responsible for approximately 21-25% of all known adverse drug reactions (ADR). NSAID medicine's most prevalent adverse effects of NSAID include functional abnormalities of the gastrointestinal tract, kidneys, cardiovascular, and central nervous systems, especially when taken long-term. Side effects, contraindications, and restrictions on the use for NSAIDs vary widely. (Kowalski, et al., 2011). NSAID toxicity's efficacy depends on NSAID toxicity pharmacological characteristics such as the bioavailability half-life and the capacity to block COX-1 and COX-2 (Crofford, 2013). With the rising usage of COX-2 inhibitors, such as DS studies have discovered that COX-2 selective drugs may correlate with an increased risk of cardiovascular diseases (A. M. Olsen, et al., 2012).

However, the side effects of NSAIDs were concluded into cardiovascular mortality, myocardial infarction, stroke, and heart failure. Renal failure, papillary necrosis, acute interstitial nephritis, weight gain, oedema, Type IV hypertension, renal tubular acidosis, hyperkalemia, and accelerated chronic kidney disease (Peterson,et al., 2006). Dyspepsia of the stomach esophagitis complications from gastroduodenal ulcers (bleeding, perforation, blockage), Colitis and small bowel erosions and strictures Hepatic higher transaminases (Bresalier, et al., 2005). Asthma/allergic pulmonary illness (in subjected individuals) made worse by aspirin and hematologic cytopenia. convulsions, aseptic meningitis, disorientation, fatigue, and nervous dizziness. delayed bone healing (Jain et al., 2009).

Table 2.1. Shared toxicities of NSAIDs (Crofford, 2013)

Organ	The adverse effects
Cardiovascular	heart failure, myocardial infarction, stroke, and cardiovascular death.
Renal	sodium retention, weight gain, edema, hypertension type iv, renal tubular acidosis, hyperkalemia, acute renal failure, papillary necrosis, interstitial nephritis, and accelerated chronic kidney disease.
Gastrointestinal	dyspepsia esophagitis gastroduodenal ulcer complications (bleeding, perforation obstruction), small bowel erosions and stricture,s colitis
Hepatic	elevated transaminases.
Asthma/Allergic	aspirin-exacerbated respiratory disease and rash
Hematologic	cytopenia.
Nervous	dizziness, confusion, drowsiness, seizures, and aseptic meningitis.
Bone	delayed healing

2.1.5. The Effects of DS on the (CVS)

In up to three-year clinical trials, some COX-2 selective and nonselective NSAIDs have been associated with an increased risk of serious cardiovascular (CVS) thrombotic events, such as myocardial infarction (MI) and stroke, which are possibly potentially fatal (Bresalier,et al., 2005; Solomon, et al., 2005). Regarding the presently available information, it is unknown whether the risk of CV thrombotic events is the same for all NSAIDs. The apparent increase in major CVS thrombotic events caused

by NSAID usage appears to be equivalent among those with and without developed CVS disease or CVS risk (Schmidt, Sorensen and Pedersen, 2018). Patients with previous episodes of CVS diseases or vulnerability factors had a greater probability of harmful CVS thrombotic events due to their higher background incidence (Connolly, et al., 2018).

Numerous observational studies reported that the increased risk of serious CVS thrombotic events began as early as the first weeks of medication. Higher dosages frequently cause an increase in CVS thrombotic risk (Bombardier, et al., 2000). The impairment caused by diminishing COX-2-mediated prostacyclin synthesis while not lowering COX-1-mediated thromboxane production may increase the risk of CVS events (Graham, 2006). There is no reliable data to support the idea that taking an aspirin reduces the risk of significant CVS thrombotic events, stroke or CV mortality (Bartolucci and Howard, 2006).

Another observational study performed in the Danish National Registry revealed that patients using NSAIDs after a MI interval had a higher risk of reinfarction, CVS-related death, and all-cause mortality commencing in the first week of treatment (Schmidt,et al., 2018). NSAID-treated patients had a mortality incidence of 20 per 100 person-years in the first year following MI, as opposed to 12 per 100 in non-NSAID exposed individuals in the same group. The increased relative risk of mortality among NSAID users continued for at least the next four years of follow-up, even though the death rate decreased after the first year post-MI (A.-M. S. Olsen, et al., 2012). Also, it has been demonstrated that NSAIDs, particularly when COX-2 inhibitors are administered, might increase blood pressure and lead to congestive heart failure in susceptible individuals (Antman,et al., 2007). The use of DS could raise cardiovascular risk due to COX-2 selectivity, which results in the blocking of (PGI2), the antithrombotic hormone prostacyclin, and the (A2) proaggregatory and (TXA2) vasoconstrictor thromboxane. PGI2 plays an essential function in CVS by regulating endothelial cell homeostasis (A. Fanelli, D. Ghisi, P. L. Aprile and F. Lapi, 2017). Rofecoxib is a potent, selective COX-2 inhibitor that lasts in the tissue for a more extended period. Unfortunately, due to the high incidence of the risk of myocardial infarction and stroke, rofecoxib's usage restricted and was eventually removed from the market (Baron, et al., 2008)

2.2. Gum Arabic (GA)

Acacia Senegal or Acacia Seyal trees, are members of the Leguminosae family, release a substance known as Gum Arabic (GA), which is a mixture of glycoproteins and polysaccharides (Dauqan and Abdullah, 2013). Sudan is valued as a cash crop (Figure 2.3). GA in the cosmetics, culinary, and the pharmaceutical industry sectors, it is regularly used as an emulsifier and stabilizer (Lelon, Jumba, Keter, Chemuku and Oduor, 2010). Adenine-induced chronic renal failure (CRF) in rats has been shown to be improved by GA therapy, according to an experimental investigation (B. H. Ali,et al., 2011; E. H. Ali and Arafa, 2011).



Figure 2.3. Gum Arabic (dry exudates particles)

2.2.1. Chemical Components of the GA

GA is a complex polysaccharide with a branched chain that is neutral or slightly acidic (Andersen et al., 2016; Anderson and Stoddart, 1966). Calcium, magnesium, and potassium salts make up its composition. 1,3-linked -D-galactopyranosyl units form the main chain. Two to five 1,3-linked -D-galactopyranosyl units make up the side chains, which are 1,6-linked to the main strand. Units of 4-O-methyl-D-glucuronopyranosyl and 4-O-arabinofuranosyl, as well as L-rhamnopyranosyl, D-

glucuronopyranosyl, and 4-O-arabinofuranosyl, are found in both the compositional main and side chains (Islam, Phillips, Sljivo, Snowden and Williams, 1997).

GA contains varying levels of galactose, arabinose, rhamnose, glucuronic acid, protein, nitrogen, and moisture (Idris, Williams and Phillips, 1998). Hydrophobic Interaction Chromatography has divided the components of GA into three major portions. According to (Weisskopf, 1988), the first fraction, arabinogalactan (AG), made up 88.4% of the total weight and had a low protein content (0.35%) and a molecular mass of 3.8X105 Da. The second portion, an arabinogalactan-protein complex (AGP), makes up 10.4% of the total weight, has a molecular mass of 1.45 106 Daltons, 11.8% of it is protein, and it comprises 11.8% of the weight. According to, (Idris,et al., 1998; Phillips and Williams, 2000), the third portion, glycoprotein (GP), accounts for 1.2% of the total gum. It has a molecular mass of 2.5 105 Da, a low molecular weight of 2.5 105 Da, and a protein content of 47.3%. The main amino acids in the AG and AGP proteins consist of hydroxyproline, serine, proline, and aspartic acid, while aspartic acid is abundant in GP (Islam et al., 1997).

2.2.2. Traditional Medicine Uses of GA

Traditional medicine uses GA for the treatment of chronic kidney disease (CKD) (B. H. Ali, Ziada and Blunden, 2009). Suliman and colleagues studied the impact of frequent GA ingestion on individuals with chronic renal failure (Suliman, Hamdouk and Elfaki, 2000). They concluded that these individuals' blood urea and serum creatinine levels decreased significantly (Al-Majed, Mostafa, Al-Rikabi and Al-Shabanah, 2002). They additionally noticed a decrease in the frequency of weekly dialysis sessions from three to two. Nevertheless, these results may require additional research to be widely accepted and confirm their validity, reliability, and efficiency level to verify their validity, reliability, and level of efficiency (Suliman,et al., 2000). Study reported on the use of GA's anti-inflammatory effects in folk medicine to treat dermatitis and gastrointestinal mucosa, respectively (Ayman M Gamal el-din, Adel M Mostafa, Othman A Al-Shabanah, Abdullah M Al-Bekairi and Mahmoud N Nagi, 2003). Numerous physiological and pharmacological studies use GA as a carrier and inert substance (A. A. Ali, Ali, Fadlalla and Khalid, 2008). Recently cited research that said GA includes antioxidants, nephron-protectors, and other therapeutic advantages (Rehman, Wingertzahn, Harper and Wapnir, 2001).

2.2.3. Antioxidant Properties of GA

According to the findings of a recent Sudanese study, GA has powerful anti-oxidative benefits in humans by enhancing total antioxidant capacity TAC and lowering oxidative stress indicators (L. Kaddam, et al., 2017). Furthermore, the antioxidant potency of GA has been experimentally demonstrated (Al-Majed,et al., 2002). Many studies have shown that GA protects against gentamicin, cisplatin nephrotoxicity, acetaminophen hepatotoxicity, and cisplatin nephrotoxicity, as well as acetaminophen hepatotoxicity and doxorubicin cardiotoxicity (Abd-Allah,et al., 2002; A. M. Gamal el-din, A. M. Mostafa, O. A. Al-Shabanah, A. M. Al-Bekairi and M. N. Nagi, 2003). The production of free radicals was the mechanism for the induction of these toxicities (Badreldin H Ali and Al Moundhri, 2006). The decreased glutathione (GSH), ascorbic acid (AA), and superoxide dismutase (SOD) levels in the animal's blood did not change significantly because of the administration of GA to the rats for eight days straight, according to Ali (B. H. Ali, 2004) (Al-Majed, Abd-Allah, Al-Rikabi, Al-Shabanah and Mostafa, 2003). This research provides no concrete proof that GA has strong antioxidant properties. There is an argument made by many Sudanese scientists that the GA can protect against nephrotoxicity, hepatotoxicity, and cardiotoxicity, respectively, are difficult to explain because GA is not a powerful antioxidant(Abd-Allah,et al., 2002; Al-Majed,et al., 2002; A. M. Gamal el-din,et al., 2003)

2.3. Anatomy of the Rat Heart

2.3.1. Background and Development

The heart, blood arteries, and lymphatics make up the rat's cardiovascular system, which is typical of most mammalian species (Scudamore, 2013). The heart is the first organ to develop in the embryo, which is derived from the cardiogenic mesoderm which differentiates into the endothelium and cardiomyocyte cells (Savolainen, Foley and Elmore, 2009). Primarily, the cardiomyocytes and endothelium forming tubes later split into four chambers (Savolainen,et al., 2009; Scudamore, 2013). All mammalian species share astonishing resemblances in their hearts. Given the widespread use of rats as a model for the phenotypes of cardiac disease, it is advantageous that the mouse heart shares many morphological

characteristics with the human heart, apart from how some venous vessels enter the atria (Wessels and Sedmera, 2003).

The mesothelium-lined pericardial sac surrounds the heart. In most routine sections, only the visceral pericardium, the mesothelial layer covering the outside of the heart, is visible. Typical mesothelial cells are squamous, fragile cells that arise from the mesoderm. They create a thin monolayer on top of a thin foundation membrane, which lines the body cavities and secretes lubricating fluid (Dullin, et al., 2017; Scudamore, 2013). Mesothelial cells prefer to transform into cuboidal when disturbed. Frond-like projections of fibrous connective tissue with a mesothelial coating can occasionally be observed in the pleura and pericardium observed in the pleura and pericardium on occasion (Dullin,et al., 2017). The epicardium comprises the mesothelial coating and a thin layer of connective tissue immediately beneath it, which also carries blood. The mesothelial covering and a thin layer of connective tissue underneath it, known as the epicardium, contain vascular supply and fat, especially near the base of the heart.

There is rich vasculature of blood visible between the cardiac fibres (Scudamore, 2013). The mouse's left and right aortic sinuses drain into the left and right ventricles with two coronary arteries, respectively. The myocardium contains these arteries predominantly. According to (B. Fernandez, et al., 2008), septal arteries that develop from either the left or right coronary arteries supply the interventricular septum. When interpreting potential phenotypic changes, it is essential to consider that the actual pattern of coronary arteries can vary quite a bit (B. Fernandez,et al., 2008).

The epicardium's main muscular mass lies underneath it. The trabeculae carnage lines the endocardial surface of the ventricles (Scudamore, 2013). The width of these trabeculae between the left and right ventricles appears to be the same, contrary to in humans (Wessels and Sedmera, 2003). Cardiomyocytes make up most of the myocardium which are cylindrical, branching fibres linked end to end to neighboring cells by intercalated discs (Borja Fernandez, et al., 2000). Adherence junctions and desmosomes, which aid in maintaining contact between nearby fibres during contraction, are present in the intercalated discs, while gap junctions facilitate the transmission of impulses between adjacent fibres (Li and Radice, 2010). One or two nuclei are in the central region of cardiomyocytes (Scudamore, 2013). Mouse hearts frequently have enlarged cardiomyocyte nuclei, especially in the

papillary muscle, which may be a sign of polyploidy or a reaction to damage (Keenan and Vidal, 2006). The myofiber's contractile protein arrangements are the culprit. The myofiber has a striated appearance due to a result of the contractile protein arrangements there in (Scudamore, 2013). Elliptical cross sections are most frequently observed due to the spiral arrangement of cardiac myocyte fibers around the heart, making it challenging to quantify the length of myofibers. Cross-sectional area measurements may be more repeatable for morphometry because cross-section width might also be challenging to measure consistently as well (Hort, 1971). Myocardium is a somewhat frequent spontaneous finding especially in certain mice strains (Scudamore, 2013). Males are more likely to develop it, it can start early in life, and it frequently impacts the right ventricle (Frith and Ward, 1988).

Another frequent spontaneous discovery in young mice is a condition known as "cardiomyopathy," which can appear in a variety of ways, including as tiny clusters of inflammatory cells (Torgersen, 1950). Comparing the prevalence and severity of these alterations with present controls or recent historical controls from the same strain kept in the same facility is crucial to determining their relevance. A rather common finding in elderly mice is atrial thrombosis, with notable strain-specific variations (Taylor, et al., 2011). The sinoatrial node, atrioventricular node, and bundles of His and Purkinje fibers make up the cardiac conduction system, which develops from the myocardial cells like in other species (Rentschler, et al., 2001; Wiese, et al., 2009). It is challenging to recognize these structures in tissues using H&E staining.

However, immunohistochemistry can identify connexin 45 in the cells (Rentschler et al., 2001). Connective tissue, which makes up the cardiac skeleton, supports the myocardial and valves. The fibrous skeleton generates annuli that keeps the lumen of the atrioventricular (AV) valve open. The fibrous tissue penetrates the AV valves, chordae tendinae, papillary muscle, and muscle at the heart's base, giving it a disordered look. That should not be confused with fibrosis or cardiomyopathy (Scudamore, 2013). In normal mice, islands of cartilaginous metaplasia can form in the cardiac skeleton near the base of the heart or in the aorta (Scudamore, 2013). Endothelium covers three structural layers of the heart valves (aortic, pulmonic, and atrioventricular). The ventricular layer is made up of elastic fibers and is the layer nearest to the blood flow. The core of the valve is the spongiosa, which is formed of collagen and proteoglycan. The fibrosa is the outermost layer made up of thick

collagen that gives structural rigidity and continues into the chordae tendinae, attaching the valve leaflet (Scudamore, 2013). Some mouse strains, such as C57Bl/6, have black melanin pigment in the valve leaflets, particularly the aortic valve. A calcium-specific stain such as Alizarin red can be used to separate the melanin pigment from the calcification of the valves (Hinton, et al., 2008). In regular H&E-stained sections, the pulmonic valve can display granular blue staining, which is considered a typical characteristic (Elwell and Mahler, 1999).

2.4. Stereology

The foundation of research is gathering quantitative data with statistical validity. The term "stereology" refers to several methods that, using mathematical and statistical tools, convert a two-dimensional image into a three-dimensional information (Kaplan, et al., 2011). William Thompson first proposed the idea of stereology in the 1930s. In 1961, Hans Elias introduced the word "stereology" at a scientific conference in Germany (Miki, et al., 2005). By introducing the director concept in 1984, Stero founded stereology as we know it presently. The director principle is a pro (H. J. Gundersen, et al., 1988) defined the optical disector as a probe in which the particles' shape, size, or orientation size, or orientation of the particles cannot affect the outcome of the estimation because of the three-dimensional designs of the probes owing to their mathematical basis. The fractionator is a sampling strategy that adopts a systematic random sampling approach to obtain accurate and unbiased results (Kaplan,et al., 2011). According to West, stereology is the most effective tool because it is the unbiased feature (the fractionator - as a sampling strategy) and independent from particle shape, size, or orientation (the optical disector - as a probe) (H. J. Gundersen and Jensen, 1987). When combined, these two characteristics result in the optical fractionator. These methods can yield data on volume, surface area, or particle quantity (Yurt, et al., 2018)

2.5. Objectives

2.5.1. General Objective

This study aims to investigate the protective role of GA in healing Heart tissue damage induced by DS in adult Wistar rats by means of stereological, light microscopic techniques, as well as biochemical analysis.

2.5.2. Special Objectives

In addition, it aims to compare the results obtained by stereological analysis with those obtained by light microscopy.

2.6. Justification

Traditional herbal therapy has been utilized for eons by rural and primitive people around the globe to treat a wide range of illnesses dates to 5000 years ago (Cornelsen,et al., 2015). More than eighty percent of the population in developing nations uses traditional herbal medicine for primary healthcare according to the World Health Organization (WHO). To close the equity gap in public health, the WHO encouraged collaboration between traditional and modern herbal medicine in a 2008 statement. The WHO also emphasized the importance of research to advance the development of traditional herbal medicine to provide appropriate, dependable, and effective treatments (Anderson and Eastwood, 1989).

Diclofenac is one of the most common medications used worldwide; diclofenac is one of the most common NSAIDs used, yet. In contrast, NSAID usage has been associated by expensive and adverse harmful effects on the cardiovascular and renal systems (Pountos,et al., 2011). For example, NSAID use has been associated with increased risk for hospitalization due to MI as well as heart failure (HF). According to recent data from the Agency for Healthcare Research and Quality, the average hospitalizations for acute MI and congestive HF cost $18,500 and $10,500, respectively (Fine, 2013).

The heart tissues were chosen for this study because, firstly, cardiac symptoms usually bring patients urgently seeking medical advice. Secondly, symptomatology of the heart could be a heavy psychological burden affecting life directly. Thirdly, treatment to heart may result without irreversible damage with high risk of death.

3. MATERIALS AND METHODS

3.1. Experimental Animals

For this experiment, forty 12-week-old Wistar albino male rats weighing 280-300g were used. The experimental animals were obtained from Ondokuz Mayis University's Experimental Animal Research Center and Surgical Applications in Samsun, Turkey. The study was carried out with the agreement of the Ondokuz Mayis University's Local Ethical Committee (approval number 2015/40). All experimental activities were carried out in accordance with the protocol. The rats were housed in cages made of stainless steel. During the experiment, the rats were kept in the animal house on a 12h light/12h dark cycle at room temperature (22±2 °C) with humidity between 40 and 50%. The rats had free access to food and water, were kept in typical laboratory settings, and were fed with standard feed (Figure 3.1).



Figure 3.1. Housing conditions of the animal

3.1.1. Formation of Experimental Animal Groups

Rats were classified randomly into four groups (10 rats per group), and all the experimental procedures were done blindly; the researcher had no clue about the animal's allocation to groups, all animals were coded, and the transcription of the codes was kept until the experiments and the stereological procedures were done.

Control group (CON): This group was not subjected to administering any substances.

Diclofenac Sodium group (DS): This group was received 3.6 mg/kg/day of DS by oral gavage (Voltaren from Novartis Health, Food and Agricultural Products Industry and Trade Inc. Kurtköy - Pendik, Istanbul, Turkey).

Gum Arabic group (GA): This group was subjected to 7.5 g/kg/day of GA by oral gavage (Gum Arabic Company, Khartoum, Sudan).

Gum Arabic + Diclofenac Sodium (GA+DS): This group was subjected to both 3.6 mg/kg/day of DS by oral gavage (Voltaren, Novartis) and 7.5 g/kg/day of GA by oral gavage (Gum Arabic Company, Khartoum, Sudan). All animals were coded using numbers; thus, all analyses were performed blindly for the experimental group to which any rat belonged.



Figure 3.2. Wistar albino rats in a cage

3.2. Materials

3.2.1. Diclofenac Sodium

Tabs (Voltaren from Novartis Health, Food and Agricultural Products Industry and Trade Inc. Kurtköy - Pendik, Istanbul), dose: 3.6 mg/kg/day, given orally every day for 15 days. An study determined the lethal dosage (LD) for DS to be 90 mg/kg (Hirose, et al., 1984). We used the recommended dose (3.6 mg/kg).

3.2.2. Gum Arabic

Powder from Khartoum, Sudan's GA Company. 7.5 g/kg/day taken orally by gavage once a day for 15 days.

3.3. Histological Procedures and Tissue Preparation

The experimental components of the investigation, including histological and stereological examination, were carried out at the faculty of medicine, Ondokuz Mayis University, Samsun, Turkey

3.3.1. Perfusion

Before perfusion, the animals were weighed. The rats weigh between 280-300 g on average. All rats received Intraperitoneal of 5 mg/kg ketamine and 2 mg/kg xylazine (bio®, Bayer, Istanbul, Turkey) for general anesthesia at the end of the experiment (Fish, Danneman, Brown and Karas, 2011). Following general anesthesia, heart perfusion was carried out using a normal saline solution and a 10% formalin solution. One day before the experiment was performed, all used solutions and supplies for perfusion were prepared; the solutions were maintained at room temperature.

The rats were placed on the operating table with their backs facing the operating table, and the chest was opened with a pair of scissors and a scalpel from the bottom of the diaphragm to the top of the chest to reveal the heat. A plastic cannula was inserted into the left ventricle's apex while the heart was beating to accomplish tissue perfusion. The scalpel was used in conjunction with this surgery to make a tiny incision in the right atrium to guarantee that the solution could flow freely. As a result of formalin fixation, tetanic contractions were seen in the rat limbs during perfusion. During perfusion, the rats in our study displayed erratic contractions (the formalin dance). The heart was now completely exposed, making it simple to separate it from the great vessels by collecting it with scissors.

3.3.2. Routine Histological Tissue Processing

The heart was taken out, placed in a container made of plastic and filled with 10% formalin, and then left to soak in the fixation solution for two weeks. The fixative solution was changed throughout the fixation phase every three days. This perfusion approach's main goal was to minimize artifacts during fixation. The normal histology procedures entailed extracting each rat's heart from a 10% formalin fixative solution

and cleaning it for one night under running water. After the washing procedure, perform the tissue follow-up steps provided in (Table 3.1.) were done tory up the tissues and eliminate the alcohol. The Thermo Scientific TM Citadel 2000 Tissue Processor (Fisher Scientific UK Ltd Bishop Meadow Road Loughborough LE11 5RG) was used to process the tissue (Figure 3.3). The rats' hearts were inserted into paraffin wax at 60 degrees. After the heart's normal histopathology procedures, they are used to create tissue blocks for cutting that are embedded in paraffin wax.

Table 3.1. Time spent treating cardiac tissues processing procedures protocol



Figure 3.3. Automated dehydration

	PROCEDURE	TIME
1.	50% Alcohol	10 hours
2.	70% Alcohol	1 hour
3.	80% Alcohol	1hour
4.	96% Alcohol I	1 hour
5.	96% Alcohol II	1 hour
6.	100% Alcohol I	1 hour
7.	100% Alcohol II	1 hour
8.	100% Alcohol III	2 hours
9.	Xylene I	1 hour
10.	Xylene II	1 hour
11.	Paraffin I	1 hour
12.	Paraffin II	1 hour

3.3.3. Toluidine Blue Staining Process

Toluidine blue was used to stain the thin sections that were obtained. 2 g of sodium borate was dissolved in 100 ml of deionized water to create a 1% solution of toluidine blue stain. 1g of toluidine blue was then added, and the mixture was gently stirred until it was completely dissolved. After that, the solution was left at room temperature for two weeks in an opaque bottle. Using a plastic pipette, a drop of toluidine blue was applied to the heart's semithin sections and let to sit for 20 to 30 seconds. After that, the slide was submerged in a container of deionized water, and the process was repeated three to four times until the section was clear.

3.3.4. Sectioning Methods

Before acquiring the desired sections of heart tissues for this investigation, the approach for heart tissue sectioning was defined by completing a pilot study with two heart tissue blocks. After picking the initial segment at random, systematic random sampling (SRS) was used to choose selected portions for stereological examination using the physical disector approach. Sectioning continued until the entire heart was cut thoroughly, resulting in approximately 25 samples of 2 consecutive sampling portions for each heart. The 5 µm thick serial sections were cut horizontally from tissue blocks with a 1/40 section interval using disposable metal microtome blades (Type N35, Feather Company, Osaka, Japan) and a rotary microtome (Leica RM2245, Nussloch, Germany), paraffin slices of the tissue blocks were cut (Figure 3.4.).



Figure 3.4. A rotary microtome (Leica RM2125RT, Nussloch, Germany)

The sampled sections were gathered on slides that had 5% gelatin (the gelatin was dissolved in 100 cc of distilled water). The gelatin-added distilled water was heated to 45°C in the float bath (MH8517 Paraffin Section float Baths) to collect the sliced tissue. As a result, during the staining process, the sections stay firmly attached to the glass slide. Before beginning, the slides containing the sampled sections were placed in an oven set at 58° C for one night (Figure 3.5.). This process is known as deparaffinization. Before beginning the staining process, microscopic slices were taken from the tissue blocks. Following SRS, an average of 25 pairs of sections were obtained from each animal and stained with Hematoxylin and Eosin (H&E).



Figure 3.5. Laboratory drying oven

3.3.5. H&E Stain

The tissue sections were stained with H&E. The table below (Table 3.2.) contains a list of the dyes and solutions used to stain the sections. The period that dye permeated the sections was measured in pilot study. After that, all parts were treated using the same methodology based on the results of the pilot study. The effectiveness

of the H&E-stained slices was examined using a light microscope (Olympus, BX51, Japan).

Table 3.2. Tissue staining procedures protocol H&E staining procedure

	PROCEDURE	TIME
1.	Xylene I	30 minutes
2.	Xylene II	30 minutes
3.	Xylene III	30 minutes
4.	100% Alcohol	5 minutes
5.	96% Alcohol	5 minutes
6.	80% Alcohol	5 minutes
7.	70% Alcohol	5 minutes
8.	Wash	5 minutes
9.	Hematoxylin	8 minutes
10.	Wash	5 minutes
11.	Eosin	2 minutes
12.	70% Alcohol	dip twice
13.	80% Alcohol	dip twice
14.	96% Alcohol	dip twice
15.	100% Alcohol	1 minute
16.	Xylene	30 minutes

3.3.6. Masson Trichrome Stain

A single animal was chosen to represent each group in the few samples that were used for the triple stain. This stain is used to investigate the formation of collagen and fibrous tissue within heart tissue because of the damaging effects of diclofenac. The table below (Table 3.3.) contains a list of the dyes and solutions used to stain the sections. The same method was then used on all the targeted samples in accordance with the results of the pilot study.

Table 3.3. Tissue staining procedures protocol for Masson trichrome stain.

	PROCEDURE	TIME
1.	xylene i	30 minutes
2.	xylene ii	30 minutes
3.	xylene iii	30 minutes
4.	100% alcohol	5 minutes
5.	96% alcohol	5 minutes
6.	80% alcohol	5 minutes
7.	70% alcohol	5 minutes
8.	wash	5 minutes
9.	Wegret hematoxylin	10 minutes
10.	wash	5 minutes
11.	acid fuchsin solution	5 minutes
12.	wash	5 minutes
13.	phosphotungstic acid	10 minutes
14.	aniline blue	10 minutes
15.	wash	5 minutes
16.	70% alcohol	dip twice
17.	80% alcohol	dip twice
18.	96% alcohol	dip twice
19.	100% alcohol	1 minute
20.	xylene	1 minute
21.	xylene	30 minutes

3.3.7. Tissue Preparation for Ultra-Thin Sectioning Process.

For the toluidine blue stained samples one animal from each group was perfused "intra-cardiac perfusion" with 4 per cent glutaraldehyde + 4 per cent paraformaldehyde solutions through the left ventricle. The samples were then submerged in a glutaraldehyde solution containing 4% glutaraldehyde for several weeks. After that, the Milloning buffer was used to wash the segment samples. After washing with buffer, they were immersed in 1 per cent osmium tetroxide in the dark for 2 hours. The samples were. rewashed for 4x15 minutes with Milloning buffer, and the procedure was completed by dehydration.

The heart's tissue samples were blocked at 45°C in a silicone embedding mold. Every 30 minutes, the temperature was raised by five degrees Celsius until it reached 62 degrees Celsius. They were incubated for 48 hours at 62°C to ensure polymerization. Using a glass blade semithin sections of 500 nm thick and 70 nm thick were cut out. Toluidine blue stain was applied to all sections.

Table 3.4 Tissue embedding silicone mold procedures protocol.

	PROCEDURE	TIME
1.	50% Acetone	15 Minutes
2.	75% Acetone	15 Minutes
3.	95% Acetone	15 Minutes
4.	100% Acetone	20 Minutes
	SUBSEQUENTLY	
5.	Propylene Oxide	20 Minutes
6.	Propylene Oxide	20 Minutes
7.	50% of Propylene Oxide + 50% Araldite Mixture	1 Hour
8.	Araldite, 100%	1 Hour

3.4. Stereology

William Thompson described the fundamentals of stereology in the 1930s (Kaplan,et al., 2011). Hans Elias introduced the term "stereology" in 1961 during a scientific symposium in Germany (Miki,et al., 2005). Stereological processes work by providing quantitative and unbiased estimates from two-dimensional sections to obtain three-dimensional data. The concepts of these processes are used to obtain data that does not depart systematically from the true value (Schmitz, et al., 2014). Furthermore, getting the real number with a small margin of error in a short amount of time is feasible (B. Z. Altunkaynak, Onger, Altunkaynak, Ayranci and Canan, 2012).

The criteria of stereological procedures are based on systematic random sampling (SRS). To ensure that the samples are well represented, they are divided into similar intervals to give each sampling location an equal chance (Brown, 2017).

3.4.1. Stereological Analysis:

The physical dissector method of stereology, which is an unbiased stereological method of particle counting, was used to estimate the total number of the cardiomyocytes of the left ventricles to identify the numerical density of the cardiomyocyte in each ventricle after calculating the volumes of the left ventricles. To determine the ideal sectioning interval and the quantity of sampled sections, a pilot study was carried out. Numerous images of the sections were captured using a microscope camera (Olympus SC50, Olympus Soft Imaging Solutions GmbH, Münster, Germany) and a set of highly effective light microscopes (Olympus BX43F, Tokyo, Japan) connected to a desktop computer (Figure 3.6). It used Olympus CellSens Entry 1.14 imaging software. The interval between imaging of 1/2 was chosen for this study. ImageJ was used to count the countable dissector particles in selected images.

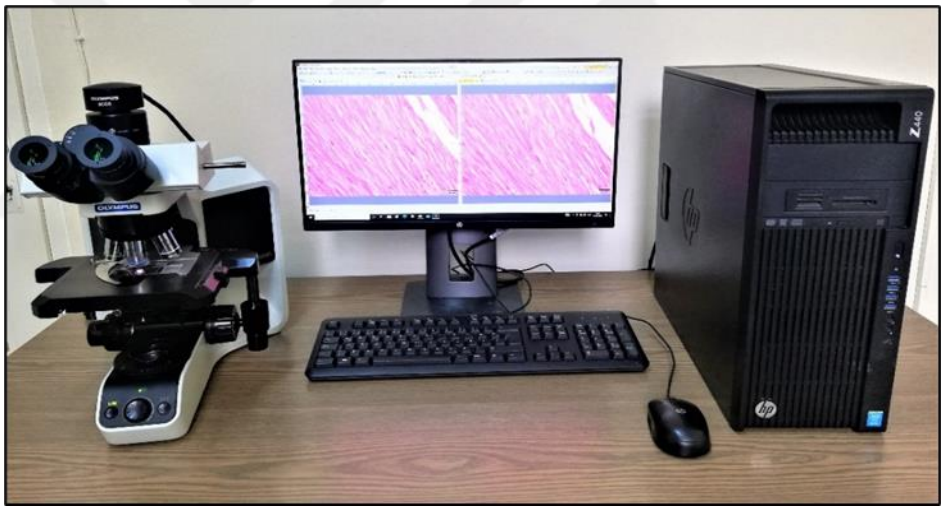


Figure 3.6. Stereological analysis system

3.4.1.1. The Total Number of The Cardiomyocytes.

Many paired photos at a magnification of x40 from two consecutive sections were taken using an Olympus SC50 microscope camera and an Olympus BX43F light microscope (both from Tokyo, Japan) connected to a desktop computer (Figure 3.6). For imaging, Olympus CellSens Entry 1.14 was employed. An unbiased counting frame and dissector counting technique are used to count the number of particles for each pair of images acquired from adjacent sections as a reference and look-up image. The inclusion line and the cardiomyocyte profiles were found to be overlaid inside the

counting frame (Figure 3.7). They were counted as extending so far as they did not touch any of the edges of the prohibited line.

Cardiomyocyte profiles (nuclei) that touched the inclusion line and the area inside the frame were tallied, but those that touched the exclusion (red) border, or its extensions were not. In the ImageJ application, the reference and look-up images are displayed and contrasted (Figure 3.8). Cardiomyocyte profiles that complied with all the unbiased counting frame rules listed in the reference part but not in the look-up section were counted, while those that did not were excluded (Muhlfeld, Nyengaard and Mayhew, 2010). The numerical density presented below was calculated using the disector particle number, the counting frame area, and the section thickness (Mouton, et al., 2017; Yurt, Kivrak,et al., 2018).

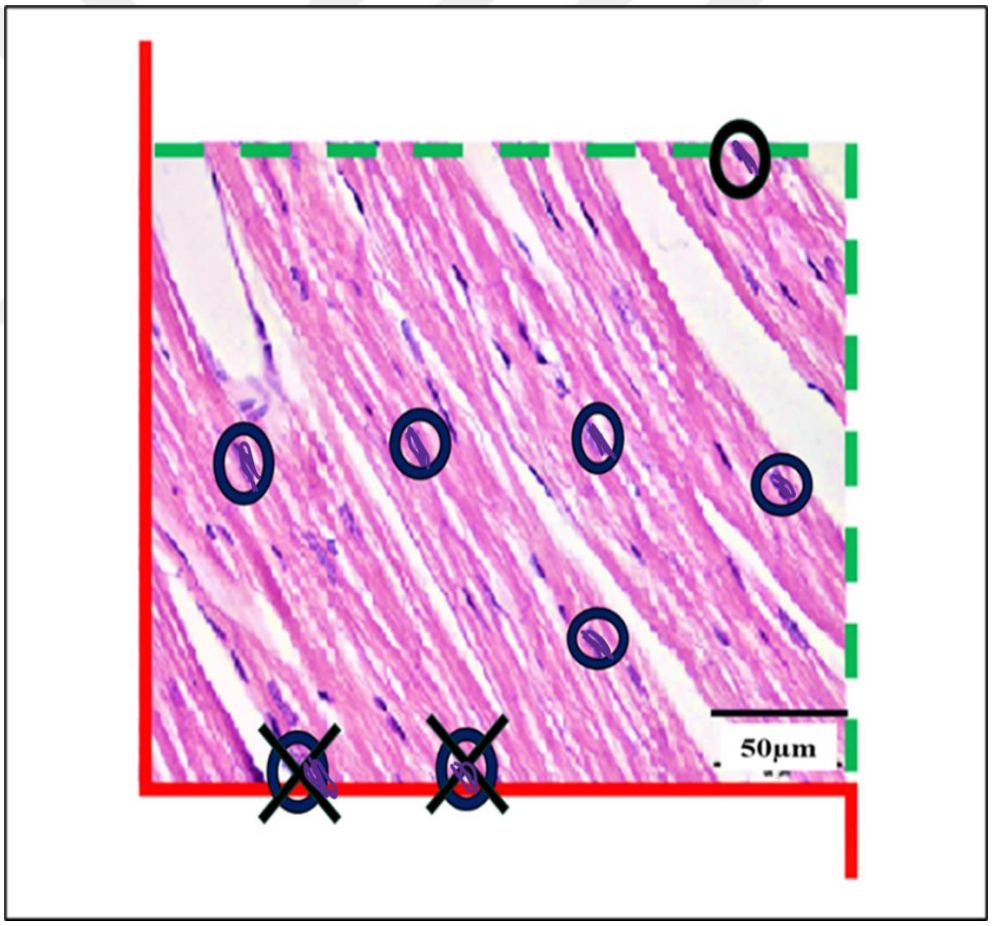


Figure 3.7. Unbiased counting frame

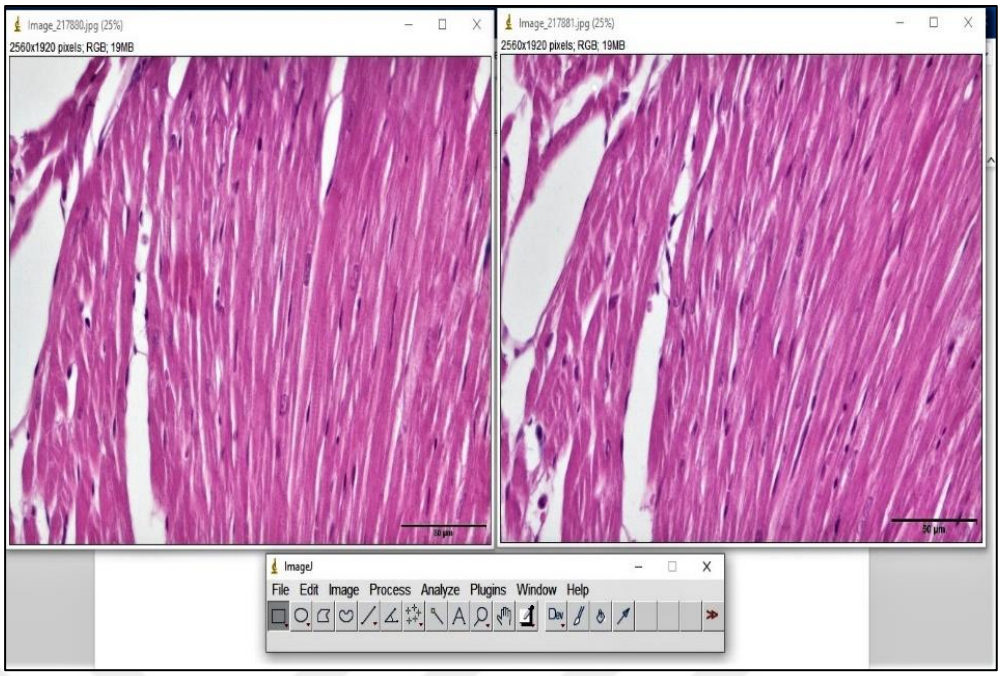


Figure 3.8. A pair of disector sections is seen in the ImageJ program

3.4.1.2. The Volume of the Left Ventricle

Cavalieri's principle was used to calculate the reference volume of each rat's left ventricle. Using the (closed polygon measurement) option in the same system's software, which lets us measure the left ventricle section area directly in μm^2, we estimated the overall size of the left ventricle for each rat from the sampled sections (Kaplan,et al., 2011). The left ventricle's reference volume (V_{ref}) can be accurately estimated by multiplying the total area of the sampled sections (A) by the distance between their areas (T) (Muhlfeld,et al., 2010; Yurt, Kivrak,et al., 2018).The sectioning interval multiplied by the section thickness equals the distance (T) (Ren and Wold, 2001). The formula below was used:

$$V_{ref} = \sum A \times T$$

3.4.1.3. The Estimation of The Total Number of The Cardiomyocytes

The total number of Cardiomyocytes (N) in the left ventricle of each rat was estimated using the physical disector by applying the following formula (West, 2012).

$$N = \sum Q \times (1/ssf) \times (1/asf)$$

$\sum$ Q: The total number of dissector particles (i.e., nucleoli of Cardiomyocytes)

ssf: The section-sampling fraction

asf: The area-sampling fraction

Step size = 2593846.154 μm^2

Counting frame size = 60066.67μm^2

Section sampling fraction was = 1/ (1/40) = 40

Area sampling fraction= 1/ (60066.67/2593846.154) = 43.18279

Total number of cardiac cells = Σ Q x (1/ (1/40)) x (1/ (60066.67/2593846.154))

3.4.1.4. The Coefficient of Variance and The Coefficient of Error

We calculated the coefficients of variance (CV) and error (CE) to make sure that our study had a suitable design precision. The CE denotes the degree of stereotypical estimation inaccuracy whereas the CV denotes group variability. Below are references to the CV and CE formulas that we used (H. J. G. Gundersen, Jensen, Kieu and Nielsen, 1999).

$$CV = \frac{\text{standard deviation}}{\text{mean}} = \frac{\sqrt{\frac{\sum(x - \bar{x})^2}{n - 1}}}{\bar{x}}$$

x: the number of cardiac cells in the individual animal; $\bar{x}$: the mean number of cardiac cells in each animal group; n: the number of animals in each group.

(Nv) for the estimate of the cardiac cells' numerical density was calculated as follows:

$A = \sum Q_i \,.\, Q_i$

$B = \sum Q_i . Q_{i+1}$

$C = \sum Q_i . Q_{i+2}$

$\text{Noise} = \sum Q$

$\text{Var}_{(srs)} = (3(\text{A-Noise}) - 4B + C)/240$

$\text{Total Var} = \text{Noise} + \text{Var}_{(srs)}$

$$CE_{(Nv)} = \frac{\sqrt{\text{Total Var}}}{\sum Q}$$

$\sum \mathbf{Q}$: the total number of disector cardiac cells counted in all sampled sections of each rat; $\mathbf{Q_i} \,.\, \mathbf{Q_i}$: the square of the disector cardiac cells in each section; $\mathbf{Q_i} . \mathbf{Q_{i+1}}$: the number of disector cardiac cells from each section (i) multiplied by the number of the disector cardiac cells from each section (i) multiplied by the number of the disector cardiac cells from the second next section (i+2) in the sequence.

$CE_{(V)}$ for the estimate of the total volume of the left ventricle was calculated as follows:

$$A = \sum A_i \,.\, A_i$$

$B = \sum A_i . A_{i+1}$

$C = \sum A_i . A_{i+2}$

$\text{Noise} = \sum 0.0724 \text{ x } 8 \text{ x } \sqrt{\sum A}$

$\text{Var}_{(srs)} = (3(\text{A-Noise}) - 4B + C)/240$

$\text{Total Var} = \text{Noise} + \text{Var}_{(srs)}$

$$CE_{(V)} = \frac{\sqrt{\text{Total Var}}}{\sum A}$$

$\sum \mathbf{A}$ is the sum area of all the left ventricle portions from each rat that were sampled; A(i). Ai is the area of each left ventricle section squared. Ai. A(i+1) is the area of each left ventricle section multiplied by the area of the next left ventricle section in the sequence. Ai. A(i+2) is the area of each left ventricle section squared. For CE and CV, the top limit is 0.05 and 0.10, respectively. Values that fall within these bounds show that the stereological design is adequately accurate.

3.4.1.5. The Estimation of The Numerical Density

$$Nv_{(myocyte)} = \sum Q_{(myocyte)}/t.\ A$$

Where $\sum \mathbf{Q}_{(myocyte)}$ is the total number of nuclei (dissector particles) counted in the reference section; t is the mean section thickness (5 um), and A is the area of the unbiased counting frame (H.-J. G. Gundersen, 1986; Kaplan,et al., 2011).

3.5. Biochemical Methods

Two days after the study ended, rats were perfused, and blood samples were taken from the heart. This delay had no impact on the level of antioxidant activity because diet supplementation with antioxidants keeps the antioxidants' activity high even after a week of ceasing the supplementation (Limberaki, Eleftheriou, Vagdatli, Kostoglou and Petrou, 2012).

Blood Sample Collection

During the perfusion and after the heart exposure, 3 ml of blood was collected from the rat's heart into blood collection tubes. Blood was collected and centrifuged at 4 °C on (HettichEB 20 centrifuge, Hettich, Tuttlingen, Germany) for 15 minutes at

2000 rpm before cycling perfusion solutions through the rats' circulatory systems (Figure 3.9). The samples of serum were stored at -80°C until biochemical analysis



Figure 3.9. Blood centrifuging machine

could be performed. The biochemistry department assessed absorbance values in serum samples to detect CAT and SOD enzyme activity.

3.5.1. Analysis of Superoxide Dismutase Enzyme Activity

Highly reactive radicals produced by enzymes such as xanthine oxidase and the mitochondrial electron chain are associated with the accumulation of superoxide anions (O2-) in cells and tissues in many diseases (Viggiano, Viggiano, Viggiano and De Luca, 2003). To protect against the damaging effects of oxygen in aerobic organisms, these molecules and other oxidant radicals shouldn't accumulate. When oxygen toxicity occurs in living tissues, the SOD-initiated enzymatic defense process catalyzes the dismutation of oxygen and metalloenzymes (Assady, Farahnak, Golestani and Esharghian, 2011). SOD enzyme activity was assessed in our study to evaluate OS using the SOD assay kit (Cayman Chemical Company, USA). The underlying idea behind the SOD assay kit is that the removal of superoxide radicals from the xanthine-xanthine oxidase reaction causes a reaction with tetrazolium compound and a purple reaction. The SOD in the sample neutralizes superoxide radicals in the medium and prevents the tetrazolium compound from reacting with

oxygen. Utilizing a microplate absorbance reader (Sunrise TM, Tecan Trading AG, Männedorf, Switzerland) at a wavelength of 450 nm, the absorbance values of the purple-colored liquids obtained after the experiment was calculated (Ukeda, Kawana, Maeda and Sawamura, 1999).



Figure 3.10. A microplate absorbance reader (Sunrise TM, TECAN)

3.5.2. Analysis of Catalase Enzyme Activity

CAT is an antioxidant enzyme that contributes to the detoxification of H_2O_2, which is a harmful byproduct of aerobic metabolism. Low levels of H_2O_2 improve the expression of stress-associated proteins and antioxidant enzymes, enabling the body to respond to oxidants. The CAT enzyme is responsible for converting the H_2O_2 molecule into oxygen and water. CAT has peroxidation activity, with low molecular weight alcohols acting as electron donors (Madeo, et al., 1999; Martins and English, 2014). Cayman's CAT Assay Kit (Cayman Chemical Company, USA) was used to determine enzyme activity in the serum to detect the oxidative effect. The method's core idea is based on the CAT enzyme reaction with methanol in the presence of H_2O_2. Formaldehyde serves as a chromogen in this reaction, giving it a pink color. After completing the required reactions, the samples' absorbance was assessed using a multi-

mode microplate reader (BioTek Synergy 4, BioTek Instruments Inc., Vermont, USA) at a wavelength of 540 nm (Figure 3.11).



Figure 3.11. A microplate absorbance reader (BioTek Synergy 4)

3.5.3. Total Phenolic Content and Antioxidant Power Determination

Sample Extract Preparation.

The current study employed ultrasound-assisted extraction with 80% methyl alcohol. 2.5 g of the material was combined with 50 mL of 80% methyl alcohol in an ultrasonic water bath for 30 minutes, followed by 2 hours at room temperature. It was centrifuged for 15 minutes at 3000 rpm to remove turbidity. The pre-analysis samples were filtered using a 0.45 Teflon filter.

3.5.4. Method to Assess the Total Phenolic Content

Singleton and Rossi (1965) 's method of determining the total phenolic content was modified (Singleton and Rossi, 1965). 2.5 ml of Folin-Ciocalteu was added onto 0.5 ml of sample diluted with the appropriate amount of methyl alcohol and left for 5 minutes in a dark place to add 7.5% sodium carbonate solution. At the end of the period, the total phenolic content was calculated by means of the standard calibration curve, which was read against the witness at 760 nm wavelength and plotted with pure gallic acid.

3.5.5. Methods to Assess The Antioxidant Power

3.5.5.1. Ferric Iron Reduction Antioxidant Power (FRAP)

The samples were diluted in the following ratios after being extracted with methyl alcohol: 10: 1: 1 (v: v: v) Acetate buffer 300 mM: 10 mM 2,4,6-tripyridyl-s-triazine (TPTZ) solution, dissolved in 40 mM HCl, was added to 20 mM FeCl3, and the absorbance at 593 nm was assessed using a spectrophotometer. Trolox-prepared solutions were used to generate a calibration curve, and the result was found. (Gao, Björk, Trajkovski and Uggla, 2000).

3.5.5.2. Determination of DPPH Free-Radical Scavenging Effect

The method described by Tural and Koca (2008) was used to assess the reducing power of the DPPH radical (2,2-diphenyl-1-picrylhydrazyl). To measure the absorbance at 517 nm, 50 L of the extract that included methyl alcohol has been added to 1 ml of DPPH solution and stored at room temperature (Tural and Koca, 2008).

3.6. Statistical Analysis

The evaluation of the numerical data of this study and the quantitative variables were provided in the form of mean ± standard deviation SD The GraphPad Prism® software program, version 9.5.1 was used for statistical analysis (GraphPad Prism 9.5.1 Software Inc., San Diego, CA, USA). The ordinary one – way ANOVA was used for analysis of the data. The data for the left ventricle volume and the total of cardiomyocytes number were compared between the groups by implementation of Tukey's multiple comparisons test to discover significant differences between the study groups. When the P-value was <0.05, the values were judged statistically significant (*), and when the P-value was ≤ 0.005, they were regarded as high significant (**).

4. RESULTS

This study was performed to investigate the possible effects of GA in healing of adverse effects of DS on rat heart tissue, and stereological, biochemical, and histopathological analyses were conducted.

4.1. Stereological Findings

The total number of cardiomyocytes of the left ventricle was calculated using the physical fractionator technique. The total volume of the left ventricle was estimated using Cavalieri's principle and calculated using the given equations in the methodology section. Those estimations were done for the study groups.

Table 4.1. Estimation of mean and SD of volume, total number, and numerıcal density of the left ventricle among all groups: CON, DS, GA, and GA+DS

Stereological Findings		Control	DS	GA	GA+DS
Total number	Mean x 10^7	3.03	2.70	3.36	3.02
	SD x 10^6	4.99	3.04	1.78	2.00
Volume	Mean (μm^3)	51704	50383	51626	50357
	SD (μm^3)	651.0	493.0	882.0	838.0
Numerical density	Mean (count/μm^3)	586.46	536.18	649.91	600.33
	SD (count/μm^3)	94.4	53.52	27.58	37.89

4.1.1. The Counted Particles of Cardiomyocytes of The Left Ventricle

The mean, SD, and the standard error of mean (SEM) of cardiomyocytes of the left ventricle and the coefficient of error (CE), coefficient of variation (CV) is shown in the following table and figures (Tables 4.2; Figures 4.1).

Table 4.2. The mean, SD, SEM, CE and CV of counted particles of cardiomyocytes of the left ventricle among all groups: CON, DS, GA, and GA+DS.

Group	Mean	SD	SEM	CE	CV%
CON	422.88	72.77	25.73	0.049	17.21%
DS	386.63	41.26	7.516	0.051	10.67%
GA	468.63	21.26	14.59	0.046	4.54%
GA+DS	432.88	29.21	10.33	0.048	6.75%

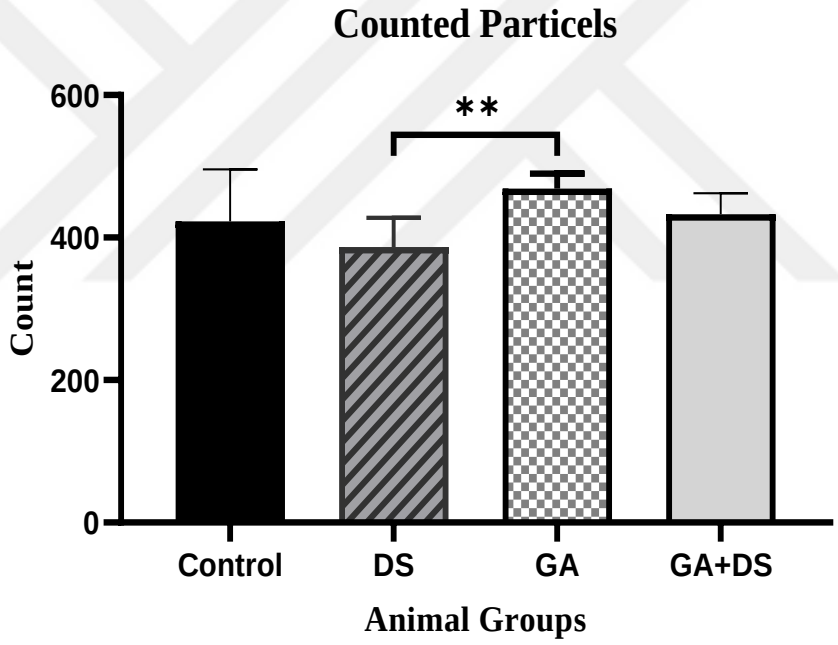


Figure 4.1. Indicates the significant differences between the groups in terms of the counted particles of the left ventricle.Very high significantly difference was observed between the GA and DS groups in terms of left ventricle counted particles ($p<0.01$)

4.1.2. The Total Volume of The Left Ventricle

The mean, SD, and SEM of the volumes of the left ventricle are shown in the following table and figures (Table 4.3; Figure 4.3).

Table 4.3. Estimation of mean, SD and SEM of volume of the left ventricle (µm³) among all groups: CON, DS, GA, and GA+DS

Group	Mean (µm³)	SD (µm³)	SEM (µm³)
CON	51704	651	230.1
DS	50383	493	174.3
GA	51626	882	311.8
GA+DS	50357	838	296.3

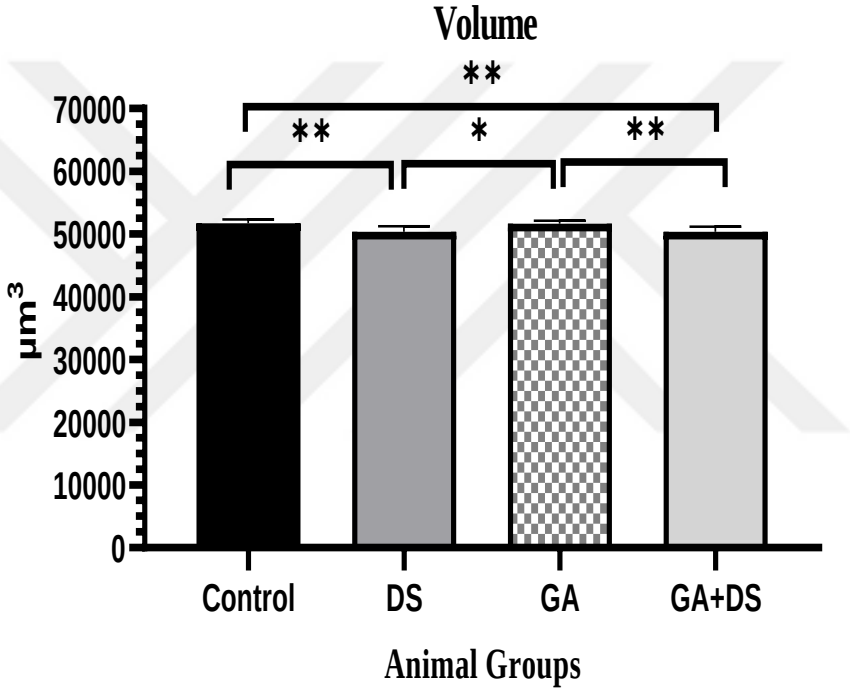


Figure 4.2. Indicates the differences between the groups regarding the volume of the left ventricle of the rat heart.The significant difference was found between the CON& GA+DS, CON&DS, GA& GA+DS and DS&GA groups in terms of left ventricle volume ($p<0.01$).

4.1.3. The Total Number of Cardiomyocytes in The left Ventricle

The mean, SD, and SEM of total number of cardiomyocytes of the left ventricle are shown in the following table and figures:

Table 4.4. The mean, SD and SEM of the total number of cardiomyocytes of the left ventricle among all groups: CON, DS, GA, and GA+DS

Group	Mean Total Number x 10^7	SD x 10^6	SEM
CON	3.03	4.99	1.76 x 10^6
DS	2.70	3.04	1.07x 10^6
GA	3.36	1.78	6.28x 10^5
GA+DS	3.02	2.00	7.07x 10^5

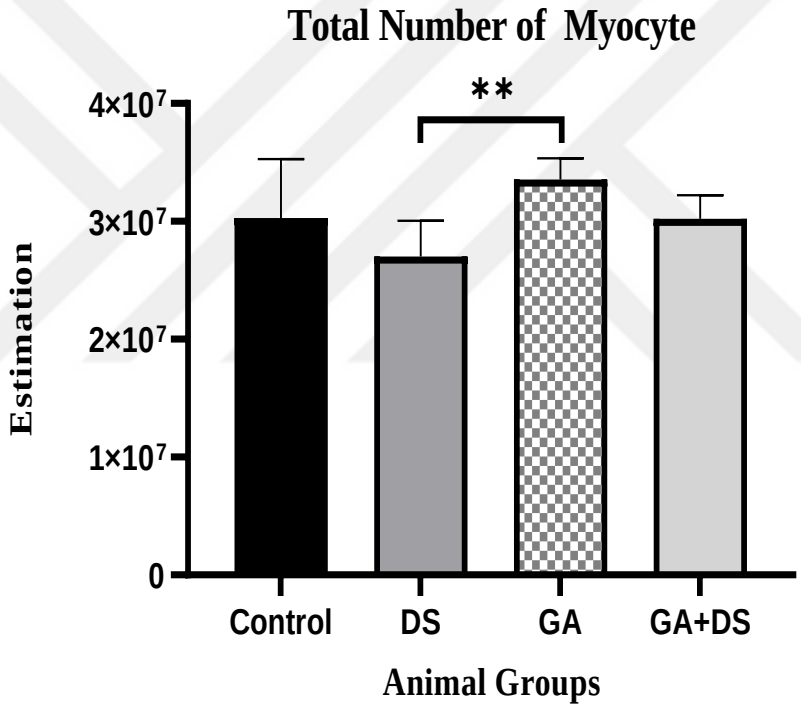


Figure 4.3. The graph shows the differences between the groups in terms of the total number of myocytes in the left ventricle of the rat heart. After a comparison was made between the total number of cardiomyocytes among all groups, there was significant difference between DS & GA groups ($p<0.01$).

4.1.4. The Numerical Density of Cardiomyocytes in The left Ventricle

The mean and SD of the numerical density of cardiomyocytes in the left ventricle volume are shown in the following table and figures:

Table 4.5. The mean and SD numerical density (count/μm^3) among all groups: CON, DS, GA, and GA+DS

Groups	Numerical Density (Mean ± SD) Count/μm^3
CON	586.46 ± 94.4
DS	536.18 ± 53.52
GA	649.91 ± 27.58
GA+DS	600.33 ± 37.89

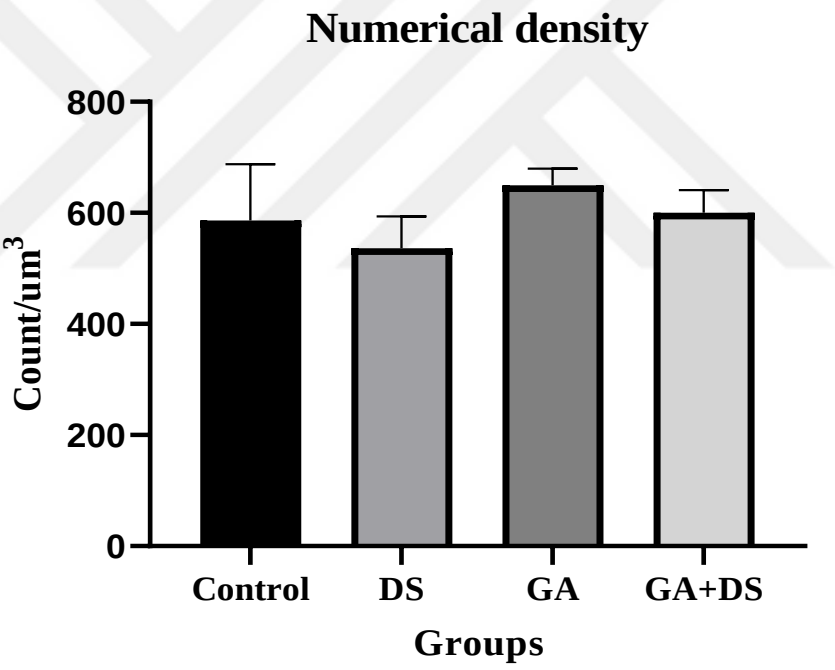


Figure 4.4. The graph shows the differences between the groups in terms of mean of the numerical density of cardiomyocytes in the left ventricle of the rat heart. After comparison was made between the groups the was no significant difference in the terms of mean of the numerical density of cardiomyocytes.

4.2. Analysis of Enzyme's Activities

4.2.1. Analysis of Catalase Enzyme Activity

Table 4.6. The mean and SEM of CAT enzyme activity nmol/min/ml 540 nm, among all groups: CON, DS, GA, and GA+DS.

Groups	Mean	SEM
CON	216.000	34.811
DS	245.370	18.610
GA	322.794	16.743
GA+ DS	279.866	41.281

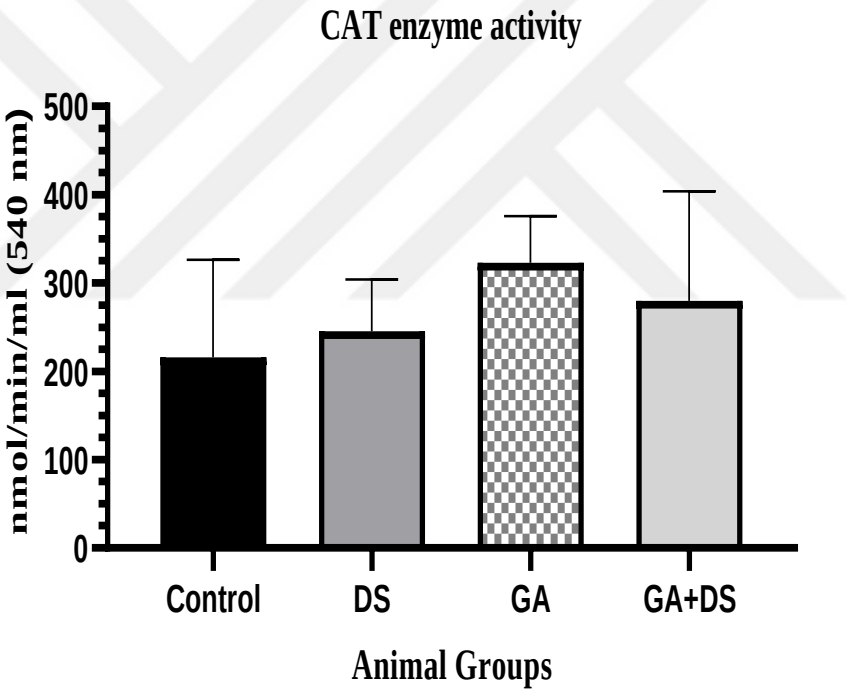


Figure 4.5. The mean and SEM of CAT enzyme activity nmol/min/ml 540 nm among all groups: CON, DS, GA, and GA+DS. As a result of the analysis of the enzyme's activities, statistical analysis of the data shows no significant difference

4.2.2. Analysis of Superoxide Dismutase Enzyme Activity

Table 4.7. The mean, the SEM of SOD enzyme activity U/ml450 nm, among all groups: CON, DS, GA, and GA+DS.

Groups	Mean	SEM
CON	27.2	0.275
DS	27.0	0.292
GA	26.6	0.407
GA+DS	26.8	0.483

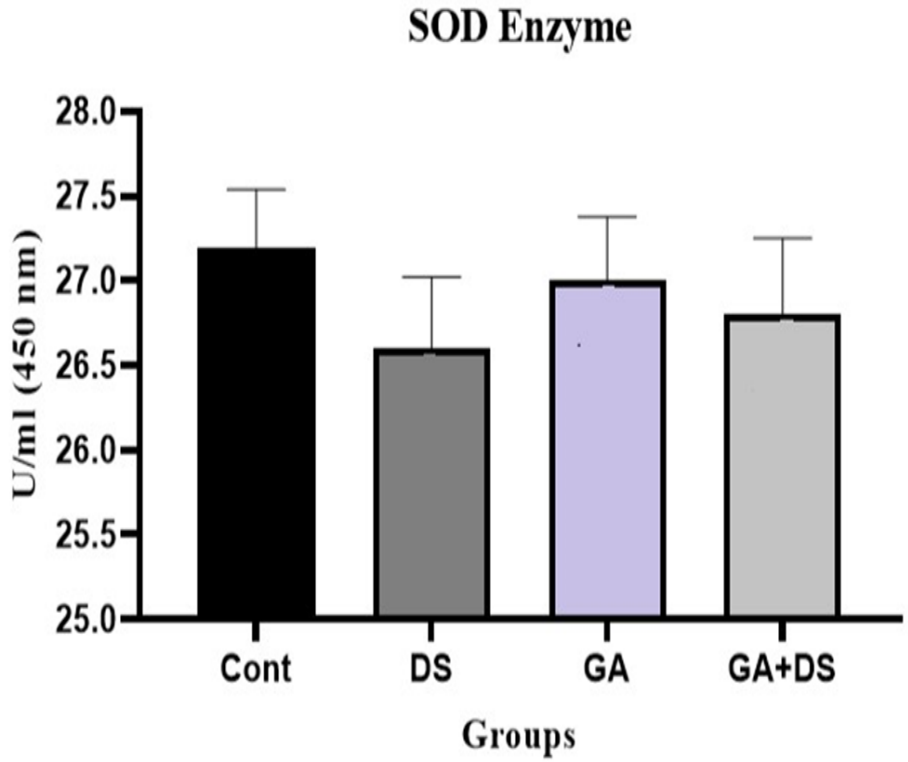


Figure 4.6. SOD enzyme activity (U/ml (450 nm)), among all groups: CON, DS, GA, and GA+DS. As a result of the analysis of the enzyme's activities, statistical analysis of the data shows no significant difference.

4.3. Light Microscopic Findings

4.3.1. Light Microscopic Findings of H&E-Stained Sections

Tissue sections were taken from the left ventricle of all experimental animals. These sections were stained with H&E left ventricle was examined by the light microscope (Figure 4.7 - 4.17).

4.3.1.1. H&E-Stained Sections: CON Group

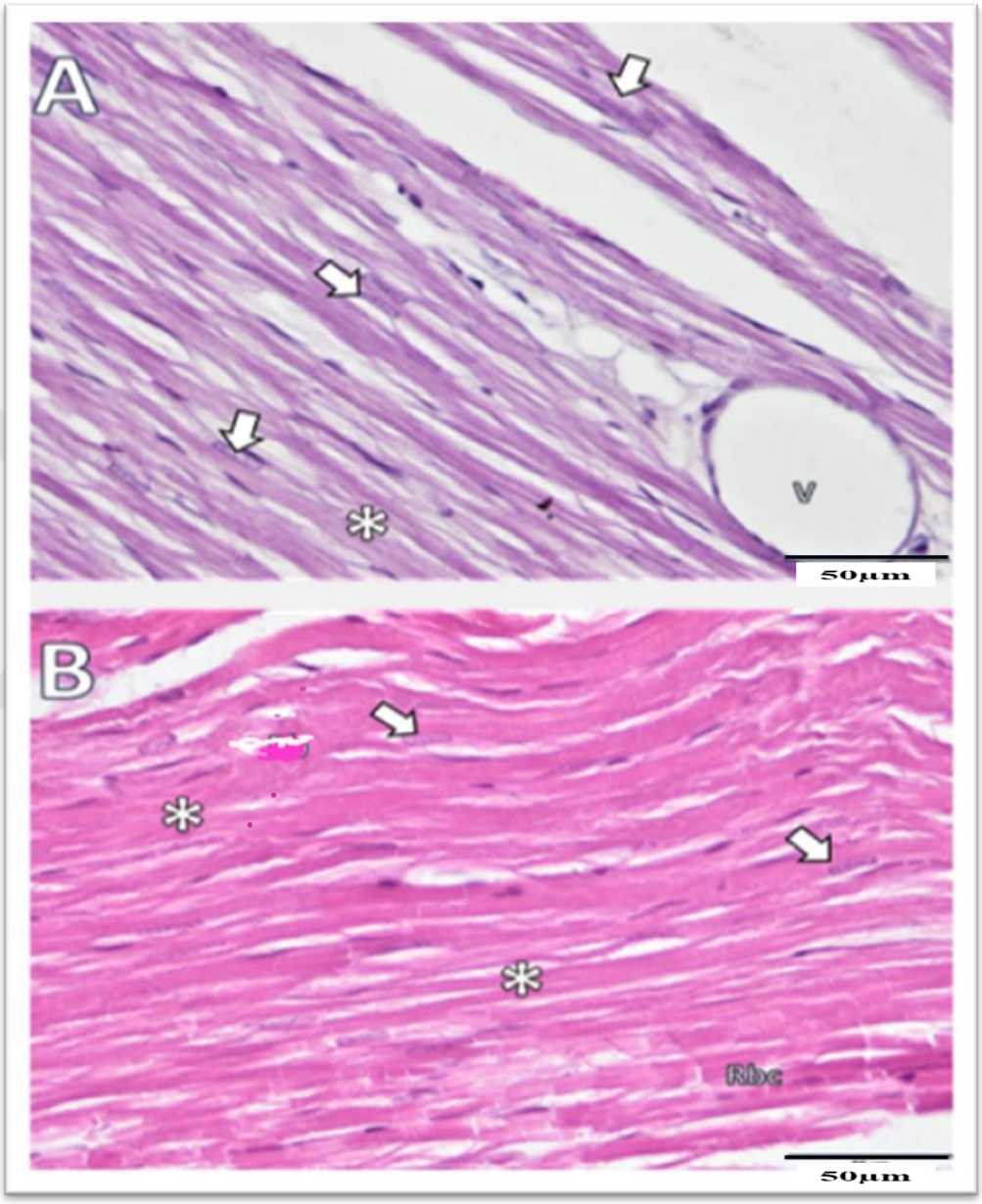


Figure 4.7. (A, B) Histological images of the left ventricle of CON stained with H&E staining are seen. The general structure of the heart tissue of the left ventricle is fine. The arrows indicate nucleus of the cardiac cell. (V) indicates the vessel. (Rbc) indicates the red blood cells. The star indicates the muscle fibres. Original magnification: X40

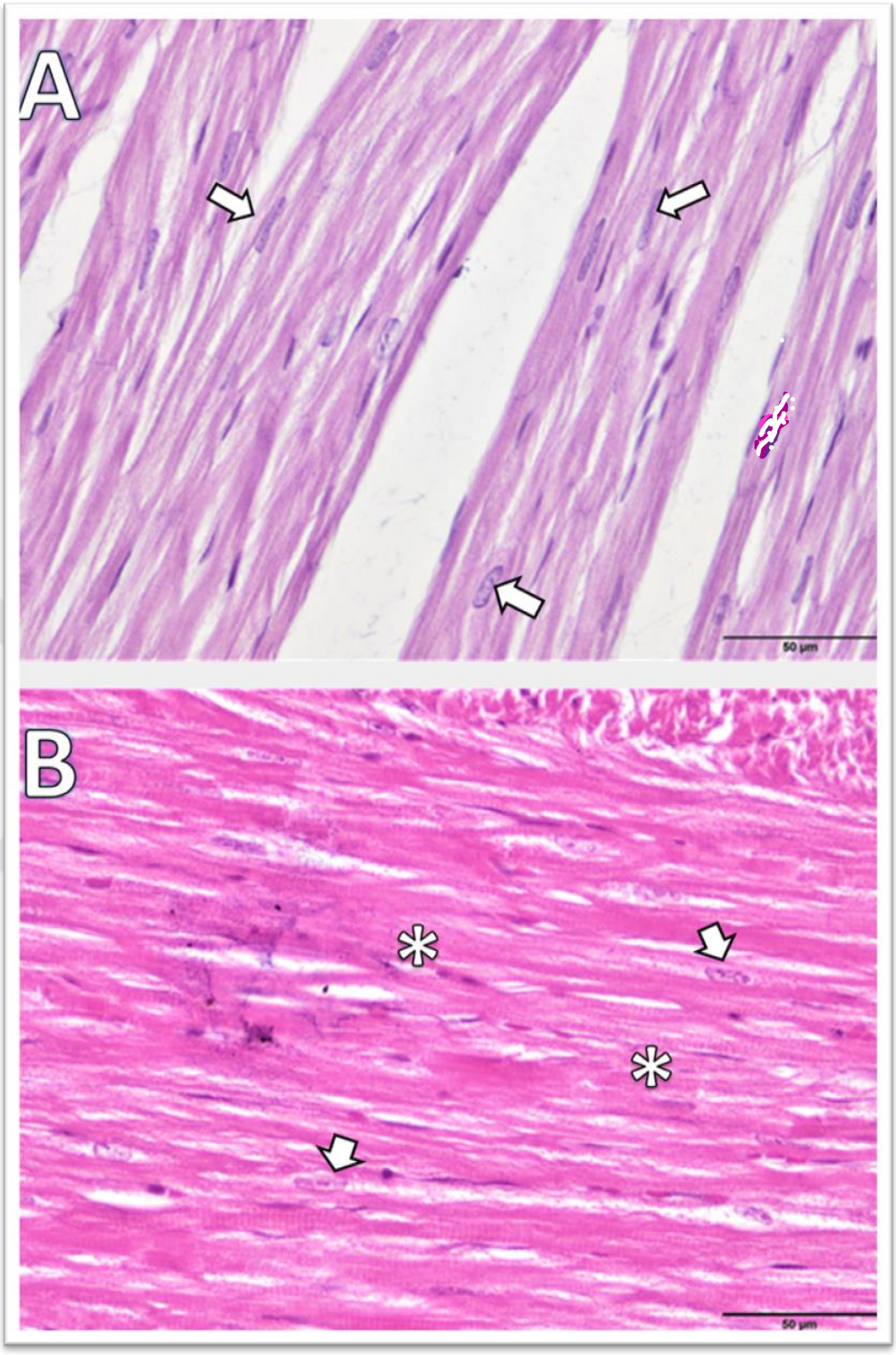


Figure 4.8. (A, B) Histological images of the left ventricle stained with H&E staining are seen. The general structure of the heart tissue of the left ventricle of CON is fine. The arrows indicate nucleus of the cardiac cell. (*) indicates the muscle fibres. Original magnification: X40

4.3.1.2. H&E-Stained Sections: DS Group

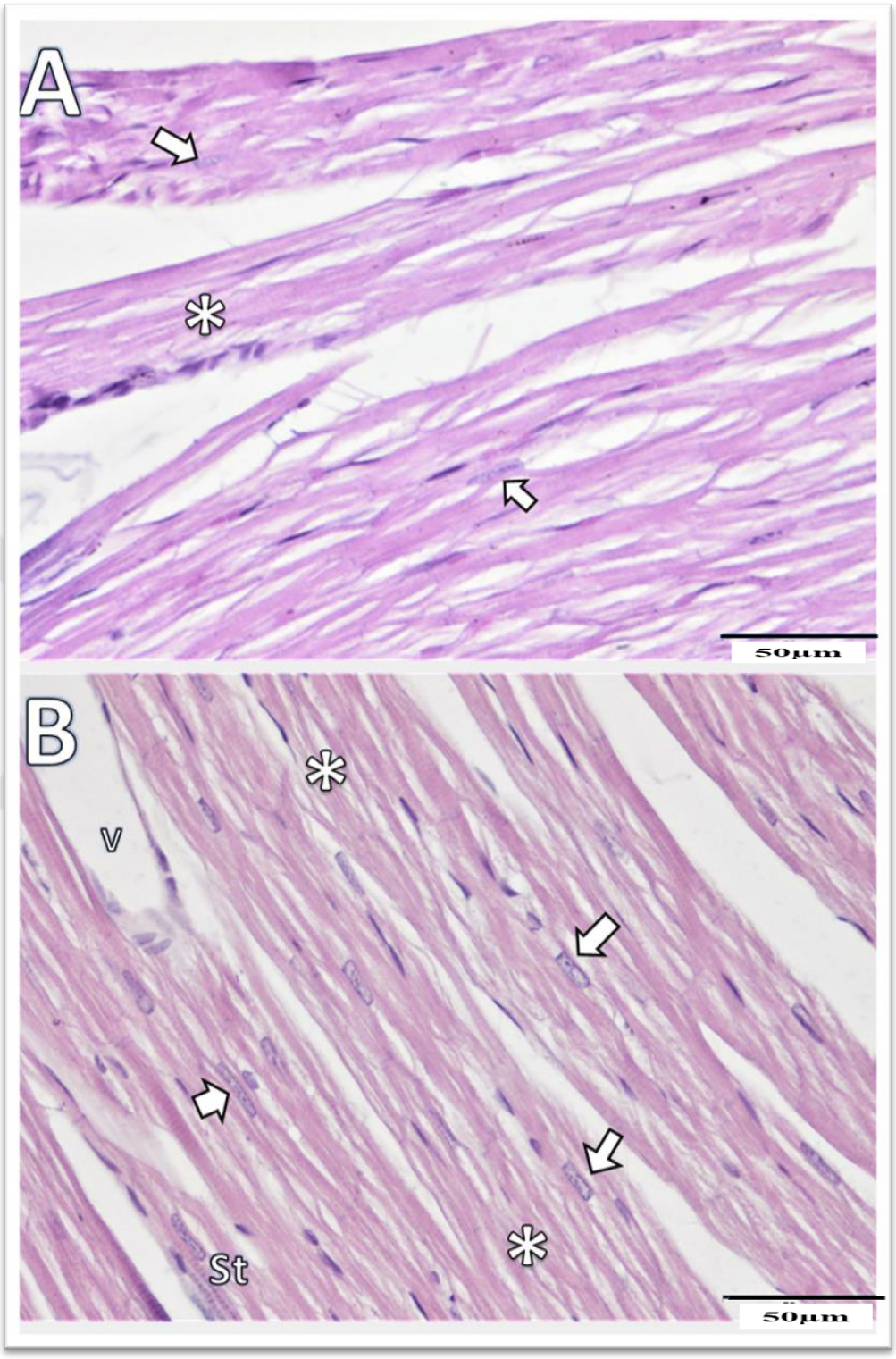


Figure 4.9. (A, B) Histological images of the left ventricle stained with H&E staining are seen of DS. The general structure of the heart tissue of the left ventricle is fine. The arrows indicate nucleus of the cardiac cell. (V) indicates the vessel. (St) indicate striation of the muscle fibres. (*) indicates the muscle fibres. Original magnification: X40

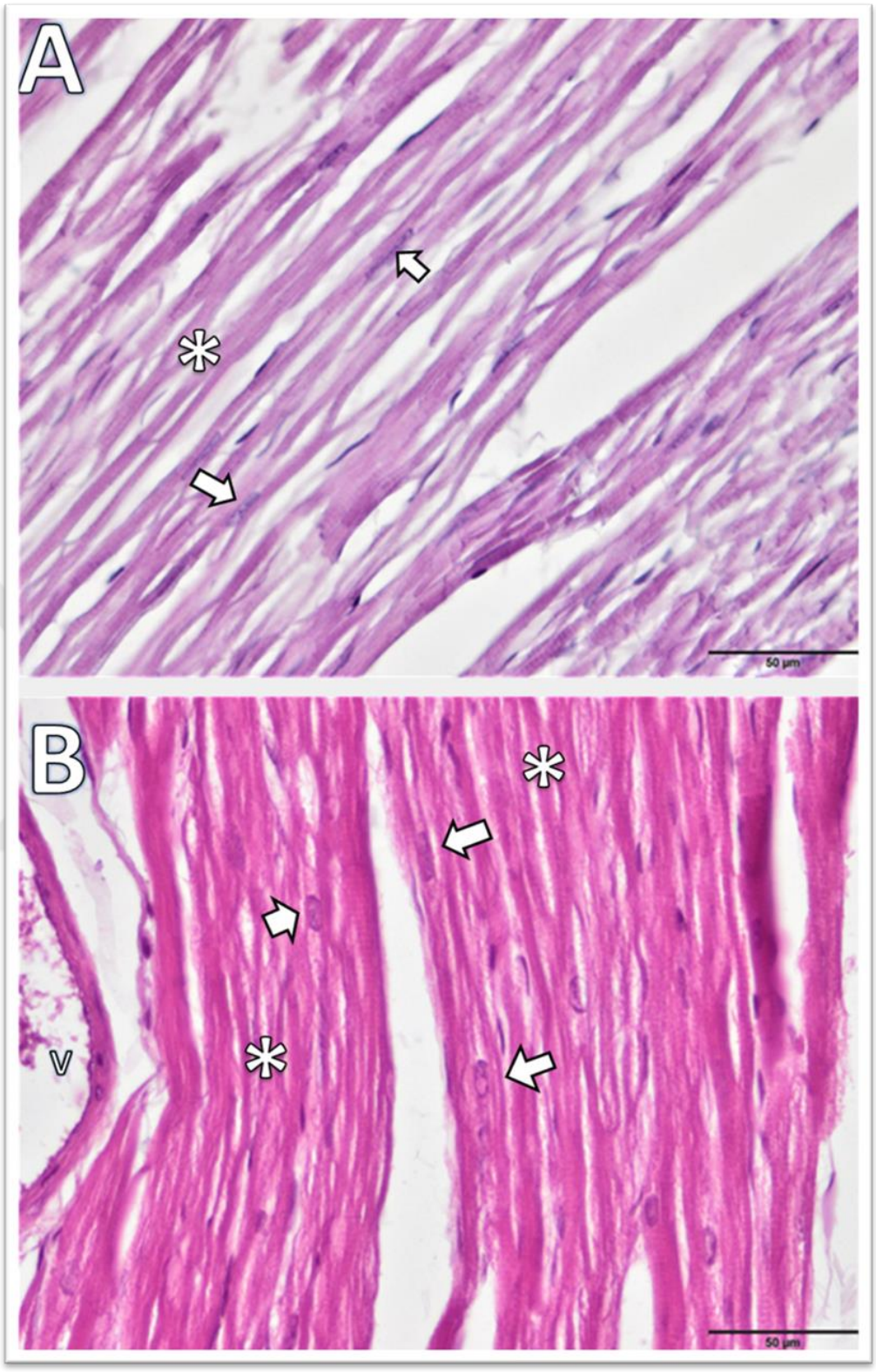


Figure 4.10. (A, B) Histological images of the left ventricle stained with H&E staining are seen. The general structure of the heart tissue of the left ventricle of DS is fine. The arrows indicate nucleus of the cardiac cell. (*) indicates the muscle fibres. Original magnification: X40

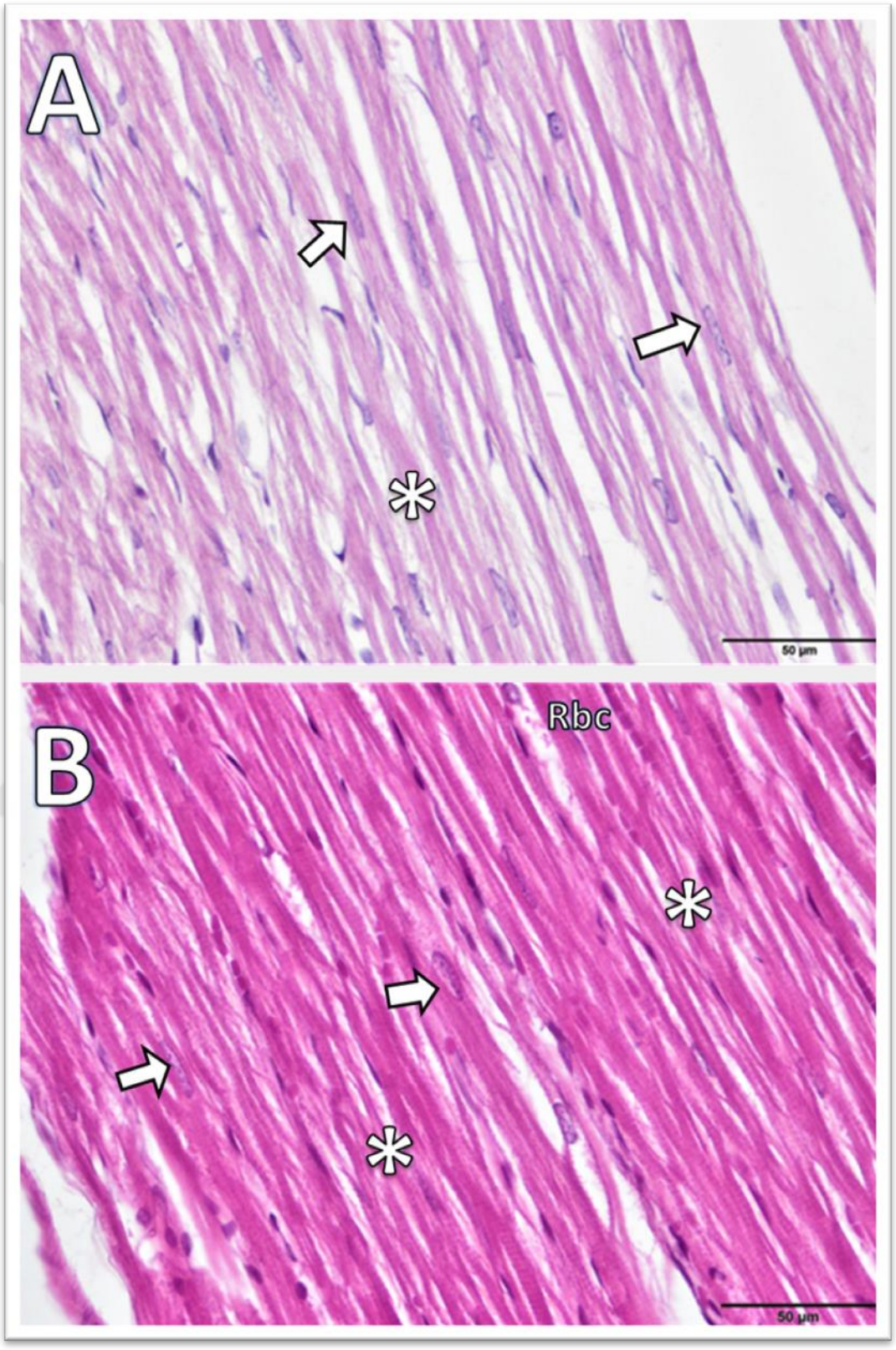


Figure 4.11. (A, B) Histological images of the left ventricle stained with H&E staining are seen. The general structure of the heart tissue of the left ventricle of DS is fine. The arrows indicate nucleus of the cardiac cell. (Rbc) indicates the red blood cells (*) indicates the muscle fibres. Original magnification: X40

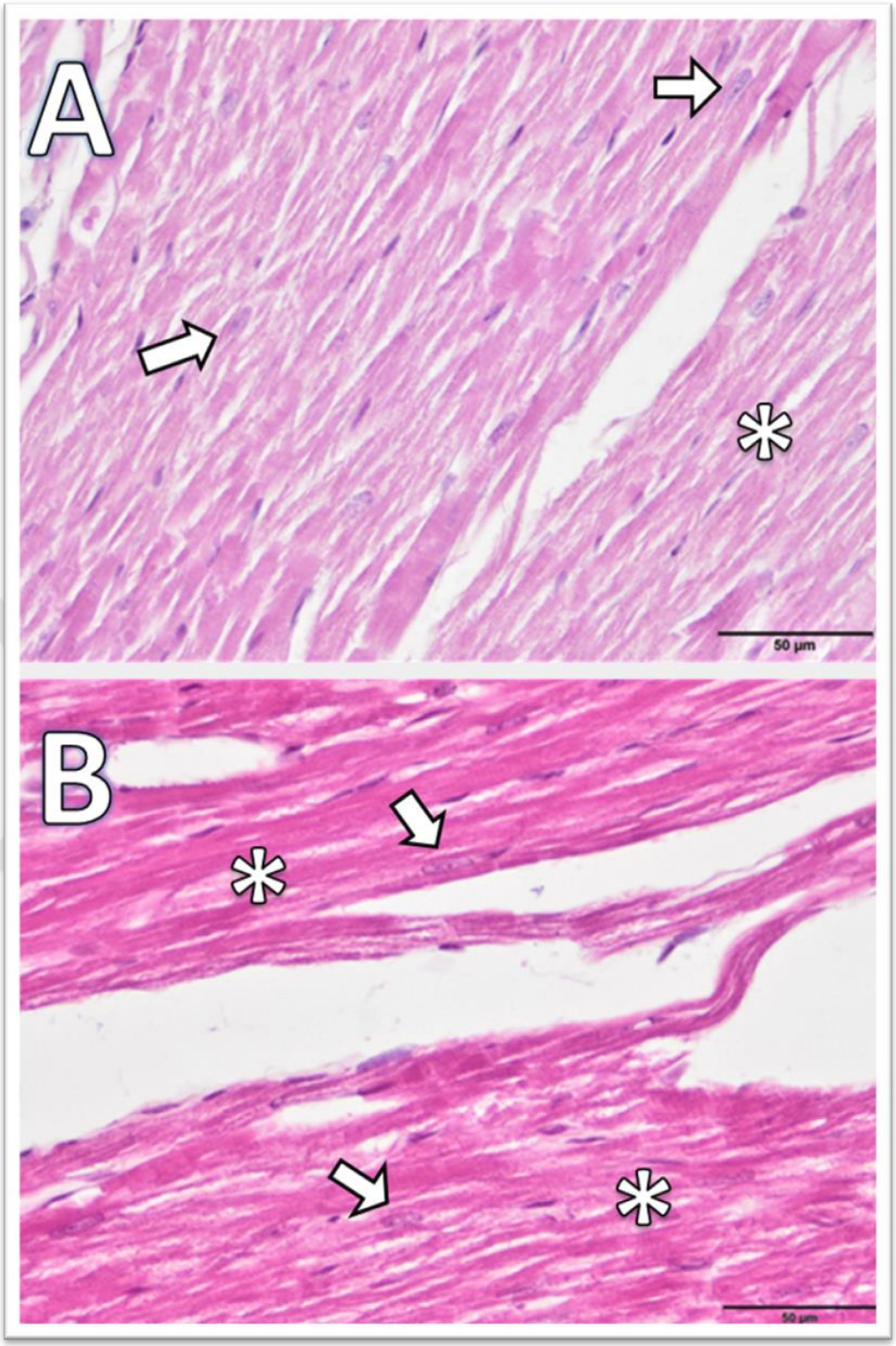


Figure 4.12. (A, B) Histological images of the left ventricle stained with H&E staining are seen. The general structure of the heart tissue of the left ventricle of DS is fine. The arrows indicate nucleus of the cardiac cell. (*) indicates the muscle fibres. Original magnification: X40

4.3.1.3. H&E-Stained Sections: GA Group

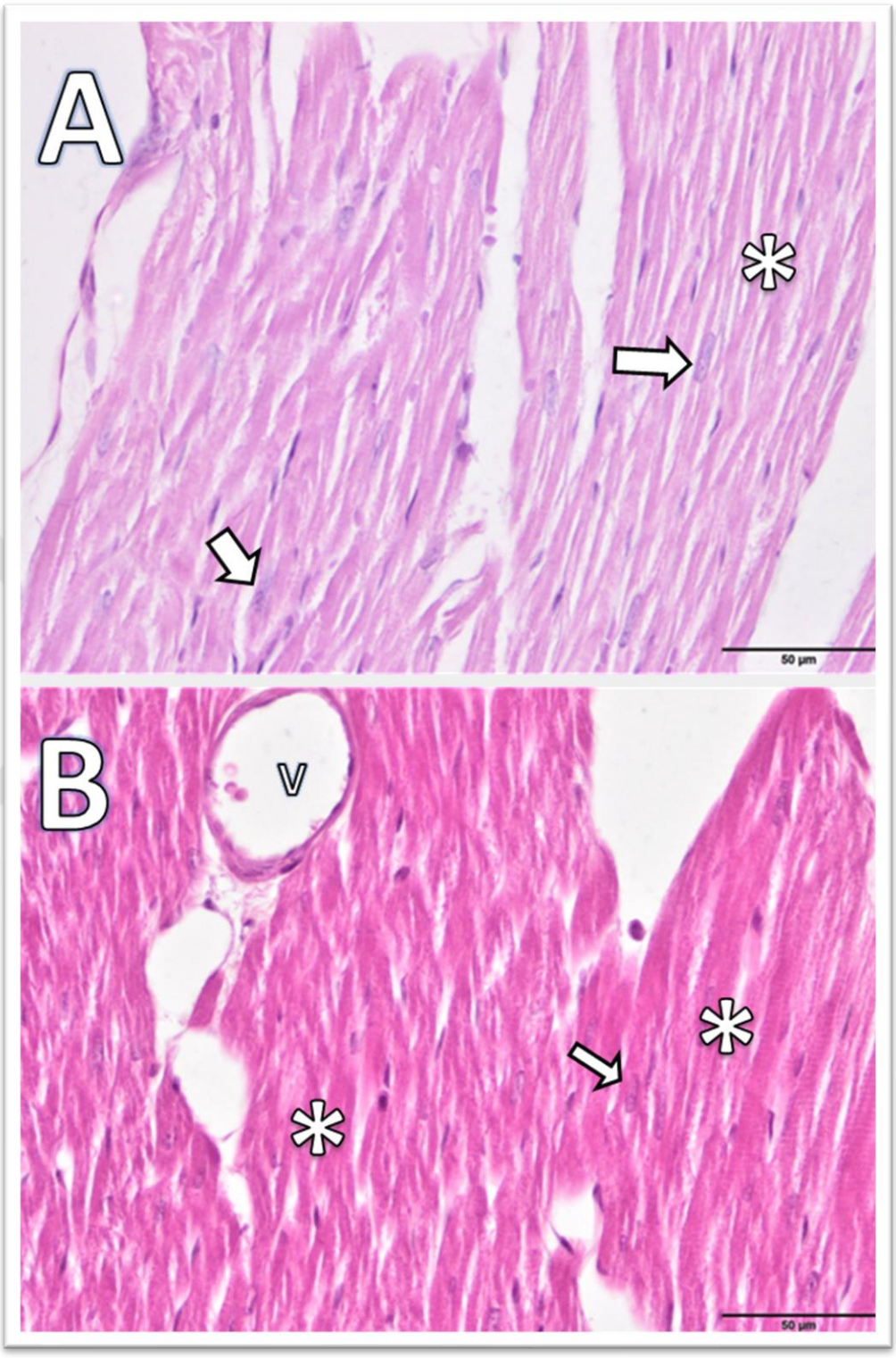


Figure 4.13. (A, B) Histological images of the left ventricle stained with H&E staining are seen. The general structure of the heart tissue of the left ventricle of GA is normal. The arrows indicate nuclei of the cardiac cells. (V) indicates the vessel (*) indicates the muscle fibres. Original magnification: X40

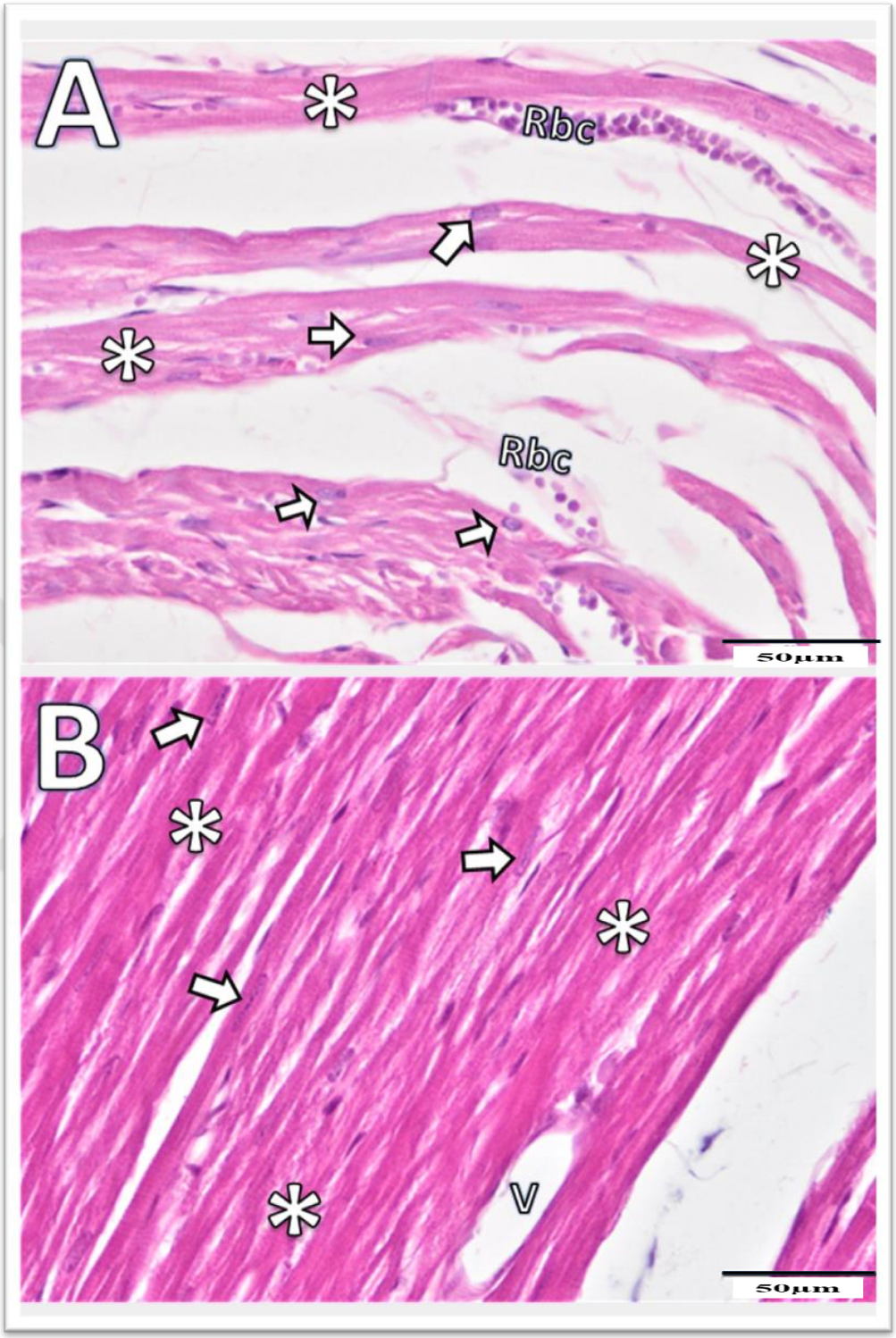


Figure 4.14. (A, B) Histological images of the left ventricle stained with H&E staining are seen. The general structure of the heart tissue of the left ventricle of GA is fine. The arrows indicate nucleus of the cardiac cell. (V) indicates the vessel. (Rbc) indicates the red blood cells. (*) indicates the muscle fibres. Original magnification: X40

4.3.1.4. H&E-Stained Sections: GA+DS Group

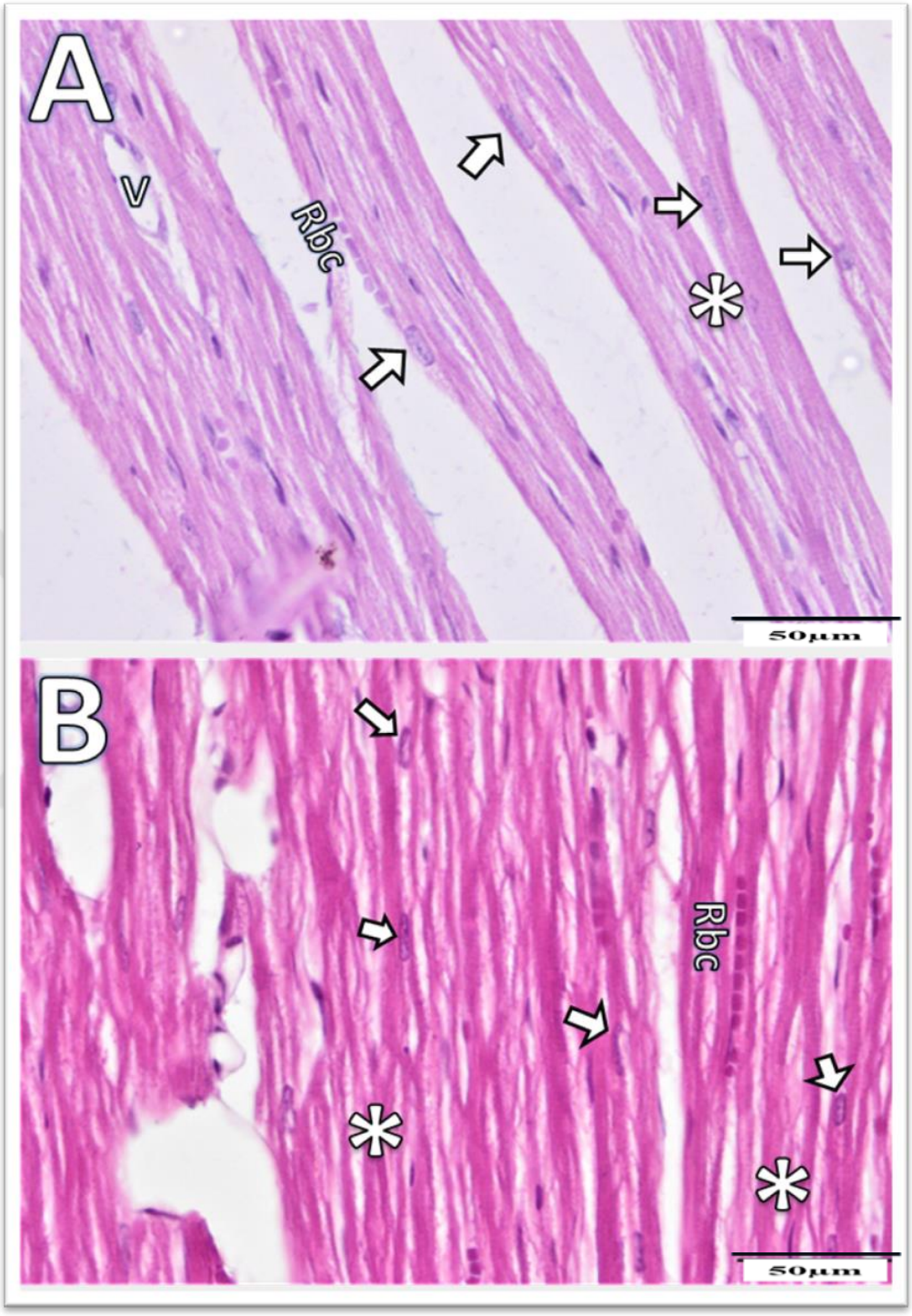


Figure 4.15. (A, B) Histological images of the left ventricle stained with H&E staining are seen. The general structure of the heart tissue of the left ventricle of GA+DS is slightly fragmented. The arrows indicate nucleus of the cardiac cell. (V) indicates the vessel. (Rbc) indicates red blood cell. The star indicates the muscle fibres. Original magnification: X40

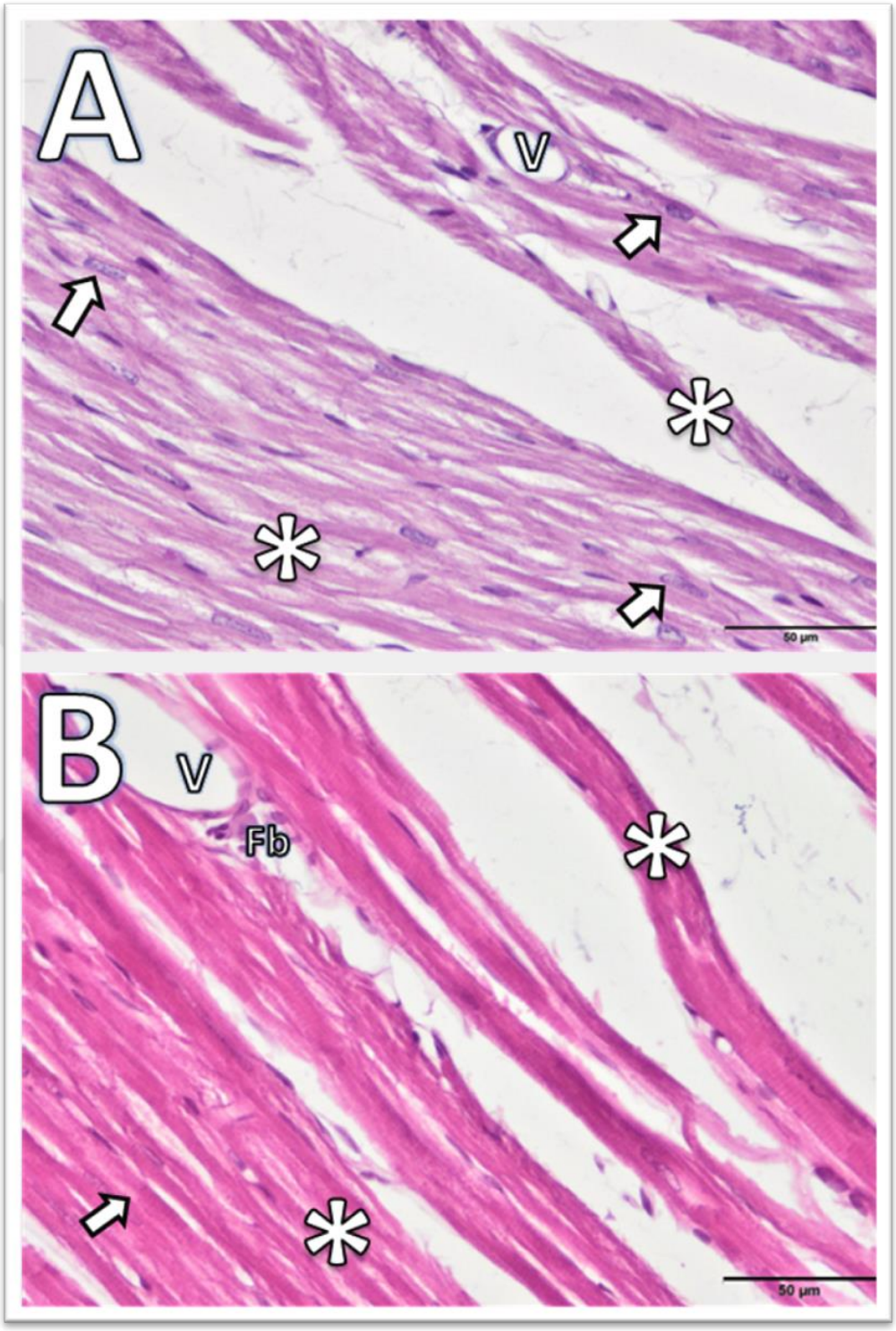


Figure 4.16. (A, B) Histological images of the left ventricle stained with H&E staining are seen. The general structure of the heart tissue of the left ventricle of GA+DS is fine. The arrows indicate nucleus of the cardiac cell. (V) indicates the vessel. (Fb) indicatesthe fibroblast cells. The star (*) indicates the muscle fibres. Original magnification: X40.

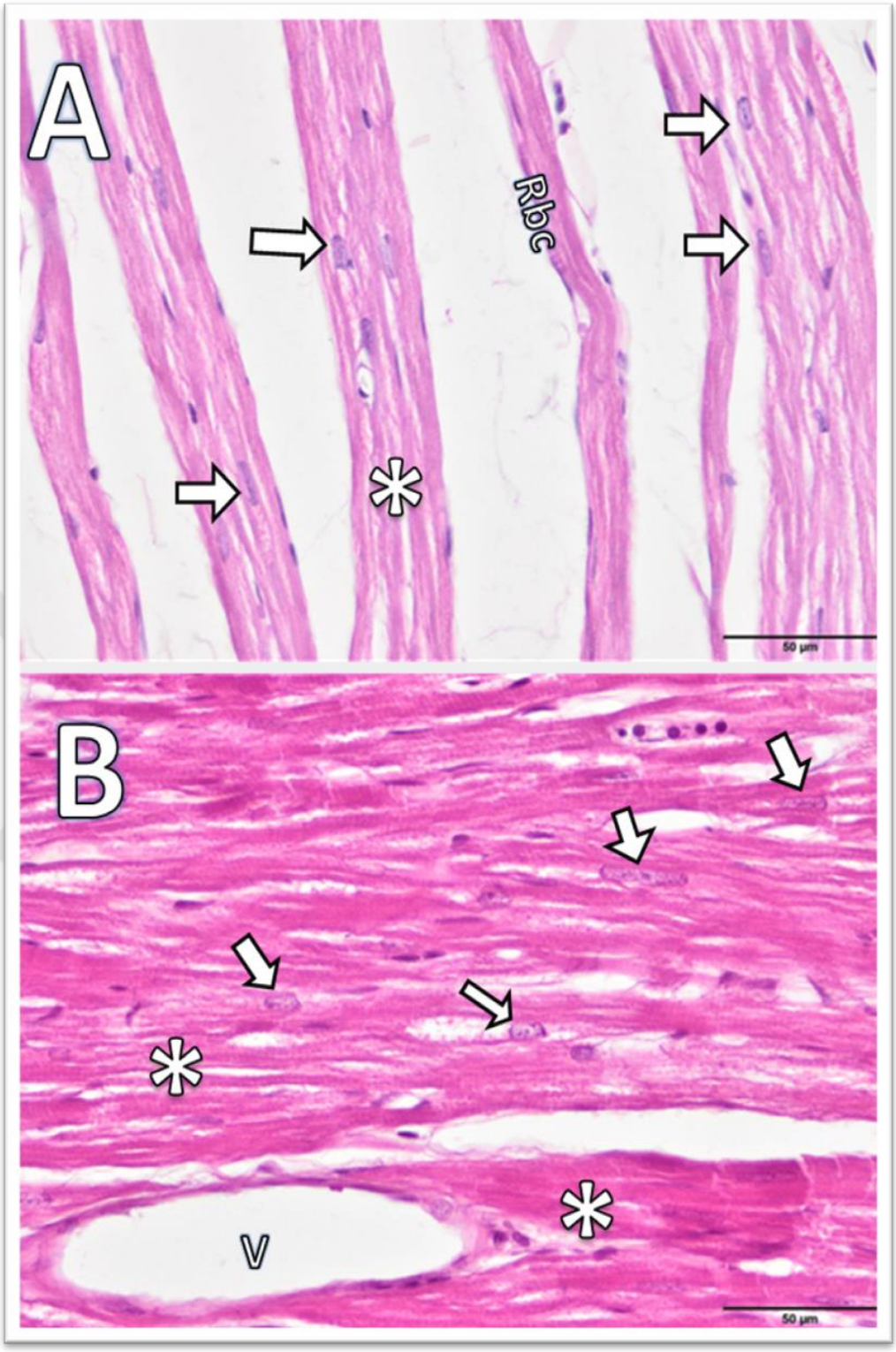


Figure 4.17. (A, B) Histological images of the left ventricle stained with H&E staining are seen. The general structure of the heart tissue of the left ventricle of GA+DS is fine. The arrows indicate nuclei of the cardiac cells. (V) indicates the vessel. (Rbc) indicate collection of red blood cells. (*) indicates the muscle fibres. Original magnification: X40.

4.3.2. Light Microscopic Findings of Toluidine Blue - Stained Sections

Tissue sections were taken from the left ventricle of all experimental animals. These sections were stained with toluidine blue stain, the slides were examined by the light microscope and the visualisations shown as follow (Figure 4.18 - 4.52).

4.3.2.1. Toluidine Blue - Stained Sections: CON Group

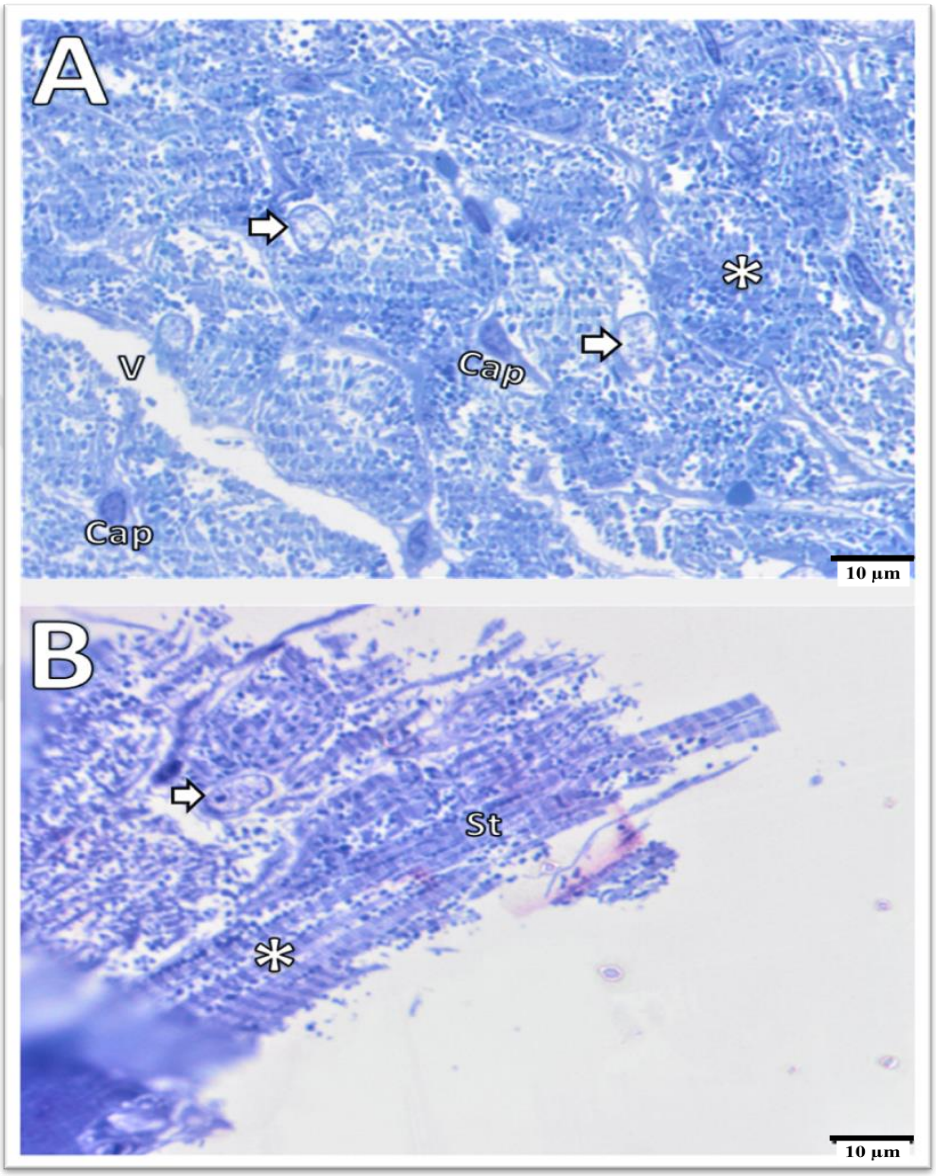


Figure 4.18. (A, B) Images of the heart tissue of the left ventricle are seen in the CON. The general structure of the heart tissue of the left ventricle is fine. The arrows indicate nuclei of the cardiac cells. (V) indicates the vessel. (Cap) indicate a blood capillary. (St) indicate the striations of the cardiac cells. (*) indicates the muscle fibres. Toluidine blue stained semi-thin resin section (0.5 µm thickness). Original magnification: X100

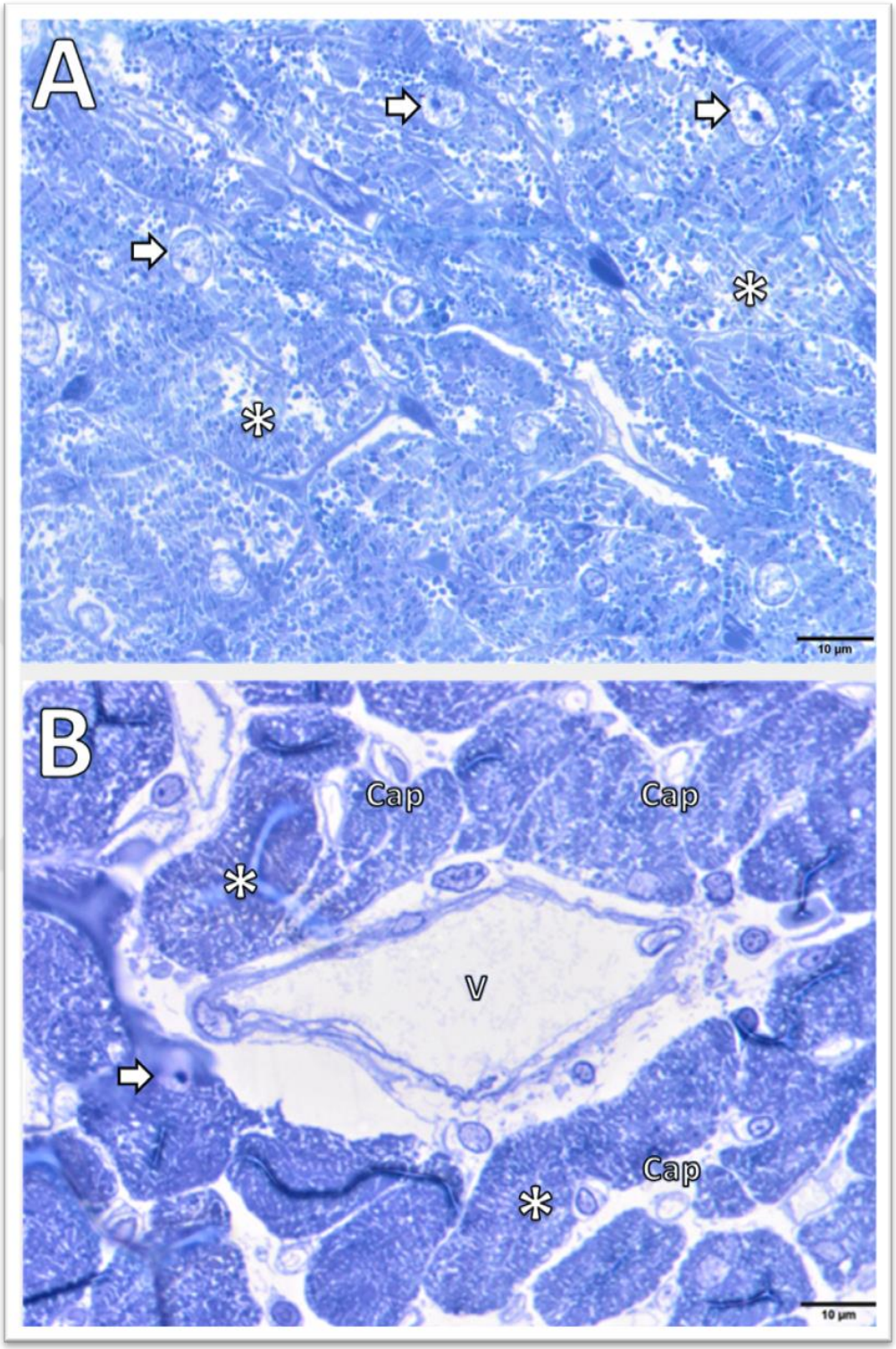


Figure 4.19. (A, B) Images of the heart tissue of the left ventricle are seen in the CON. The general structure of the heart tissue of the left ventricle is fine. The arrows indicate nuclei of the cardiac cells. (V) indicates the vessel. (Cap) indicate a blood capillary. (*) indicates the muscle fibres. Toluidine blue stained semi-thin resin section (0.5 µm thickness). Original magnification: X100

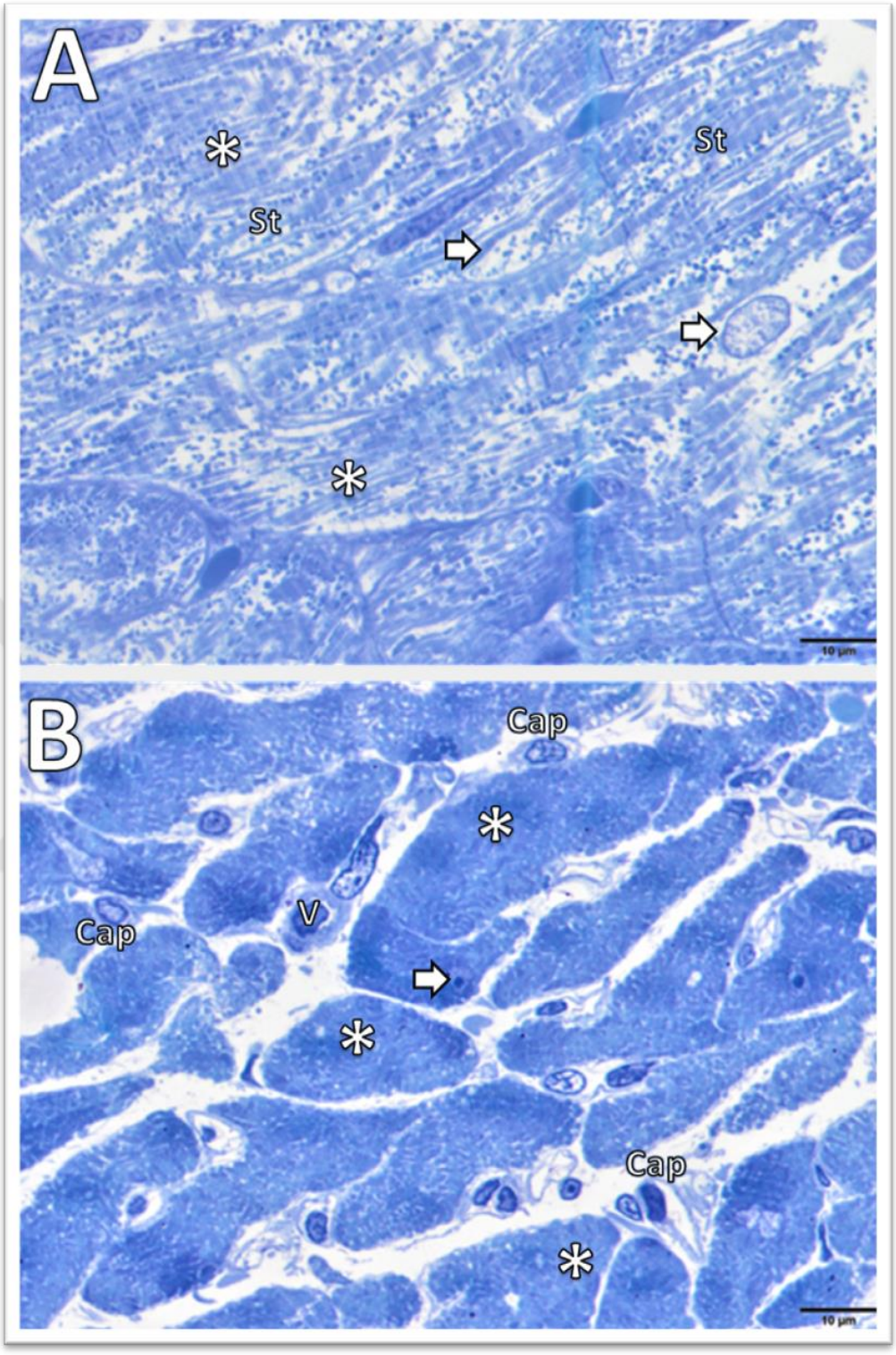


Figure 4.20. (A, B) Images of the heart tissue of the left ventricle are seen in the CON. The general structure of the heart tissue of the left ventricle is fine. The arrows indicate nuclei of the cardiac cells. (V) indicates the vessel. (Cap) indicate a blood capillary. (St) indicate the striations of the cardiac cells. (*) indicates the muscle fibres. Toluidine blue stained semi-thin resin section (0.5 µm thickness). Original magnification: X100

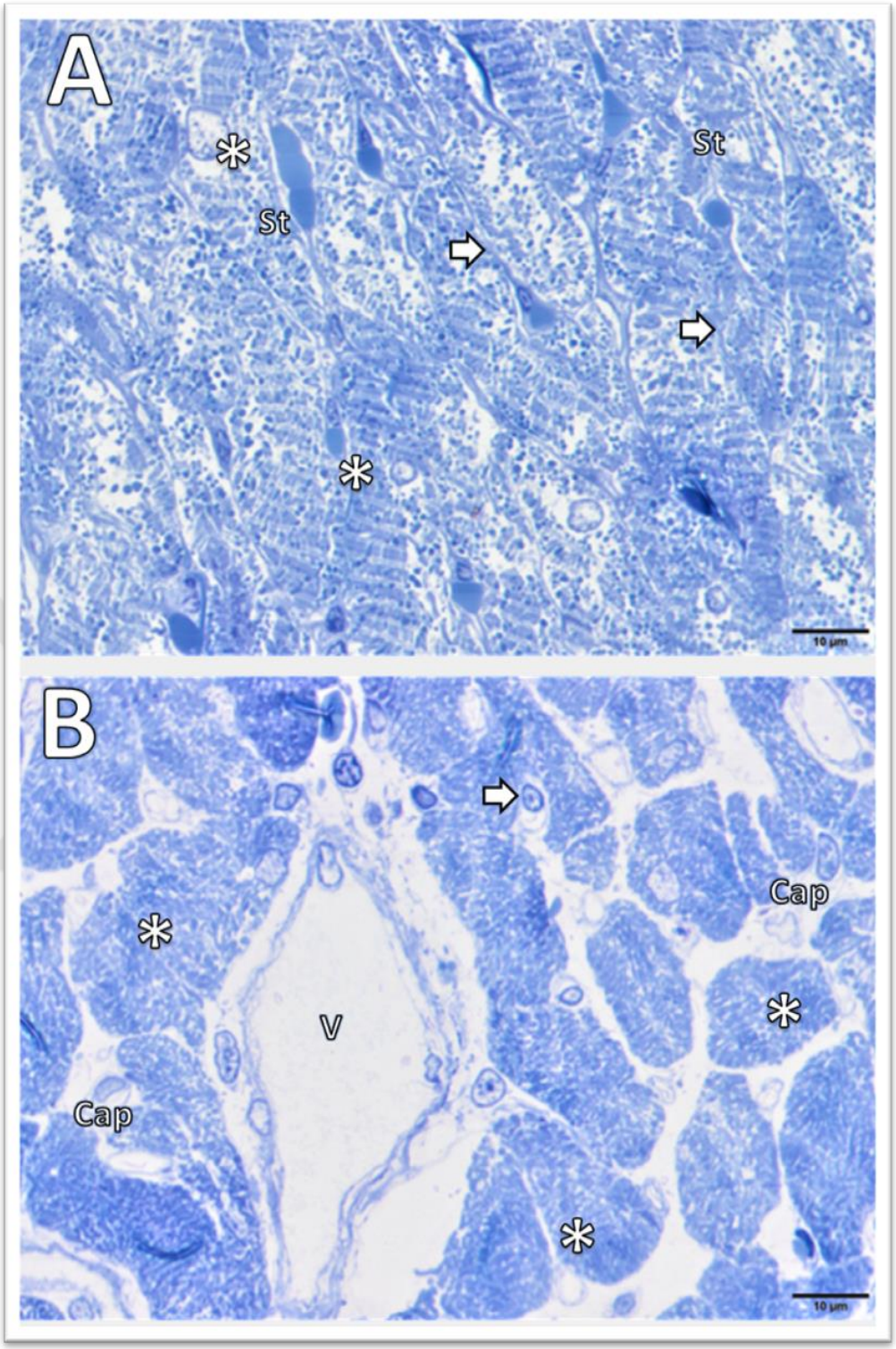


Figure 4.21. (A, B) Images of the heart tissue of the left ventricle are seen in the CON. The general structure of the heart tissue of the left ventricle is fine. The arrows indicate nuclei of the cardiac cells. (V) indicates the vessel. (Cap) indicate a blood capillary. (St) indicate the striations of the cardiac cells. (*) indicates the muscle fibres. Toluidine blue stained semi-thin resin section (0.5 µm thickness). Original magnification: X100

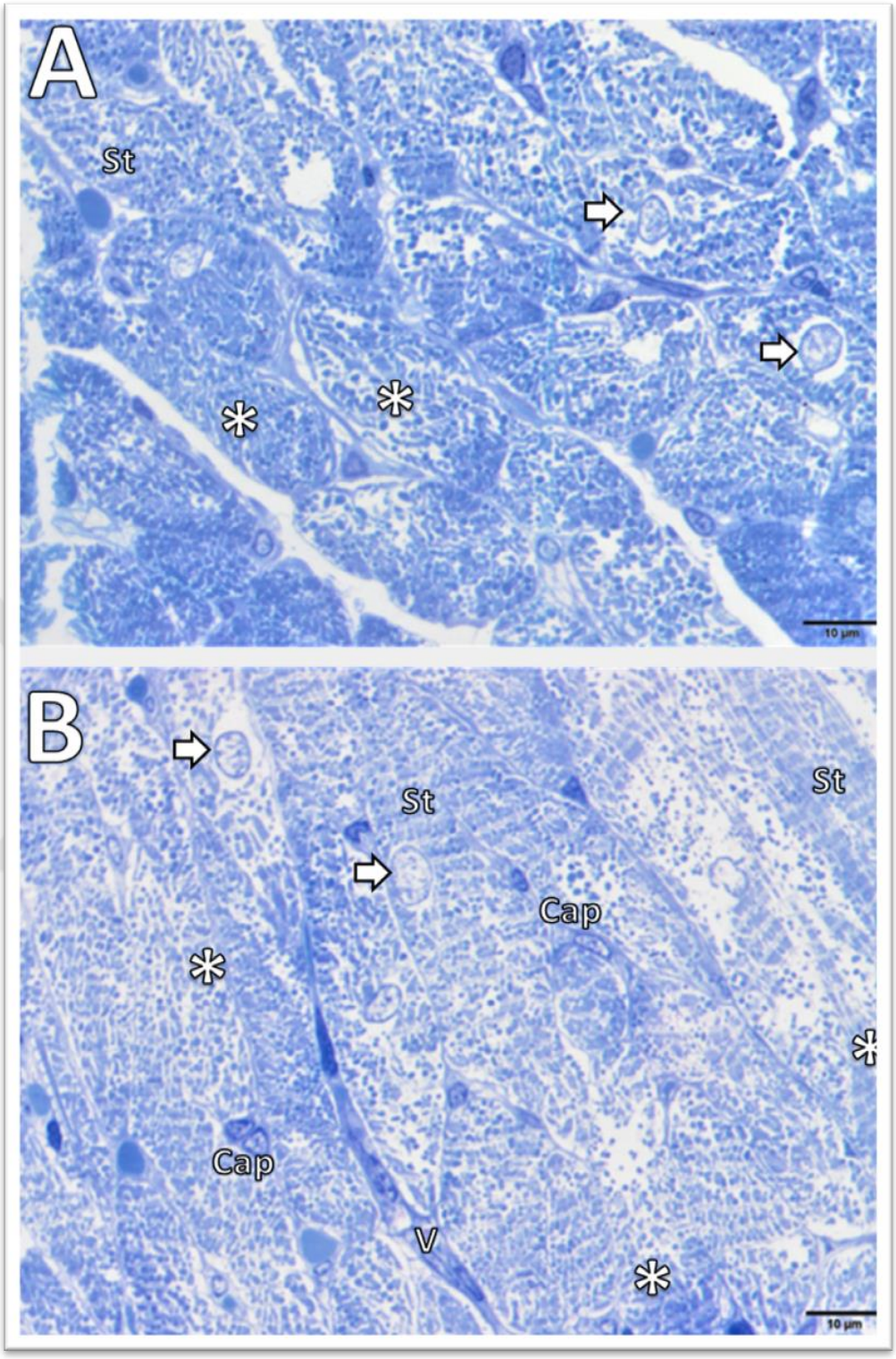


Figure 4.22. (A, B) Images of the heart tissue of the left ventricle are seen in the CON. The general structure of the heart tissue of the left ventricle is fine. The arrows indicate nuclei of the cardiac cells. (V) indicates the vessel. (Cap) indicate a blood capillary. (St) indicate the striations of the cardiac cells. (*) indicates the muscle fibres. Toluidine blue stained semi-thin resin section (0.5 µm thickness). Original magnification: X100

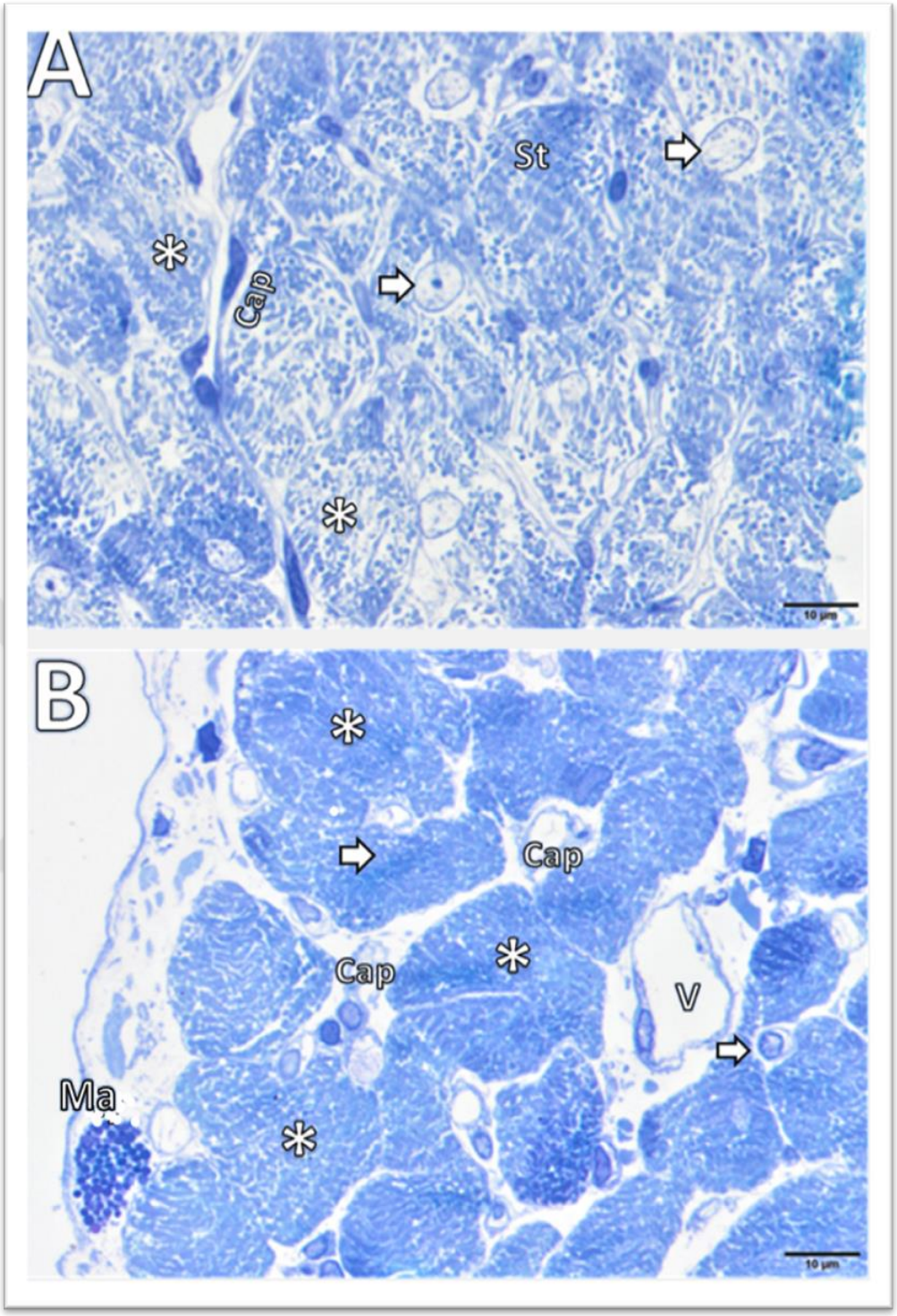


Figure 4.23. (A, B) Images of the heart tissue of the left ventricle are seen in the CON. The general structure of the heart tissue of the left ventricle is fine. The arrows indicate nuclei of the cardiac cells. (V) indicates the vessel. (Cap) indicate a blood capillary. (St) indicate the striations of the cardiac cells. (Ma) mast cells. (*) indicates the muscle fibres. Toluidine blue stained semi-thin resin section (0.5 µm thickness). Original magnification: X100

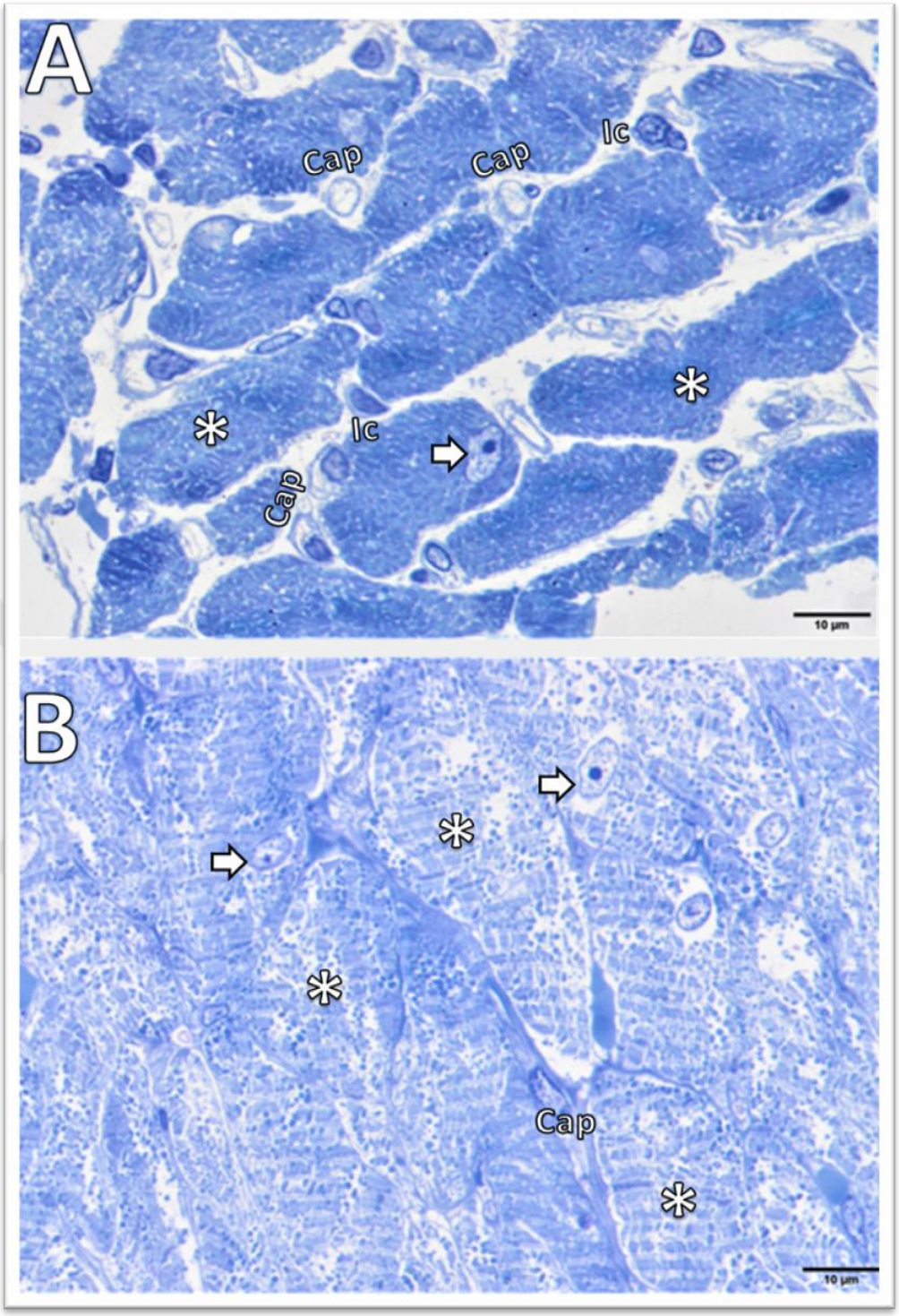


Figure 4.24. (A, B) Images of the heart tissue of the left ventricle are seen in the CON. The general structure of the heart tissue of the left ventricle is fine. The arrows indicate nuclei of the cardiac cells. (Cap) indicate a blood capillary. (Ic) indicate interstitial cell. (*) indicates the muscle fibres. Toluidine blue stained semi-thin resin section (0.5 µm thickness). Original magnification: X100

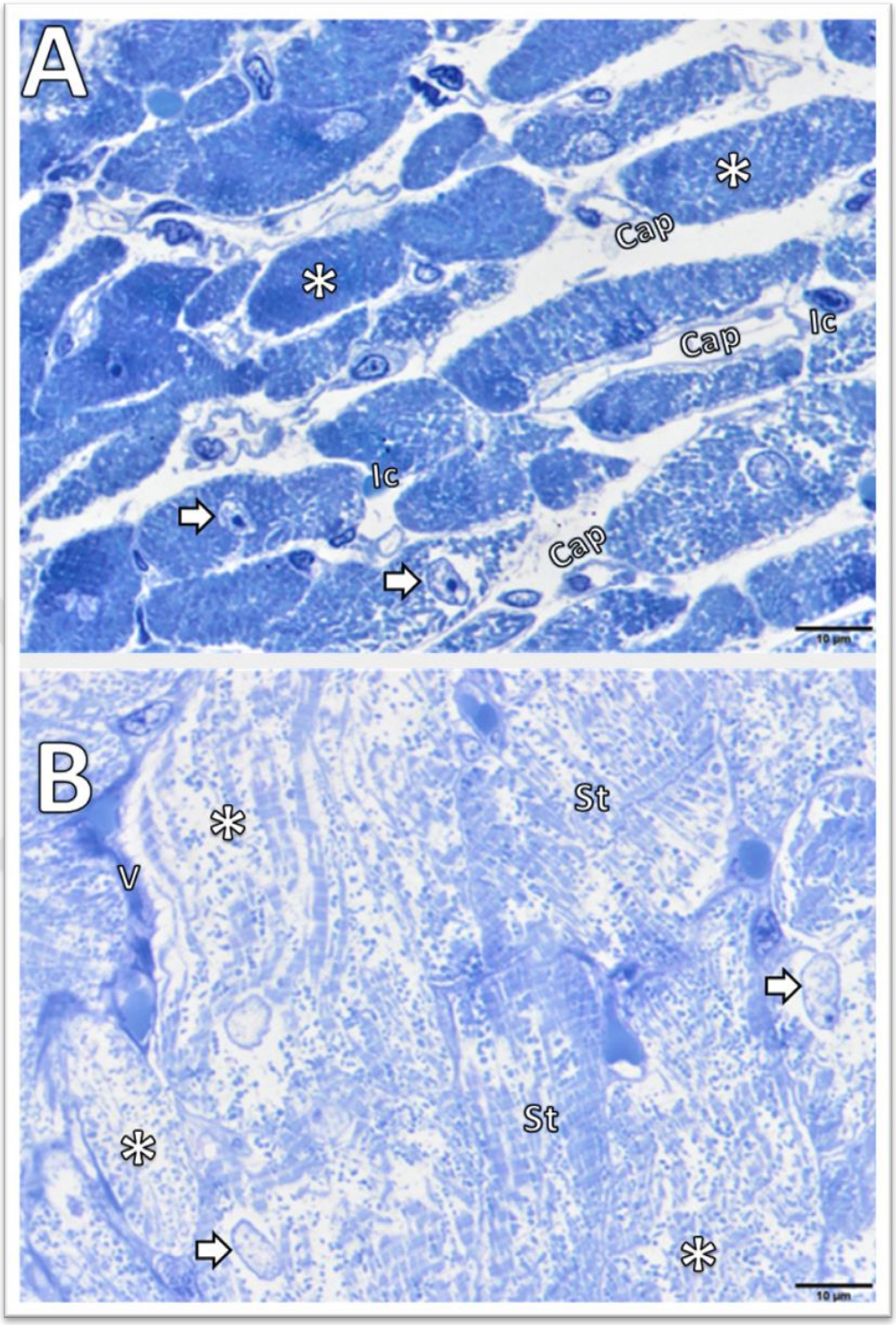


Figure 4.25. (A, B) Images of the heart tissue of the left ventricle are seen in the CON. The general structure of the heart tissue of the left ventricle is fine. The arrows indicate nuclei of the cardiac cells. (V) indicates the vessel. (Cap) indicate a blood capillary. (Ic) indicate interstitial cell. (St) indicate the striations of the cardiac cells. (*) indicates the muscle fibres. Toluidine blue stained semi-thin resin section (0.5 µm thickness). Original magnification: X100

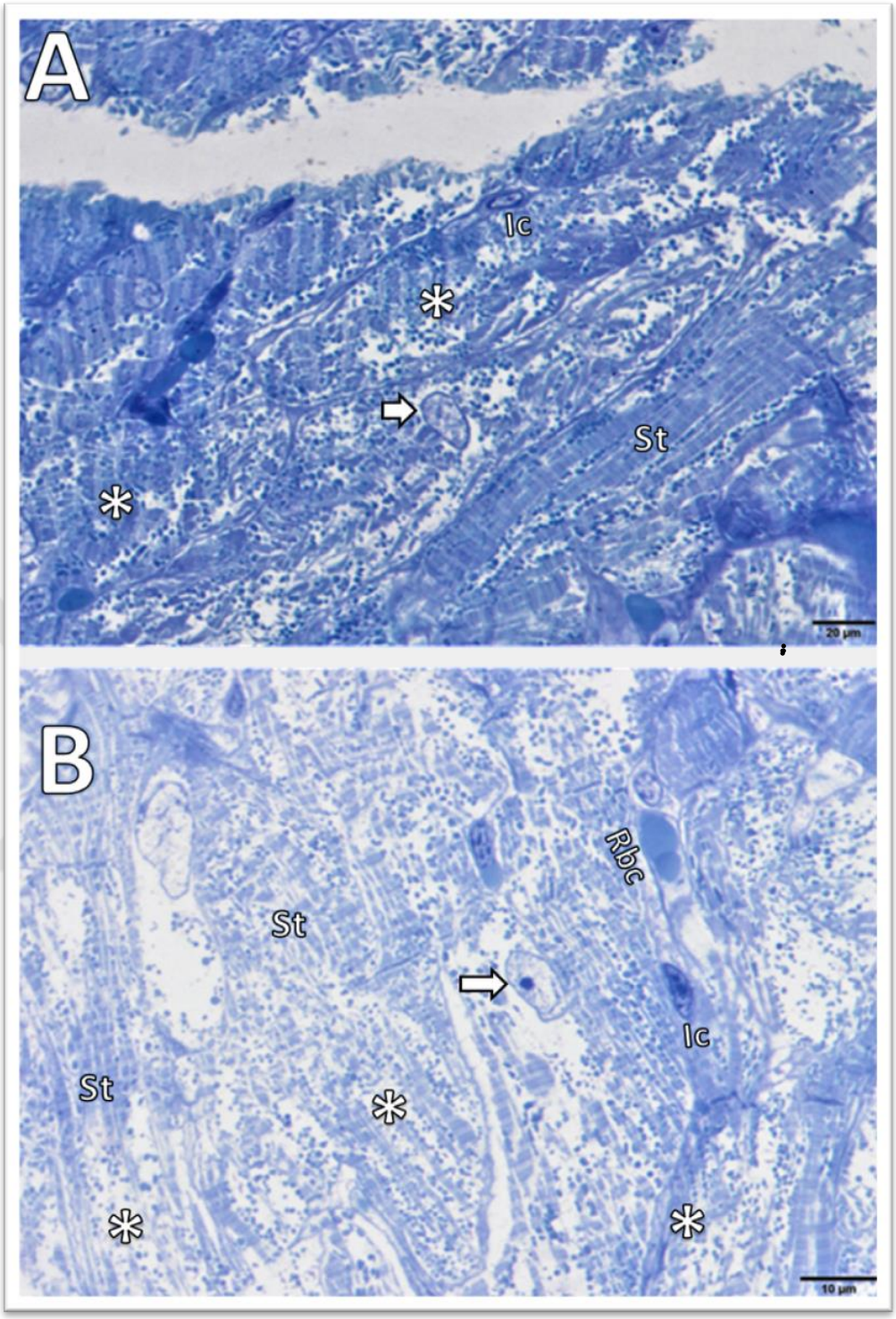


Figure 4.26. (A, B) Images of the heart tissue of the left ventricle are seen in the CON. The general structure of the heart tissue of the left ventricle is fine. The arrows indicate nuclei of the cardiac cells. (Rbc) indicate collection of red blood cells. (Ic) indicate interstitial cell. (St) indicate the striations of the cardiac cells. (*) indicates the muscle fibres. Toluidine blue stained semi-thin resin section (0.5 µm thickness). Original magnification: X100

4.3.2.2. Toluidine Blue - Stained Sections: DS Group

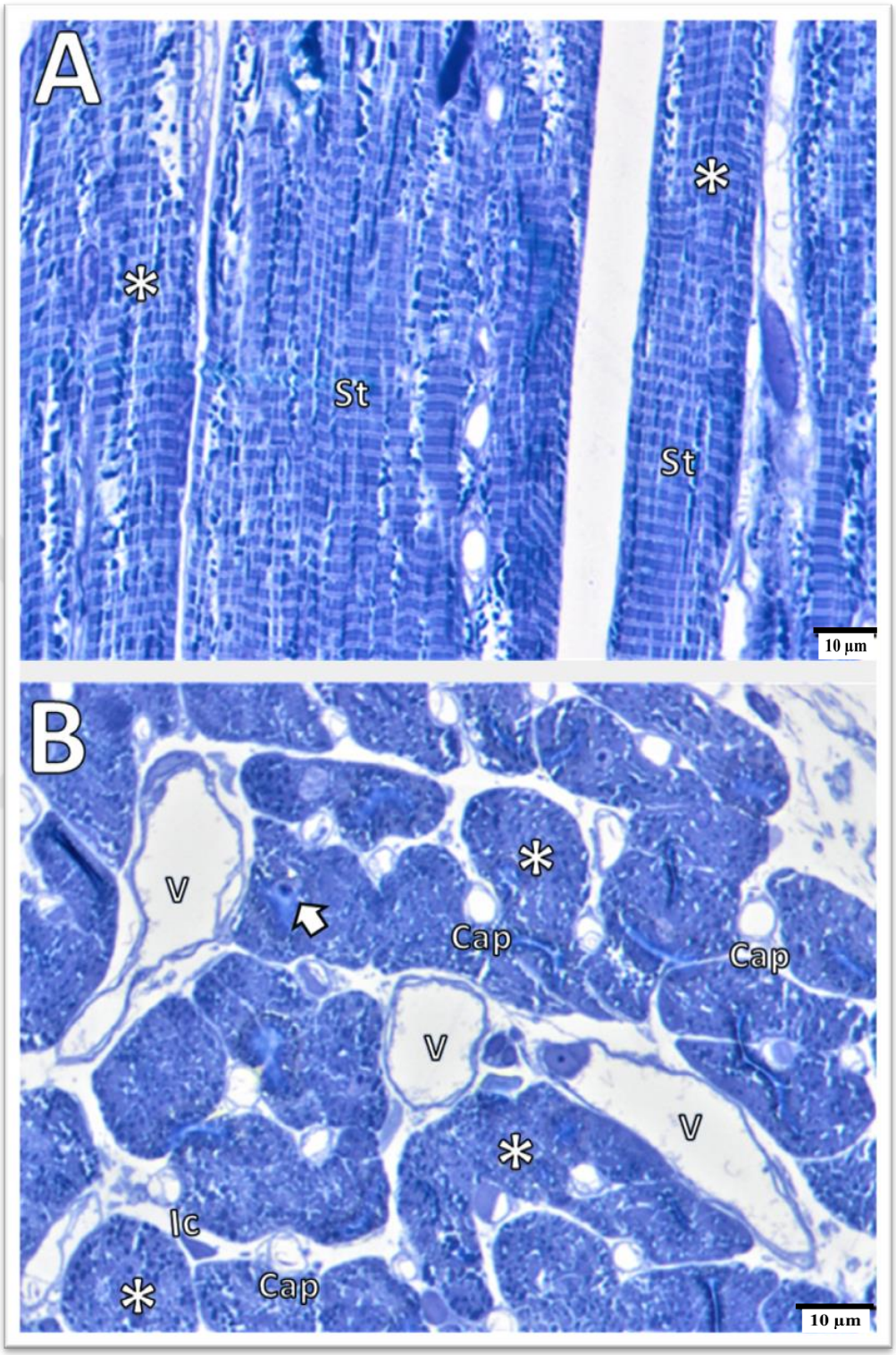


Figure 4.27. (A, B) Images of the heart tissue of the left ventricle are seen in the DS. The general structure of the heart tissue of the left ventricle is fine. The arrows indicate nuclei of the cardiac cells. (V) indicates the vessel. (Cap) indicate a blood capillary. (St) indicate the striations of the cardiac cells. (*) indicates the muscle fibres. Toluidine blue stained semi-thin resin section (0.5 µm thickness). Original magnification: X100

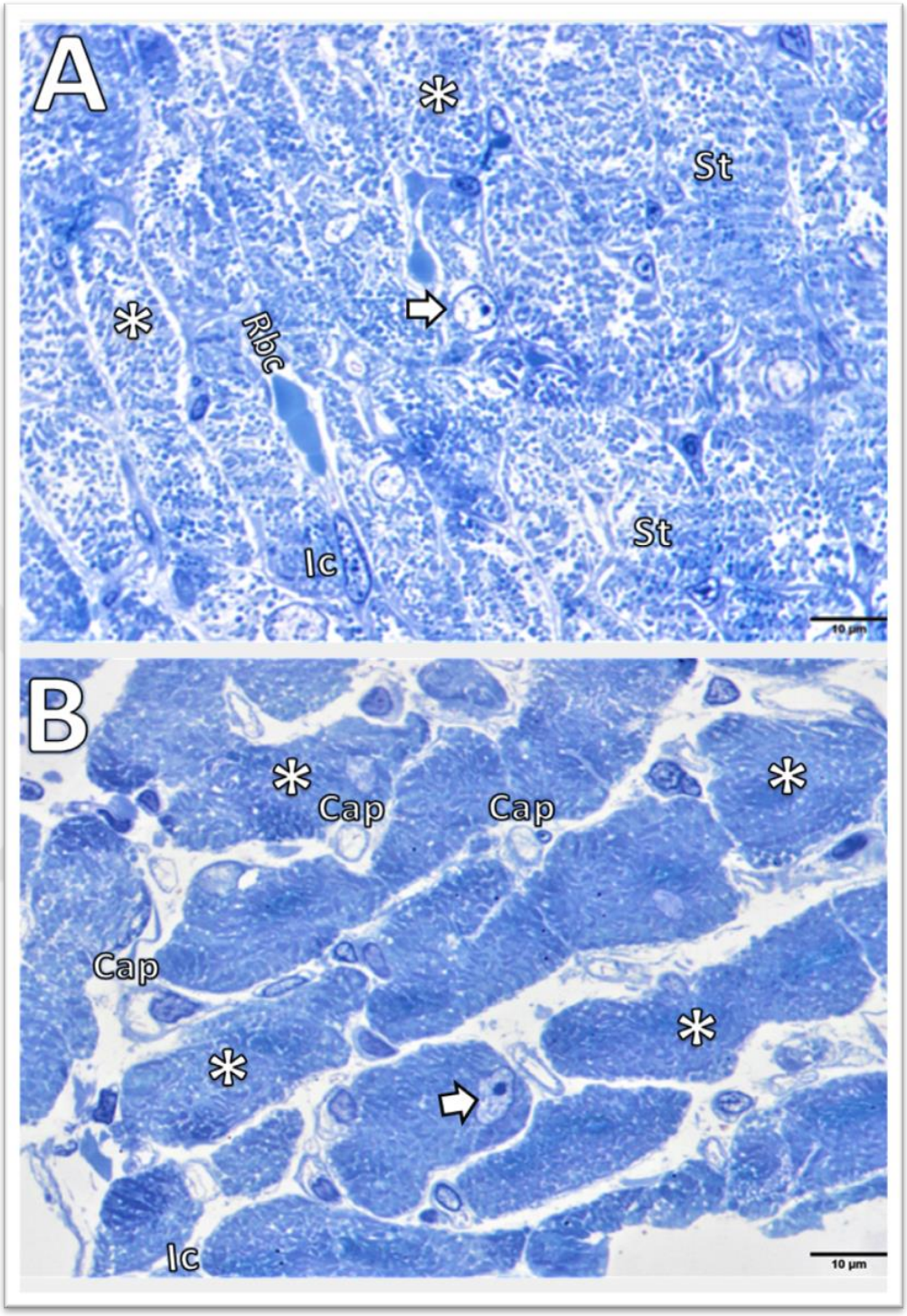


Figure 4.28. (A, B) Images of the heart tissue of the left ventricle are seen in the DS. The general structure of the heart tissue of the left ventricle is fine. The arrows indicate nuclei of the cardiac cells. (Rbc) indicate collection of red blood cells. (Cap) indicate a blood capillary. (Ic) indicate interstitial cell. (St) indicate the striations of the cardiac cells. (*) indicates the muscle fibres. Toluidine blue stained semi-thin resin section (0.5 µm thickness). Original magnification: X100

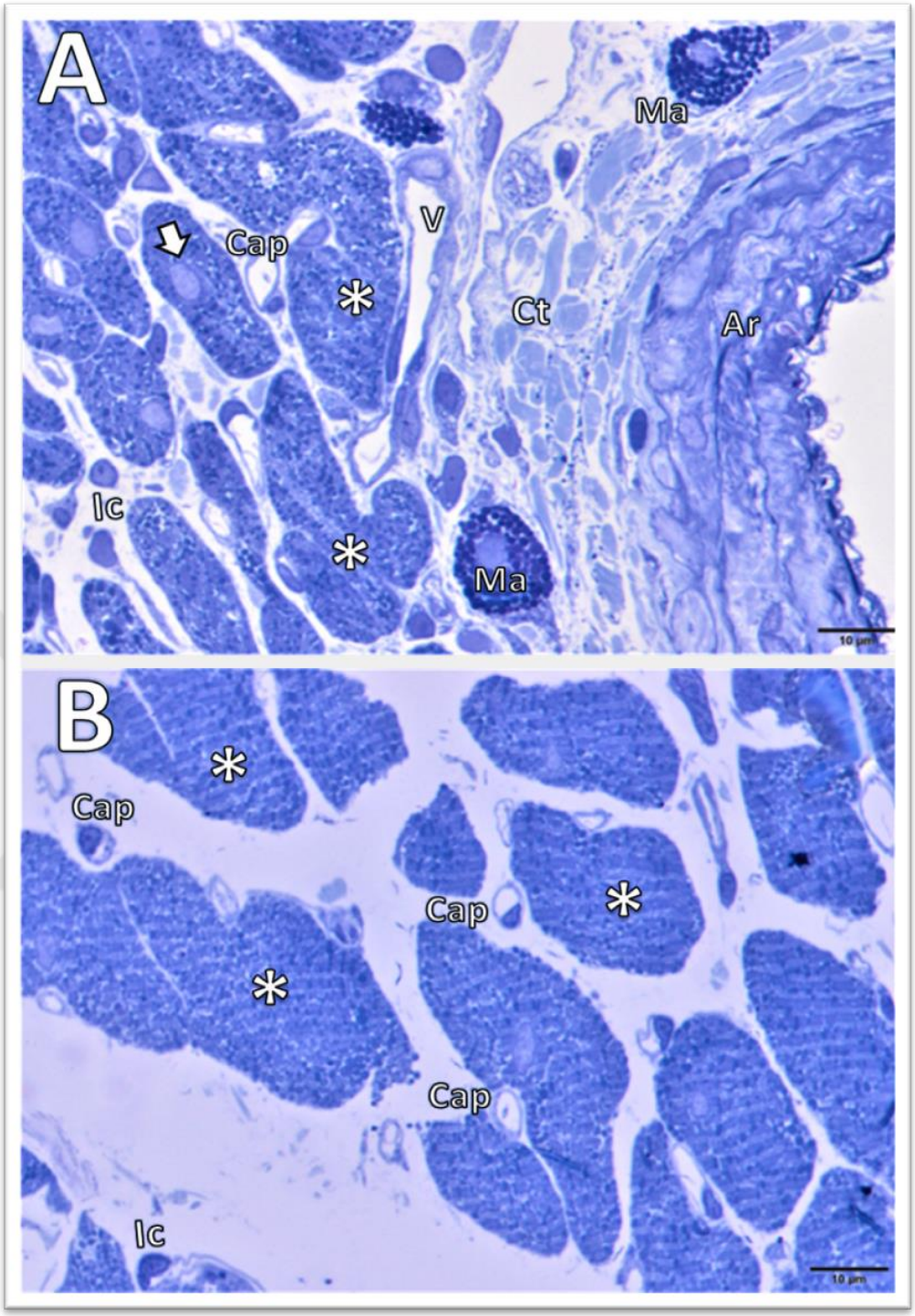


Figure 4.29. (A, B) Images of the heart tissue of the left ventricle are seen in the DS. The general structure of the heart tissue of the left ventricle is fine. The arrows indicate nuclei of the cardiac cells. (V) indicates the vessel. (Rbc) indicate collection of red blood cells. (Cap) indicate a blood capillary. (Ct) indicate connective tissue. (Ic) indicate interstitial cell. (Ar) indicate artery. (Ma) mast cell. (*) indicates the muscle fibres. Toluidine blue stained semi-thin resin section (0.5 µm thickness). Original magnification: X100

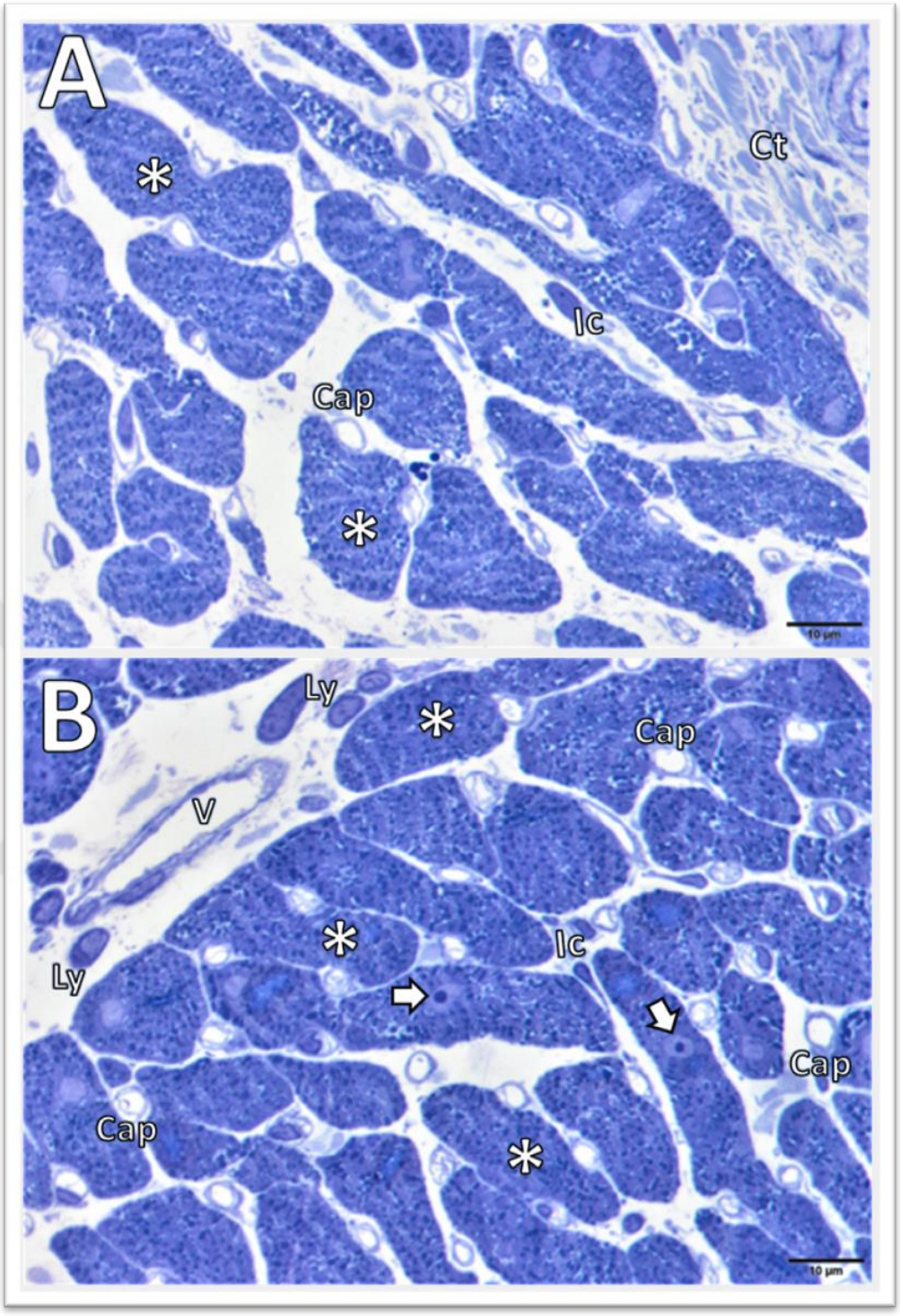


Figure 4.30. (A, B) Images of the heart tissue of the left ventricle are seen in the DS. The general structure of the heart tissue of the left ventricle is fine. The arrows indicate nuclei of the cardiac cells. (V) indicates the vessel. (Cap) indicate a blood capillary. (Ct) indicate connective tissue. (Ic) indicate interstitial cell. (Ly) indicate lymphocyte. (*) indicates the muscle fibres. Toluidine blue stained semi-thin resin section (0.5 µm thickness). Original magnification: X100

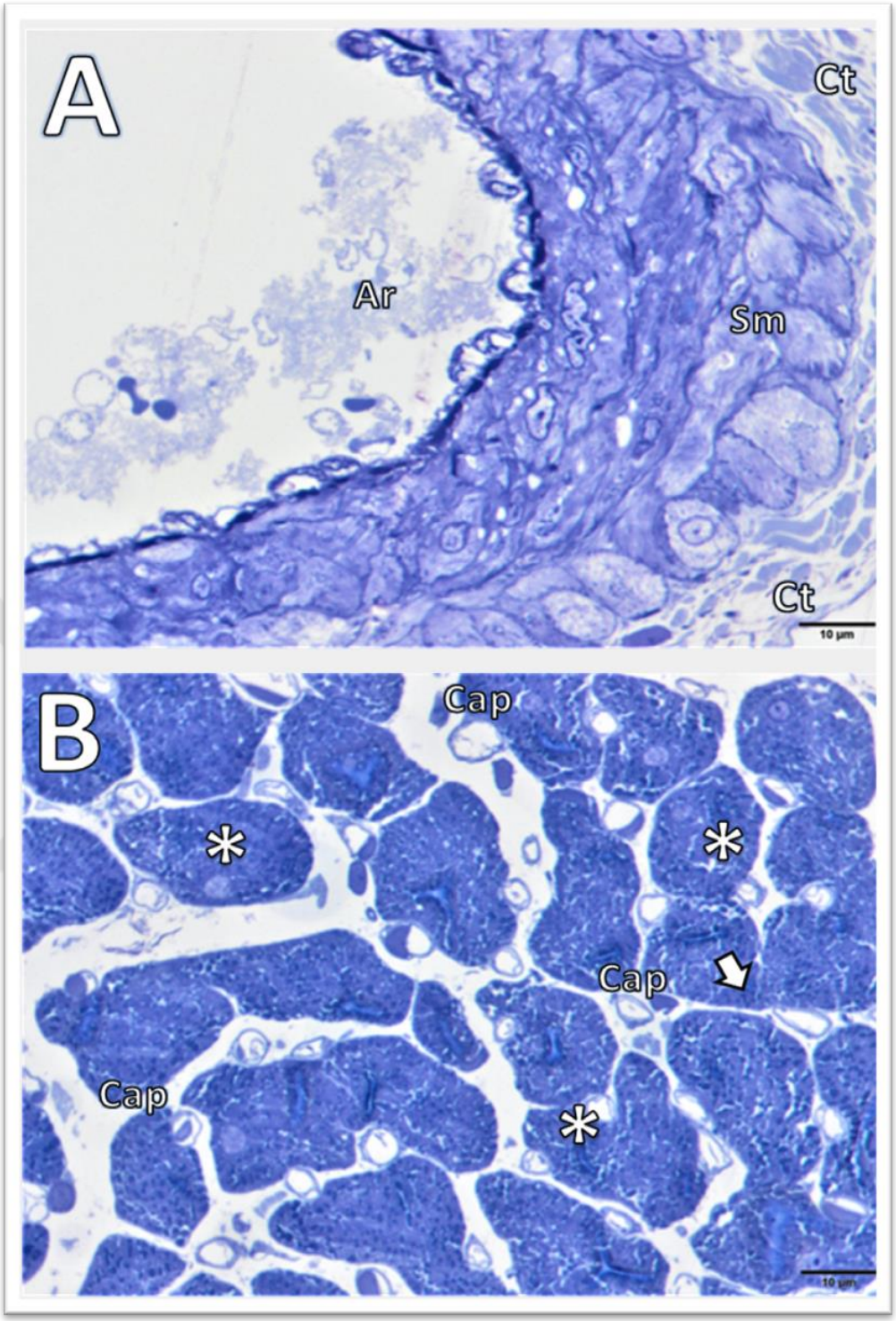


Figure 4.31. (A, B) Images of the heart tissue of the left ventricle are seen in the DS. The general structure of the heart tissue of the left ventricle is fine. The arrows indicate nuclei of the cardiac cells. (Cap) indicate a blood capillary. (Ct) indicate connective tissue. The letters (Sm) Smooth muscle cell. The letters (Ar) indicate the artery. (*) indicates the muscle fibres. Toluidine blue stained semi-thin resin section (0.5 µm thickness). Original magnification: X100

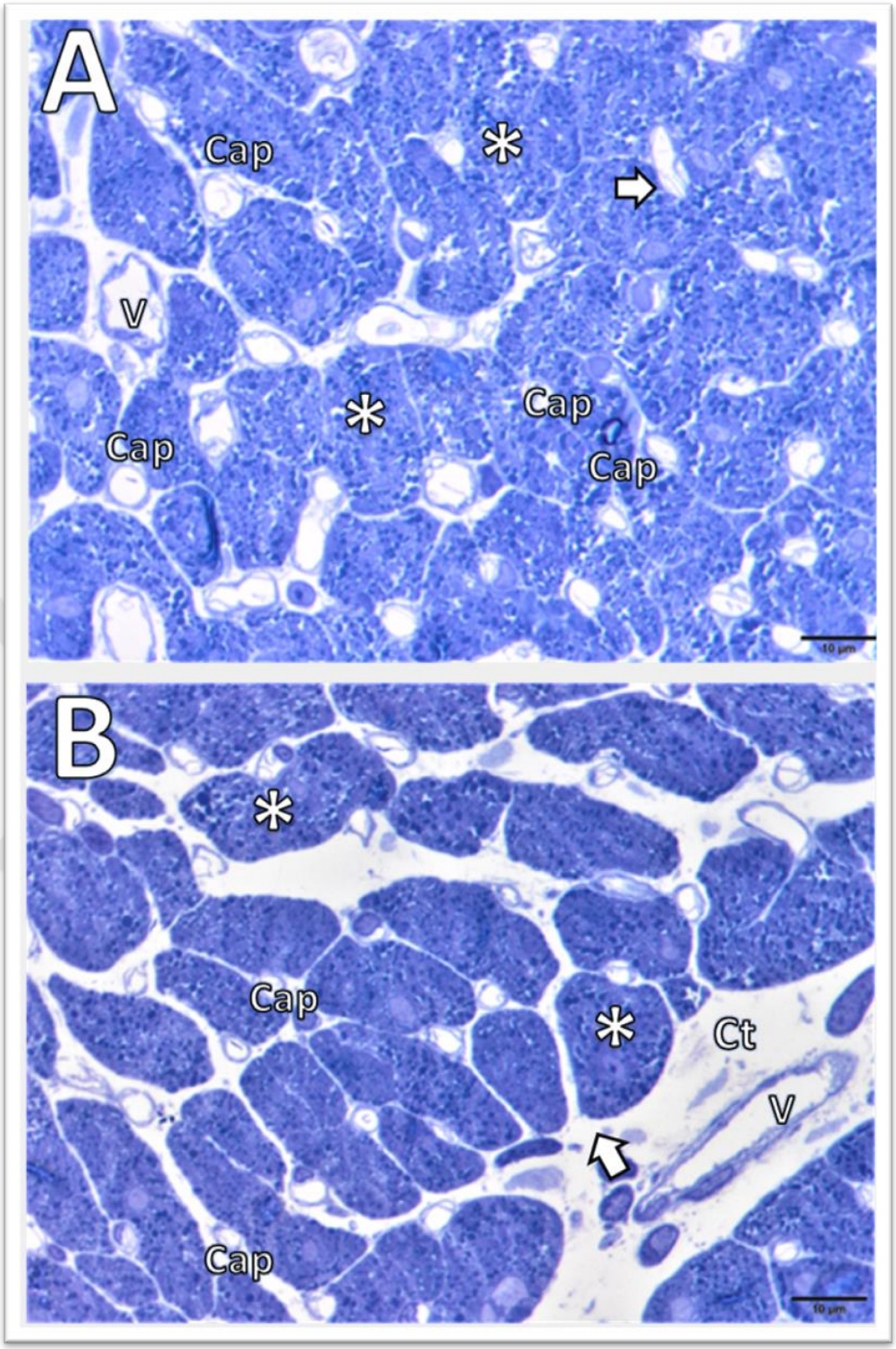


Figure 4.32. (A, B) Images of the heart tissue of the left ventricle are seen in the DS. The general structure of the heart tissue of the left ventricle is fine. The arrows indicate nuclei of the cardiac cells. (V) indicates the vessel (Cap) indicate a blood capillary. (Ct) indicate connective tissue. (*) indicates the muscle fibres. Toluidine blue stained semi-thin resin section (0.5 µm thickness). Original magnification: X100.

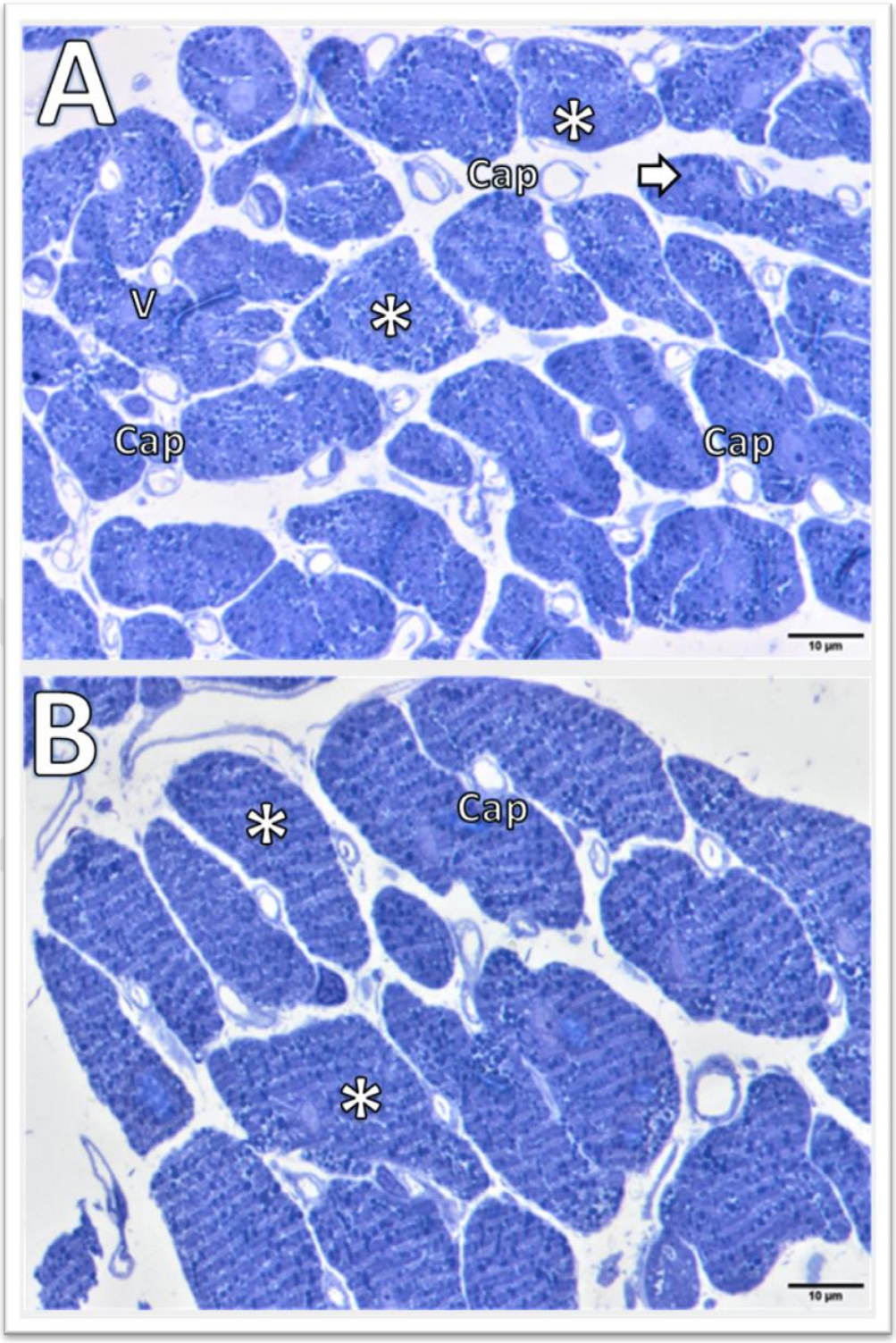


Figure 4.33. (A, B) Images of the heart tissue of the left ventricle are seen in the DS. The general structure of the heart tissue of the left ventricle is fine. The arrows indicate nuclei of the cardiac cells. (V) indicates the vessel. (Cap) indicate a blood capillary. (*) indicates the muscle fibres. Toluidine blue stained semi-thin resin section (0.5 µm thickness). Original magnification: X100

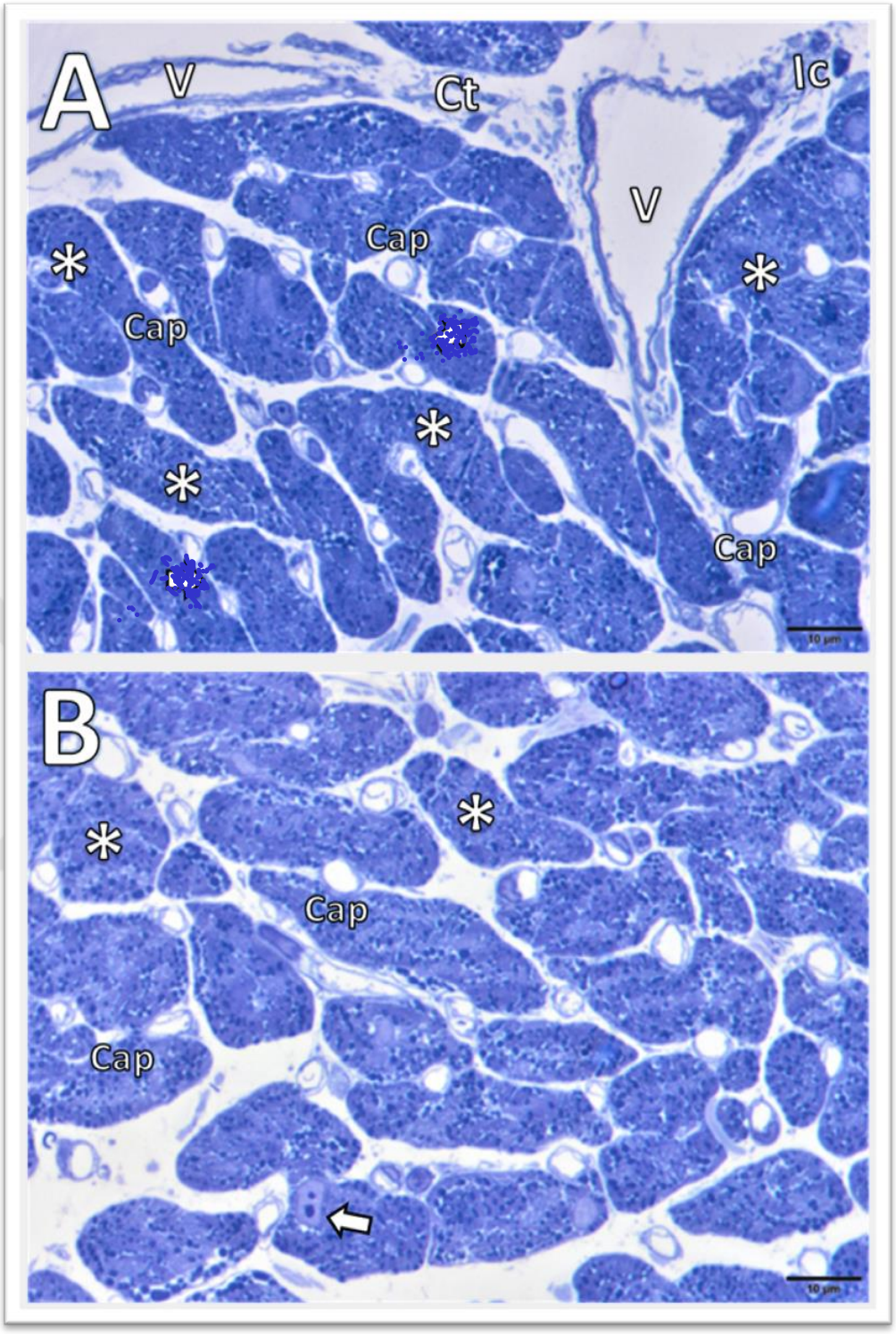


Figure 4.34. (A, B) Images of the heart tissue of the left ventricle are seen in the DS. The general structure of the heart tissue of the left ventricle is fine. The arrows indicate nuclei of the cardiac cells. (V) indicates the vessel. (Cap) indicate a blood capillary. (Ct) indicate connective tissue. (Ic) indicate interstitial cell. (*) indicates the muscle fibres. Toluidine blue stained semi-thin resin section (0.5 µm thickness). Original magnification: X100

4.3.2.3. Toluidine Blue - Stained Sections; GA Group

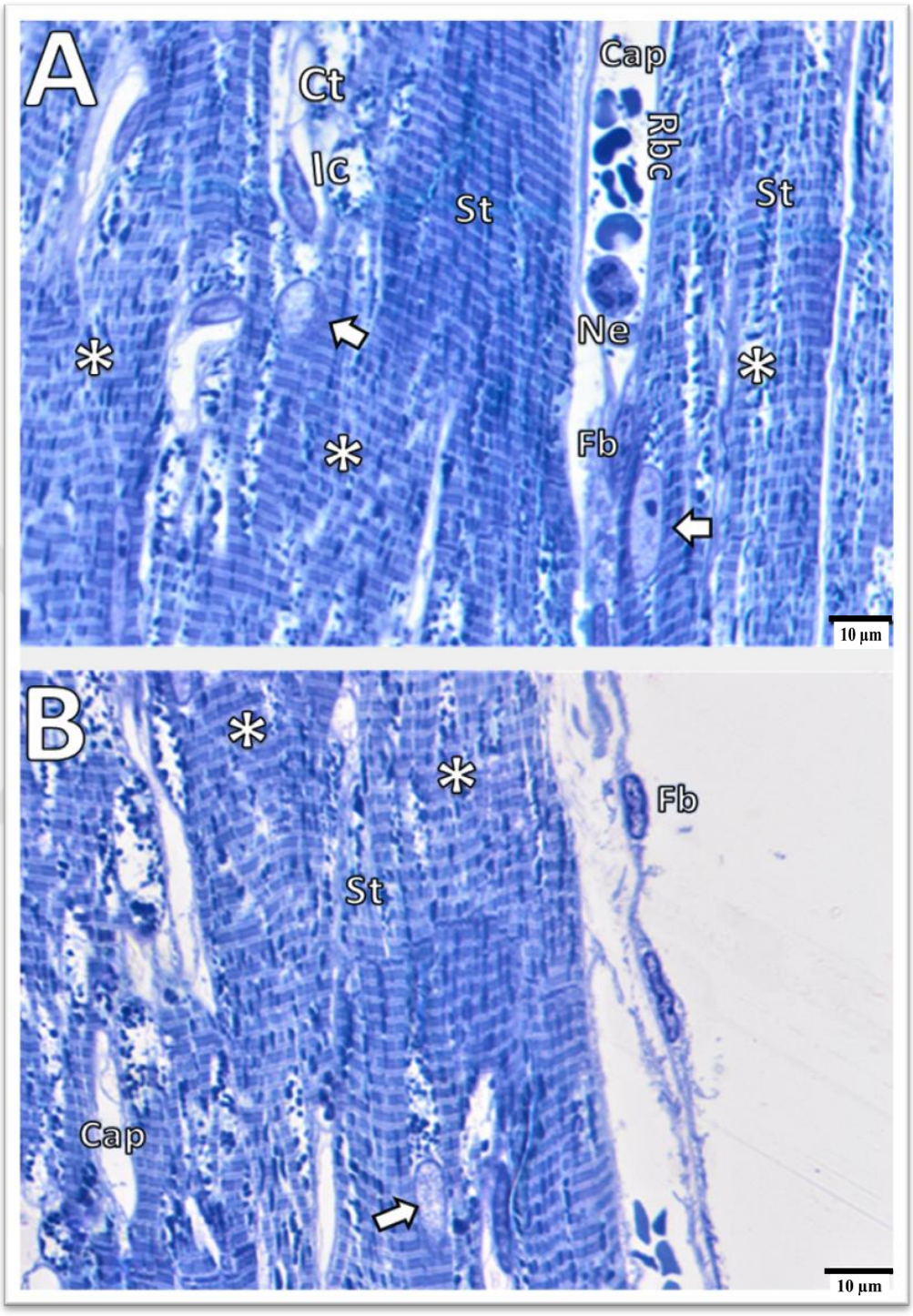


Figure 4.35. (A, B) Images of the heart tissue of the left ventricle are seen in the GA. The general structure of the heart tissue of the left ventricle is fine. The arrows indicate nuclei of the cardiac cells. (V) indicates the vessel. (Rbc) indicate collection of red blood cells. (Cap) indicate a blood capillary. (Ct) indicate connective tissue. (Ic) indicate interstitial cell. The letters (Fb) indicate the fibroblast cell. (Ne) indicate neutrophil. (St) indicate the striations of the cardiac cells. (*) indicates the muscle fibres. Toluidine blue stained semi-thin resin section (0.5 µm thickness). Original magnification: X100

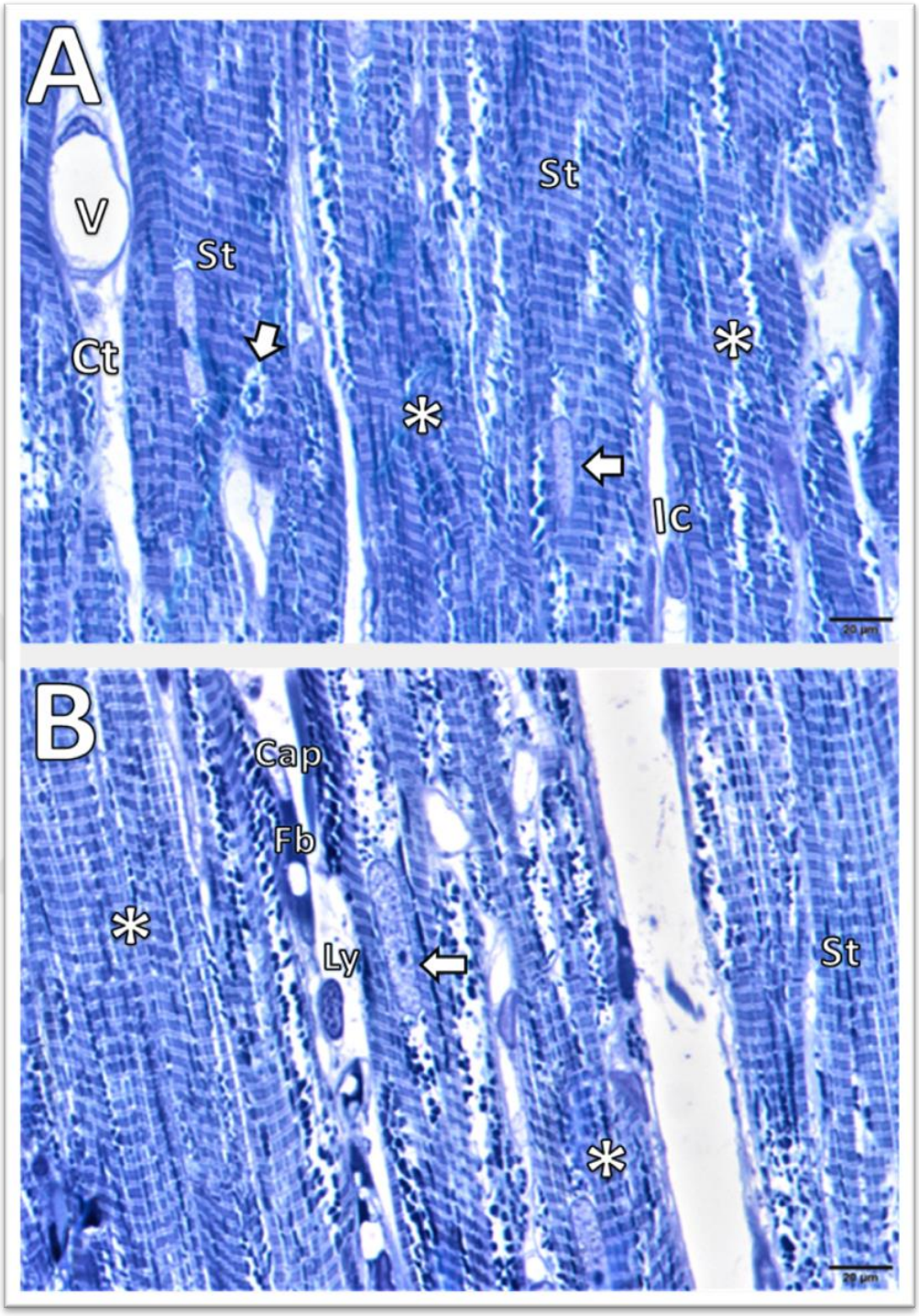


Figure 4.36. (A, B) Images of the heart tissue of the left ventricle are seen in the GA. The general structure of the heart tissue of the left ventricle is fine. The arrows indicate nuclei of the cardiac cells. (V) indicates the vessel. (Cap) indicate a blood capillary. (Ct) indicate connective tissue. (Ic) indicate interstitial cell. (Fb) indicate the fibroblast cell. (Ly) indicate lymphocyte. (St) indicate the striations of the cardiac cells. (*) indicates the muscle fibres. Toluidine blue stained semi-thin resin section (0.5 µm thickness). Original magnification: X100

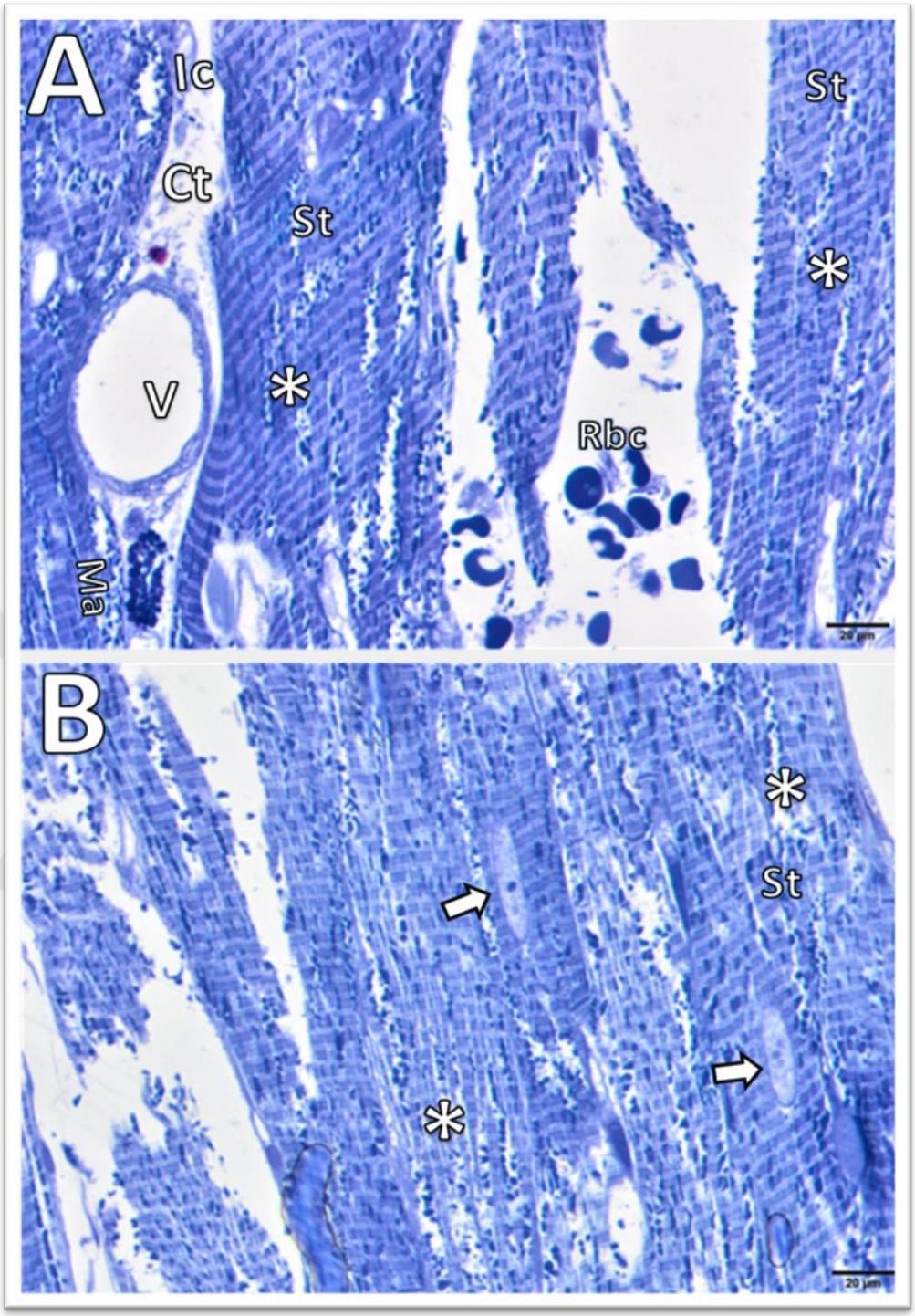


Figure 4.37. (A, B) Images of the heart tissue of the left ventricle are seen in the GA. The general structure of the heart tissue of the left ventricle is fine. The arrows indicate nuclei of the cardiac cells. (V) indicates the vessel. (Rbc) indicate collection of red blood cells. (Cap) indicate a blood capillary. (Ct) indicate connective tissue. (Ic) indicate interstitial cell. (St) indicate the striations of the cardiac cells. (Ma) mast cells. (*) indicates the muscle fibres. Toluidine blue stained semi-thin resin section (0.5 µm thickness). Original magnification: X100

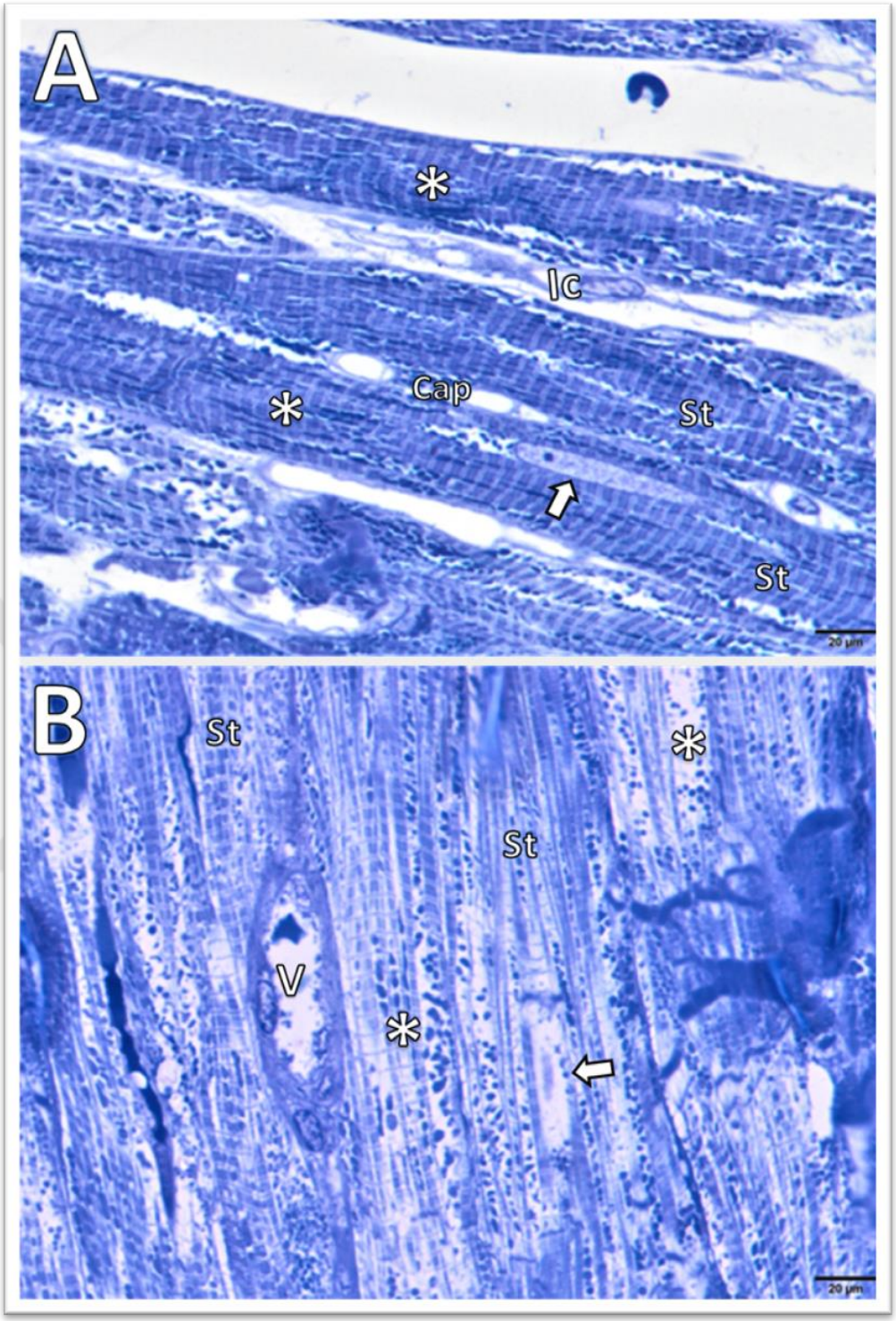


Figure 4.38. (A, B) Images of the heart tissue of the left ventricle are seen in the GA. The general structure of the heart tissue of the left ventricle is fine. The arrows indicate nuclei of the cardiac cells. (V) indicates the vessel. (Cap) indicate a blood capillary. (Ic) indicate interstitial cell. (St) indicate the striations of the cardiac cells. (Ma) mast cells. (*) indicates the muscle fibres. Toluidine blue stained semi-thin resin section (0.5 µm thickness). Original magnification: X100

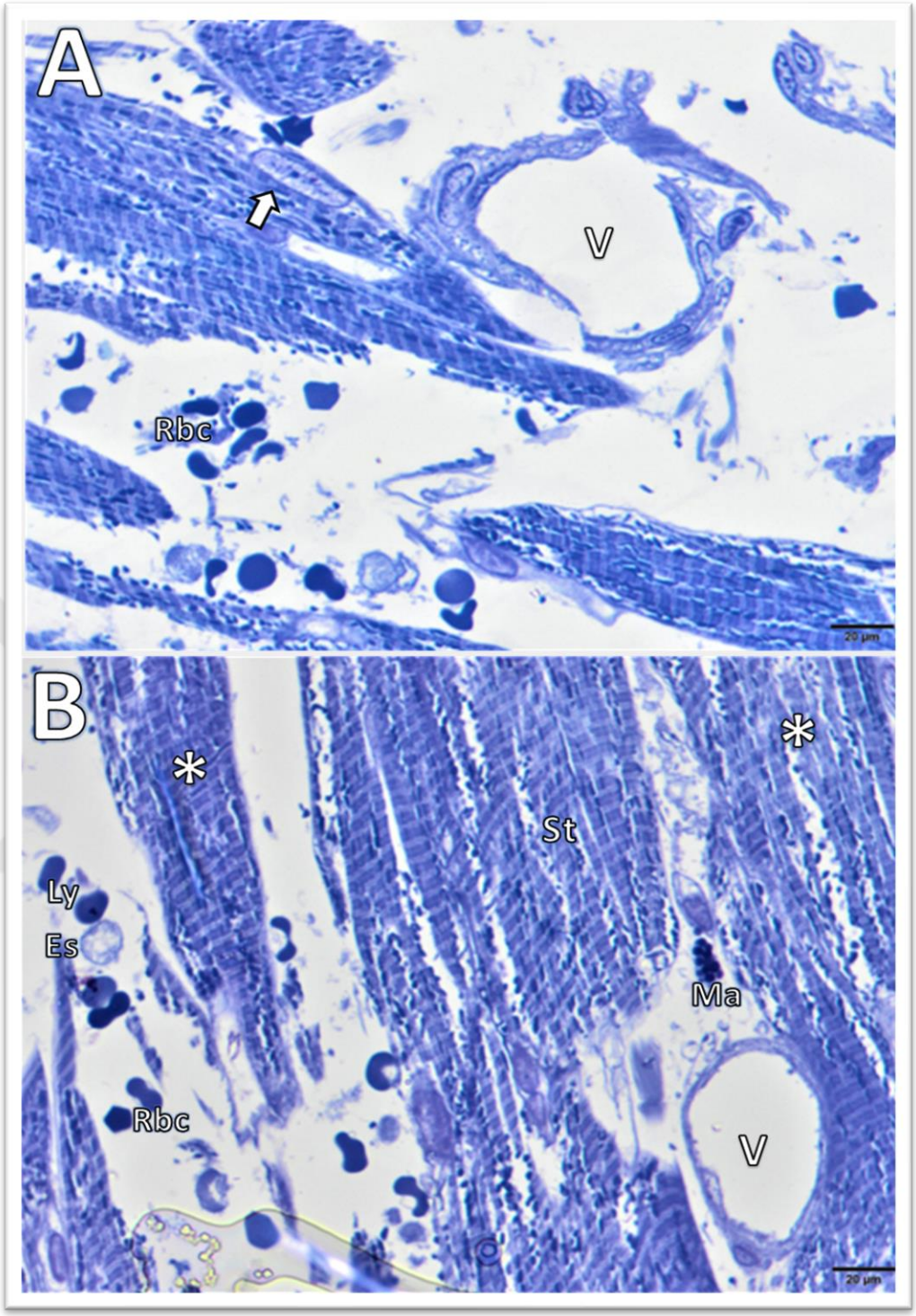


Figure 4.39. (A, B) Images of the heart tissue of the left ventricle are seen in the GA. The general structure of the heart tissue of the left ventricle is fine. The arrows indicate nuclei of the cardiac cells. (V) indicates the vessel. (Rbc) indicate collection of red blood cells. (Ic) indicate interstitial cell. (Es) indicate Eosinophil. (Ly) indicate lymphocyte. (St) indicate the striations of the cardiac cells. (Ma) mast cells. (*) indicates the muscle fibres. Toluidine blue stained semi-thin resin section (0.5 µm thickness). Original magnification: X100

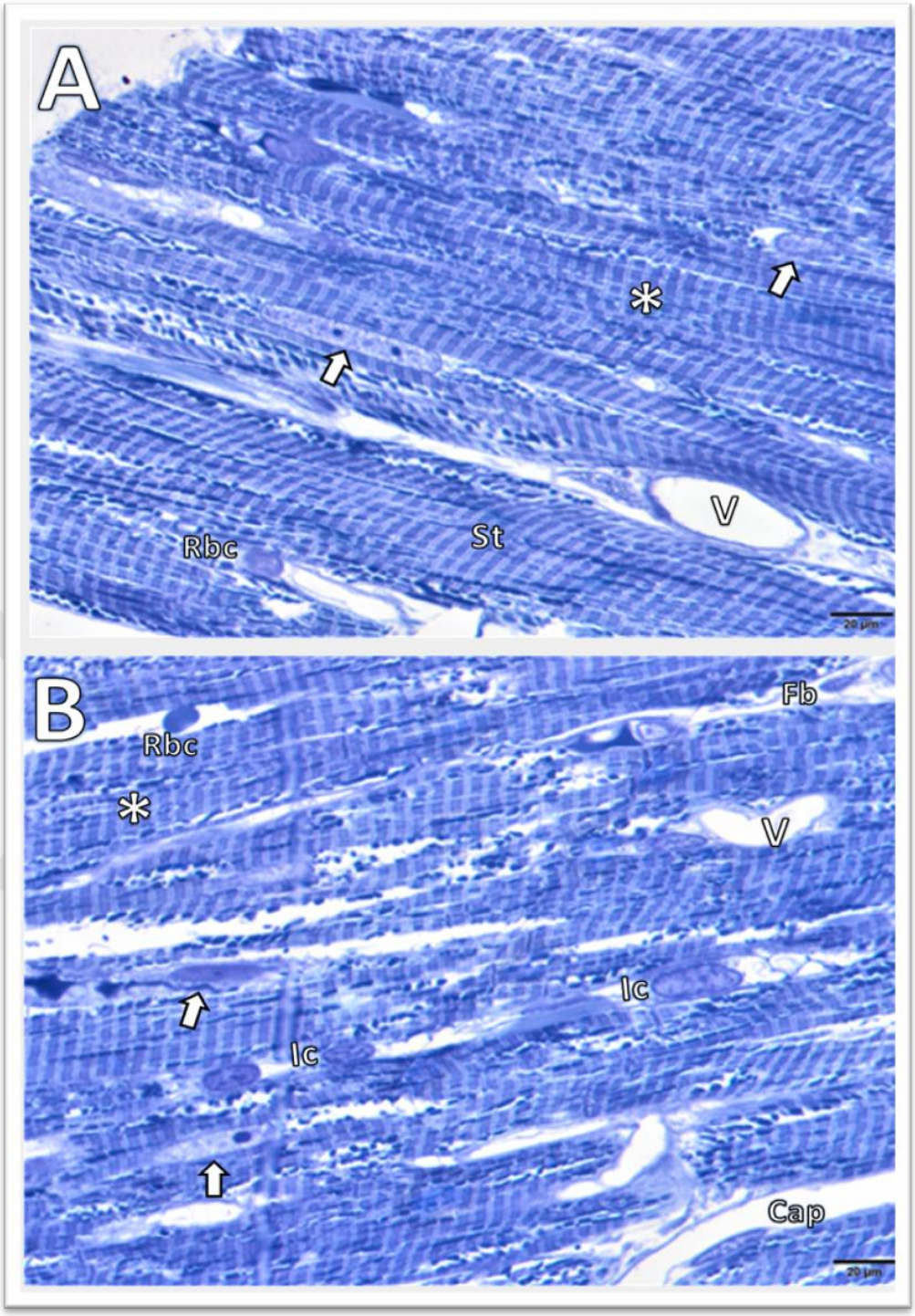


Figure 4.40. (A, B) Images of the heart tissue of the left ventricle are seen in the GA. The general structure of the heart tissue of the left ventricle is fine. The arrows indicate nuclei of the cardiac cells. (V) indicates the vessel. (Rbc) indicate collection of red blood cells. (Cap) indicate a blood capillary. (Ct) indicate connective tissue. (Ic) indicate interstitial cell. The letters (Fb) indicate the fibroblast cell. (St) indicate the striations of the cardiac cells. (*) indicates the muscle fibres. Toluidine blue stained semi-thin resin section (0.5 µm thickness). Original magnification: X100

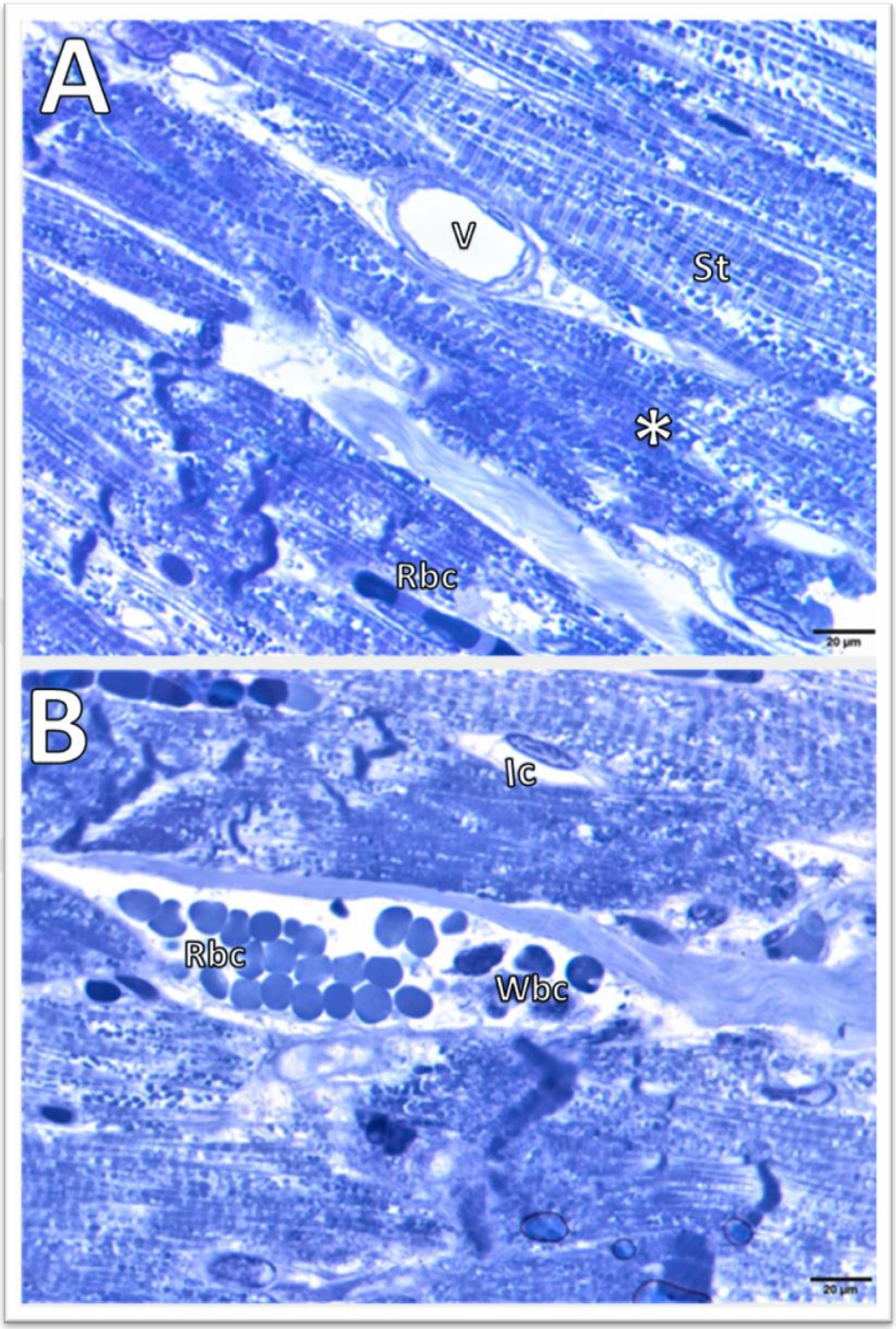


Figure 4.41. (A, B) Images of the heart tissue of the left ventricle are seen in the GA. The general structure of the heart tissue of the left ventricle is fine. The arrows indicate nuclei of the cardiac cells. (V) indicates the vessel. (Rbc) indicate collection of red blood cells. (Ic) indicate interstitial cell. (Wbc) indicate the white blood cells. (St) indicate the striations of the cardiac cells. (*) indicates the muscle fibres. Toluidine blue stained semi-thin resin section (0.5 µm thickness). Original magnification: X100

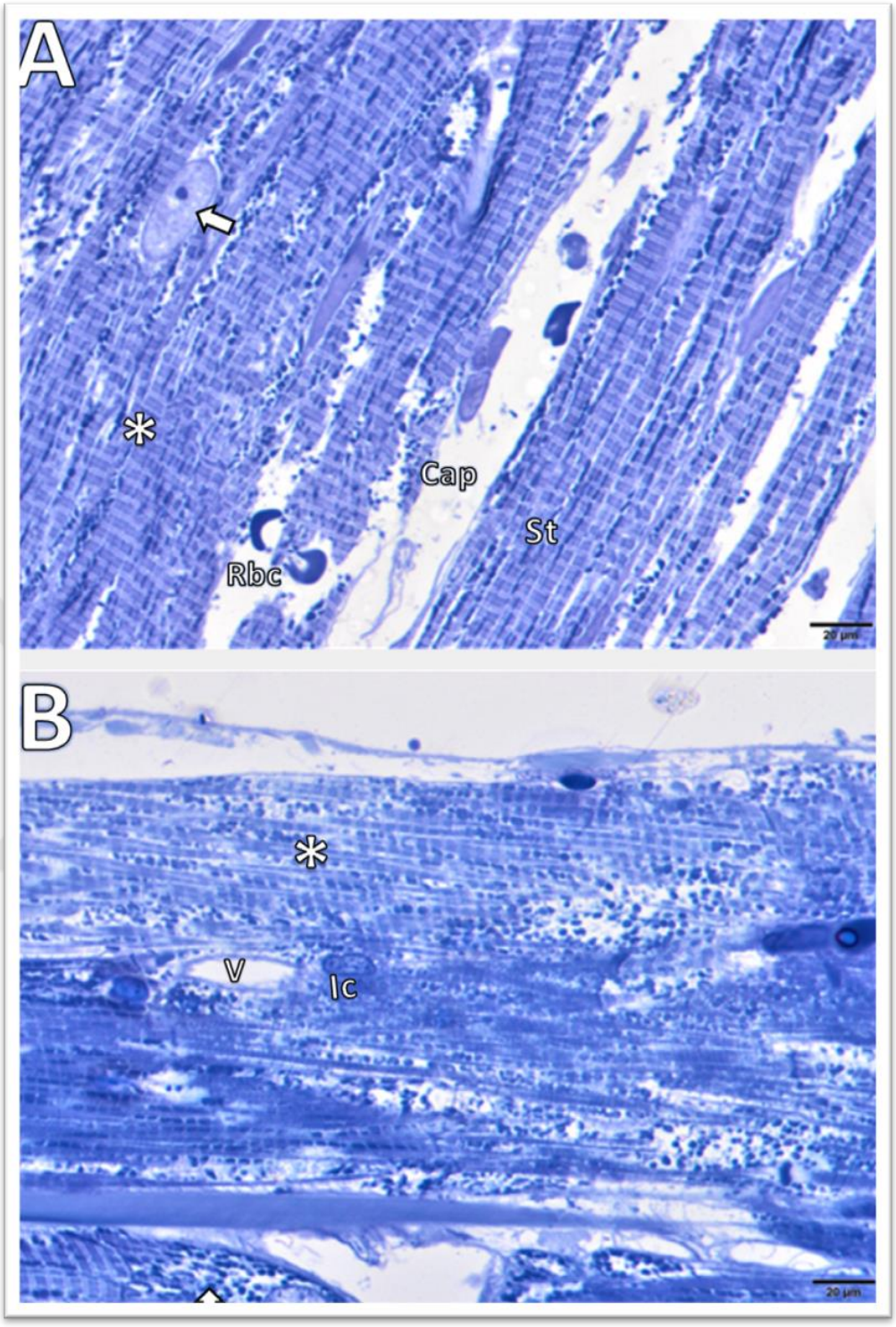


Figure 4.42. (A, B) Images of the heart tissue of the left ventricle are seen in the GA. The general structure of the heart tissue of the left ventricle is fine. The arrows indicate nuclei of the cardiac cells. (V) indicates the vessel. (Rbc) indicate collection of red blood cells. (Cap) indicate a blood capillary. (Ic) indicate interstitial cell. (St) indicate the striations of the cardiac cells. (*) indicates the muscle fibres. Toluidine blue stained semi-thin resin section (0.5 µm thickness). Original magnification: X100

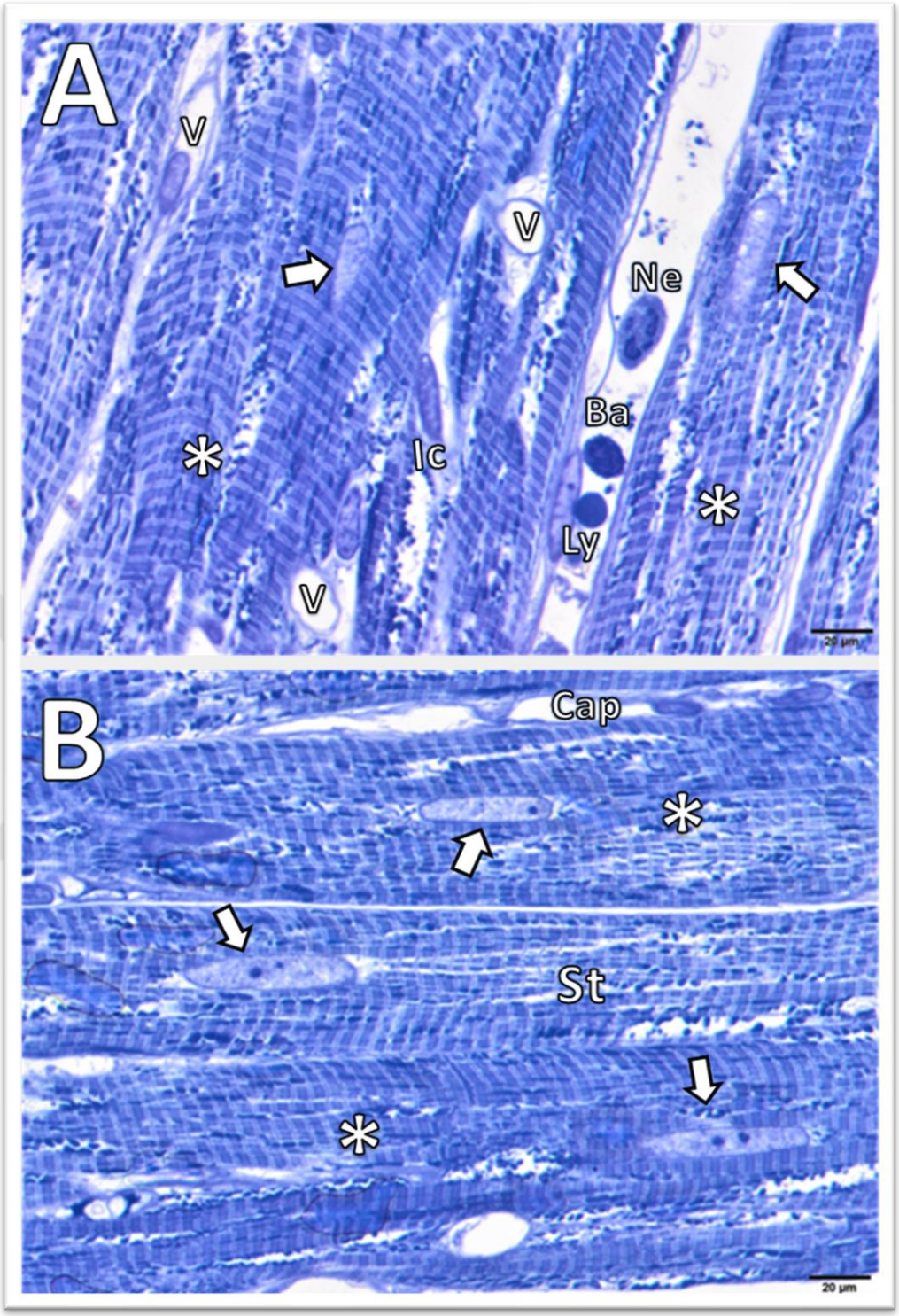


Figure 4.43. (A, B) Images of the heart tissue of the left ventricle are seen in the GA. The general structure of the heart tissue of the left ventricle is fine. The arrows indicate nuclei of the cardiac cells. (V) indicates the vessel. (Cap) indicate a blood capillary. (Ba) indicate Basophil. (Ic) indicate interstitial cell. (Ly) indicate lymphocyte. (Ne) indicate neutrophil. (St) indicate the striations of the cardiac cells. (*) indicates the muscle fibres. Toluidine blue stained semi-thin resin section (0.5 µm thickness). Original magnification: X100

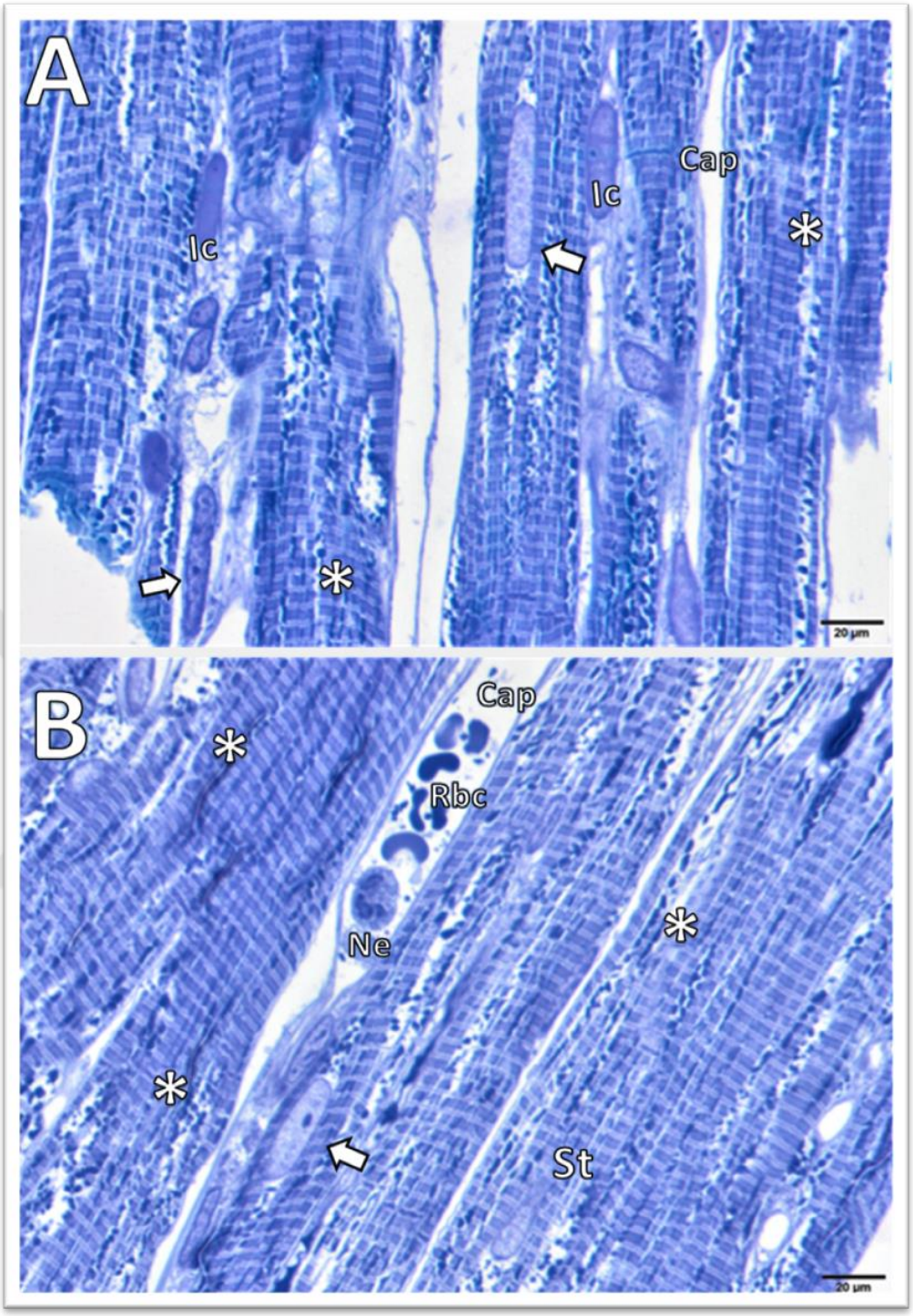


Figure 4.44. (A, B) Images of the heart tissue of the left ventricle are seen in the GA. The general structure of the heart tissue of the left ventricle is fine. The arrows indicate nuclei of the cardiac cells. (Rbc) indicate collection of red blood cells. (Cap) indicate a blood capillary. (Ic) indicate interstitial cell. (Ne) indicate neutrophil. (St) indicate the striations of the cardiac cells. (*) indicates the muscle fibres. Toluidine blue stained semi-thin resin section (0.5 µm thickness). Original magnification: X100

4.3.2.4. Toluidine Blue - Stained Sections; GA+DS Group

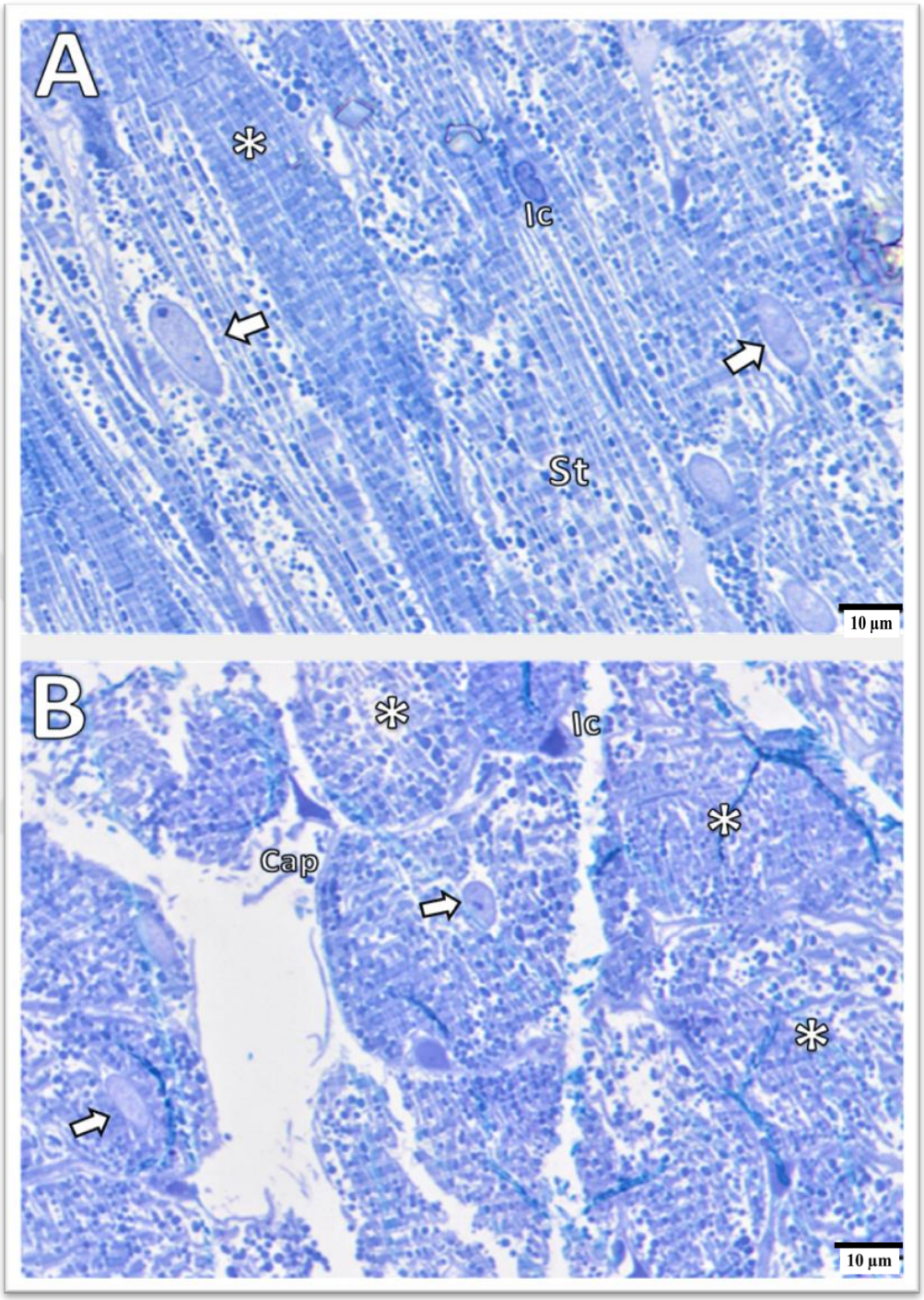


Figure 4.45. (A, B) Images of the heart tissue of the left ventricle are seen in the GA+DS. The general structure of the heart tissue of the left ventricle is fine. The arrows indicate nuclei of the cardiac cells. (Cap) indicate a blood capillary. (Ic) indicate interstitial cell. (St) indicate the striations of the cardiac cells. (*) indicates the muscle fibres. Toluidine blue stained semi-thin resin section (0.5 µm thickness). Original magnification: X100.

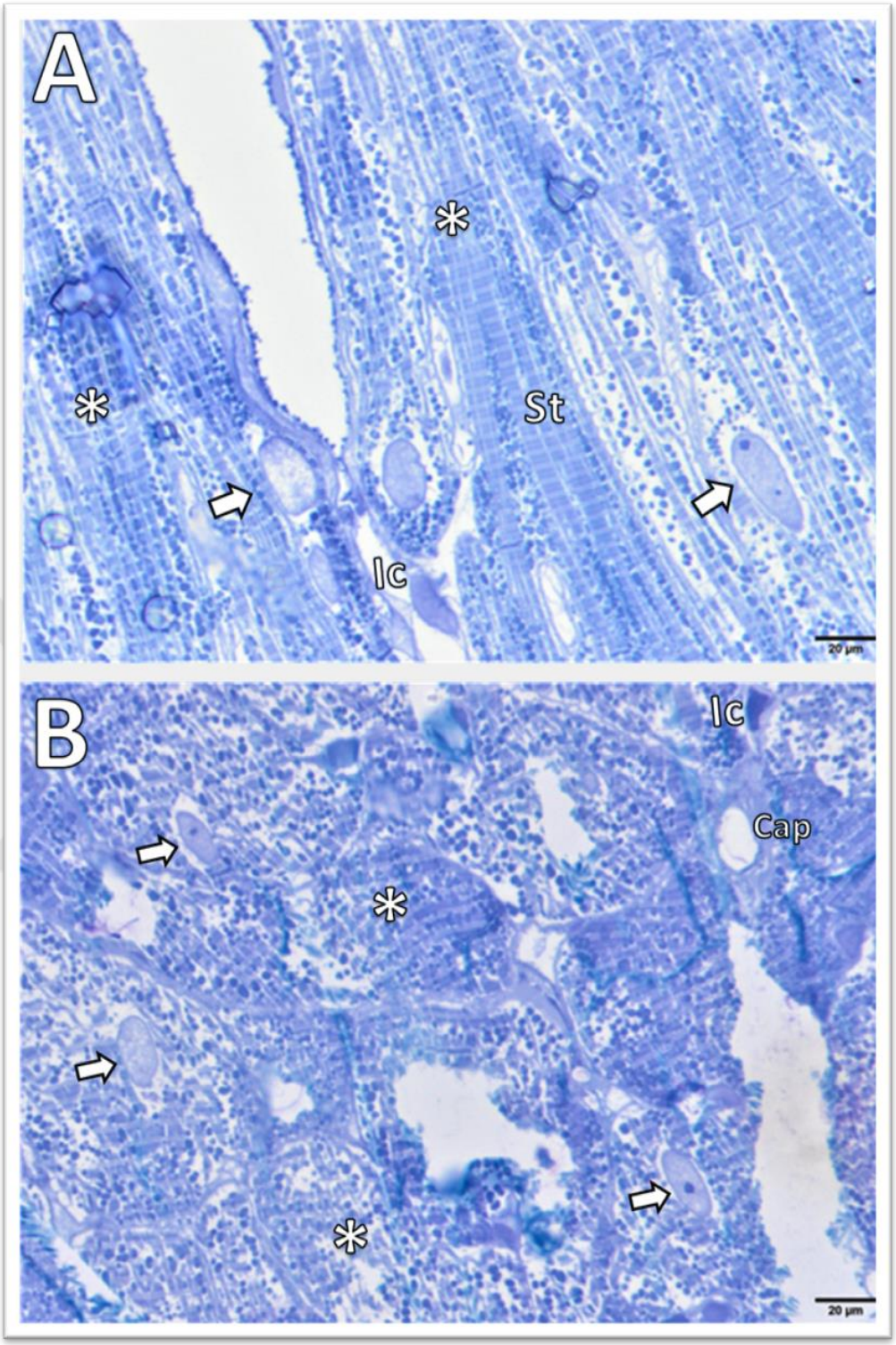


Figure 4.46. (A, B) Images of the heart tissue of the left ventricle are seen in the GA+DS. The general structure of the heart tissue of the left ventricle is fine. The arrows indicate nuclei of the cardiac cells. (Cap) indicate a blood capillary. (Ic) indicate interstitial cell. (*) indicates the muscle fibres. (St) indicate the striations of the cardiac cells. Toluidine blue stained semi-thin resin section (0.5 µm thickness). Original magnification: X100

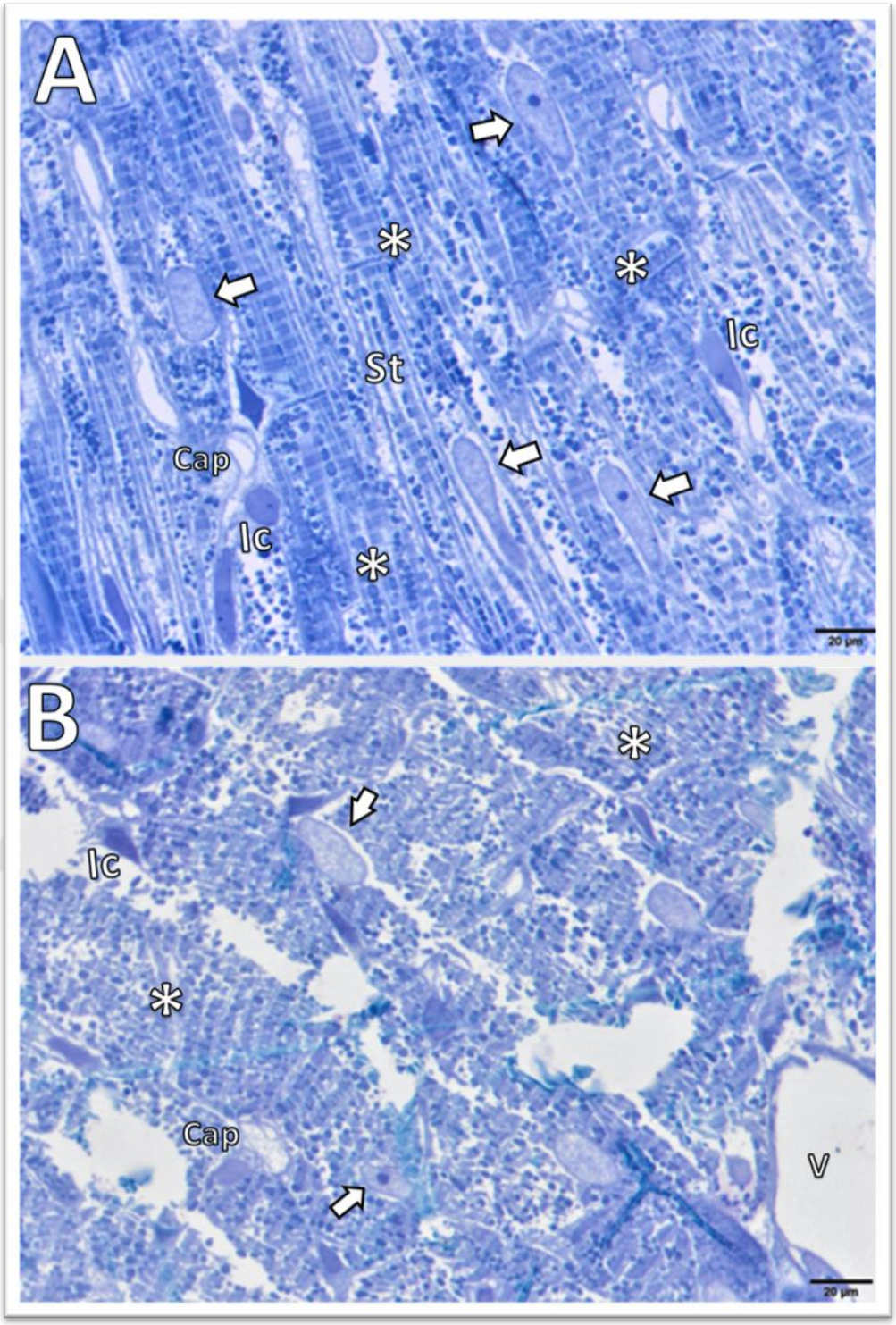


Figure 4.47. (A, B) Images of the heart tissue of the left ventricle are seen in the GA+DS. The general structure of the heart tissue of the left ventricle is fine. The arrows indicate nuclei of the cardiac cells. (Cap) indicate a blood capillary. (Ic) indicate interstitial cell. The letters (St) indicate the striations of the cardiac cells. (V) indicates the vessel. (*) indicates the muscle fibres. Toluidine blue stained semi-thin resin section (0.5 µm thickness). Original magnification: X100

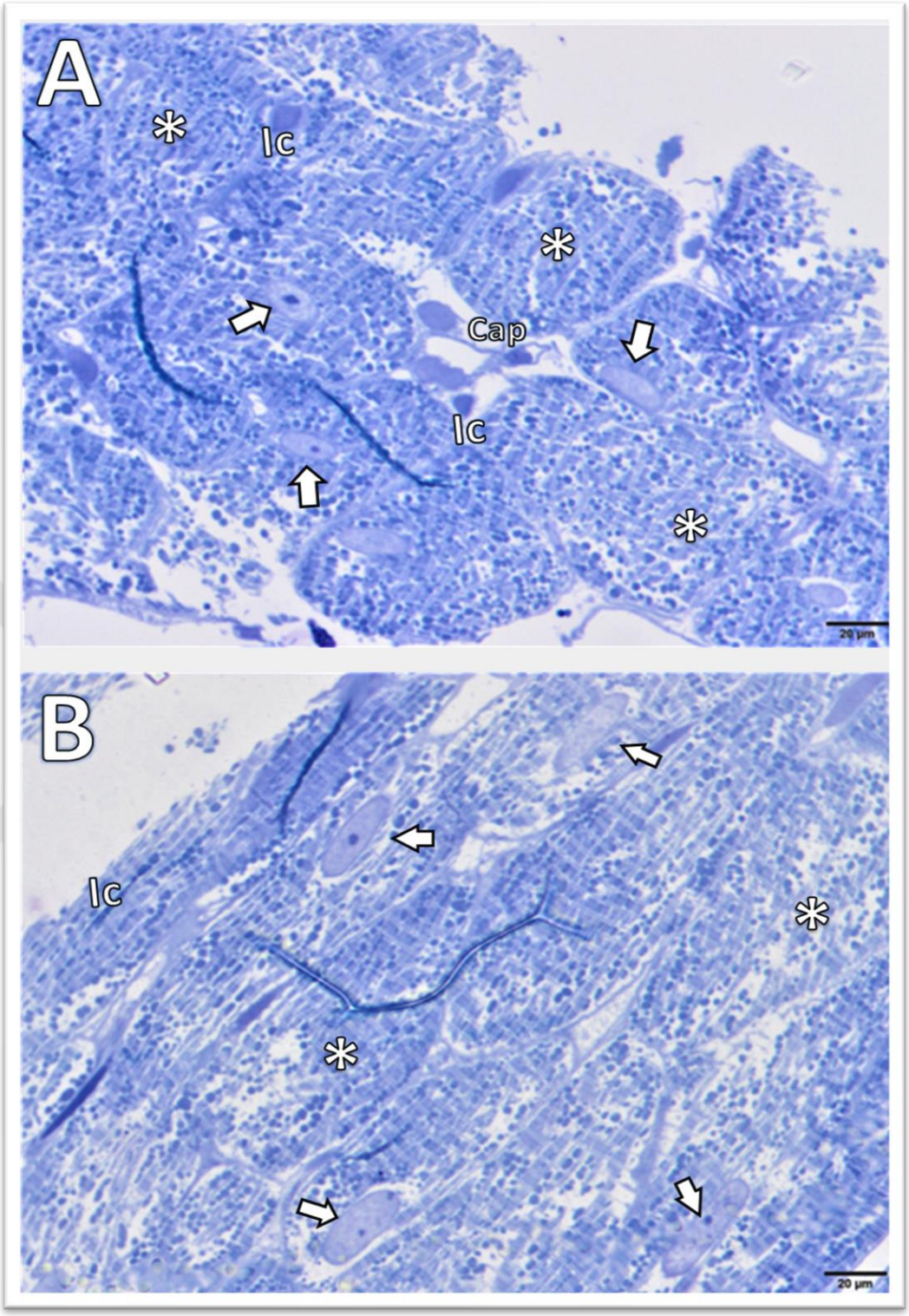


Figure 4.48. (A, B) Images of the heart tissue of the left ventricle are seen in the GA+DS. The general structure of the heart tissue of the left ventricle is fine. The arrows indicate nuclei of the cardiac cells. (Cap) indicate a blood capillary. (Ic) indicate interstitial cell. (*) indicates the muscle fibres. Toluidine blue stained semi-thin resin section (0.5 µm thickness). Original magnification: X100

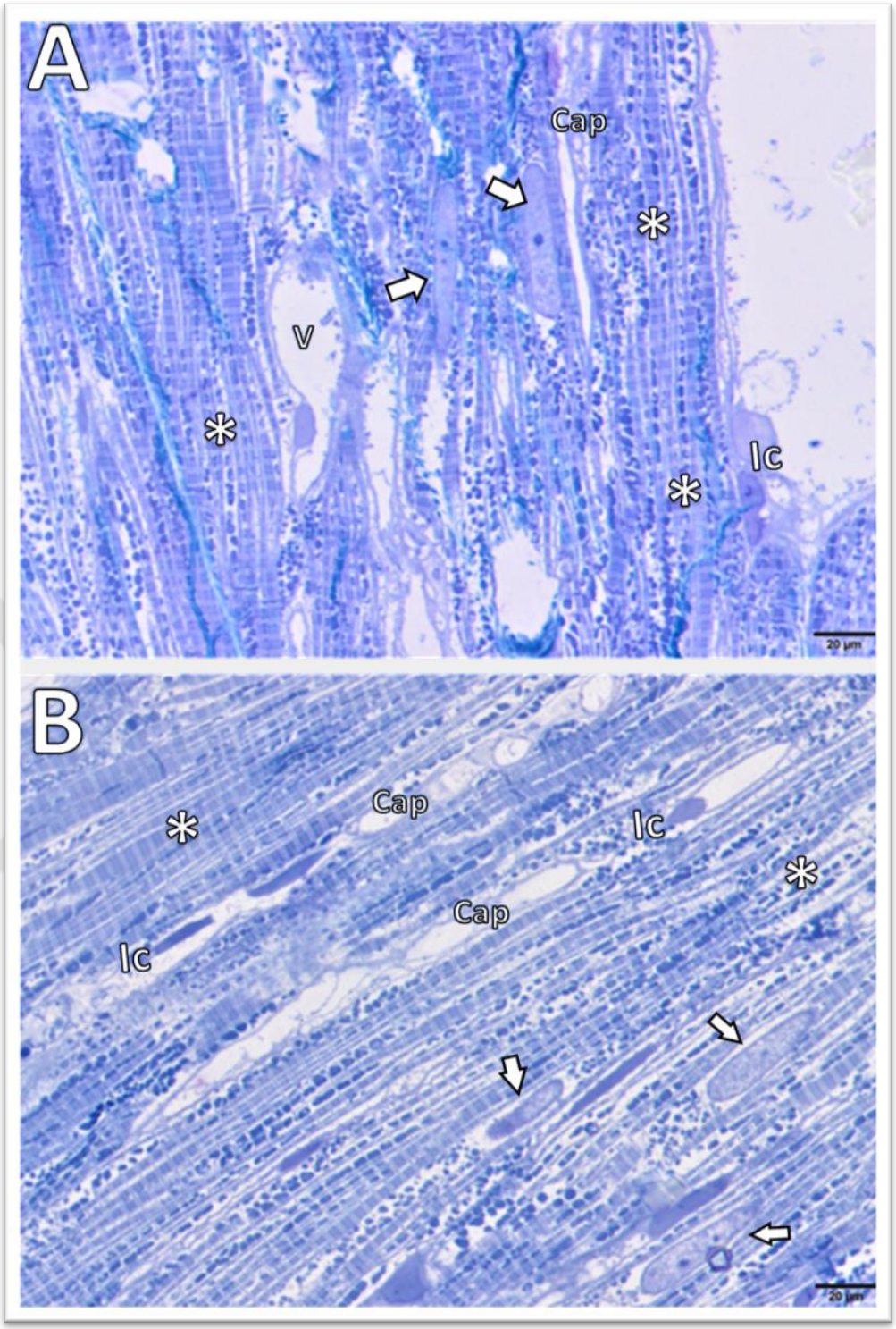


Figure 4.49. (A, B) Images of the heart tissue of the left ventricle are seen in the GA+DS. The general structure of the heart tissue of the left ventricle is fine. The arrows indicate nuclei of the cardiac cells. (V) indicates the vessel. (Cap) indicate a blood capillary. (Ic) indicate interstitial cell. (*) indicates the muscle fibres. Toluidine blue stained semi-thin resin section (0.5 µm thickness). Original magnification: X100

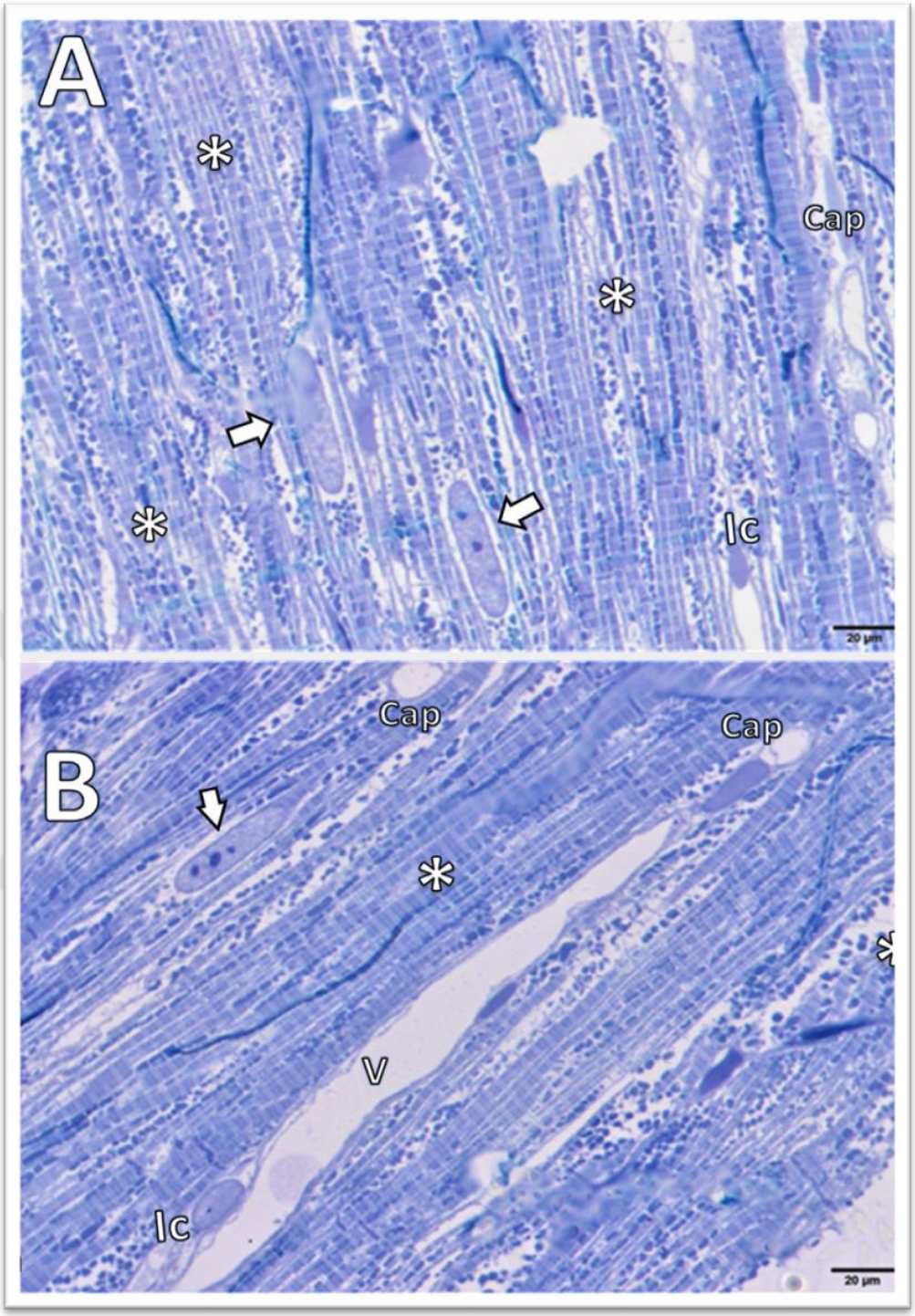


Figure 4.50. (A, B) Images of the heart tissue of the left ventricle are seen in the GA+DS. The general structure of the heart tissue of the left ventricle is fine. The arrows indicate nuclei of the cardiac cells. (V) indicates the vessel. (Cap) indicate a blood capillary. (Ic) indicate interstitial cell. (*) indicates the muscle fibres. Toluidine blue stained semi-thin resin section (0.5 µm thickness). Original magnification: X100

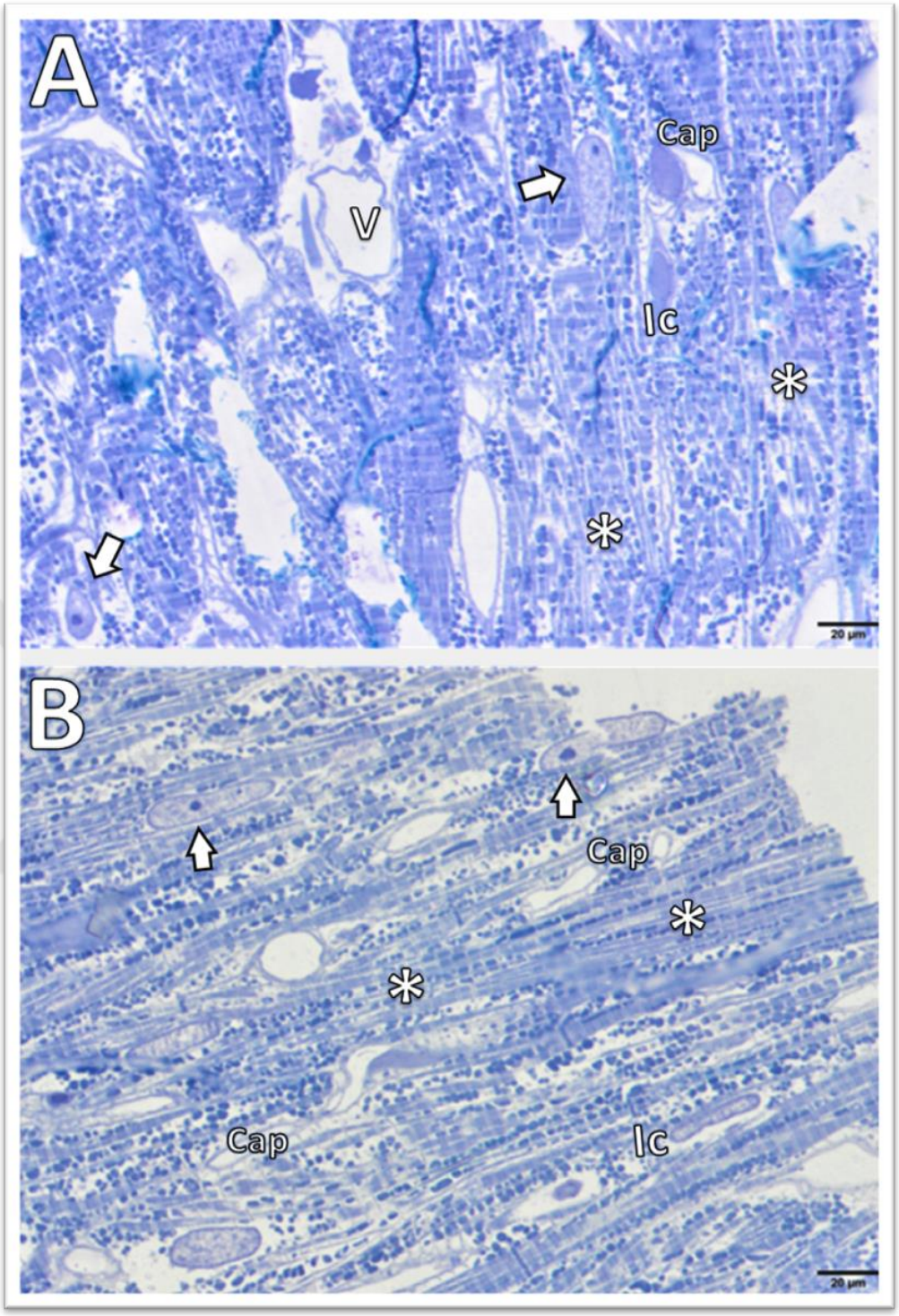


Figure 4.51. (A, B) Images of the heart tissue of the left ventricle are seen in the GA+DS. The general structure of the heart tissue of the left ventricle is fine. The arrows indicate nuclei of the cardiac cells. (V) indicates the vessel. (Cap) indicate a blood capillary. (Ic) indicate interstitial cell. (*) indicates the muscle fibres. Toluidine blue stained semi-thin resin section (0.5 µm thickness). Original magnification: X100

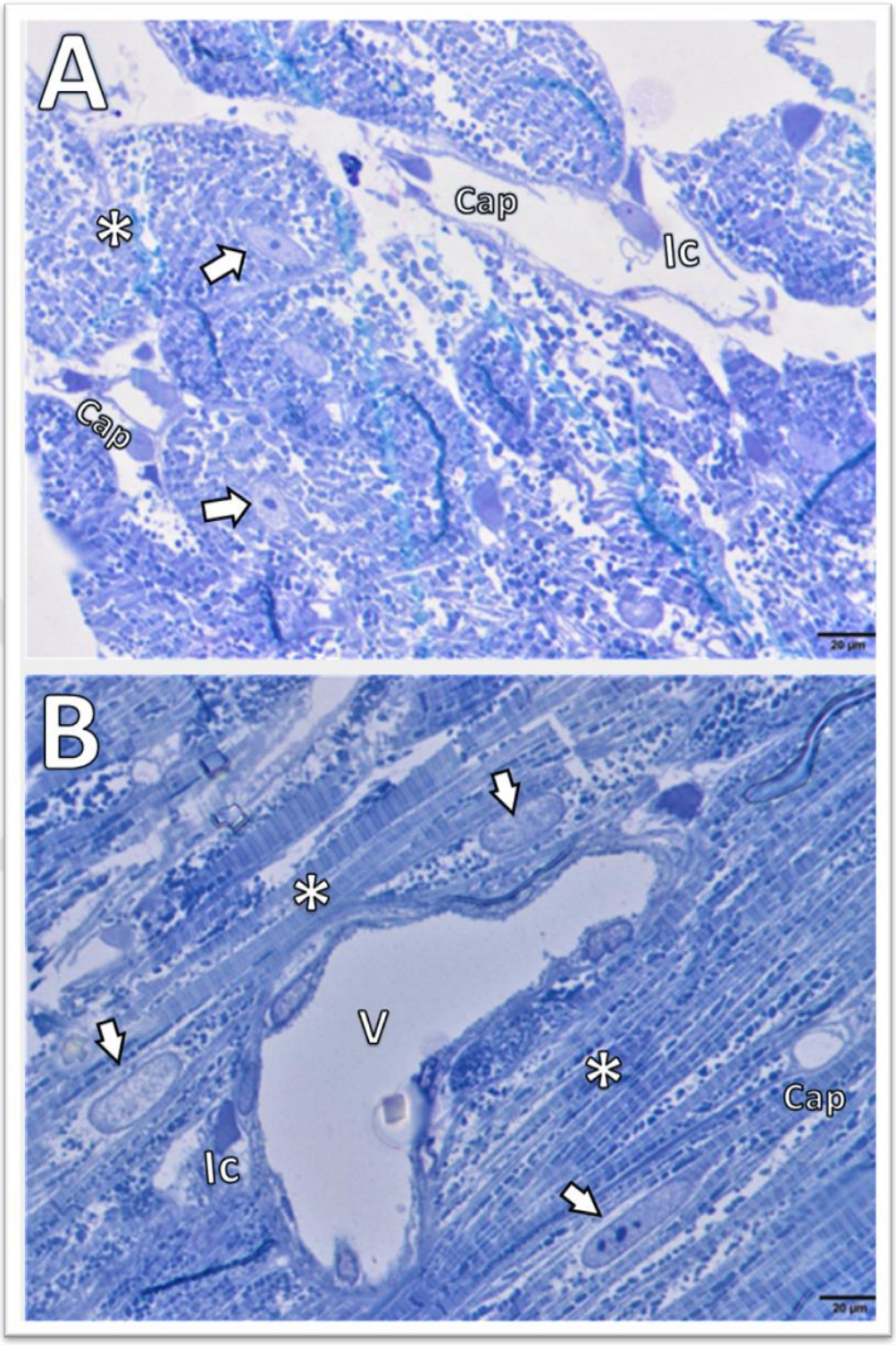


Figure 4.52. (A, B) Images of the heart tissue of the left ventricle are seen in the GA+DS. The general structure of the heart tissue of the left ventricle is fine. The arrows indicate nuclei of the cardiac cells. (V) indicates the vessel. Cap) indicate a blood capillary. (Ic) indicate interstitial cell. (*) indicates the muscle fibres. Toluidine blue stained semi-thin resin section (0.5 µm thickness). Original magnification: X100

4.3.3. Findings of Toluidine Blue - Stained Sections

Each cardiomyocyte has an elongated-shaped nucleus; the nuclei of cardiomyocytes and the cell features are seen. Cardiomyocytes of LV normally appeared except for some defragmentation of the tissue due to artifact of processing. The typical vascular and capillaries distribution between the cardiomyocytes were clearly noticed, especially in the transverse sections, longitudinal sections fortunately revealed the whole lengths of the myocytes with their unique features of the branching and striations.

4.3.4. Light Microscopic Findings of Masson Trichrome- Stained Sections

Tissue sections were taken from the left ventricle of all experimental animals. These sections were stained with toluidine blue stain, the slides were examined by the light microscope and the visualisations were shown as follow (Figures 4.53- 4.76**).**

4.3.4.1. Masson Trichrome- Stained Sections: CON Group

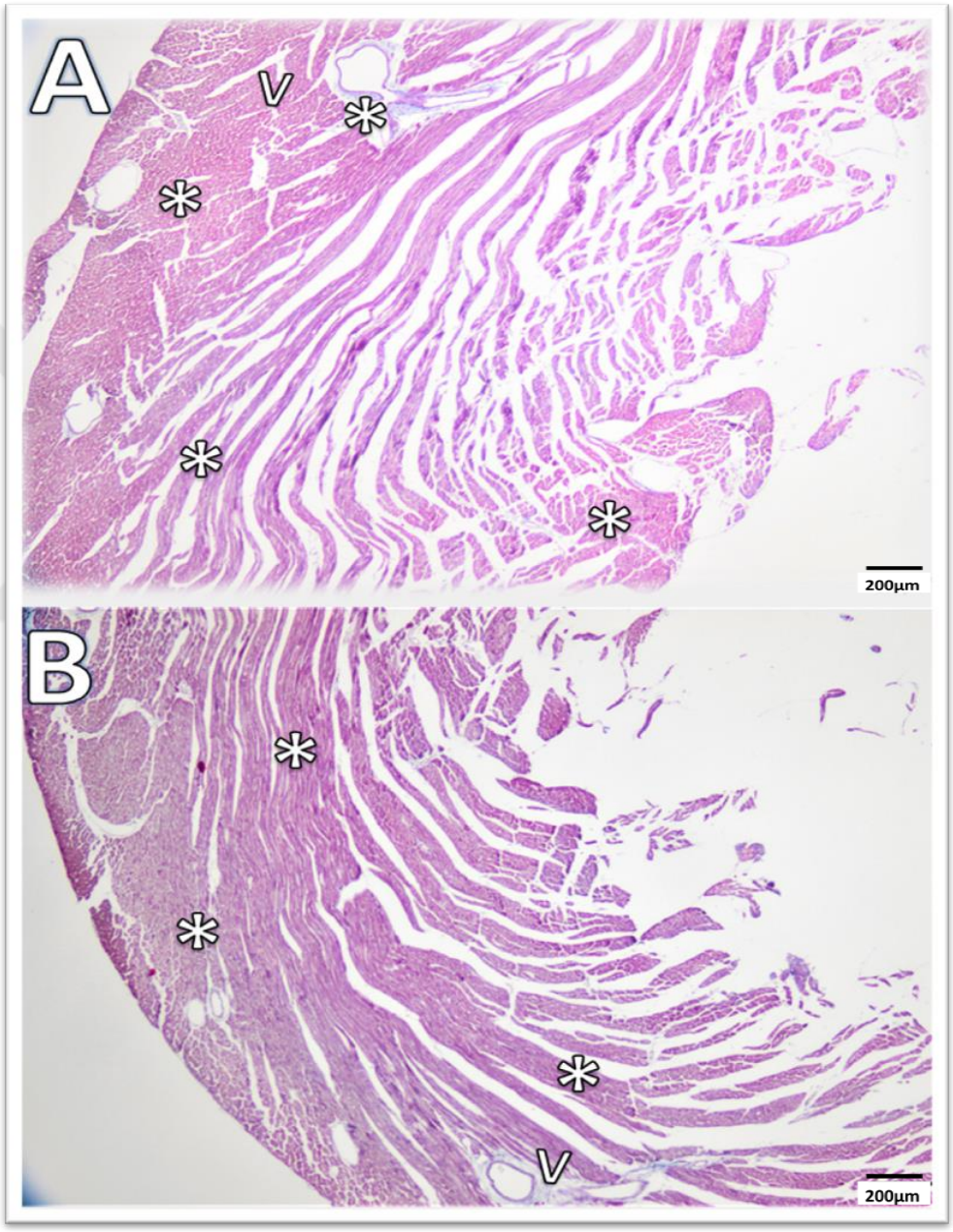


Figure 4.53. (A, B) Images of the heart tissue of the left ventricle are seen in the CON. The general structure of the heart tissue of the left ventricle is fine. The arrows indicate nuclei of the cardiac cells. (V) indicates the vessel. (*) indicates the muscle fibres. Masson trichrome stained section (5 µm thickness). Original magnification: X10.

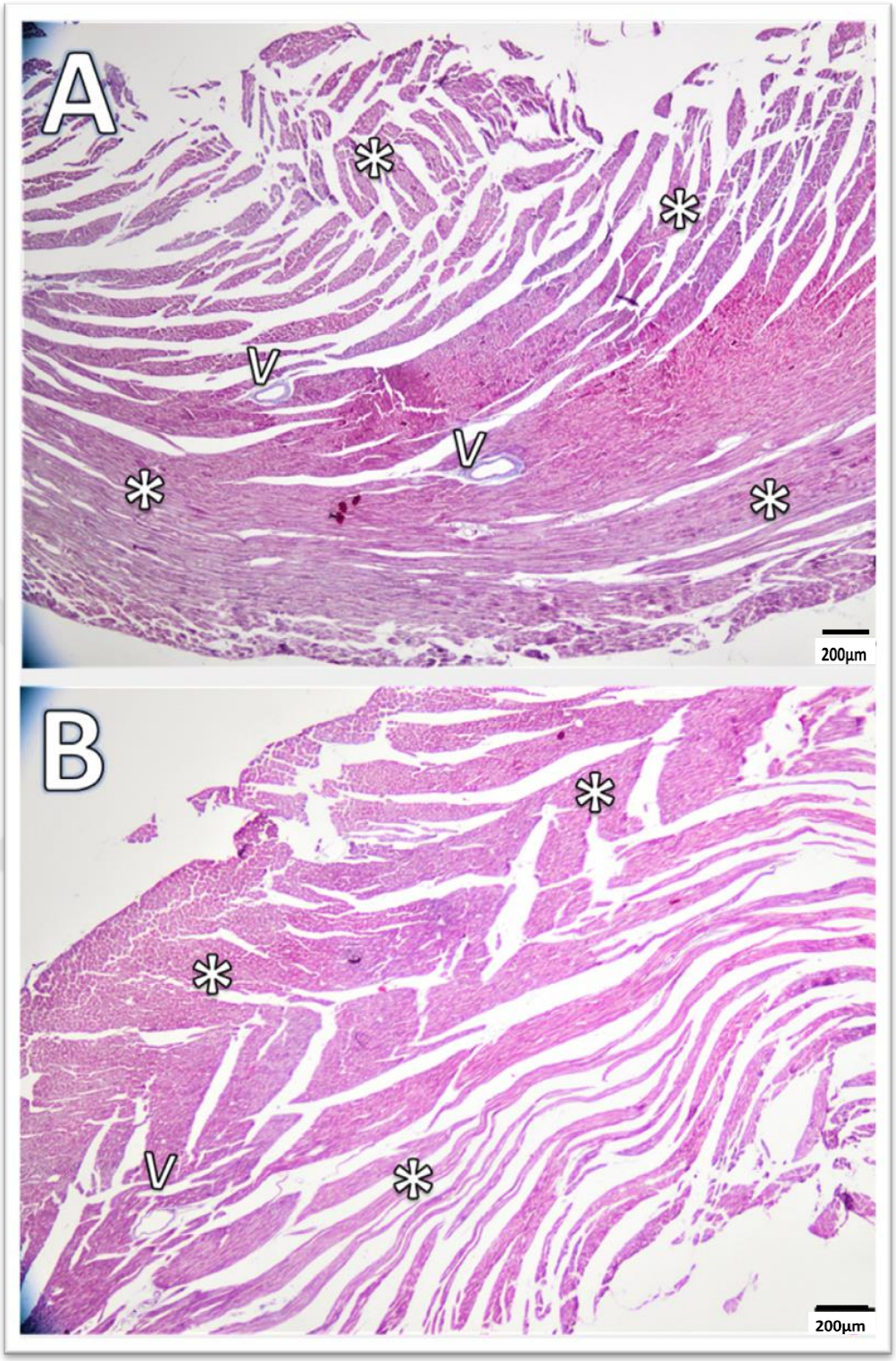


Figure 4.54. (A, B) Images of the heart tissue of the left ventricle are seen in the CON. The general structure of the heart tissue of the left ventricle is fine. The arrows indicate nuclei of the cardiac cells. (V) indicates the vessel. (*) indicates the muscle fibres. Masson trichrome stained section (5 µm thickness). Original magnification: X10.

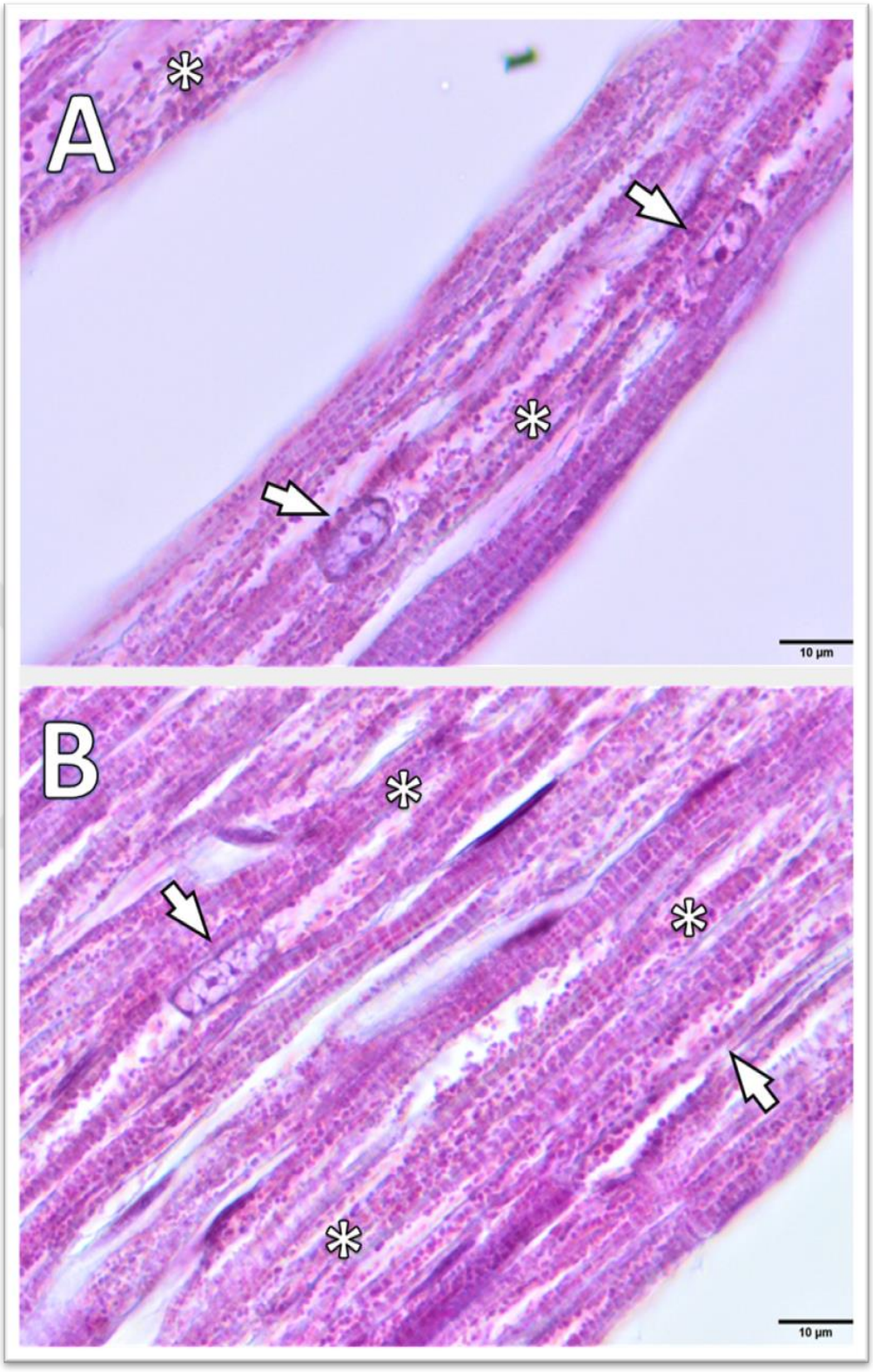


Figure 4.55. (A, B) Images of the heart tissue of the left ventricle are seen in the CON. The general structure of the heart tissue of the left ventricle is fine. The arrows indicate nuclei of the cardiac cells. (*) indicates the muscle fibres. Masson trichrome stained section (5 µm thickness). Original magnification: X100

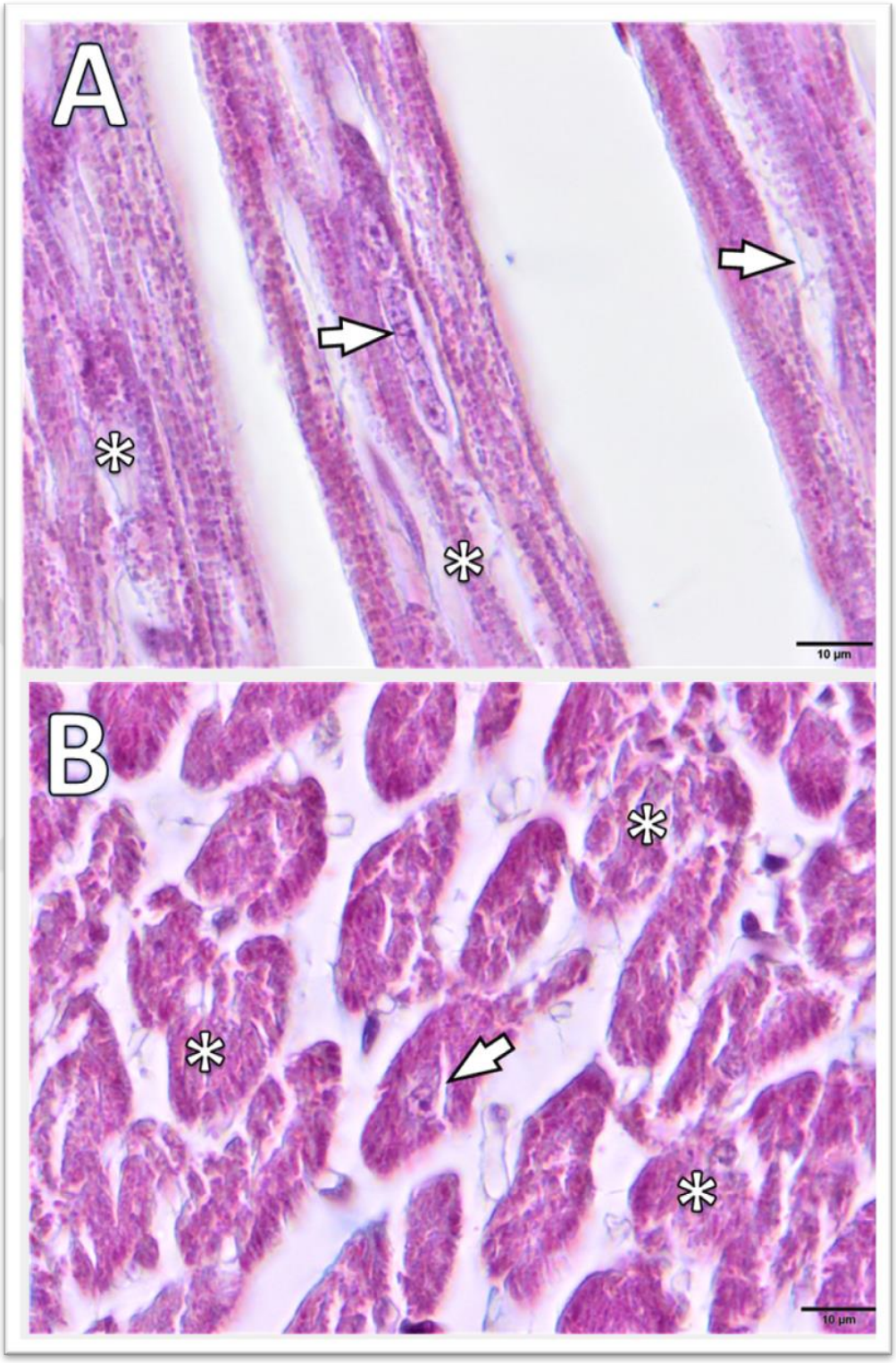


Figure 4.56. (A, B) Images of the heart tissue of the left ventricle are seen in the CON. The general structure of the heart tissue of the left ventricle is fine. The arrows indicate nuclei of the cardiac cells. (*) indicates the muscle fibres. Masson trichrome stained section (5 µm thickness). Original magnification: X100

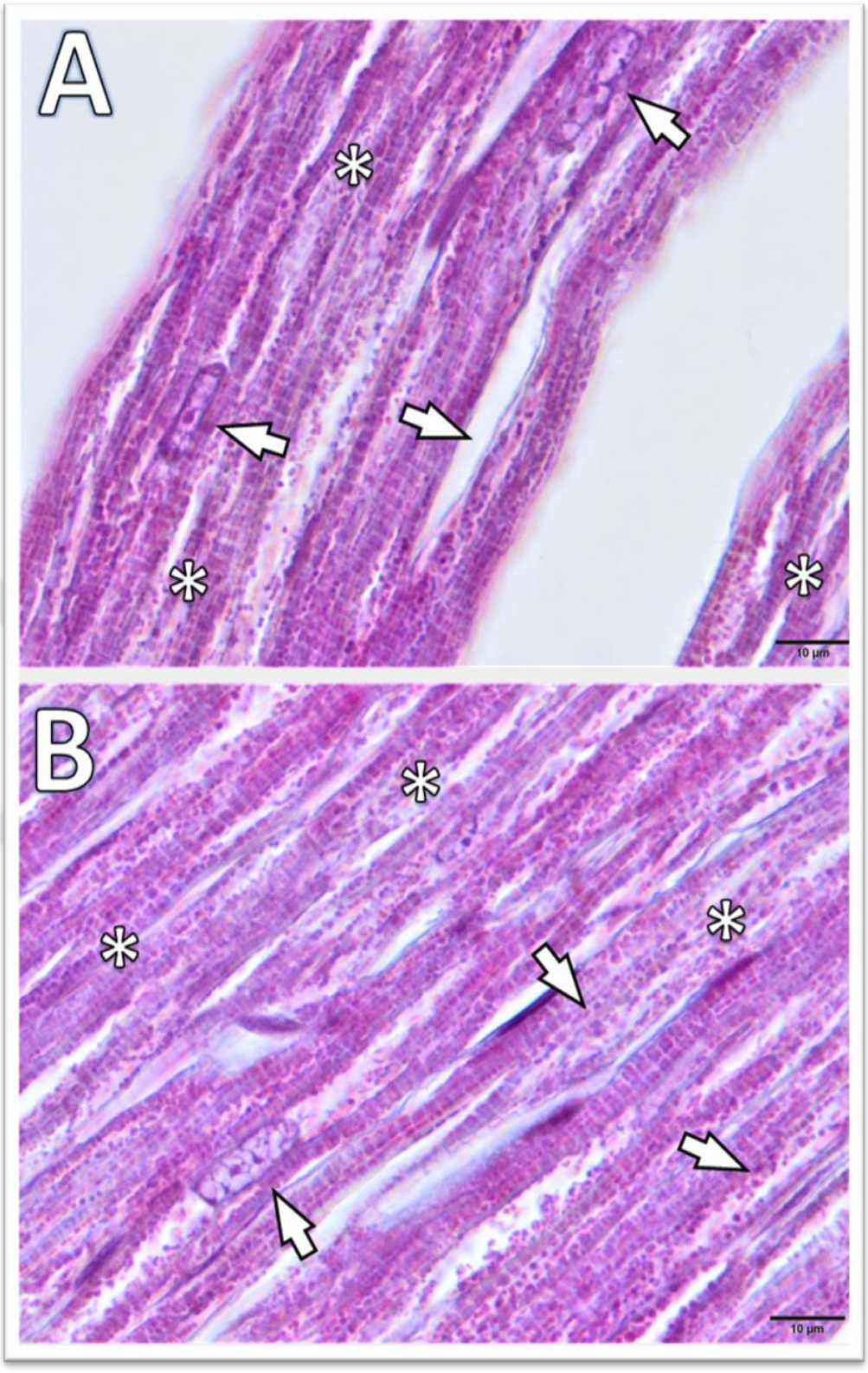


Figure 4.57. (A, B) Images of the heart tissue of the left ventricle are seen in the CON. The general structure of the heart tissue of the left ventricle is fine. The arrows indicate nuclei of the cardiac cells. (*) indicates the muscle fibres. Masson trichrome stained section (5 µm thickness). Original magnification: X100.

4.3.4.2. Masson Trichrome Stained Sections: DS Group

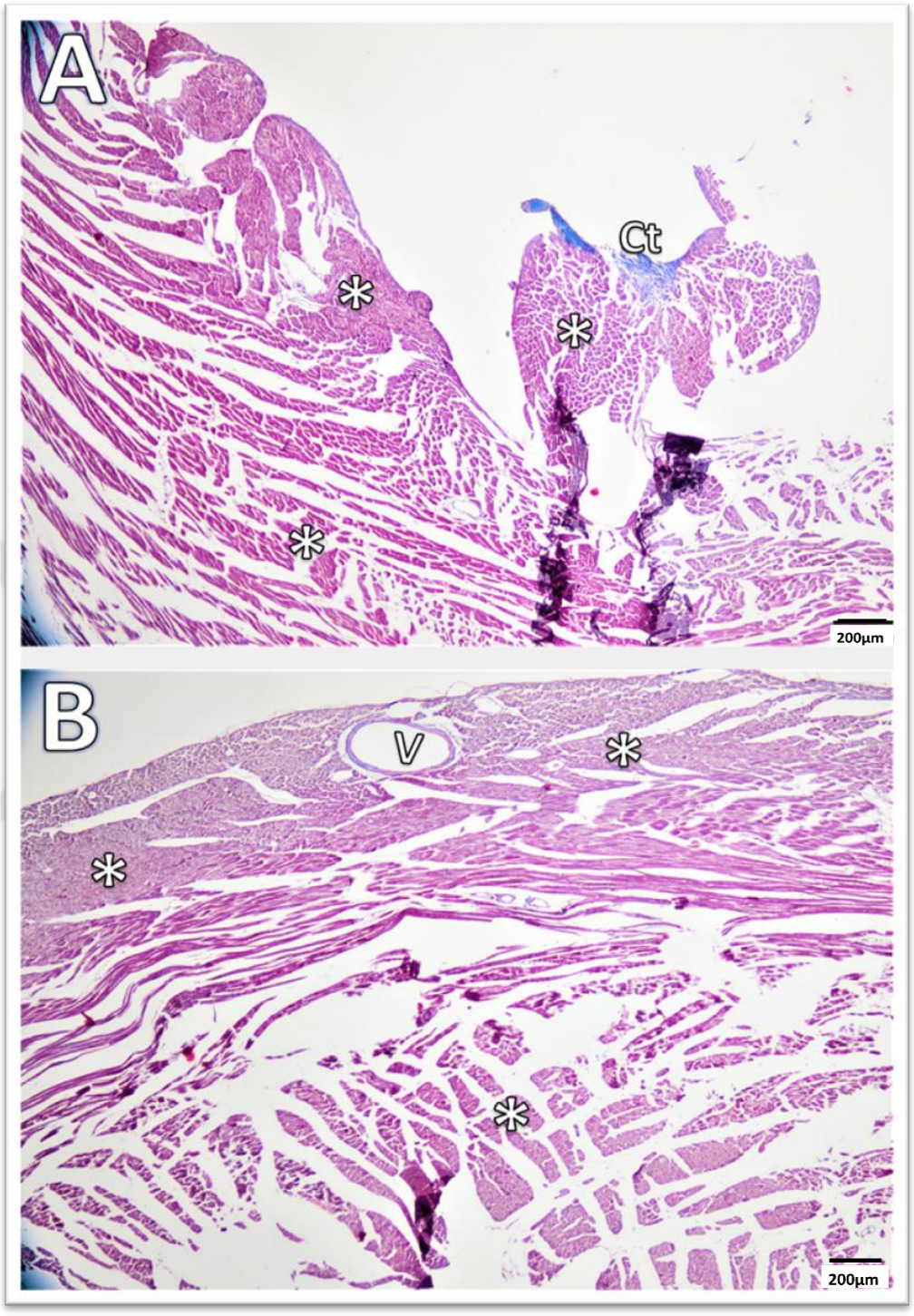


Figure 4.58. (A, B) Images of the heart tissue of the left ventricle are seen in the DS. The general structure of the heart tissue of the left ventricle is fine. The arrows indicate nuclei of the cardiac cells. (V) indicates the vessel. (Ct) indicate the muscle fibres. Masson trichrome stained section (5 µm thickness). Original magnification: X10.

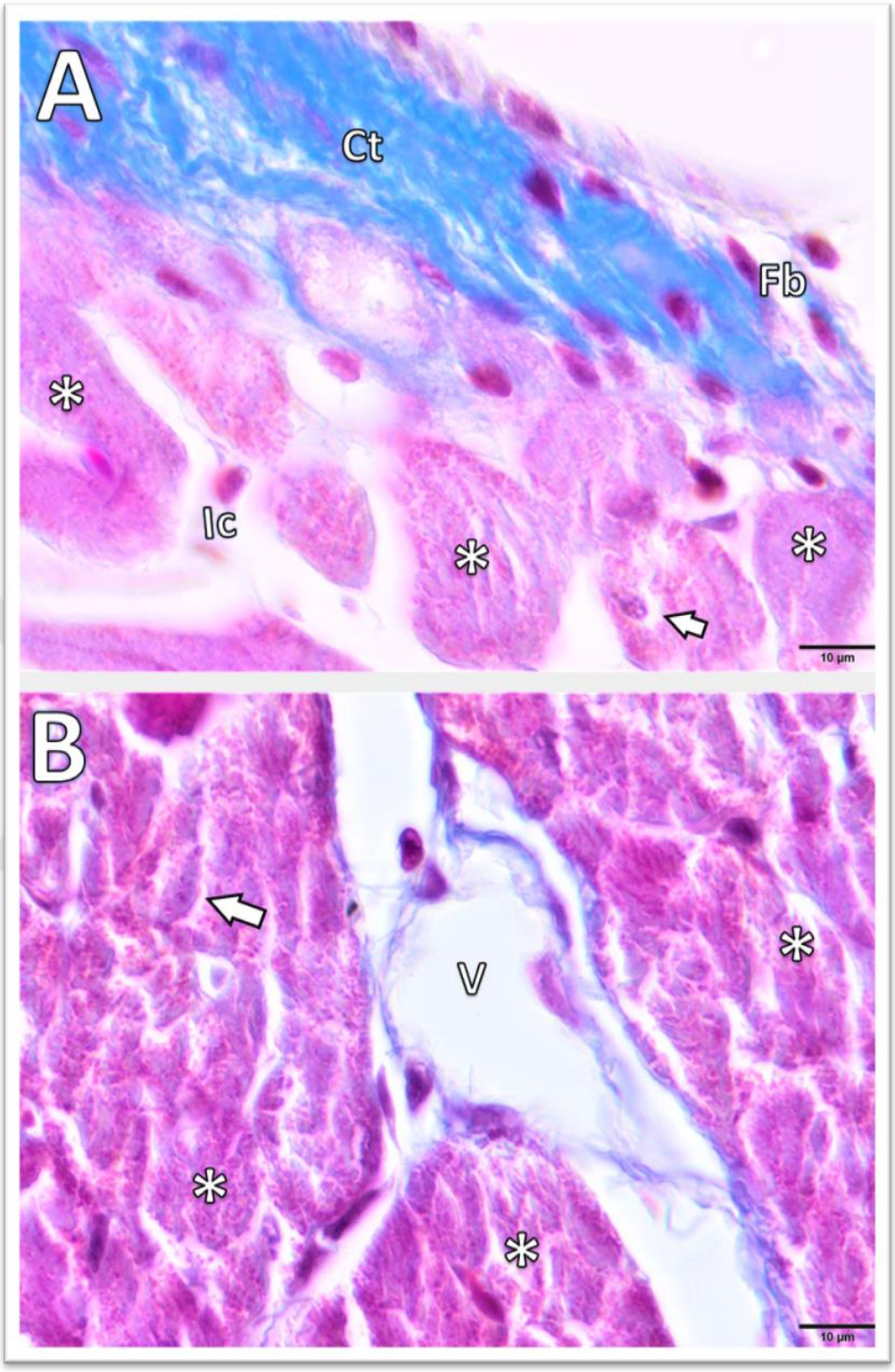


Figure 4.59. (A, B) Images of the heart tissue of the left ventricle are seen in the DS. The general structure of the heart tissue of the left ventricle is fine. The arrows indicate nuclei of the cardiac cells. (V) indicates the vessel. (Ct) indicate connective tissue. (Ic) indicate interstitial cell. (Fb) indicate the fibroblast cell. (*) indicates the muscle fibres. Masson trichrome stained section (5 µm thickness). Original magnification: X100

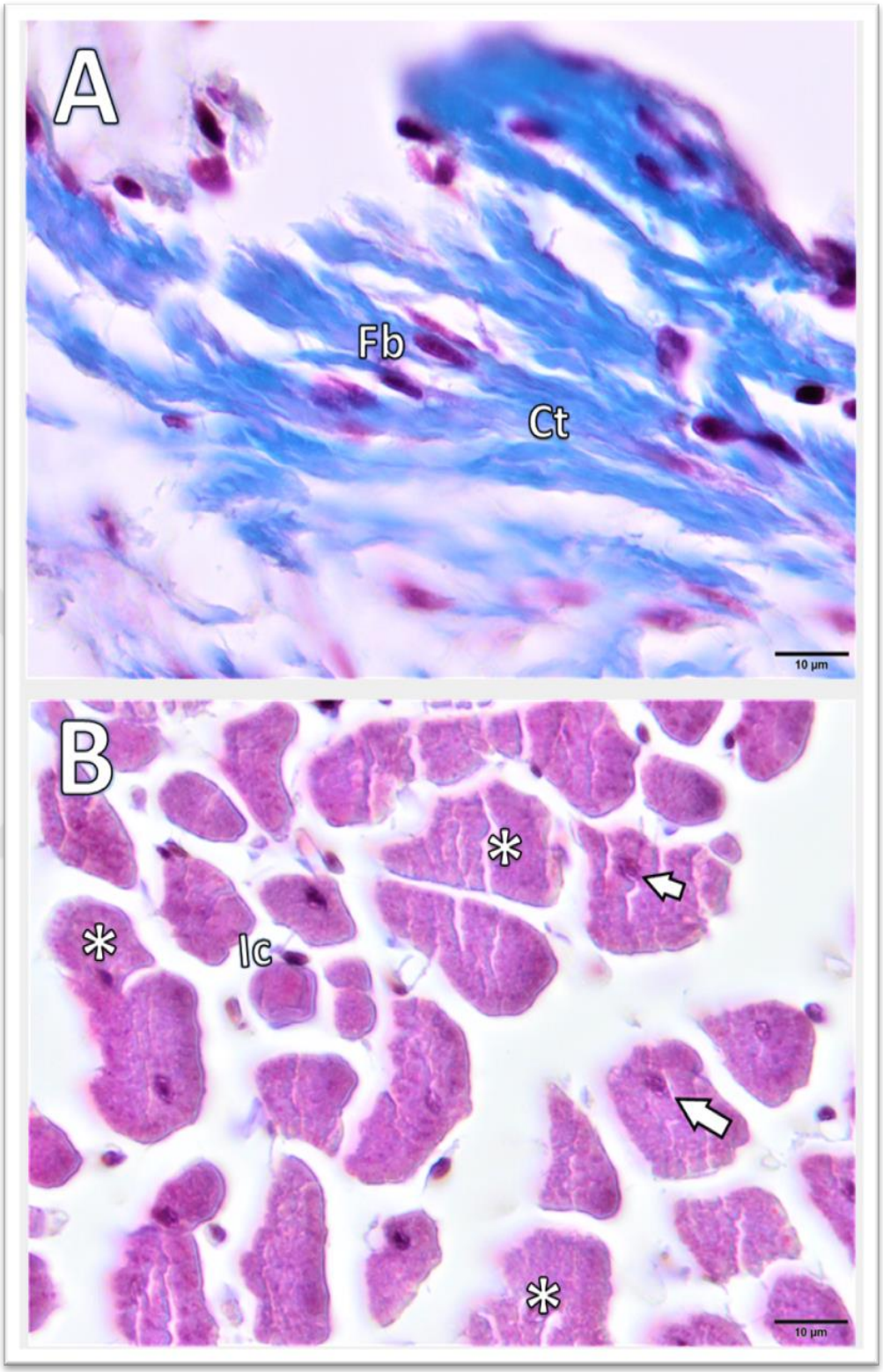


Figure 4.60. (A, B) Images of the heart tissue of the left ventricle are seen in the DS. The general structure of the heart tissue of the left ventricle is fine. The arrows indicate nuclei of the cardiac cells. (Ct) indicate connective tissue. (Ic) indicate interstitial cell. (Fb) indicate the fibroblast cell. (*) indicates the muscle fibres. Masson trichrome stained section (5 µm thickness). Original magnification: X100

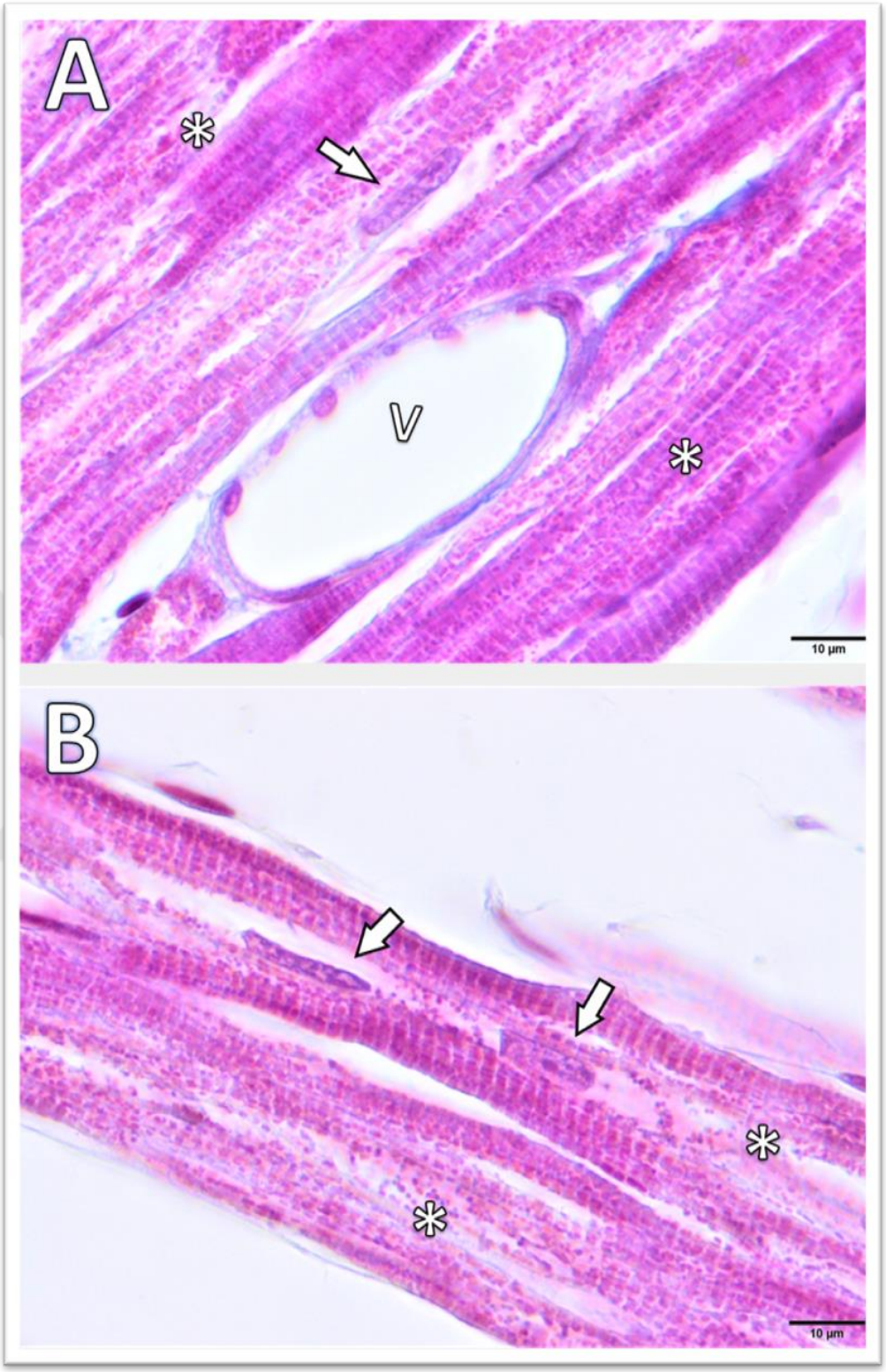


Figure 4.61. (A, B) Images of the heart tissue of the left ventricle are seen in the DS. The general structure of the heart tissue of the left ventricle is fine. The arrows indicate nuclei of the cardiac cells. (V) indicates the vessel. (*) indicates the muscle fibres. Masson trichrome stained section (5 µm thickness). Original magnification: X100

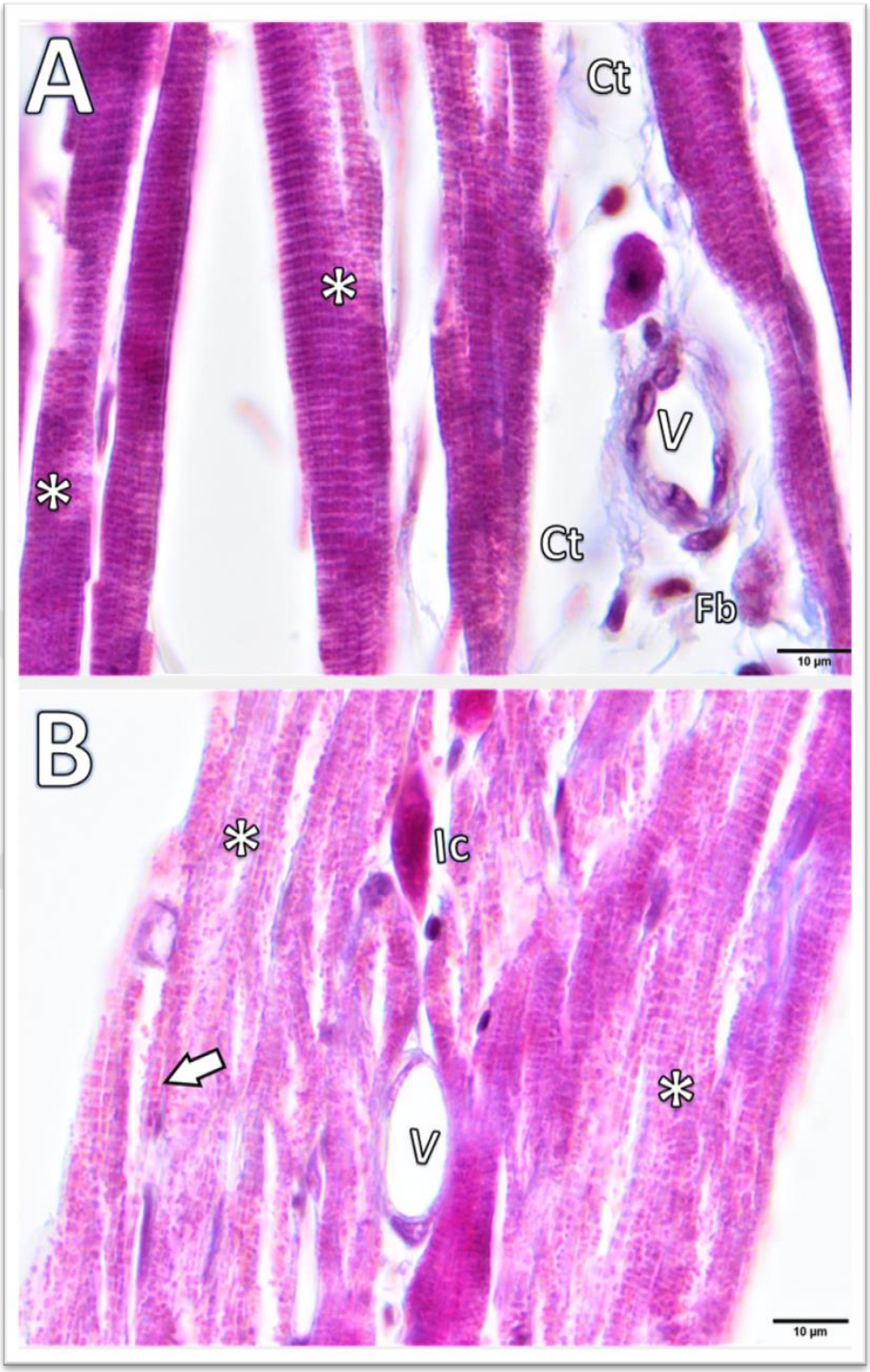


Figure 4.62. (A, B) Images of the heart tissue of the left ventricle are seen in the DS.The general structure of the heart tissue of the left ventricle is fine. The arrows indicate nuclei of the cardiac cells. (V) indicates the vessel. (Ct) indicate connective tissue. (Ic) indicate interstitial cell. The letters (Fb) indicate the fibroblast cell. (*) indicates the muscle fibres. Masson trichrome stained section (5 µm thickness). Original magnification: X100

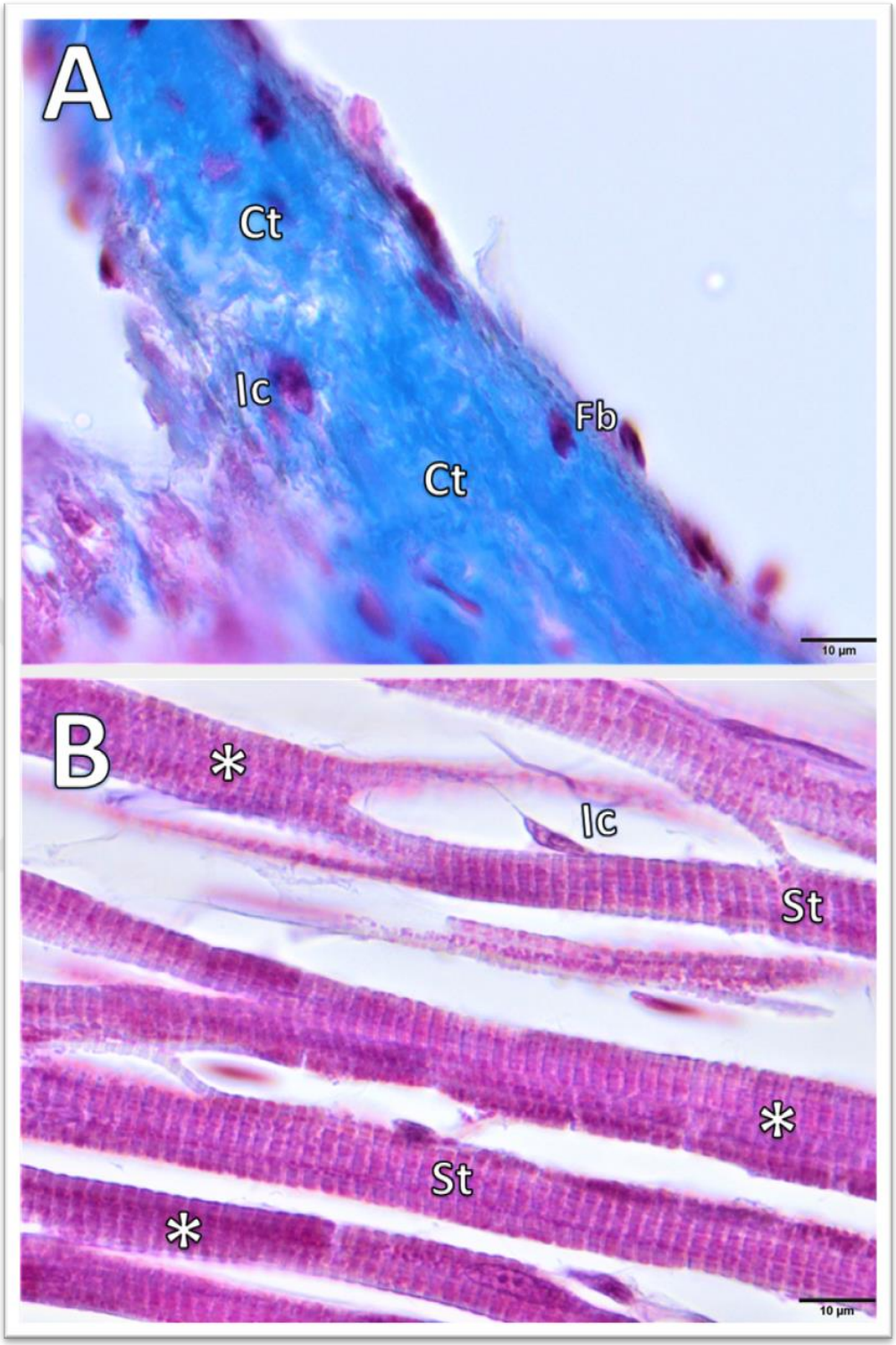


Figure 4.63. (A, B) Images of the heart tissue of the left ventricle are seen in the DS. Thegeneral structure of the heart tissue of the left ventricle is fine. The arrows indicate nuclei of the cardiac cells. (Ct) indicate connective tissue. (Ic) indicate interstitial cell. The letters (Fb) indicate the fibroblast cell. (St) indicate the striations of the. (*) indicates the muscle fibres. Masson trichrome stained section (5 µm thickness). Original magnification: X100

4.3.4.3. Masson Trichrome- Stained Sections: GA Group

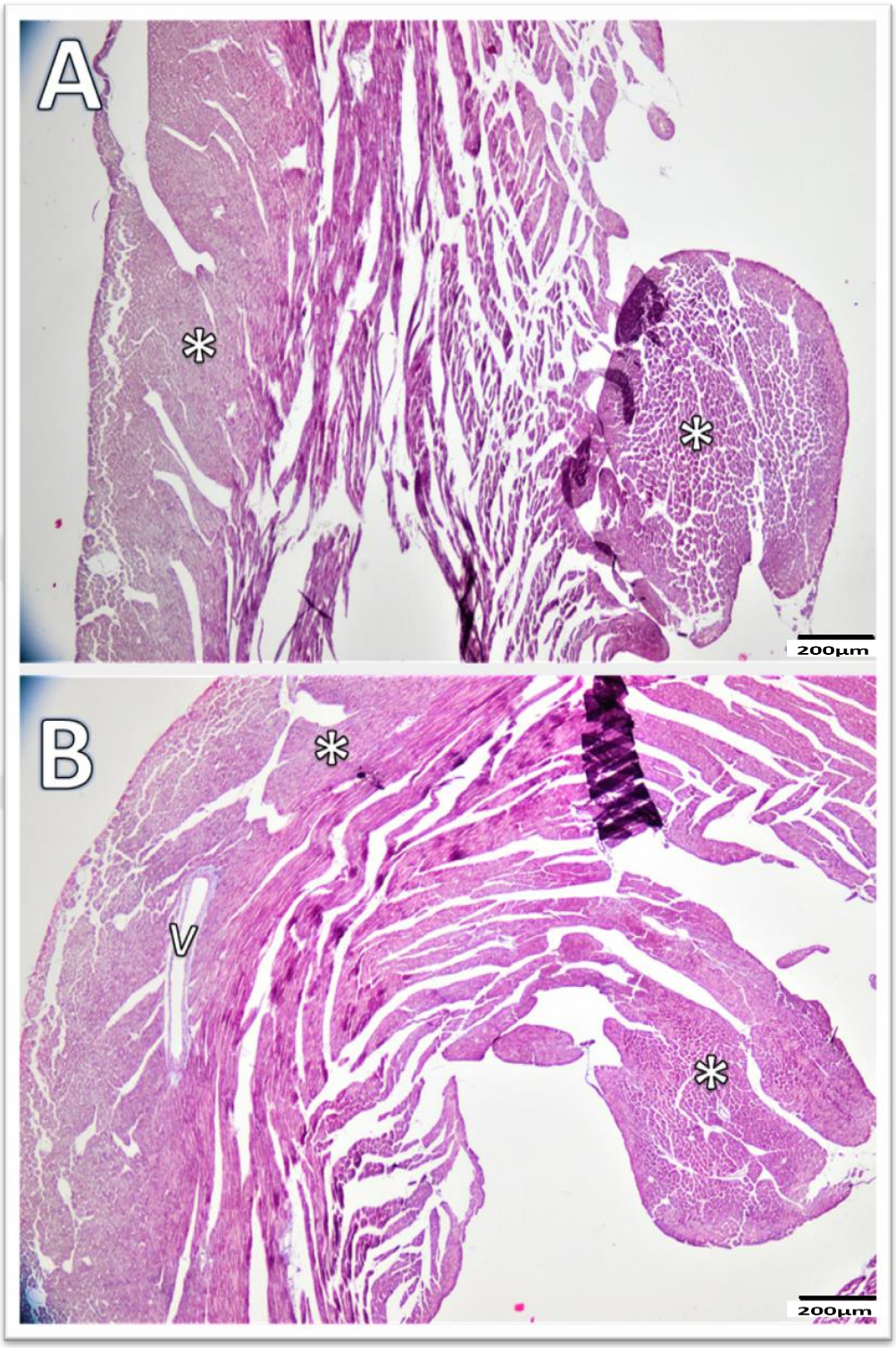


Figure 4.64. (A, B) Images of the heart tissue of the left ventricle are seen in the GA. The general structure of the heart tissue of the left ventricle is fine. (V) indicates the vessel. (*) indicates the muscle fibres. Masson trichrome stained section (5 µm thickness). Original magnification: X10.

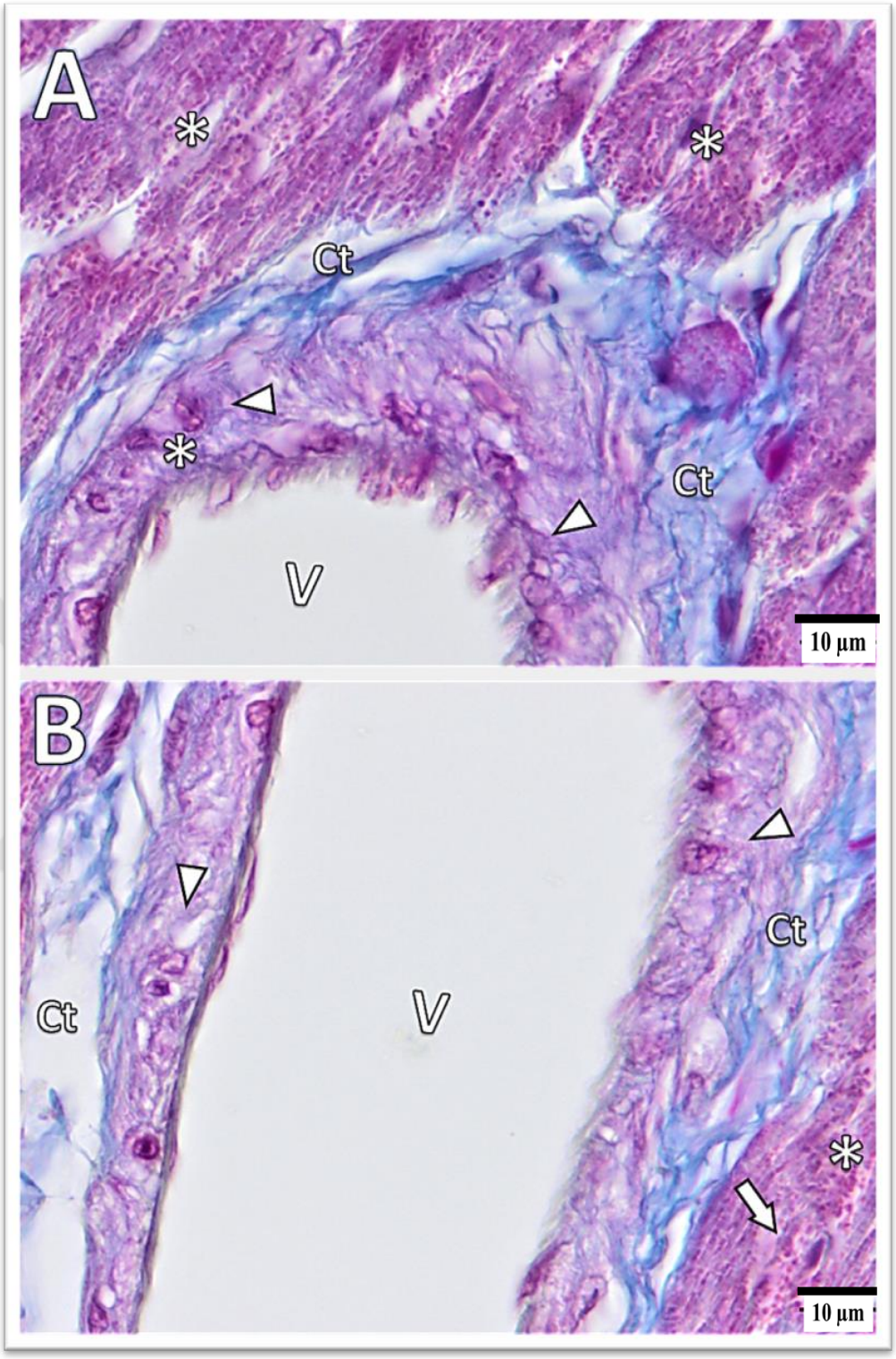


Figure 4.65. (A, B) Images of the heart tissue of the left ventricle are seen in the GA. The general structure of the heart tissue of the left ventricle is fine. The arrows indicate nuclei of the cardiac cells. (V) indicates the vessel. (Ct) indicate connective tissue. Arrowhead indicates the vascular smooth muscle cell. (*) indicates the muscle fibres. Masson trichrome stained section (5 µm thickness). Original magnification: X100.

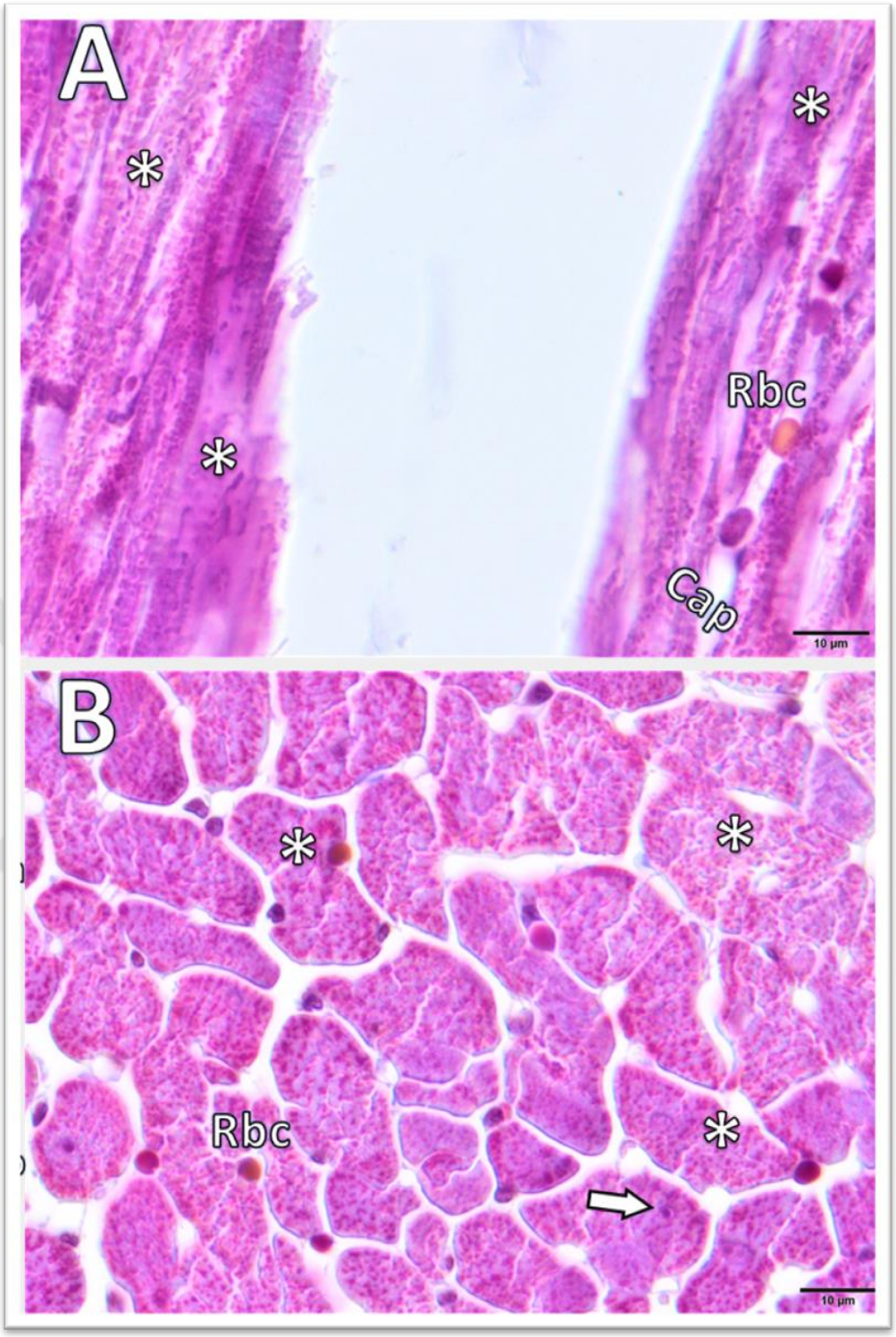


Figure 4.66. (A, B) Images of the heart tissue of the left ventricle are seen in the GA. The general structure of the heart tissue of the left ventricle is fine. The arrows indicate nuclei of the cardiac cells. (Rbc) indicate collection of red blood cells. (Cap) indicate a blood capillary. (*) indicates the muscle fibres. Masson trichrome stained section (5 µm thickness). Original magnification: X100

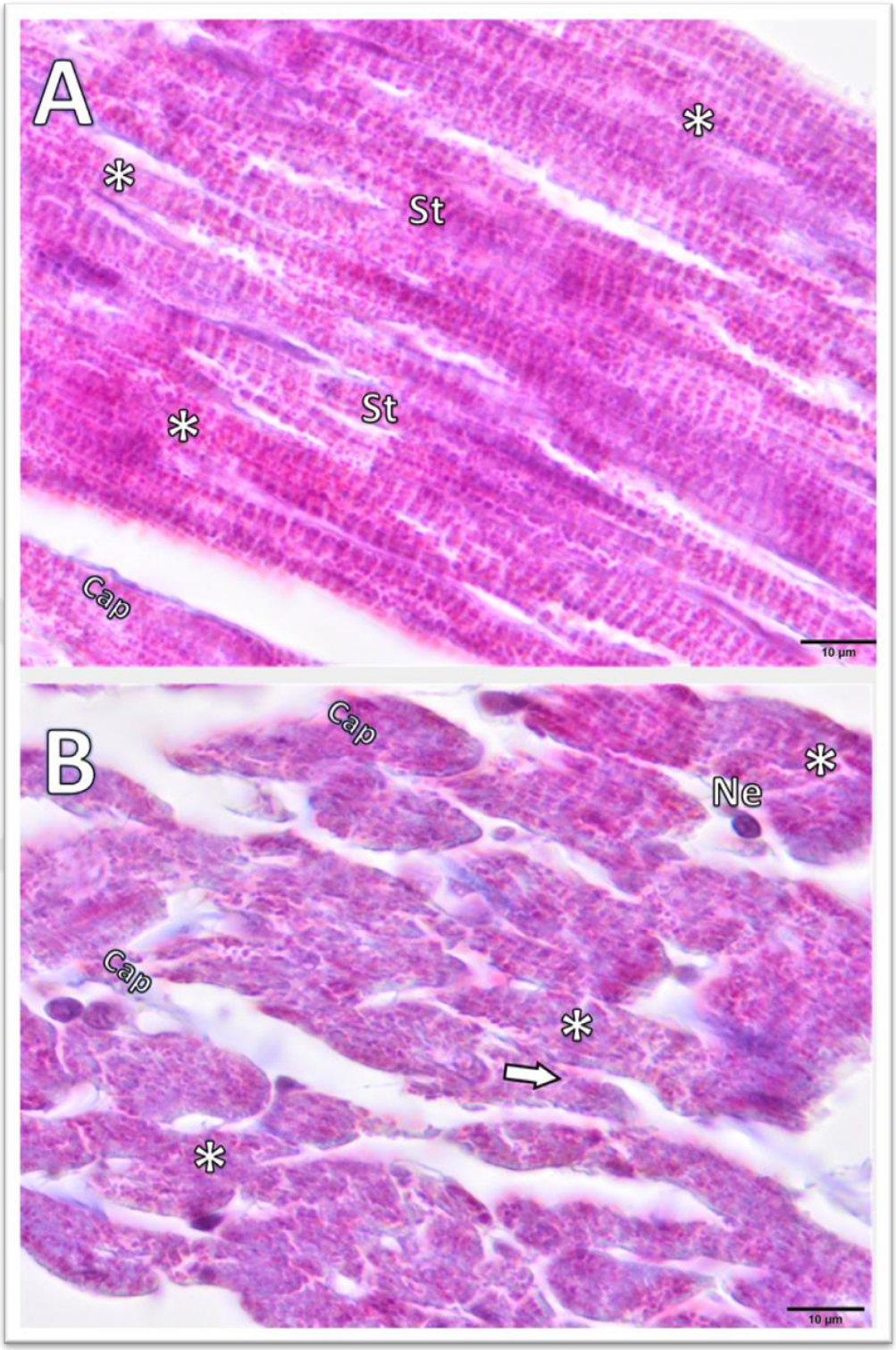


Figure 4.67. (A, B) Images of the heart tissue of the left ventricle are seen in the GA. The general structure of the heart tissue of the left ventricle is fine. The arrows indicate nuclei of the cardiac cells (Cap) indicate a blood capillary. (Ne) indicate the Neutrophil. (St) indicate the striations of the. (*) indicates the muscle fibres. Masson trichrome stained section (5 µm thickness). Original magnification: X100

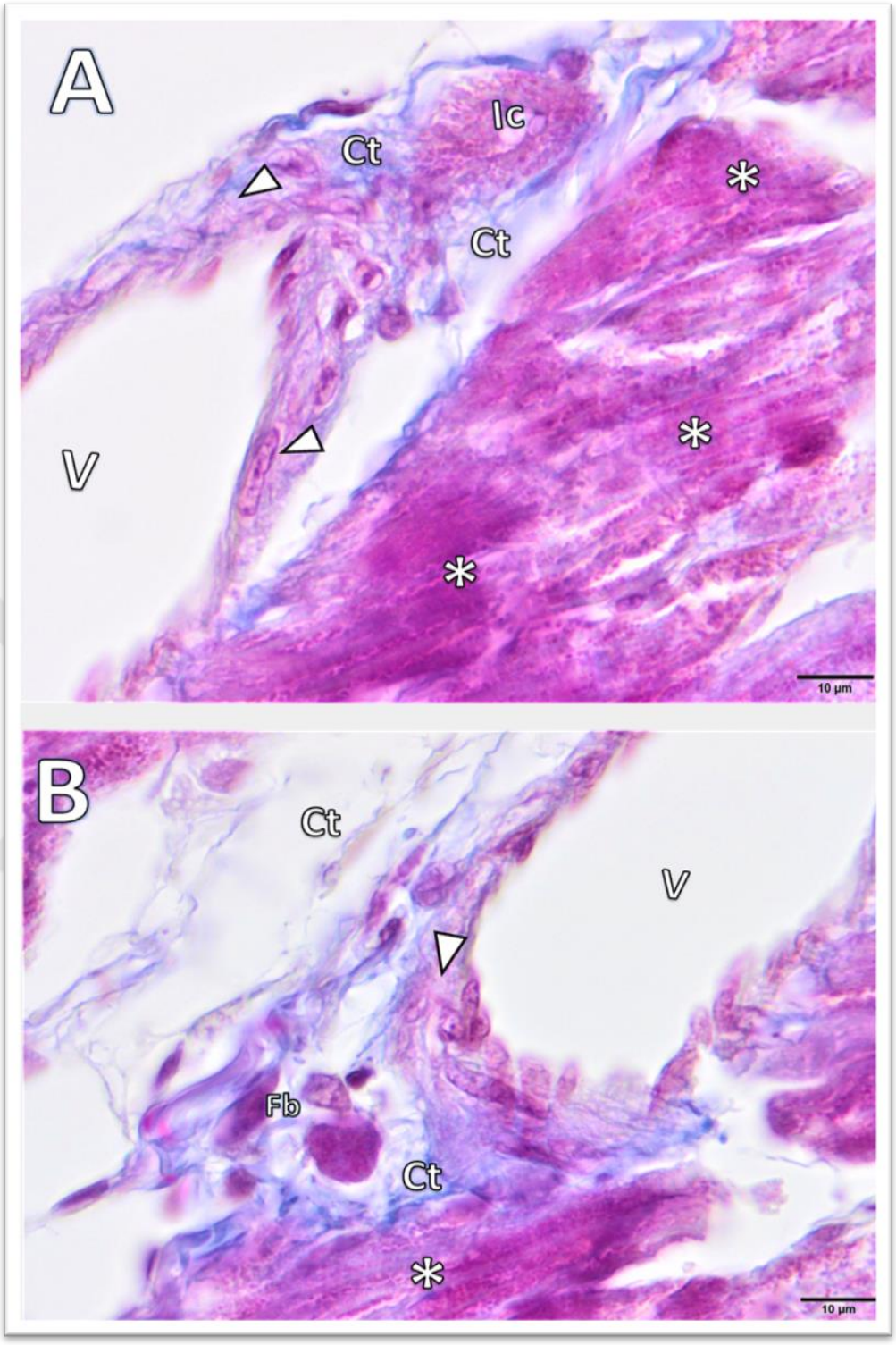


Figure 4.68. (A, B) Images of the heart tissue of the left ventricle are seen in the GA. The general structure of the heart tissue of the left ventricle is fine. The arrows indicate nuclei of the cardiac cells. (V) indicates the vessel. (Ct) indicate connective tissue. (Ic) indicate interstitial cell. (Fb) indicate the fibroblast cell. Arrowhead indicates the vascular smooth muscle cell. (*) indicates the muscle fibres. Masson trichrome stained section (5 µm thickness). Original magnification: X100

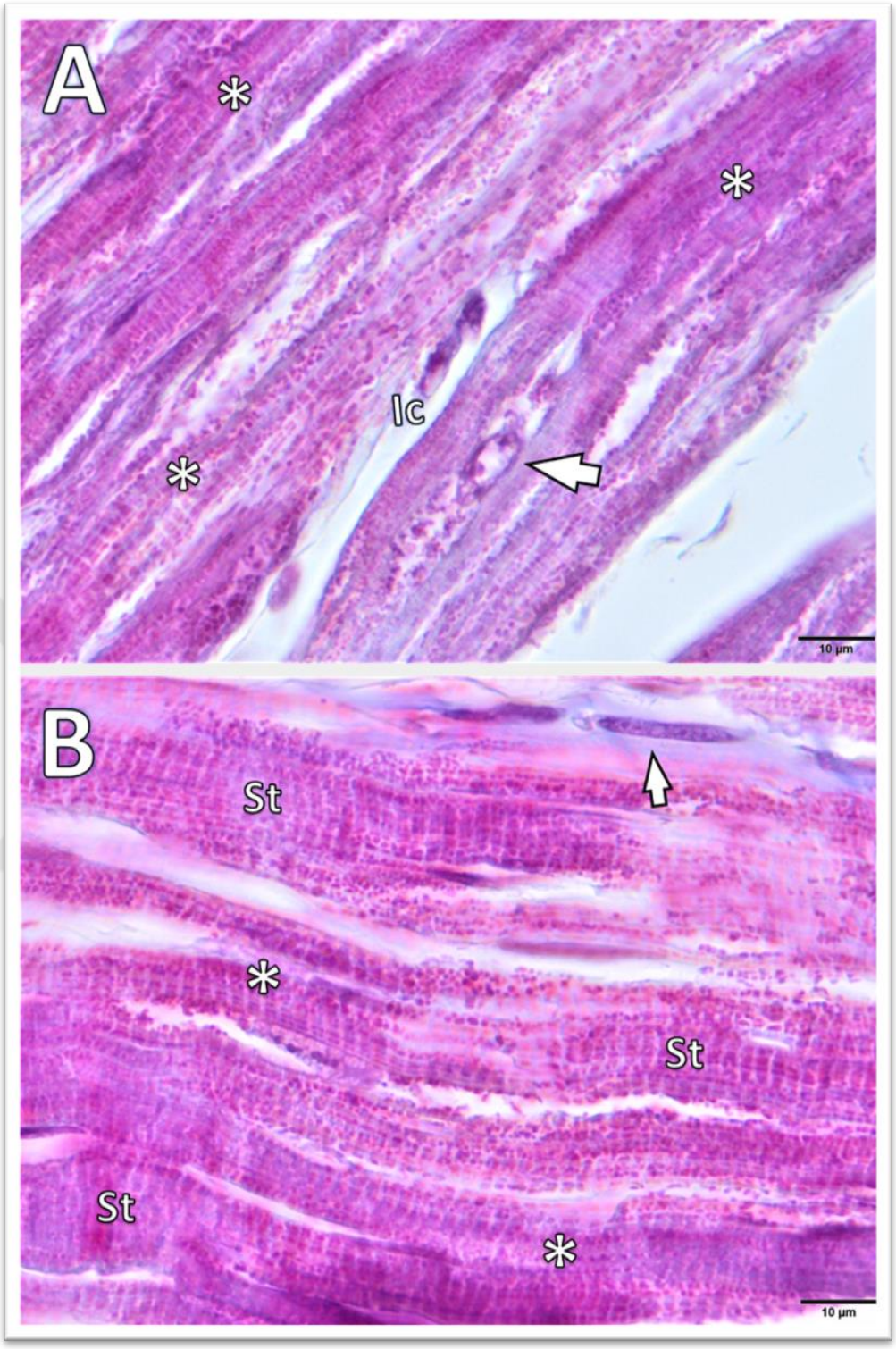


Figure 4.69. (A, B) Images of the heart tissue of the left ventricle are seen in the GA. The general structure of the heart tissue of the left ventricle is fine. The arrows indicate nuclei of the cardiac cells. (Ic) indicate interstitial cell. (St) indicate the striations of the. (*) indicates the muscle fibres. Masson trichrome stained section (5 µm thickness). Original magnification: X100

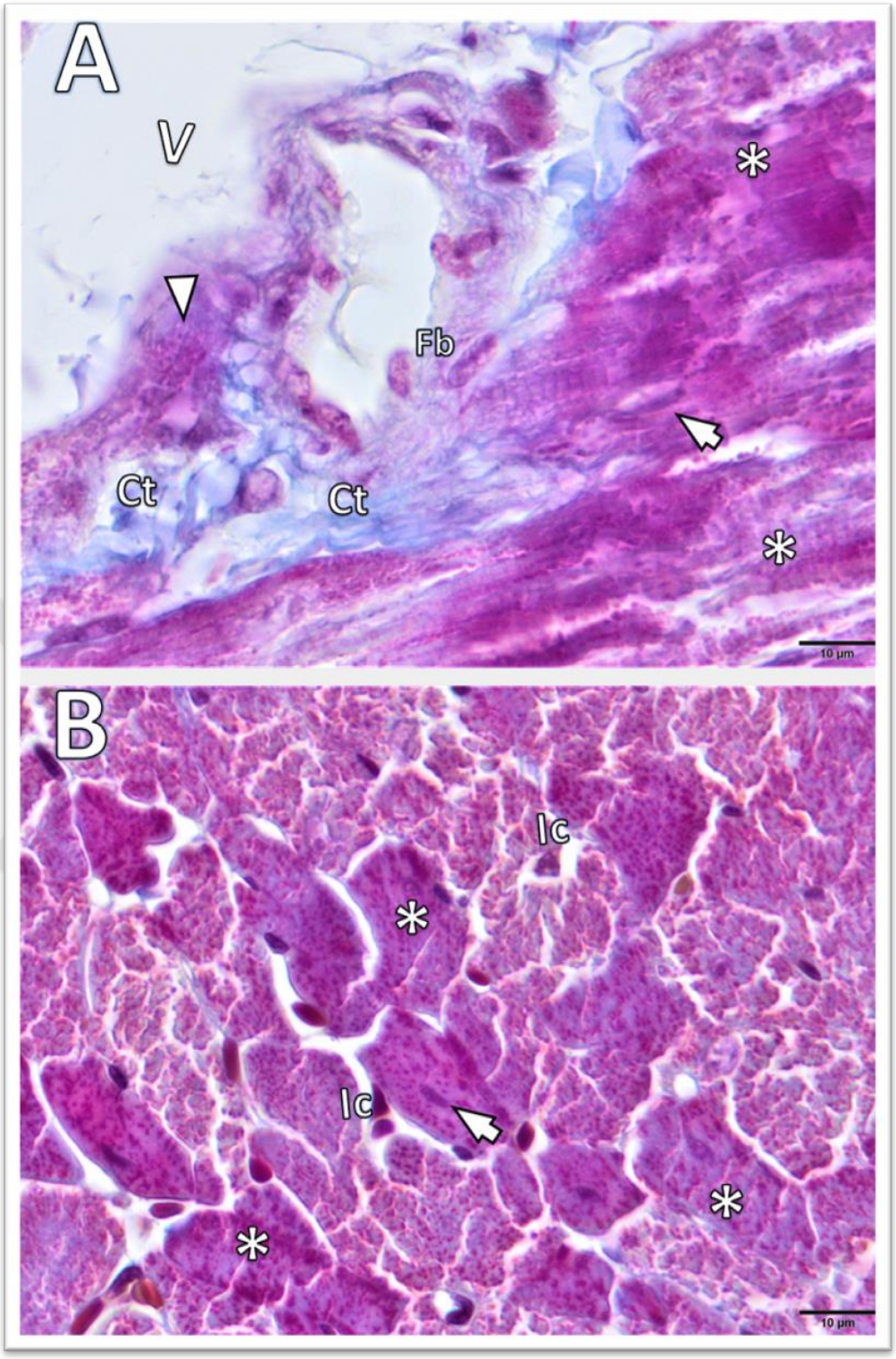


Figure 4.70. (A, B) Images of the heart tissue of the left ventricle are seen in the GA. The general structure of the heart tissue of the left ventricle is fine. The arrows indicate nuclei of the cardiac cells. (V) indicates the vessel. (Ct) indicate connective tissue. (Ic) indicate interstitial cell (*) indicates the muscle fibres. Masson trichrome stained section (5 µm thickness). Original magnification: X100

4.3.4.4. Masson Trichrome- Stained Sections: (GA+DS) Group

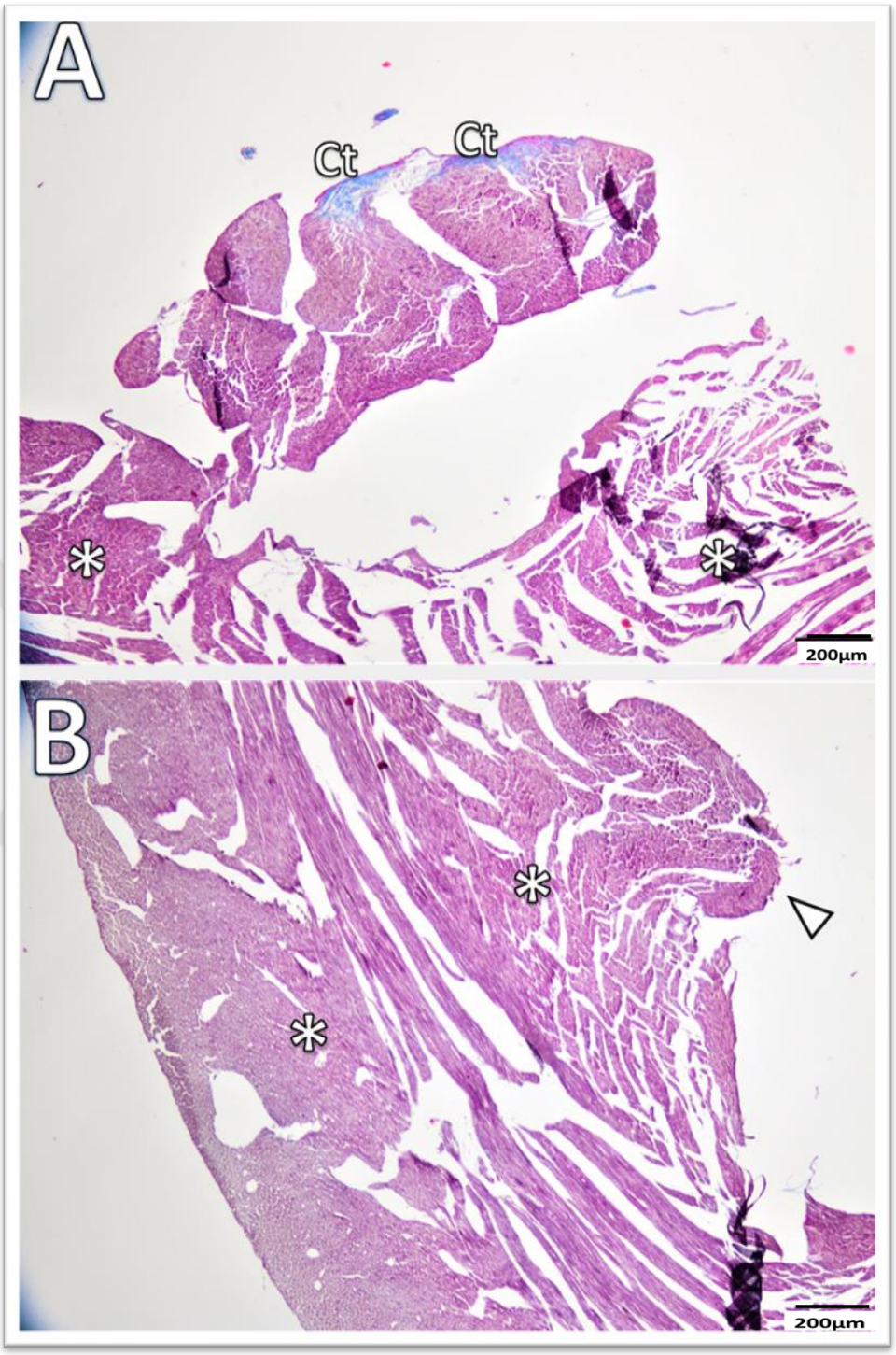


Figure 4.71. (A, B) Images of the heart tissue of the left ventricle are seen in the GA+DS. The general structure of the heart tissue of the left ventricle is fine. The arrows indicate nuclei of the cardiac cells (Ct) indicate connective tissue. (*) indicates the muscle fibres. Masson trichrome stained section (5 µm thickness). Original magnification: X10.

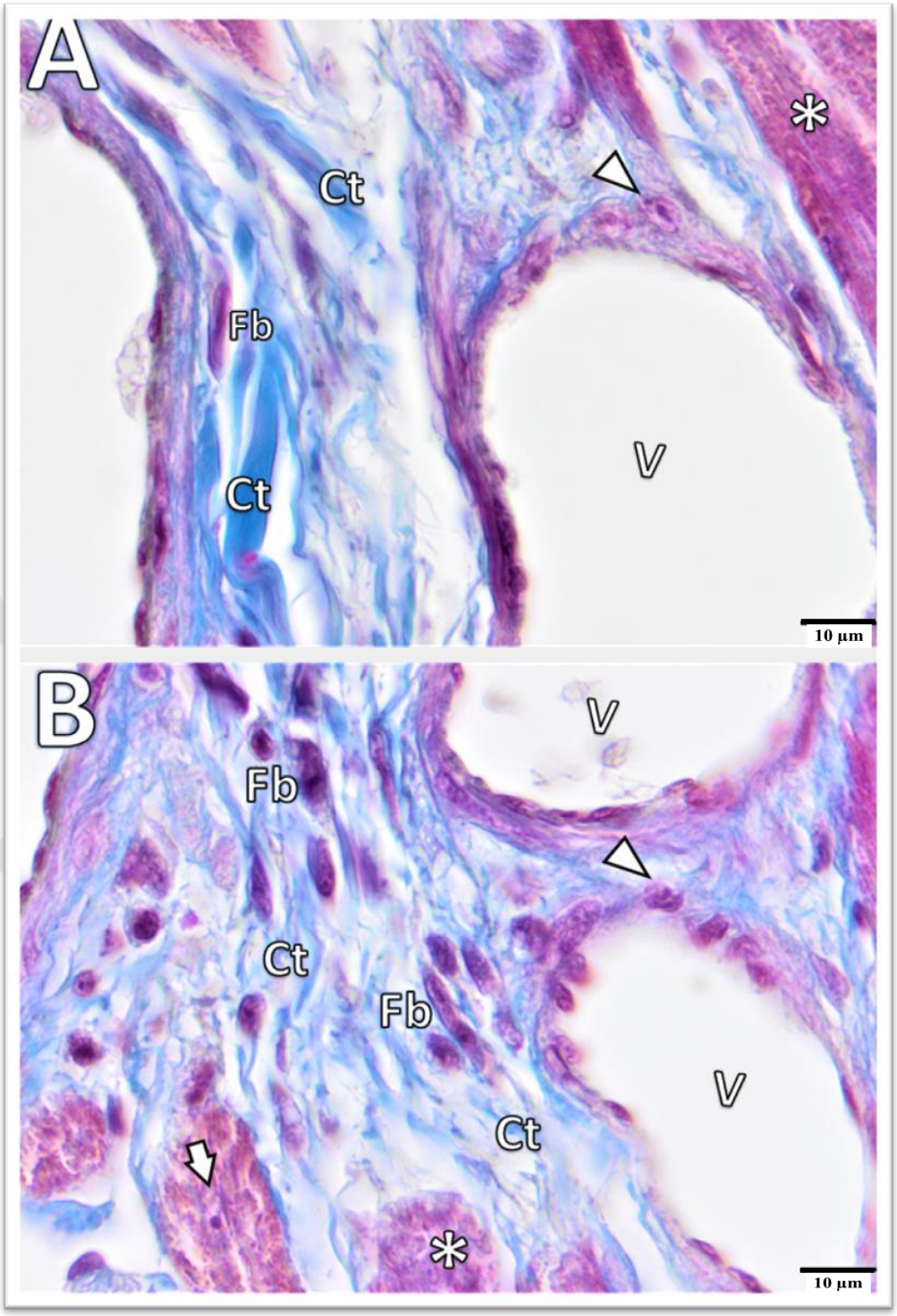


Figure 4.72. (A, B) Images of the heart tissue of the left ventricle are seen in the GA+DS. The general structure of the heart tissue of the left ventricle is fine. The arrows indicate nuclei of the cardiac cells. (V) indicates the vessel. (Ct) indicate connective tissue. Arrowhead indicates the vascular smooth muscle cell. (Fb) indicate the fibroblast cell. (*) indicates the muscle fibres. Masson trichrome stained section (5 µm thickness). Original magnification: X100

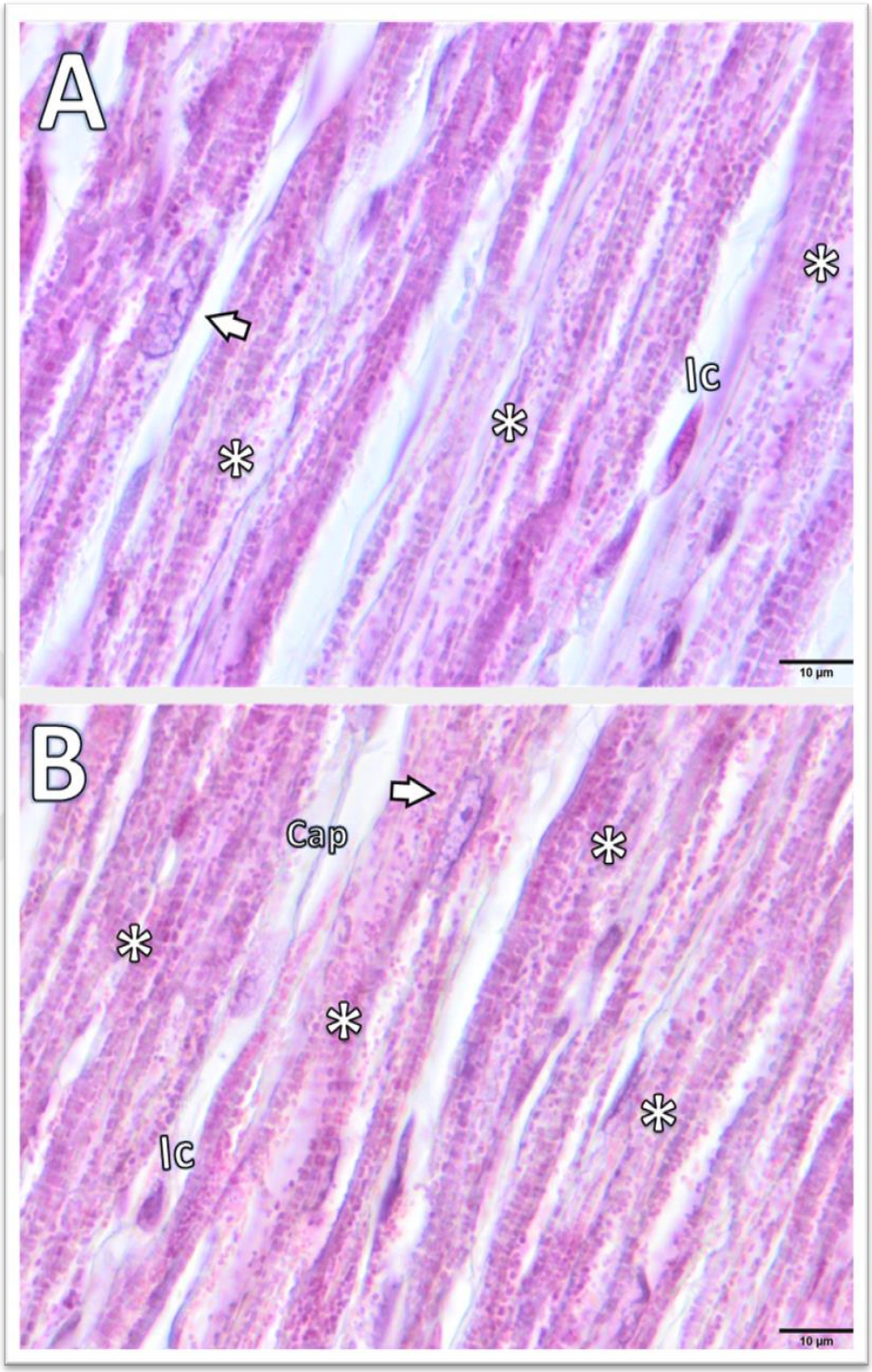


Figure 4.73. (A, B) Images of the heart tissue of the left ventricle are seen in the GA+DS. The general structure of the heart tissue of the left ventricle is fine. The arrows indicate nuclei of the cardiac cells. (Cap) indicate a blood capillary. (Ic) indicate interstitial cell. (*) indicates the muscle fibres. Masson trichrome stained section (5 µm thickness). Original magnification: X100

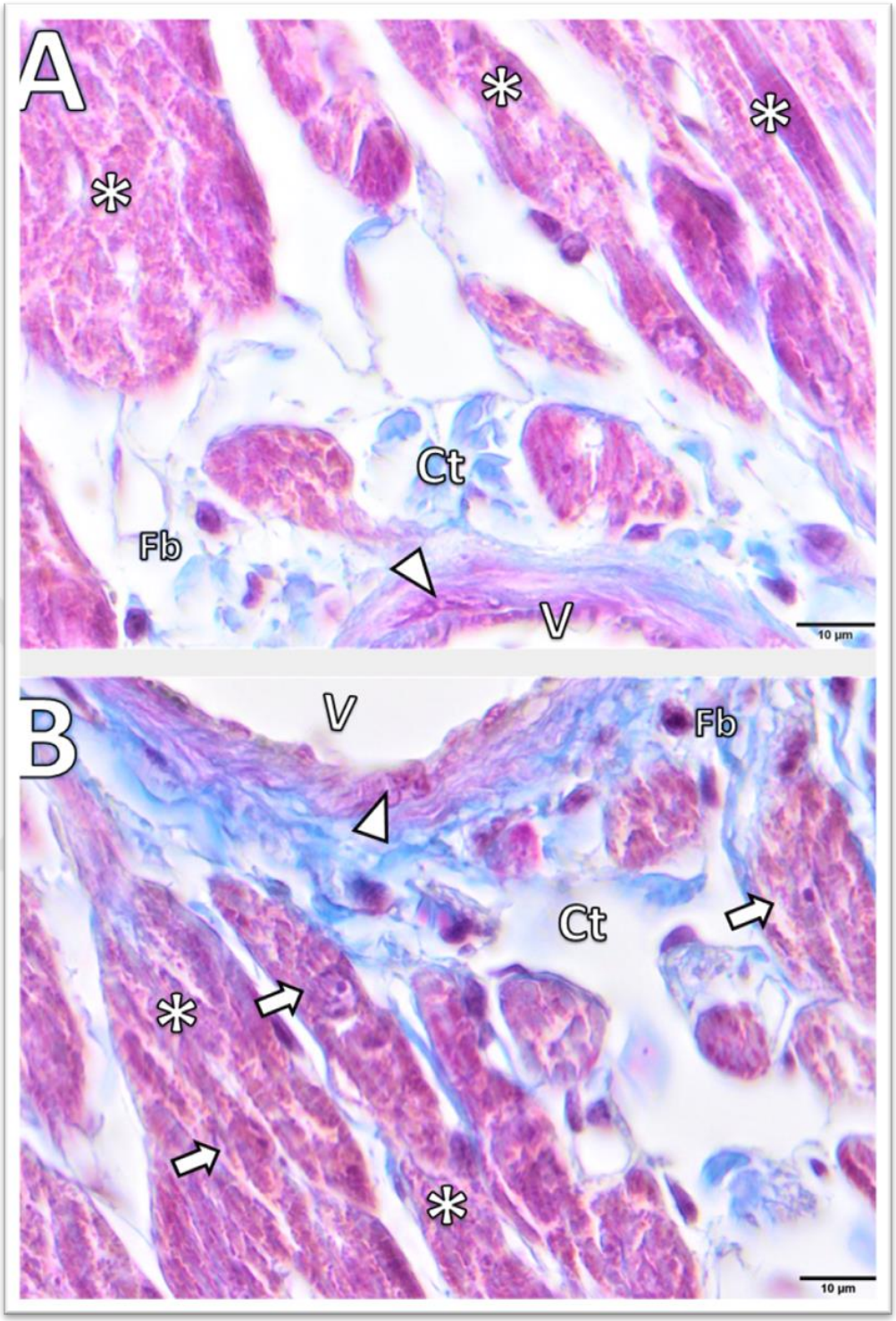


Figure 4.74. (A, B) Images of the heart tissue of the left ventricle are seen in the GA+DS. The general structure of the heart tissue of the left ventricle is fine. The arrows indicate nuclei of the cardiac cells. (V) indicates the vessel. (Ct) indicate connective tissue. (Fb) indicate the fibroblast cell. Arrowhead indicates the vascular smooth muscle cell. (*) indicates the muscle fibres. Masson trichrome stained section (5 µm thickness). Original magnification: X100

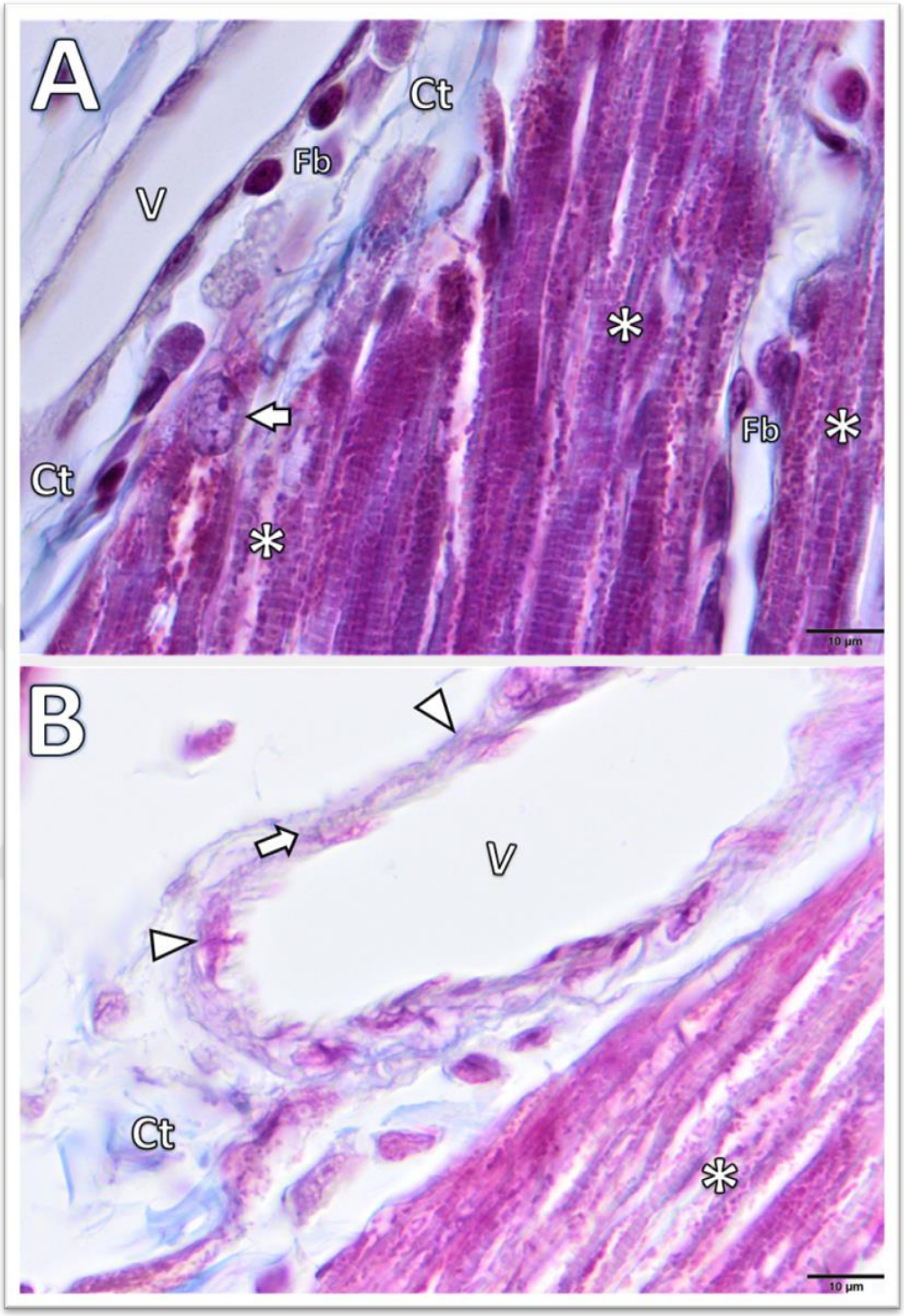


Figure 4.75. (A, B) Images of the heart tissue of the left ventricle are seen in the GA+DS. The general structure of the heart tissue of the left ventricle is fine. The arrows indicate nuclei of the cardiac cells. (V) indicates the vessel. Arrowhead indicates the vascular smooth muscle cell. (Ct) indicate connective tissue. (Fb) indicate the fibroblast cell. (*) indicates the muscle fibres. Masson trichrome stained section

(5 µm thickness). Original magnification: X100

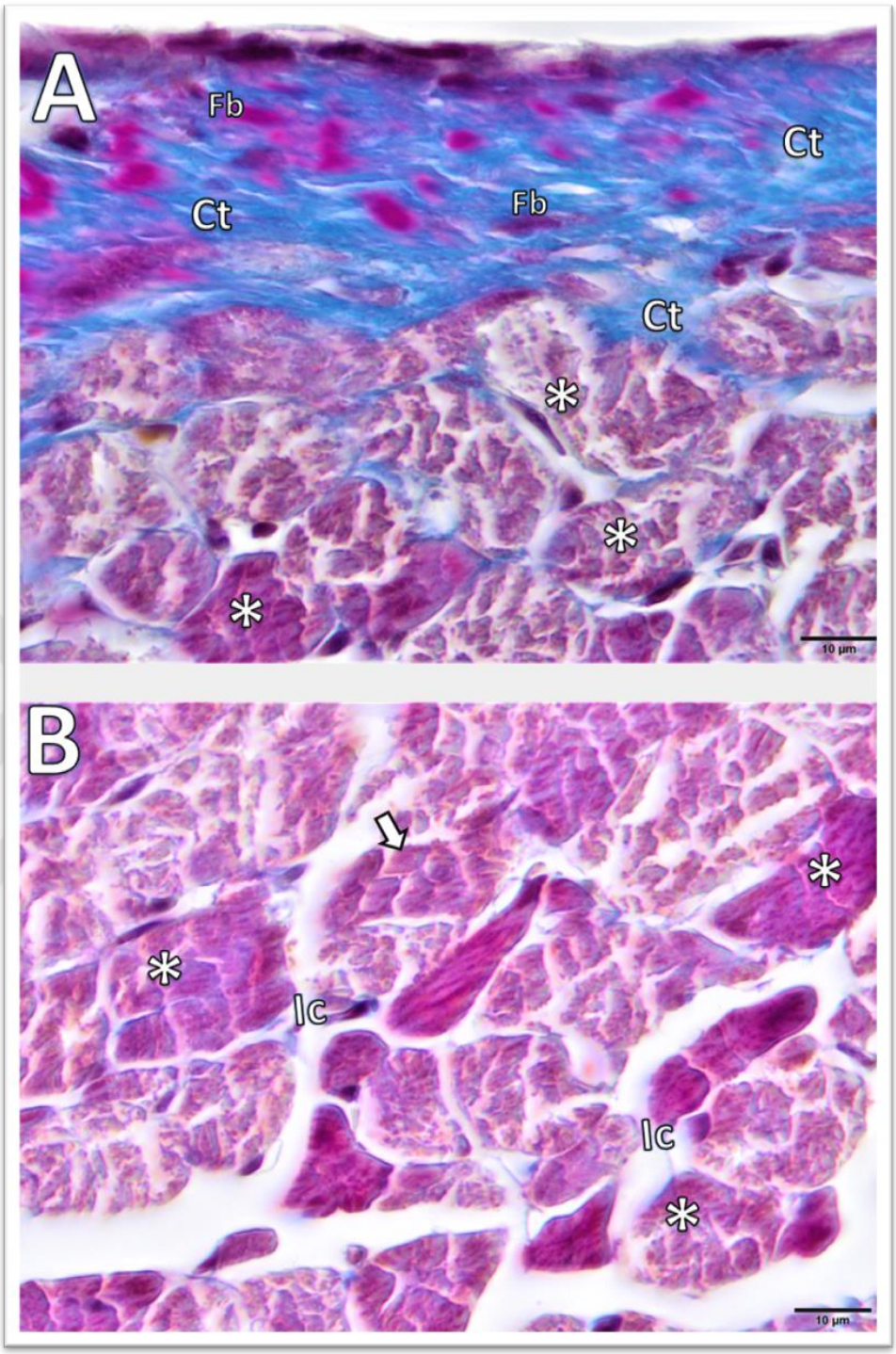


Figure 4.75. (A, B) Images of the heart tissue of the left ventricle are seen in the GA+DS. The general structure of the heart tissue of the left ventricle is fine. The arrows indicate nuclei of the cardiac cells. (Ct) indicate connective tissue. (Ic) indicate interstitial cell. (Fb) indicate the fibroblast cell. (*) indicates the muscle fibres. Masson trichrome stained section (5 µm thickness). Original magnification: X100

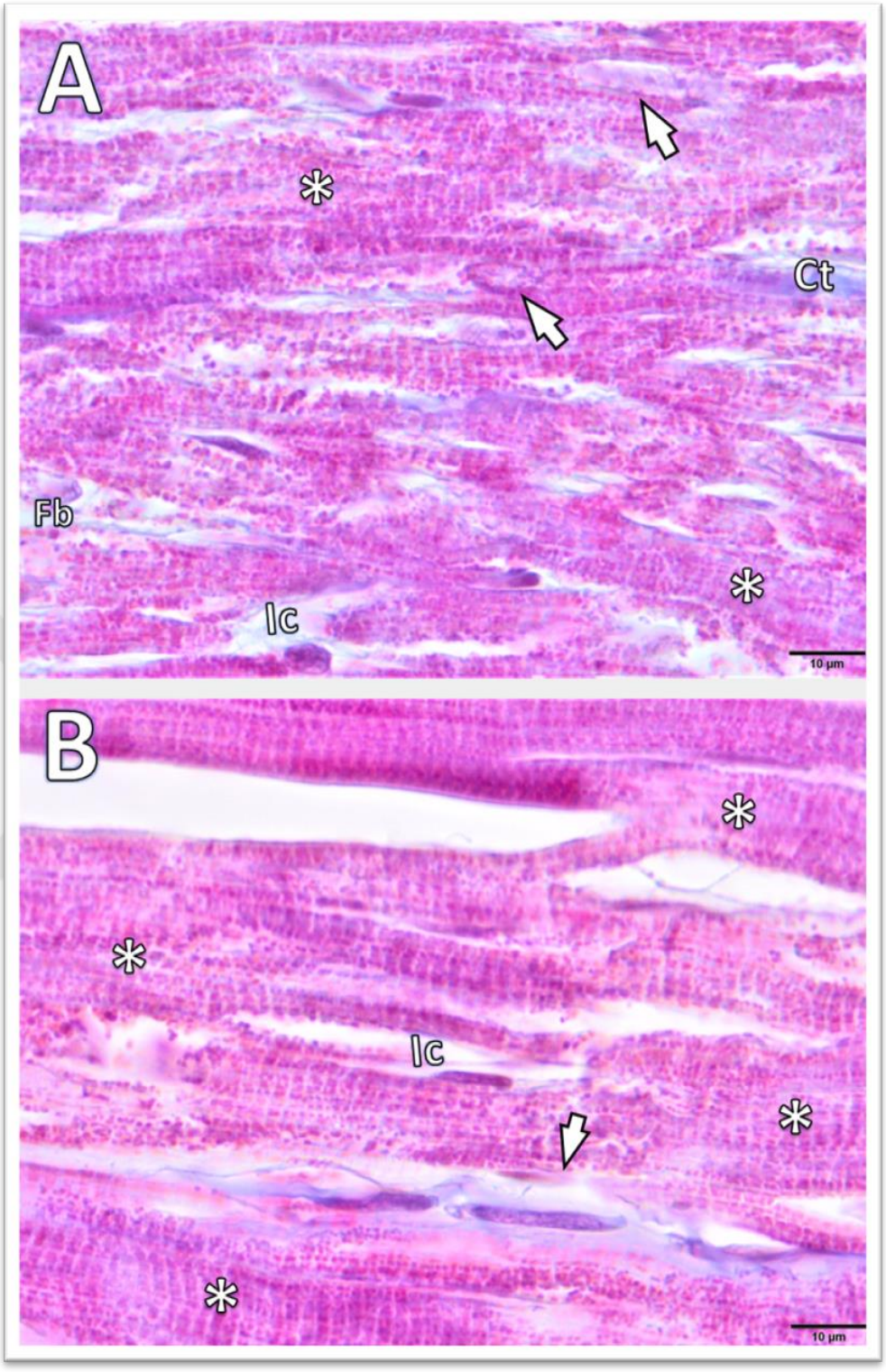


Figure 4.76. (A, B) Images of the heart tissue of the left ventricle are seen in the GA+DS. The general structure of the heart tissue of the left ventricle is fine. The arrows indicate nuclei of the cardiac cells. (Ct) indicate connective tissue. (Ic) indicate interstitial cell. (Fb) indicate the fibroblast cell. (*) indicates the muscle fibres. Masson trichrome stained section (5 µm thickness). Original magnification: X100

4.3.4.5. Findings Of Masson Trichrome- Stained Sections

The same findings of some degrees of defragmentation, disorganization, vacuolations, and cell discontinuation in many pictures were noted among all groups.The damage that replaced by the fibrous tissue appear very clear stained (fine blue) in the DS and GA+DS groups.

5. DISCUSSION

This study investigated the possible healing effects of GA on the apoptotic and degenerative effects of DS on rat hearts. Biochemical, stereological, light microscopic analysis were conducted.

The morphological characteristics of the left ventricle (LV) in terms of volume, numerical density, and the total number of cardiomyocytes of LV reflect its functional and normal morphological status. Thus, obtaining quantitative data with statistical reliability is crucial for accurate and unbiased results. Histological sections usually deliver qualitative analysis showing if the tissue is undergoing pathological changes. However, the impact of this change in terms of statistically significant numbers can be obtained through stereology. Statistically significant changes can give clues about the degree of the pathological changes or the effect of the experimental drug under study.

Regarding stereological analysis, the total number of cardiomyocytes of the LV in the control group was $3.03\ X10^7 \pm 4.99\ X10^6$. The total number in the literature was counted as $3.41\ X10^7$ for 3-month-old female Wistar rats (Brüel and Nyengaard, 2005). As well as another study which performed in Three-month-old female Wistar rats estimated the total number of cardiomyocytes of the LV in the control group $3.45\ X10^7$ which is also in the common range (Bruel, Christoffersen and Nyengaard, 2007). Female Wistar rats, 8 months of age counted $3.79\ X10^7$ (Bruel, Oxlund and Nyengaard, 2002). Thus, this study's total number of Cardiomyocytes of the LV fall in the normal range for control groups. Moreover, there were significant differences between DS and GA groups concerning the total number of Cardiomyocytes and the volume of LV.

Stereological techniques were proven effective in detecting changes in the Cardiac volume and total number of cardiomyocytes under toxicities. The physical disector was used to estimate the total number of rat embryos, fetuses, 3-day-old pups and young adults of Sprague Dawley rats. The total number of cardiac muscle nuclei (CMNs) for all age groups is shown. The total number of CMNs in the heart was significantly increased from 11-day-old embryos to adult group when comparing following age groups each other ($P < 0.05$) (M. E. Altunkaynak, et al., 2011).

The optical fractionator method of (Stereo Investigator) was used to estimate the cardiac volume and ventricular wall in prenatally exposed to diclofenac sodium rats. Stereological studies revealed that there were no differences between the GA and CON groups, but there were statistically significant differences between the diclofenac

sodium exposed group and groups of (GA and CON) ($P < 0.05$) (Fikret, Mikail, Murat Cetin and Huseyin, 2015).

Biochemical analysis was performed. serum SOD and CAT levels were investigated; SOD is the primary antioxidant, while GSH and Ascorbate were play the role of main antioxidant against Oxidative Stress (OS) in the heart (Parildar, et al., 2008). Moreover, the left ventricle relays mainly on SOD as scavengers more than CAT and GSH (Suh et al., 2001). However, biochemical analysis of enzyme activities shows no significant difference between groups. It contradicts the results obtained by (Al-Yahya, et al., 2009) , in which the GA-treated group showed restoration of GSH bladder contents. The dose of GA used in the mentioned study was (7.5 gm/kg/day) in drinking water, which is like our dose. We even used a longer duration, and our dose was administered by oral gavage. However, the biochemical analysis done by Al-Yahya and co-workers was performed in tissue samples. In contrast, our biochemical analysis was performed in the blood sample, which may explain the contradiction between the two studies. The lack of significance on the biochemical results may be attributed to the toxicity of DS requiring a higher dose and/or a different route of administration. However, studies show that the toxicity of DS may not be confined to OS; this drug may affect the transport systems in the cell membrane. OS does not seem to be the sole reason for cell death, as indicated by the inefficiency of the administration of an antioxidant and a radical scavenger in minimizing the effect of DS (Norimitsu Morioka, Kei Kumagai, Katsuya Morita, Shigeo Kitayama and Toshihiro Dohi, 2004).

Microscopic findings were obtained using light microscopy in paraffin sections stained with Hematoxylin and Eosin and Masson Trichrome stains, Also, toluidine blue-stained resin sections were used for evaluation. Images taken in toluidine blue staining showed a regular appearance in the control group. Each Cardiac myocyte has an elongated-shaped nucleus; the nuclei of cardiomyocytes and the cell features are seen. Cardiomyocytes LV normally appeared except for some defragmentation of the tissue due to artifact of processing. Connective tissue was observed in DS and GA+DS groups among the cardiac tissue, especially in the inner muscular layer and around the vessels. The typical vascular and capillaries distribution between the cardiomyocytes were clearly noticed especially in the transverse sections. longitudinal sections fortunately revealed the whole lengths of the myocytes with their unique features of

the branching and striations. The same findings of some degrees of defragmentation, disorganization, vacuolations, and cell discontinuation in many pictures were noted among all groups. Regarding the Trichrome stain findings, the general structure seemed damaged by autolysis, but the severity of damage that replaced by the fibrous tissue (connective tissue and collagen that appear very clear stained clear blue) in the DS and GA+DS groups. according to these observations we can suppose that damage is a result of adverse effects of diclofenac sodium which (Gado and Aldahmash, 2013) is cause tissue toxicity and degeneration.

According to our knowledge, the role of GA on the heart as an antioxidant has not yet to be investigated, the heart (Abd-Allah,et al., 2002). This role among other tissues was investigated, and promising results were reported in the kidneys (Al-Majed,et al., 2003; Al-Majed,et al., 2002; B. H. Ali, et al., 2013; B. H. Ali, Al Za'abi, Ramkumar, Yasin and Nemmar, 2014), the liver (A. M. Gamal el-din,et al., 2003) and the gonads(Ahmed, Fedail, Musa, Musa and Sifaldin, 2016; Fedail, et al., 2016). However, some contradicted results emerged, while many reports supported the effectiveness of GA as an antioxidant (Lamis Kaddam, Fdl-Elmula and Saeed, 2018). Some reports suggested that its role is less significant than proposed (Cindoruk, et al., 2007).

It is reported that oral administration of GA in the drinking water for rats at a three-graded concentration of 2.5, 5.0 or 10.0% w/v for eight days did not lead to any significant change in the concentrations of antioxidants like GSH and superoxide dismutase in the kidney or liver. The report concluded that the beneficial effects of GA are unlikely due to its antioxidant properties (B. H. Ali, 2004). It is also suggested that GA can pass through the gut and get absorbed to reach adequate concentrations in circulation to apply its antioxidant effect to other organs rather than the intestine (B. H. Ali, 2004). However, we administered GA orally to mimic its use in folk medicine and traditions in the local community. Our study adds to the literature by confirming that GA does not affect heart tissue as an antioxidant. To our knowledge, a stereological investigation of the effect of GA on the histology of the CVS was only done after.

The probable explanation could be elaborated in the following factors: there are limitations regarding the applications of the driven results obtained from animals on humans. Animal models cannot mimic the same disease development or ageing process duration (Gandhi and Abramov, 2012). Also, it looks crucial to administer

antioxidants in the early stages or prior to disease development. Other factors include issues related to the dosage differences between animal models and humans; using an antioxidant that scavenges ROS rather than eliminating the source of their production is also a contributing factor. Lastly, there are different mechanisms of OS with different sources of ROS. Thus, multiple antioxidants would be more beneficial (Gandhi and Abramov, 2012)

The dose of DS applied in our study was 3.6 mg/kg. It was kept as the same dose used by Yurt and co-workers (Yurt, Kaplan and Kivrak, 2018). Their study is the most like ours in terms of using an antioxidant substance to investigate its effect on minimizing damage caused by DS on the nervous tissue. Examples of doses from other studies investigating the use effect of DS on the nervous tissue include 1 mg/kg, intraperitoneal administration for 15 days (Gokcimen et al., 2007). Another study on pregnant rats was administrated, DS (1 mg/kg, i.m) for 15 days to the group on gestation of days 5–20, and 9–11 represent the critical period of organogenesis for cardiovascular and midline development in rats, equivalent to 3–6 weeks after fertilization in human embryos (Fikret,et al., 2015). However, the use of different doses, i.e., 3.9, 9 and 18 mg/kg, intraperitoneal administration for seven days in which the effect was dose dependent (Elibol, OĞUR and Doğru, 2019).

The offspring of Wistar albino rats were arranged into two groups, four weeks old and 20 weeks old, after prenatal administration of DS (1 mg/kg for intraperitoneal administration 15 days) to their mothers. The 20-week-old group showed a decrease in the number of Cardiac myocytes. Also, there was a decrease in the number of granule cells in the DG in the 4-week-old group, while they increased in the 20-week-old group. The latter results are because granular cells in the DG proliferate mostly postnatally, which indicates the possible role of DS in increasing their rate of proliferation. The same results were obtained when administering DS postnatally. The dose of 15 mg/kg through intramuscular for seven days was applied postoperatively to rats with acute subdural hematoma (ASDH) (Turkmen, et al., 2016). Also, DS was administered intraperitoneally to Wistar rats at a dose of 12.5 mg/kg for three days. The results on the nervous system were manifested in the cerebral cortex and the cerebellum in the presence of ballooned red neurons (Ilic, et al., 2011). This phenomenon was not detected in the cardiac tissue.

However, some of these studies were prenatal, while others were postnatal. Many factors are reported to contribute to the effect of DS on the cardiac tissue, including the dose, route of administration and duration (Andrea Fanelli, Daniela Ghisi, Pierangelo Lora Aprile and Francesco Lapi, 2017). Those studies used intraperitoneal and intramuscular injections, while we used the oral route to administer DS. On the other hand, our study was concerned about adult heart tissue rather than the developing one. All these factors may explain the need for significant results in our study.

This study is the first report on the effect of GA as an antioxidant to minimize the harmful effect of DS on cardiac tissue. Stereological, histological, and biochemical analyses indicate no significant protective effect of GA since the used DS did not create a side effect on the number of Cardiac myocytes. However, our qualitative results of the stereological, histological, and biochemical investigations showed the opposite. The DS impaired most of the CVS functions and caused irreversible structure damage. Moreover, a protective result was seen after GA exposure. This was indicated by the fact that most of the cardiomyocytes have a stable structure.

The use of multiple antioxidants would get significantly positive results. The administration of DS through the oral route also contributed to the study's negative results. Most studies with positive results used intraperitoneal, intramuscular, or intrathecal injections. Also, most of those results were done on developing hearts, i.e., prenatal exposure to DS. However, postnatal studies found no significant results, which indicates that the oral administration of DS in the dose used in this study has no significant effect on the adult rat cardiac tissue.

6. CONCLUSIONS AND RECOMMENDATIONS

6.1. Conclusions

DS, although it can affect the developing heart, shows harmful effects on the structure of the adult heart and function when administered by oral gavage for 15 days at a dose of 3.6 mg/kg.

Administration of DS postnatally via other routes with higher doses and for a longer duration would give different results.

Biochemical investigations showed no change in antioxidant levels following the administration of GA by oral gavage for 15 days at a dose of 7.5 g/kg. On the other hand, there need to be more significant biochemical results because the toxicity of DS requires a higher dose and/or a different route of administration.

However, our qualitative analysis showed a toxic effect of DS and GA on the Cardiomyocytes of the left ventricle; if GA is simultaneously used with DS, it shows a protective effect on the Heart tissue since amount of fibrous tissue and collagen was decreased after GA exposure.

To our knowledge, stereological analysis of the effect of GA on the histology of the CVS was not done before. This is the first study in this manner; many reports praise the antioxidant role of GA in the kidneys, liver, gonads, and nervous tissue, with other contradicting reports suggesting that there is no role for GA as an antioxidant in oral administration.

6.2. Recommendations

Further investigations are required, considering the following points:

- Administration of DS via other routes with a higher dose and longer duration.
- Administration of GA through the same route and dose, but the starting date of administration should be before the DS exposure.
- Using multiple antioxidants rather than one.
- Biochemical analyses are to be done in tissue samples rather than blood samples.
- For the sake of time and effort, an optical fractionator is recommended for stereological analysis.

REFERENCES

Abd-Allah, A. R., Al-Majed, A. A., Mostafa, A. M., Al-Shabanah, O. A., Din, A. G. and Nagi, M. N. (2002). Protective effect of arabic gum against cardiotoxicity induced by doxorubicin in mice: a possible mechanism of protection. *J Biochem Mol Toxicol,* 16(5), 254-259. doi:10.1002/jbt.10046

Ahmed, A. A., Fedail, J. S., Musa, H. H., Musa, T. H. and Sifaldin, A. Z. (2016). Gum Arabic supplementation improved antioxidant status and alters expression of oxidative stress gene in ovary of mice fed high fat diet. *Middle East Fertility Society Journal,* 21(2), 101-108. doi:10.1016/j.mefs.2015.10.001

Al-Majed, A. A., Abd-Allah, A. R., Al-Rikabi, A. C., Al-Shabanah, O. A. and Mostafa, A. M. (2003). Effect of oral administration of Arabic gum on cisplatin-induced nephrotoxicity in rats. *J Biochem Mol Toxicol,* 17(3), 146-153. doi:10.1002/jbt.10072

Al-Majed, A. A., Mostafa, A. M., Al-Rikabi, A. C. and Al-Shabanah, O. A. (2002). Protective effects of oral arabic gum administration on gentamicin-induced nephrotoxicity in rats. *Pharmacol Res,* 46(5), 445-451. doi:10.1016/s1043661802001251

Al-Yahya, A. A., Al-Majed, A. A., Gado, A. M., Daba, M. H., Al-Shabanah, O. A. and Abd-Allah, A. R. (2009). Acacia Senegal gum exudate offers protection against cyclophosphamide-induced urinary bladder cytotoxicity. *Oxid Med Cell Longev,* 2(4), 207-213. doi:10.4161/oxim.2.4.8878

Ali, A. A., Ali, K. E., Fadlalla, A. E. and Khalid, K. E. (2008). The effects of gum arabic oral treatment on the metabolic profile of chronic renal failure patients under regular haemodialysis in Central Sudan. *Nat Prod Res,* 22(1), 12-21. doi:10.1080/14786410500463544

Ali, B. H. (2004). Does gum Arabic have an antioxidant action in rat kidney? *Ren Fail,* 26(1), 1-3. doi:10.1081/jdi-120028536

Ali, B. H., Al-Husseni, I., Beegam, S., Al-Shukaili, A., Nemmar, A., Schierling, S., et al. (2013). Effect of gum arabic on oxidative stress and inflammation in adenine-induced chronic renal failure in rats. *PLoS One,* 8(2), e55242. doi:10.1371/journal.pone.0055242

Ali, B. H. and Al Moundhri, M. S. (2006). Agents ameliorating or augmenting the nephrotoxicity of cisplatin and other platinum compounds: a review of some recent research. *Food and chemical toxicology,* 44(8), 1173-1183.

Ali, B. H., Al Za'abi, M., Ramkumar, A., Yasin, J. and Nemmar, A. (2014). Anemia in adenine-induced chronic renal failure and the influence of treatment with gum acacia thereon. *Physiol Res,* 63(3), 351-358. doi:10.33549/physiolres.932685

Ali, B. H., Ziada, A., Al Husseni, I., Beegam, S., Al-Ruqaishi, B. and Nemmar, A. (2011). Effect of Acacia gum on blood pressure in rats with adenine-induced chronic renal failure. *Phytomedicine,* 18(13), 1176-1180. doi:10.1016/j.phymed.2011.03.005

Ali, B. H., Ziada, A. and Blunden, G. (2009). Biological effects of gum arabic: a review of some recent research. *Food Chem Toxicol,* 47(1), 1-8. doi:10.1016/j.fct.2008.07.001

Ali, E. H. and Arafa, N. M. (2011). Comparative protective action of curcumin, memantine and diclofenac against scopolamine-induced memory dysfunction. *Fitoterapia,* 82(4), 601-608. doi:10.1016/j.fitote.2011.01.016

Altman, R., Bosch, B., Brune, K., Patrignani, P. and Young, C. (2015). Advances in NSAID development: evolution of diclofenac products using pharmaceutical technology. *Drugs,* 75, 859-877.

Altunkaynak, B. Z., Onger, M. E., Altunkaynak, M. E., Ayranci, E. and Canan, S. (2012). A brief introduction to stereology and sampling strategies: basic concepts of stereology. *Neuroquantology,* 10(1), 31-43.

Altunkaynak, M. E., Altunkaynak, B. Z., Unal, D., Yildirim, S., Can, I. and Unal, B. (2011). Stereological and histological analysis of the developing rat heart. *Anat Histol Embryol,* 40(6), 402-410. doi:10.1111/j.1439-0264.2011.01085.x

Andersen, D. C., Jensen, C. H., Baun, C., Hvidsten, S., Zebrowski, D. C., Engel, F. B., et al. (2016). Persistent scarring and dilated cardiomyopathy suggest incomplete regeneration of the apex resected neonatal mouse myocardium--A 180 days follow up study. *J Mol Cell Cardiol,* 90, 47-52. doi:10.1016/j.yjmcc.2015.11.031

Anderson, D. and Eastwood, M. (1989). The safety of gum arabic as a food additive and its energy value as an ingredient: a brief review. *Journal of Human Nutrition and Dietetics,* 2(3), 137-144.

Anderson, D. and Stoddart, J. (1966). Studies on uronic acid materials: Part XV. The use of molecular-sieve chromatography in studies on acacia senegal gum (Gum Arabic). *Carbohydrate Research,* 2(2), 104-114.

Antman, E. M., Bennett, J. S., Daugherty, A., Furberg, C., Roberts, H. and Taubert, K. A. (2007). Use of nonsteroidal antiinflammatory drugs: an update for clinicians: a scientific statement from the American Heart Association. *Circulation,* 115(12), 1634-1642.

Assady, M., Farahnak, A., Golestani, A. and Esharghian, M. (2011). Superoxide Dismutase (SOD) Enzyme Activity Assay in Fasciola spp. Parasites and Liver Tissue Extract. *Iran J Parasitol,* 6(4), 17-22.

Atzeni, F., Masala, I. F. and Sarzi-Puttini, P. (2018). A Review of Chronic Musculoskeletal Pain: Central and Peripheral Effects of Diclofenac. *Pain Ther,* 7(2), 163-177. doi:10.1007/s40122-018-0100-2

Aygun, D., Kaplan, S., Odaci, E., Onger, M. E. and Altunkaynak, M. E. (2012). Toxicity of non-steroidal anti-inflammatory drugs: a review of melatonin and diclofenac sodium association. *Histol Histopathol,* 27(4), 417-436. doi:10.14670/HH-27.417

Baron, J. A., Sandler, R. S., Bresalier, R. S., Lanas, A., Morton, D. G., Riddell, R., et al. (2008). Cardiovascular events associated with rofecoxib: final analysis of the APPROVe trial. *The Lancet,* 372(9651), 1756-1764. doi:https://doi.org/10.1016/S0140-6736(08)61490-7

Bartolucci, A. A. and Howard, G. (2006). Meta-analysis of data from the six primary prevention trials of cardiovascular events using aspirin. *The American journal of cardiology,* 98(6), 746-750.

Baskar, R., Sparatore, A., Del Soldato, P. and Moore, P. K. (2008). Effect of S-diclofenac, a novel hydrogen sulfide releasing derivative inhibit rat vascular smooth muscle cell proliferation. *Eur J Pharmacol,* 594(1-3), 1-8. doi:10.1016/j.ejphar.2008.07.029

Bombardier, C., Laine, L., Reicin, A., Shapiro, D., Burgos-Vargas, R., Davis, B., et al. (2000). Comparison of upper gastrointestinal toxicity of rofecoxib and naproxen in patients with rheumatoid arthritis. *New England Journal of Medicine,* 343(21), 1520-1528.

Bresalier, R. S., Sandler, R. S., Quan, H., Bolognese, J. A., Oxenius, B., Horgan, K., et al. (2005). Cardiovascular events associated with rofecoxib in a colorectal adenoma chemoprevention trial. *N Engl J Med,* 352(11), 1092-1102. doi:10.1056/NEJMoa050493

Brown, D. L. (2017). Bias in image analysis and its solution: unbiased stereology. *J Toxicol Pathol,* 30(3), 183-191. doi:10.1293/tox.2017-0013

Bruel, A., Christoffersen, T. E. and Nyengaard, J. R. (2007). Growth hormone increases the proliferation of existing cardiac myocytes and the total number of cardiac myocytes in the rat heart. *Cardiovasc Res,* 76(3), 400-408. doi:10.1016/j.cardiores.2007.06.026

Brüel, A. and Nyengaard, J. R. (2005). Design–based stereological estimation of the total number of cardiac myocytes in histological sections. *Basic Research in Cardiology,* 100(4), 311-319. doi:10.1007/s00395-005-0524-9

Bruel, A., Oxlund, H. and Nyengaard, J. R. (2002). Growth hormone increases the total number of myocyte nuclei in the left ventricle of adult rats. *Growth Horm IGF Res,* 12(2), 106-115. doi:10.1054/ghir.2002.0269

Chan, F. K., Lanas, A., Scheiman, J., Berger, M. F., Nguyen, H. and Goldstein, J. L. (2010). Celecoxib versus omeprazole and diclofenac in patients with osteoarthritis and rheumatoid arthritis (CONDOR): a randomised trial. *The Lancet,* 376(9736), 173-179.

Cindoruk, M., Kerem, M., Karakan, T., Salman, B., Akin, O., Alper, M., et al. (2007). Peroxisome proliferators-activated alpha agonist treatment ameliorates hepatic damage in rats with obstructive jaundice: an experimental study. *BMC Gastroenterol,* 7(1), 44. doi:10.1186/1471-230X-7-44

Conaghan, P. G. (2012). A turbulent decade for NSAIDs: update on current concepts of classification, epidemiology, comparative efficacy, and toxicity. *Rheumatol Int,* 32(6), 1491-1502. doi:10.1007/s00296-011-2263-6

Connolly, S. J., Eikelboom, J. W., Bosch, J., Dagenais, G., Dyal, L., Lanas, F., et al. (2018). Rivaroxaban with or without aspirin in patients with stable coronary artery disease: an international, randomised, double-blind, placebo-controlled trial. *Lancet,* 391(10117), 205-218. doi:10.1016/S0140-6736(17)32458-3

Cornelsen, P. A., Quintanilha, R. C., Vidotti, M., Gorin, P. A., Simas-Tosin, F. F. and Riegel-Vidotti, I. C. (2015). Native and structurally modified gum arabic: exploring the effect of the gum's microstructure in obtaining electroactive nanoparticles. *Carbohydr Polym,* 119, 35-43. doi:10.1016/j.carbpol.2014.11.020

Crofford, L. J. (2013). Use of NSAIDs in treating patients with arthritis. *Arthritis Research & Therapy,* 15(3), S2. doi:10.1186/ar4174

Dauqan, E. and Abdullah, A. (2013). Utilization of gum arabic for industries and human health. *American Journal of Applied Sciences,* 10(10), 1270.

Dullin, C., Ufartes, R., Larsson, E., Martin, S., Lazzarini, M., Tromba, G., et al. (2017). muCT of ex-vivo stained mouse hearts and embryos enables a precise match between 3D virtual histology, classical histology and immunochemistry. *PLoS One,* 12(2), e0170597. doi:10.1371/journal.pone.0170597

Egadu, S. P., Mucunguzi, P. and Obua, J. (2007). Uses of tree species producing gum arabic in Karamoja, Uganda. *African journal of ecology,* 45, 17-21.

Elibol, B., OĞUR, B. and Doğru, H. (2019). Prenatal exposure of diclofenac sodium alters the behavioral development of young Wistar rats. *Turkish Journal of Biology,* 43(5), 305-313.
Elwell, M. and Mahler, J. (1999). Heart, blood vessels and lymphatic vessels. *Pathology of the Mouse*, 362.
Fanelli, A., Ghisi, D., Aprile, P. L. and Lapi, F. (2017). Cardiovascular and cerebrovascular risk with nonsteroidal anti-inflammatory drugs and cyclooxygenase 2 inhibitors: latest evidence and clinical implications. *Therapeutic advances in drug safety,* 8(6), 173-182.
Fanelli, A., Ghisi, D., Aprile, P. L. and Lapi, F. (2017). Cardiovascular and cerebrovascular risk with nonsteroidal anti-inflammatory drugs and cyclooxygenase 2 inhibitors: latest evidence and clinical implications. *Ther Adv Drug Saf,* 8(6), 173-182. doi:10.1177/2042098617690485
Fedail, J. S., Ahmed, A. A., Musa, H. H., Ismail, E., Sifaldin, A. Z. and Musa, T. H. (2016). Gum arabic improves semen quality and oxidative stress capacity in alloxan induced diabetes rats. *Asian Pacific Journal of Reproduction,* 5(5), 434-441. doi:10.1016/j.apjr.2016.07.014
Fernandez, B., Buehler, A., Wolfram, S., Kostin, S., Espanion, G., Franz, W. M., et al. (2000). Transgenic myocardial overexpression of fibroblast growth factor-1 increases coronary artery density and branching. *Circulation research,* 87(3), 207-213.
Fernandez, B., Duran, A. C., Fernandez, M. C., Fernandez-Gallego, T., Icardo, J. M. and Sans-Coma, V. (2008). The coronary arteries of the C57BL/6 mouse strains: implications for comparison with mutant models. *J Anat,* 212(1), 12-18. doi:10.1111/j.1469-7580.2007.00838.x
Fikret, G., Mikail, K., Murat Cetin, R. and Huseyin, A. (2015). Effects of prenatally exposed diclofenac sodium on rat heart tissue: a stereological and histological study. *Turk J Med Sci,* 45(3), 474-480. doi:10.3906/sag-1404-173
Fine, M. (2013). Quantifying the impact of NSAID-associated adverse events. *Am J Manag Care,* 19(14 Suppl), s267-272.
Fish, R., Danneman, P. J., Brown, M. and Karas, A. (2011). *Anesthesia and analgesia in laboratory animals*: Academic press.
Frith, C. and Ward, J. M. (1988). Color atlas of neoplastic and non-neoplastic lesions in aging mice.
Gado, A. M. and Aldahmash, B. A. (2013). Antioxidant effect of Arabic gum against mercuric chloride-induced nephrotoxicity. *Drug Des Devel Ther,* 7, 1245-1252. doi:10.2147/DDDT.S50928
Gamal el-din, A. M., Mostafa, A. M., Al-Shabanah, O. A., Al-Bekairi, A. M. and Nagi, M. N. (2003). Protective effect of arabic gum against acetaminophen-induced hepatotoxicity in mice. *Pharmacological research,* 48(6), 631-635.
Gamal el-din, A. M., Mostafa, A. M., Al-Shabanah, O. A., Al-Bekairi, A. M. and Nagi, M. N. (2003). Protective effect of arabic gum against acetaminophen-induced hepatotoxicity in mice. *Pharmacol Res,* 48(6), 631-635. doi:10.1016/s1043-6618(03)00226-3
Gan, T. J. (2010). Diclofenac: an update on its mechanism of action and safety profile. *Curr Med Res Opin,* 26(7), 1715-1731. doi:10.1185/03007995.2010.486301

Gandhi, S. and Abramov, A. Y. (2012). Mechanism of oxidative stress in neurodegeneration. *Oxid Med Cell Longev,* 2012, 428010. doi:10.1155/2012/428010

Gao, X., Björk, L., Trajkovski, V. and Uggla, M. (2000). Evaluation of antioxidant activities of rosehip ethanol extracts in different test systems. *Journal of the Science of Food and Agriculture,* 80(14), 2021-2027.

Gevrek, F., Kara, M., RAĞBETLİ, M. Ç. and ASLAN, H. (2015). Effects of prenatally exposed diclofenac sodium on rat heart tissue: a stereological and histological study. *Turkish Journal of Medical Sciences,* 45(3), 474-480.

Glover, D. A., Ushida, K., Phillips, A. O. and Riley, S. G. (2009). Acacia(sen) SUPERGUM™ (Gum arabic): An evaluation of potential health benefits in human subjects. *Food Hydrocolloids,* 23(8), 2410-2415. doi:10.1016/j.foodhyd.2009.06.020

Graham, D. J. (2006). COX-2 inhibitors, other NSAIDs, and cardiovascular risk: the seduction of common sense. *Jama,* 296(13), 1653-1656.

Gundersen, H.-J. G. (1986). Stereology of arbitrary particles* a review of unbiased number and size estimators and the presentation of some new ones, in memory of william r. thompson. *Journal of microscopy,* 143(1), 3-45.

Gundersen, H. J., Bagger, P., Bendtsen, T. F., Evans, S. M., Korbo, L., Marcussen, N., et al. (1988). The new stereological tools: disector, fractionator, nucleator and point sampled intercepts and their use in pathological research and diagnosis. *APMIS,* 96(10), 857-881. doi:10.1111/j.1699-0463.1988.tb00954.x

Gundersen, H. J. and Jensen, E. B. (1987). The efficiency of systematic sampling in stereology and its prediction. *J Microsc,* 147(Pt 3), 229-263. doi:10.1111/j.1365-2818.1987.tb02837.x

Gundersen, H. J. G., Jensen, E. B. V., Kieu, K. and Nielsen, J. (1999). The efficiency of systematic sampling in stereology—reconsidered. *Journal of microscopy,* 193(3), 199-211.

Haugen, I. K., Ramachandran, V. S., Misra, D., Neogi, T., Niu, J., Yang, T., et al. (2015). Hand osteoarthritis in relation to mortality and incidence of cardiovascular disease: data from the Framingham heart study. *Ann Rheum Dis,* 74(1), 74-81. doi:10.1136/annrheumdis-2013-203789

Hawkey, C. J. (2000). Nonsteroidal anti-inflammatory drug gastropathy. *Gastroenterology,* 119(2), 521-535.

Hinton, R. B., Jr., Alfieri, C. M., Witt, S. A., Glascock, B. J., Khoury, P. R., Benson, D. W., et al. (2008). Mouse heart valve structure and function: echocardiographic and morphometric analyses from the fetus through the aged adult. *Am J Physiol Heart Circ Physiol,* 294(6), H2480-2488. doi:10.1152/ajpheart.91431.2007

Hirose, K., Jyoyama, H., Kojima, Y., Eigyo, M., Hatakeyama, H., Asanuma, F., et al. (1984). Pharmacological properties of 2-[4-(2-thiazolyloxy)-phenyl]-propionic acid (480156-S), a new non-steroidal antiinflammatory agent. *Arzneimittelforschung,* 34(3), 280-286.

Hort, W. (1971). Quantitative morphology and structural dynamics of the myocardium. *Methods and achievements in experimental pathology,* 5, 3-21.

Idris, O., Williams, P. and Phillips, G. (1998). Characterisation of gum from Acacia senegal trees of different age and location using multidetection gel permeation chromatography. *Food Hydrocolloids,* 12(4), 379-388.

Ilic, S., Drmic, D., Franjic, S., Kolenc, D., Coric, M., Brcic, L., et al. (2011). Pentadecapeptide BPC 157 and its effects on a NSAID toxicity model: diclofenac-induced gastrointestinal, liver, and encephalopathy lesions. *Life Sci,* 88(11-12), 535-542. doi:10.1016/j.lfs.2011.01.015

Islam, A., Phillips, G., Sljivo, A., Snowden, M. and Williams, P. (1997). A review of recent developments on the regulatory, structural and functional aspects of gum arabic. *Food Hydrocolloids,* 11(4), 493-505.

Jain, T., Koley, K., Vadlamudi, V., Ghosh, R., Roy, S., Tiwari, S., et al. (2009). Diclofenac-induced biochemical and histopathological changes in white leghorn birds (Gallus domesticus). *Indian journal of pharmacology,* 41(5), 237.

Kaddam, L., Fadl-Elmula, I., Eisawi, O. A., Abdelrazig, H. A., Salih, M. A., Lang, F., et al. (2017). Gum Arabic as novel anti-oxidant agent in sickle cell anemia, phase II trial. *BMC Hematol,* 17, 4. doi:10.1186/s12878-017-0075-y

Kaddam, L., Fdl-Elmula, I. and Saeed, A. (2018). Gum Arabic Beneficial Effects, Clinical Applications, and Future Prospective. *Gum Arabic* (s. 211-220): Elsevier.

Kaplan, S., Odacı, E., Canan, S., Onger, M. E., Aslan, H. and Unal, B. (2011). The Disector Counting Technique. *Neuroquantology,* 10(1), 44-53. doi:10.14704/nq.2012.10.1.425

Keenan, C. M. and Vidal, J. D. (2006). Standard morphologic evaluation of the heart in the laboratory dog and monkey. *Toxicol Pathol,* 34(1), 67-74. doi:10.1080/01926230500369915

Khalid, S. A., Musa, A. M., Saeed, A. M., Abugroun, E. A., Sid Ahmed, E. O., Ghalib, M. B., et al. (2014). Manipulating dietary fibre: Gum Arabic making friends of the colon and the kidney. *Bioactive Carbohydrates and Dietary Fibre,* 3(2), 71-76. doi:10.1016/j.bcdf.2014.01.005

Kowalski, M., Makowska, J., Blanca, M., Bavbek, S., Bochenek, G., Bousquet, J., et al. (2011). Hypersensitivity to nonsteroidal anti-inflammatory drugs (NSAIDs)–classification, diagnosis and management: review of the EAACI/ENDA# and GA2LEN/HANNA. *Allergy,* 66(7), 818-829.

Lelon, J., Jumba, I., Keter, J., Chemuku, W. and Oduor, F. (2010). Assessment of physical properties of gum arabic from Acacia senegal varieties in Baringo District, Kenya. *African Journal of Plant Science,* 4(4), 95-98.

Li, J. and Radice, G. L. (2010). A new perspective on intercalated disc organization: implications for heart disease. *Dermatol Res Pract,* 2010, 207835. doi:10.1155/2010/207835

Limberaki, E., Eleftheriou, P., Vagdatli, E., Kostoglou, V. and Petrou, C. (2012). Serum antioxidant status among young, middle-aged and elderly people before and after antioxidant rich diet. *Hippokratia,* 16(2), 118-123.

Madeo, F., Frohlich, E., Ligr, M., Grey, M., Sigrist, S. J., Wolf, D. H., et al. (1999). Oxygen stress: a regulator of apoptosis in yeast. *J Cell Biol,* 145(4), 757-767. doi:10.1083/jcb.145.4.757

Martins, D. and English, A. M. (2014). Catalase activity is stimulated by H2O2 in rich culture medium and is required for H2O2 resistance and adaptation in yeast. *Redox biology,* 2, 308-313.

Miki, T., Satriotomo, I., Li, H. P., Matsumoto, Y., Gu, H., Yokoyama, T., et al. (2005). Application of the physical disector to the central nervous system: estimation

of the total number of neurons in subdivisions of the rat hippocampus. *Anat Sci Int,* 80(3), 153-162. doi:10.1111/j.1447-073x.2005.00121.x

Morioka, N., Kumagai, K., Morita, K., Kitayama, S. and Dohi, T. (2004). Nonsteroidal anti-inflammatory drugs potentiate 1-methyl-4-phenylpyridinium (MPP+)-induced cell death by promoting the intracellular accumulation of MPP+ in PC12 cells. *J Pharmacol Exp Ther,* 310(2), 800-807. doi:10.1124/jpet.104.065300

Morioka, N., Kumagai, K., Morita, K., Kitayama, S. and Dohi, T. (2004). Nonsteroidal anti-inflammatory drugs potentiate 1-methyl-4-phenylpyridinium (MPP+)-induced cell death by promoting the intracellular accumulation of MPP+ in PC12 cells. *Journal of Pharmacology and Experimental Therapeutics,* 310(2), 800-807.

Mouton, P. R., Phoulady, H. A., Goldgof, D., Hall, L. O., Gordon, M. and Morgan, D. (2017). Unbiased estimation of cell number using the automatic optical fractionator. *J Chem Neuroanat,* 80, A1-A8. doi:10.1016/j.jchemneu.2016.12.002

Muhlfeld, C., Nyengaard, J. R. and Mayhew, T. M. (2010). A review of state-of-the-art stereology for better quantitative 3D morphology in cardiac research. *Cardiovasc Pathol,* 19(2), 65-82. doi:10.1016/j.carpath.2008.10.015

Nair, B. and Taylor-Gjevre, R. (2010). A Review of Topical Diclofenac Use in Musculoskeletal Disease. *Pharmaceuticals (Basel),* 3(6), 1892-1908. doi:10.3390/ph3061892

Nasir, O., Babiker, S. and Salim, A.-M. M. (2016). Protective effect of gum Arabic supplementation for type 2 diabetes mellitus and its complications. *Int J Multidiscip Curr Res,* 4, 288-294.

Olsen, A.-M. S., Fosbøl, E. L., Lindhardsen, J., Folke, F., Charlot, M., Selmer, C., et al. (2012). Long-term cardiovascular risk of nonsteroidal anti-inflammatory drug use according to time passed after first-time myocardial infarction: a nationwide cohort study. *Circulation,* 126(16), 1955-1963.

Olsen, A. M., Fosbol, E. L., Lindhardsen, J., Folke, F., Charlot, M., Selmer, C., et al. (2012). Long-term cardiovascular risk of nonsteroidal anti-inflammatory drug use according to time passed after first-time myocardial infarction: a nationwide cohort study. *Circulation,* 126(16), 1955-1963. doi:10.1161/CIRCULATIONAHA.112.112607

Ong, C. K., Lirk, P., Tan, C. H. and Seymour, R. A. (2007). An evidence-based update on nonsteroidal anti-inflammatory drugs. *Clin Med Res,* 5(1), 19-34. doi:10.3121/cmr.2007.698

Parildar, H., Dogru-Abbasoglu, S., Mehmetcik, G., ÖZDEMIRLER, G., Kocak-Toker, N. and Uysal, M. (2008). Lipid peroxidation potential and antioxidants in the heart tissue of β-alanine-or taurine-treated old rats. *Journal of nutritional science and vitaminology,* 54(1), 61-65.

Patel, S. and Goyal, A. (2015). Applications of Natural Polymer Gum Arabic: A Review. *International Journal of Food Properties,* 18(5), 986-998. doi:10.1080/10942912.2013.809541

Peterson, K., McDonagh, M., Thakurta, S., Dana, T., Roberts, C., Chou, R., et al. (2006). Drug class review nonsteroidal antiinflammatory drugs (NSAIDs). *Update,* 4.

Phillips, G. O. and Williams, P. A. (2000). *Handbook of hydrocolloids*: CRC press Boca Raton, FL.

Pountos, I., Theodora, G., Howard, B. and Giannoudis, P. (2011). Nonsteroidal anti-inflammatory drugs: prostaglandins, indications, and side effects. *International Journal of Interferon, Cytokine and Mediator Research*. doi:10.2147/ijicmr.S10200

Rehman, K., Wingertzahn, M. A., Harper, R. G. and Wapnir, R. A. (2001). Proabsorptive action of gum arabic: regulation of nitric oxide metabolism in the basolateral potassium channel of the small intestine. *Journal of pediatric gastroenterology and nutrition,* 32(5), 529-533.

Ren, J. and Wold, L. E. (2001). *Biological procedures online,* 3, 43-53.

Rentschler, S., Vaidya, D. M., Tamaddon, H., Degenhardt, K., Sassoon, D., Morley, G. E., et al. (2001). Visualization and functional characterization of the developing murine cardiac conduction system. *Development,* 128(10), 1785-1792.

Ricciotti, E. and FitzGerald, G. A. (2011). Prostaglandins and inflammation. *Arterioscler Thromb Vasc Biol,* 31(5), 986-1000. doi:10.1161/ATVBAHA.110.207449

Sanchez, C., Nigen, M., Mejia Tamayo, V., Doco, T., Williams, P., Amine, C., et al. (2018). Acacia gum: History of the future. *Food Hydrocolloids,* 78, 140-160. doi:10.1016/j.foodhyd.2017.04.008

Savolainen, S. M., Foley, J. F. and Elmore, S. A. (2009). Histology atlas of the developing mouse heart with emphasis on E11.5 to E18.5. *Toxicol Pathol,* 37(4), 395-414. doi:10.1177/0192623309335060

Schmidt, M., Sorensen, H. T. and Pedersen, L. (2018). Diclofenac use and cardiovascular risks: series of nationwide cohort studies. *bmj,* 362, k3426. doi:10.1136/bmj.k3426

Schmitz, C., Eastwood, B. S., Tappan, S. J., Glaser, J. R., Peterson, D. A. and Hof, P. R. (2014). Current automated 3D cell detection methods are not a suitable replacement for manual stereologic cell counting. *Front Neuroanat,* 8, 27. doi:10.3389/fnana.2014.00027

Scudamore, C. L. (2013). *A Practical Guide to the Histology of the Mouse*: John Wiley & Sons.

Singleton, V. L. and Rossi, J. A. (1965). Colorimetry of total phenolics with phosphomolybdic-phosphotungstic acid reagents. *American journal of Enology and Viticulture,* 16(3), 144-158.

Solomon, S. D., McMurray, J. J., Pfeffer, M. A., Wittes, J., Fowler, R., Finn, P., et al. (2005). Cardiovascular risk associated with celecoxib in a clinical trial for colorectal adenoma prevention. *N Engl J Med,* 352(11), 1071-1080. doi:10.1056/NEJMoa050405

Suliman, S., Hamdouk, M. and Elfaki, M. (2000). *Gum Arabic fibre as a supplemnt to low protein diet in chronic renal failure patients.* Paper presented at the Sudan Association of Physicians 17th Conference.

Taylor, M., Graw, S., Sinagra, G., Barnes, C., Slavov, D., Brun, F., et al. (2011). Genetic variation in titin in arrhythmogenic right ventricular cardiomyopathy-overlap syndromes. *Circulation,* 124(8), 876-885. doi:10.1161/CIRCULATIONAHA.110.005405

Todd, P. A. and Sorkin, E. M. (1988). Diclofenac sodium. A reappraisal of its pharmacodynamic and pharmacokinetic properties, and therapeutic efficacy. *Drugs,* 35(3), 244-285. doi:10.2165/00003495-198835030-00004

Torgersen, J. (1950). The developmental anatomy of the heart and the etiology of congenital heart disease. *Acta radiol,* 33(2), 131-146. doi:10.3109/00016925009133882

Tural, S. and Koca, I. (2008). Physico-chemical and antioxidant properties of cornelian cherry fruits (Cornus mas L.) grown in Turkey. *Scientia Horticulturae,* 116(4), 362-366.

Turkmen, A. P., Kaplan, S., Aksoy, A., Altunkaynak, B., Yurt, K., Elibol, E., et al. (2016). Effects of diclofenac sodium on the hippocampus of rats with acute subdural hematoma: histological, stereological, and molecular approach. *Folia Neuropathol,* 54(2), 167-179. doi:10.5114/fn.2016.60808

Ukeda, H., Kawana, D., Maeda, S. and Sawamura, M. (1999). Spectrophotometric Assay for Superoxide Dismutase Based on the Reduction of Highly Water-soluble Tetrazolium Salts by Xanthine-Xanthine Oxidase. *Biosci Biotechnol Biochem,* 63(3), 485-488. doi:10.1271/bbb.63.485

Varas-Lorenzo, C., Riera-Guardia, N., Calingaert, B., Castellsague, J., Salvo, F., Nicotra, F., et al. (2013). Myocardial infarction and individual nonsteroidal anti-inflammatory drugs meta-analysis of observational studies. *Pharmacoepidemiology and drug safety,* 22(6), 559-570.

Viggiano, A., Viggiano, D., Viggiano, A. and De Luca, B. (2003). Quantitative histochemical assay for superoxide dismutase in rat brain. *J Histochem Cytochem,* 51(7), 865-871. doi:10.1177/002215540305100702

Weisskopf, K. (1988). Characterization of polyethylene terephthalate by gel permeation chromatography (GPC). *Journal of Polymer Science Part A: Polymer Chemistry,* 26(7), 1919-1935.

Wessels, A. and Sedmera, D. (2003). Developmental anatomy of the heart: a tale of mice and man. *Physiological genomics,* 15(3), 165-176.

West, M. J. (2012). Introduction to stereology. *Cold Spring Harbor Protocols,* 2012(8), pdb. top070623.

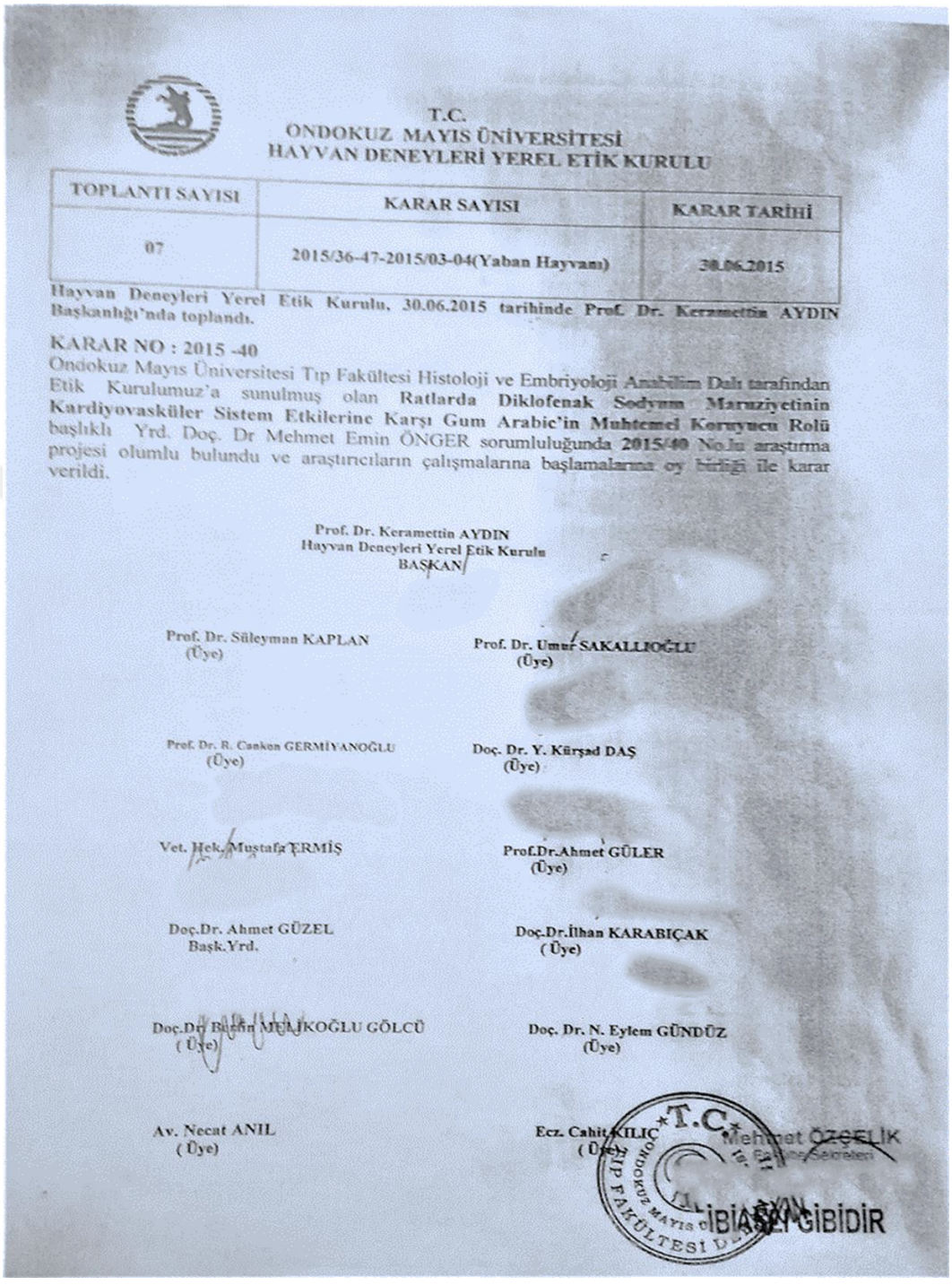
Wiese, C., Grieskamp, T., Airik, R., Mommersteeg, M. T., Gardiwal, A., de Gier-de Vries, C., et al. (2009). Formation of the sinus node head and differentiation of sinus node myocardium are independently regulated by Tbx18 and Tbx3. *Circ Res,* 104(3), 388-397. doi:10.1161/CIRCRESAHA.108.187062

Yurt, K. K., Kaplan, S. and Kivrak, E. G. (2018). The neuroprotective effect of melatonin on the hippocampus exposed to diclofenac sodium during the prenatal period. *J Chem Neuroanat,* 87, 37-48. doi:10.1016/j.jchemneu.2017.05.006

Yurt, K. K., Kivrak, E. G., Altun, G., Mohamed, H., Ali, F., Gasmalla, H. E., et al. (2018). A brief update on physical and optical disector applications and sectioning-staining methods in neuroscience. *J Chem Neuroanat,* 93, 16-29. doi:10.1016/j.jchemneu.2018.02.009

Zhao, F., Li, J., Mo, L., Tan, M., Zhang, T., Tang, Y., et al. (2016). Changes in Neurons and Synapses in Hippocampus of Streptozotocin-Induced Type 1 Diabetes Rats: A Stereological Investigation. *Anat Rec (Hoboken),* 299(9), 1174-1183. doi:10.1002/ar.23344

APPENDIX 1: ETHICAL COMMITTEE DICISTION



T.C.
ONDOKUZ MAYIS ÜNİVERSİTESİ
HAYVAN DENEYLERİ YEREL ETİK KURULU

TOPLANTI SAYISI	KARAR SAYISI	KARAR TARİHİ
07	2015/36-47-2015/03-04(Yaban Hayvanı)	30.06.2015

Hayvan Deneyleri Yerel Etik Kurulu, 30.06.2015 tarihinde Prof. Dr. Keramettin AYDIN Başkanlığı'nda toplandı.

KARAR NO : 2015 -40

Ondokuz Mayıs Üniversitesi Tıp Fakültesi Histoloji ve Embriyoloji Anabilim Dalı tarafından Etik Kurulumuz'a sunulmuş olan **Ratlarda Diklofenak Sodyum Maruziyetinin Kardiyovasküler Sistem Etkilerine Karşı Gum Arabic'in Muhtemel Koruyucu Rolü** başlıklı Yrd. Doç. Dr Mehmet Emin ÖNGER sorumluluğunda **2015/40** No.lu araştırma projesi olumlu bulundu ve araştırıcıların çalışmalarına başlamalarına oy birliği ile karar verildi.

Prof. Dr. Keramettin AYDIN
Hayvan Deneyleri Yerel Etik Kurulu
BAŞKAN

Prof. Dr. Süleyman KAPLAN (Üye)

Prof. Dr. Umur SAKALLIOĞLU (Üye)

Prof. Dr. R. Canken GERMİYANOĞLU (Üye)

Doç. Dr. Y. Kürşad DAŞ (Üye)

Vet. Hek. Mustafa ERMİŞ

Prof.Dr.Ahmet GÜLER (Üye)

Doç.Dr. Ahmet GÜZEL
Başk.Yrd.

Doç.Dr.İlhan KARABIÇAK (Üye)

Doç.Dr. Bilgin MUMCUOĞLU GÖLCÜ (Üye)

Doç. Dr. N. Eylem GÜNDÜZ (Üye)

Av. Necat ANIL (Üye)

Ecz. Cahit KILIÇ (Üye)

T.C. Mehmet ÖZÇELİK
Fak. Dönem Sekreteri
ONDOKUZ MAYIS ÜNİVERSİTESİ TIP FAKÜLTESİ
İBİARESLİ GİBİDİR

CURRICULUM VITEA

Abuzar Mubarak OMER OSMAN, a holder of B.Sc of Basic Medical Sciences (Human Anatomy) Shendi University - Faculty of Medicine and Health Sciences- Sudan- July 2002. And M.Sc of Human Anatomy- Alzheim Alazhari University – Faculty of Graduate Studies-Sudan- June 2011. Now earned a Ph.D. of histology and embryology from Ondokuz Mayıs University-Faculty of Medicine Department of Histology and Embryology 2015-2023- Samsun- Turkey.(21.06.2023)

ORCID ID: https://orcid.org/ 0000-0001-7985-5279

Publications :

1. **Osman, A.**, , A. M., Önger, M. E., Kaplan, S., Mahdi, A., Osman, M. S., . Elamin, A. Y., Abdelghani, N. (2023). Investigation of possible histological and morphological changes in kidney induced by obesity and leptin. Paper presented at the 4th International ACHARAKA Congress on Medicine, Nursing, and Health Sciences, Izmir.
2. **Osman, A.**, Önger, M. E., Kaplan, S., Osman, M. S., Mahdi, A., Abdelghani, N., & Elamin, A. Y. (2023). The possible effect of Gum Arabic in healing of cardiovascular injury induced by diclofenac: a stereological and histological study in a rat model. Paper presented at the 4th International ACHARAKA Congress on Medicine, Nursing, and Health Sciences, Izmir.
3. Elamin, A. Y., Önger, M. E., Kaplan, S., Abdelghani, N., Mahdi, A., Osman, M. S., **Osman, A.,** Hiba. H. s. Omer. (2023). Dose-dependent cytotoxic effects of agomelatine on BV2 cells: impact of duration. Paper presented at the 4th International ACHARAKA Congress on Medicine, Nursing, and Health Sciences, Izmir.
4. Elamin, A. Y., Önger, M. E., Kaplan, S., Abdelghani, N., Mahdi, A., Osman, M. S., **Osman, A.,** Hiba H.s. Omer (2023). LPS-induced toxicity: evaluating dose-dependent effects of LPS on HT-22 cell viability. Paper presented at the 4th International ACHARAKA Congress on Medicine, Nursing, and Health Sciences, Izmir.